DIFFRACTION ANALYSIS OF VERTEBRATE MUSCLE CROSSBRIDGE ARRANGEMENTS

Thesis submitted for the Degree of

Doctor of Philosophy

by

JEFFREY JON HARFORD

Biopolymer Group,

Department of Metallurgy and Materials Science,

Imperial College of Science and Technology,

University of London.

FEBRUARY 1984

ABSTRACT

The myosin crossbridge arrangement in vertebrate skeletal muscle was analysed by optical diffraction of electron micrographs, Fourier synthesis of equatorial X-ray diffraction data and by modelling low-angle X-ray layer line data from living muscle.

The appearance of the crossbridge arrangement in human muscle in axial projection along the thick filament was studied by optical diffraction of electron micrographs of longitudinally cryosectioned muscle and by computer modelling of the diffraction data. Realistic models indicate that the crossbridges in this fixed/relaxed preparation are projecting approximately perpendicular to the thick filament backbone and that the crossbridges have a true axial repeat of 42.9nm. The three crossbridge levels within this repeat are not equally spaced. C-protein, or an isoform of it, is the most abundant non-myosin protein associated with the thick filament. This labels the thick filament with a periodicity approximately 1% greater than the axial repeat of the crossbridge arrangement (i.e. 42.9nm).

The appearance of the crossbridge distribution projected onto a plane perpendicular to the fibre axis was studied by Fourier synthesis from the equatorial X-ray diffraction data from live frog and fish muscles. A method is developed to enable the correct density map to be picked from the numerous plausible maps produced by Fourier synthesis. The method was tested with simple muscle-like models and then applied to equatorial X-ray diffraction data from vertebrate skeletal muscle.

The three-dimensional arrangement of myosin crossbridges in live Plaice fish muscle was studied by low-angle X-ray

diffraction. The intensity distributions along these layer lines are consistent with the crystalline lattice of crossbridges suggested by electron micrographs of the transversely sectioned thick filament backbone in bony fish. The layer line spacings are very similar to those from frog sartorius muscle (i.e. 42.9nm, 21.5nm, 14.3nm etc.,). The row-line sampling of the layer lines was the same on the equator and all the observed layer lines. The 00 and 10 peaks predominate on all layer lines with l=3N (N=integer) and the 11 and 20 peaks predominate on layer lines with l=3N+1. This crystalline sampling of the myosin layer lines allows a much less ambiguous analysis of the relaxed crossbridge arrangement than has been possible with other vertebrate muscles. Preliminary models for the resting arrangement of myosin crossbridges in Plaice fish muscle are presented.

ACKNOWLEDGEMENTS

Throughout the period of this project at the Department of Metallurgy and Materials Science at Imperial College of Science and Technology, University of London, I was funded by the Muscular Dystrophy Association of America and am extremely grateful to them for their support during this work.

It is with pleasure that I acknowledge my very deep gratitude for the constant encouragement and enthusiasm afforded by my supervisor, Dr. John Squire, in all stages of this work. I greatly appreciate his willingness to help at all times.

I would like to thank my colleagues Dr. Alan Freundlich and Dr. Pradeep Luther for their kind help both in the laboratory and in many discussions; also Fred Huggins and Tom Rutherford for their excellent technical assistance in maintaining the X-ray generators at Imperial College and Kings College, respectively.

During the last year of this project X-ray facilities at the MRC Biophysics Unit, Kings College, Drury Lane were used and I am grateful for this provision and the help of Drs. Michael Spencer and Helen Saibil while working there.

Drs. Michael Sjöström and Anne Christine Edman (Umea University, Sweden) kindly provided the excellent cryosections of human muscle tissue which were analysed as part of this project. This work has thus been published as a co-authored paper in the Journal of Molecular Biology. I am indebted to them for the work which their considerable expertise has made possible.

Finally I would like to express my sincere appreciation to my mother for the considerable sacrifices on her part which have enabled me to pursue an academic career this far, and to my wife, Aurelia, for her patience during the prolonged period of completing this thesis.

CONTENTS

		PAGE
CHAPTER 1	Structure of the Vertebrate Muscle A-Band.	6
CHAPTER 2	Materials and Methods	86
CHAPTER 3	C-zone Analysis	153
CHAPTER 4	Analysis of Equatorial Diffraction Data.	203
CHAPTER 5	X-ray Diffraction of Live Plaice Fin Muscle.	228
CHAPTER 6	Discussion	284
	References	306
	Appendix A	322

CHAPTER 1 : STRUCTURE OF THE VERTEBRATE MUSCLE A-BAND

1.1. INTRODUCTION 8

1.1.1. Muscle Fibre and its activation. 11

1.1.2. The Sarcomere. 12

1.1.3. Thin Filaments and Regulation. 16

1.1.4. The Contractile Cycle. 21

1.1.5. The Pattern of interactions of the Actin monomers and the Myosin Crossbridges. 22

1.2. THE MYOSIN MOLECULE 25

1.2.1. The Shape of the Myosin Molecule. 25

1.2.2. Polypeptide Chain Arrangement. 28

1.2.3. Proteolytic Fragments of the Myosin Molecule. 28

1.2.4. Properties of the Myosin Molecule. 29

1.2.5. Association of the Properties of HMM-S1 with with the Myosin Heavy and Light Chains. 31

1.2.6. Flexibility of the Myosin Molecule. 32

1.3. THICK FILAMENT STRUCTURE 34

1.3.1. The Surface Arrangement of Crossbridges. 34

1.3.2. Non-myosin Proteins of the A-Band. 44

1.3.2.A. C-Protein and C-Zone Structure. 44

1.3.2.B. M-Proteins and M-band Structure. 51

1.4. X-RAY DIFFRACTION FROM FROG SARTORIUS MUSCLE 53

1.4.1. Reflections Arising from the Thick Filaments. 53

1.4.1.A. Myosin Layer Line Pattern. 53

1.4.1.B. Additional Meridional Reflections. 57

1.4.2. Reflections Arising from the Thin Filaments. 61

1.4.2.A. The Actin Layer Lines. 61

1.4.2.B. Additional Meridional Reflections from the Thin Filaments. 64

1.4.3. Arrangement of Crossbridges in Rigor Muscle. 64

1.4.4. Arrangement of Crossbridges in Active Muscle. 65

1.5. LATERAL ARRANGEMENT OF MUSCLE FILAMENTS 67

1.5.1. The Equatorial Diffraction Pattern. 67

1.5.2. The Three-Dimensional Crossbridge Lattice in Vertebrate Skeletal Muscle. 72

1.5.2.A. Interpretation of the Myosin Layer Line Sampling in terms of the Regular Superlattice. 72

1.5.2.B. The Statistical Superlattice. 73

1.5.2.C. Reinterpretation of the Myosin Layer Line Sampling in terms of the Statistical Superlattice. 82

CHAPTER ONE

1.1. INTRODUCTION.

All muscles appear to involve interactions between actin- and myosin-containing structures, fuelled by ATP hydrolysis. The high degree of structural order in striated muscles has enabled a great deal of progress in our understanding of the structural basis of this interaction. However our knowledge of the ultrastructure of the actin-containing filaments and the three-dimensional arrangement of these and the myosin containing filaments in the sarcomere is not matched by the relatively poorly understood structure of the myosin filaments in the extensively studied insect flight and frog sartorius muscles. Ironically it is in the invertebrate crustacean muscles, where the filament arrangement does not show the same degree of order, that the arrangement of the myosin crossbridges was first clearly demonstrated; in some cases indirectly by X-ray diffraction and in others directly by studying isolated myosin filaments.

This is just one example which highlights the importance of searching for new ultrastructural tools and new experimental approaches for ultrastructural research when previously used combinations fail to bear the essential fruit.

The work described in this thesis has involved the use of new ultrastructural tools or approaches to define the arrangement of myosin and in particular the myosin crossbridges in the filaments of vertebrate skeletal muscle.

X-ray diffraction patterns of living muscle in theory contain the necessary information to define the configuration of the myosin crossbridge at the starting point of its contractile cycle. Extracting this information from the richly informative

patterns of relaxed insect and frog sartorius muscles is complicated due to the randomness in the structures. The muscles in the bony fish in the present work are devoid of these complications and ought to provide a better tool for this type of study.

Equatorial X-ray diffraction data of higher resolution has resulted from recording patterns with linear position sensitive detectors. This much needed increase in the number of recorded equatorial reflections means that Fourier synthesis of the data generates an increased number of density maps many of which are plausible. A new approach to selecting the correct map and therefore establishing the projected appearance of the crossbridge arrangement down the fibre axis is presented.

The technique of Cryosectioning has considerably improved the preservation of ultrastructural detail observed in muscle tissue through the electron microscope. This has enabled a detailed optical diffraction analysis of the C-zone structure in human muscle. It has thus been possible to confirm directly the imperfections in the arrangement of the myosin crossbridge surface lattice and the presence of other components.

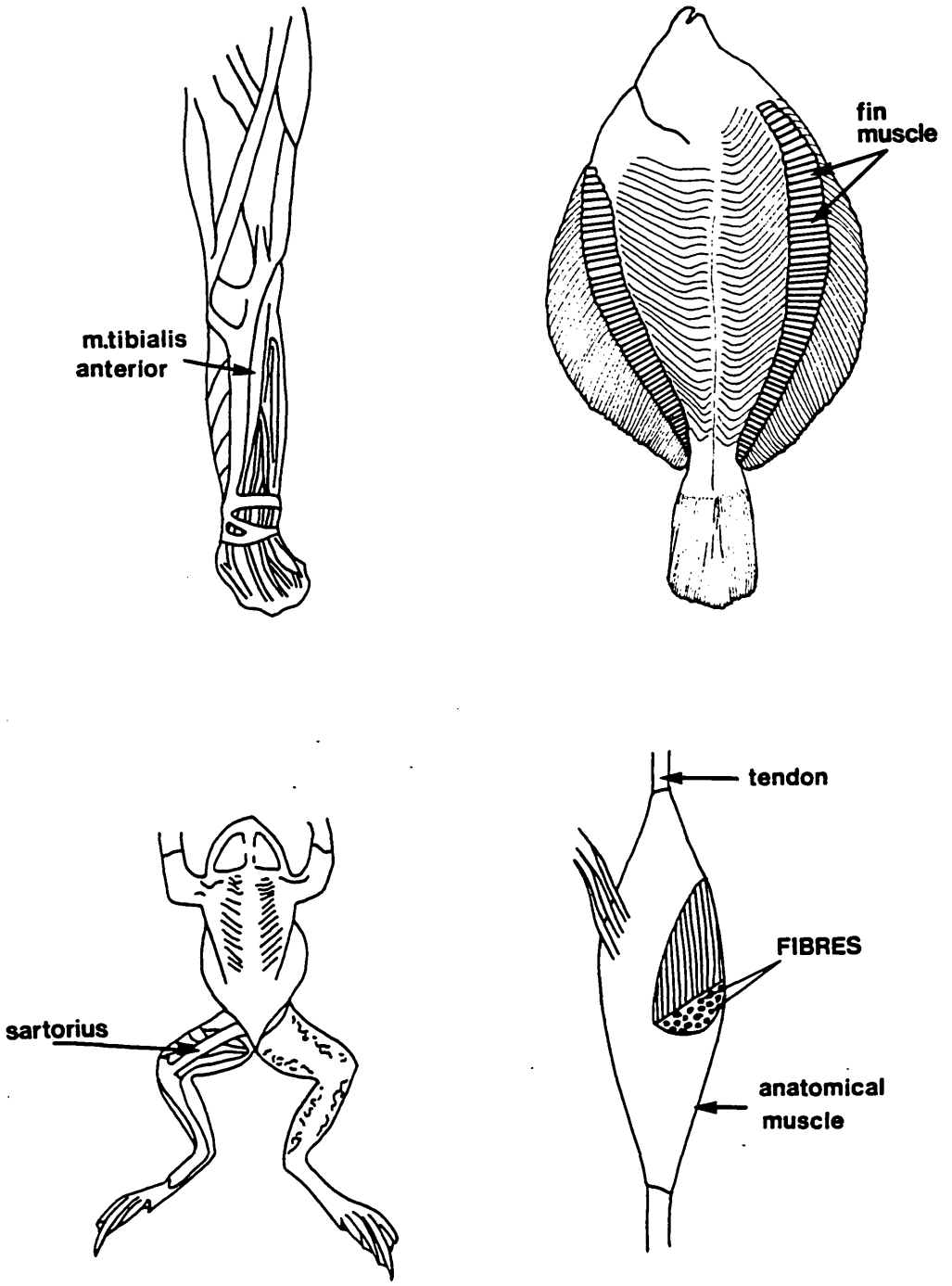


FIGURE 1 Diagram showing the anatomical muscles used in this study. (a) M.tibialis anterior muscle from the human leg. (b) Fin muscle from the Plaice fish. (c) Frog sartorius muscle (used for calibration). (d) Diagram of the basic anatomy of a skeletal muscle consisting of muscle fibres contained within a membrane of connective tissue and attached by tendons to the skeleton.

1.1.1. Muscle Fibre and its Activation.

The three basic muscle types i.e. skeletal, cardiac and smooth muscles, differ in the arrangement of their contractile proteins and by the manner in which the stimulus for contraction of these muscles is transported to the contractile machinery. These characteristics of the various muscle types clearly depend on the function performed by the muscle in the living organism. Smooth muscle forms the muscular part of the walls of some hollow organs such as the intestines, whereas cardiac muscle forms the walls of the heart. Although these muscles receive a motor nerve supply from the autonomic nervous system thay are essentially involuntary. Thus cardiac, and single unit smooth muscles, undergo contraction even when deprived of their motor nerve innervation. Their contractile proteins are far less well organised than in skeletal muscle, which only contracts on arrival of nerve impulses at the neuromuscular junction; skeletal muscle is under voluntary control. When a vertebrate skeletal muscle contracts it does so as a result of trains of high-frequency impulses reaching it from the motor nerve fibre from the central nervous system. The response of the muscle depends on how the fibres are innervated. Tonic (slow) muscle fibres receive many nerve endings along their length and the contractile response is confined to the nerve muscle junction. Twitch fibres, which are further differentiated into fast and slow twitch, typically have only a single motor nerve terminal on their surface and the nerve impulse causes contraction throughout the whole length of the fibre, and in all fibres within the motor unit, due to the rapid propagation of an electrical wave along the surface membrane.

Muscle fibres are typically 2 to 50 millimetres long and 10 to 100μm wide. The change in membrane potential caused by the nervous impulse spreads inwards to myofibrils through the T-tubule system which is an extension of the fibre's surface membrane (sarcolemma; Franzini-Armstrong and Porter, 1964; Page, 1964; Huxley, 1964). On either side of these tubules along most of their length are vesicles (terminal cisternae) belonging to the sarcoplasmic reticulum. These are not continuous with the T-tubules or the sarcolemma. The vesicles are depolarised and liberate calcium ions when the membrane potential changes the adjacent T-tubules. Activation of the actomyosin ATPase then occurs when the calcium ion concentration in the sarcoplasm of the muscle cell rises from about 0.1 to 10 micromolar. This rise in calcium concentration is the ultimate message received by the myofibrillar proteins before contraction occurs. This activity ceases when the calcium is taken up by the vesicles of the sarcoplasmic reticulum, reducing the calcium ion concentration below about 0.1 micromolar.

The contractile proteins are arranged in myofibrils 1 to 2 μm in diameter which extend from one end of the fibre to the other. The actin and myosin proteins are located in the bands of low (I-band) and high (A-band) refractive index, respectively, which alternate along the length of the myofibril (Figure 1.1).

1.1.2. The Sarcomere.

The functional unit of the myofibril, the Sarcomere, (Figure 1.1.(e)), is defined as being between two Z-disc structures. The sarcomere length is about 2.3 μm in resting frog sartorius muscle, but can range from 2.0 to about 3.7 μm. The actin and myosin molecules are arranged into filaments in the I-

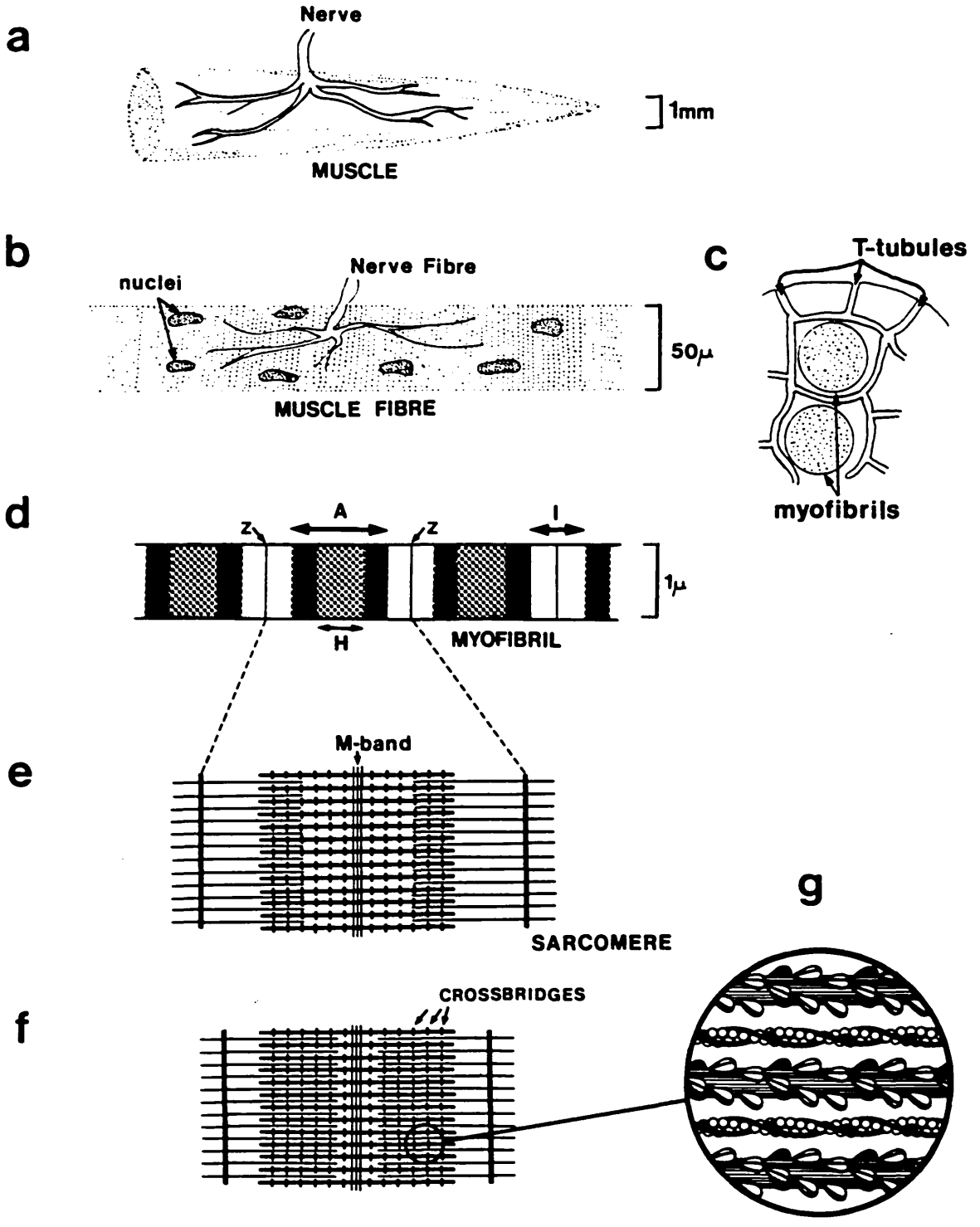


FIGURE 1.1. SCHEMATIC DIAGRAM OF THE ORGANISATION OF SKELETAL MUSCLE FROM THE ANATOMICAL TO THE FILAMENT LEVEL (see text for details). Inset (g) courtesy of Dr.J.M.Squire.

band and A-band respectively, although the thin filaments partly overlap the A-band (Hanson and Huxley, 1953; Huxley, 1953; 1957).

The thin filaments, which are about 1μm long and 80Å wide, are composed of actin and about 34% by weight of the regulatory proteins, tropomyosin and troponin (Hanson and Huxley, 1953; 1957). The thick filaments, 1.6μm long and 140Å wide, are composed of myosin and about 5% wt of other proteins (Hanson and Huxley, 1953; 1957; Page, 1964; Page and Huxley, 1963).

The thin filaments are attached regularly to the Z-discs so that their attached ends form an almost square (rhomboidal) lattice (Knappeis and Carlsen, 1963; Figure 1.1.2). Further away from the Z-disc, the thin filaments are not ordered laterally until they overlap the thick filaments (Elliott et al, 1963). At the M-band three to five prominent transverse lines are formed by the layers of M-bridges (Pepe, 1967). These lie perpendicular to the thick filament axis and link adjacent thick filaments at their midpoints in a regular hexagonal lattice (Knappeis and Carlsen, 1968). This lattice is less regular at the end of the A-band due to some flexibility in the thick filaments. The thin filaments become aligned at the trigonal points of the hexagonal array of thick filaments where the two sets of filaments overlap (Elliott et al, 1963).

The muscle changes length by a sliding movement of one of these sets of filaments, relative to the other, without any appreciable change of length of either kind of filament (Huxley and Hanson, 1954; Huxley and Niedergerke, 1954; Figure 1.1.1). The lateral spacing of the filaments varies inversely with the square root of the sarcomere length, so that sarcomere length changes are accompanied by no change in volume of the sarcomere

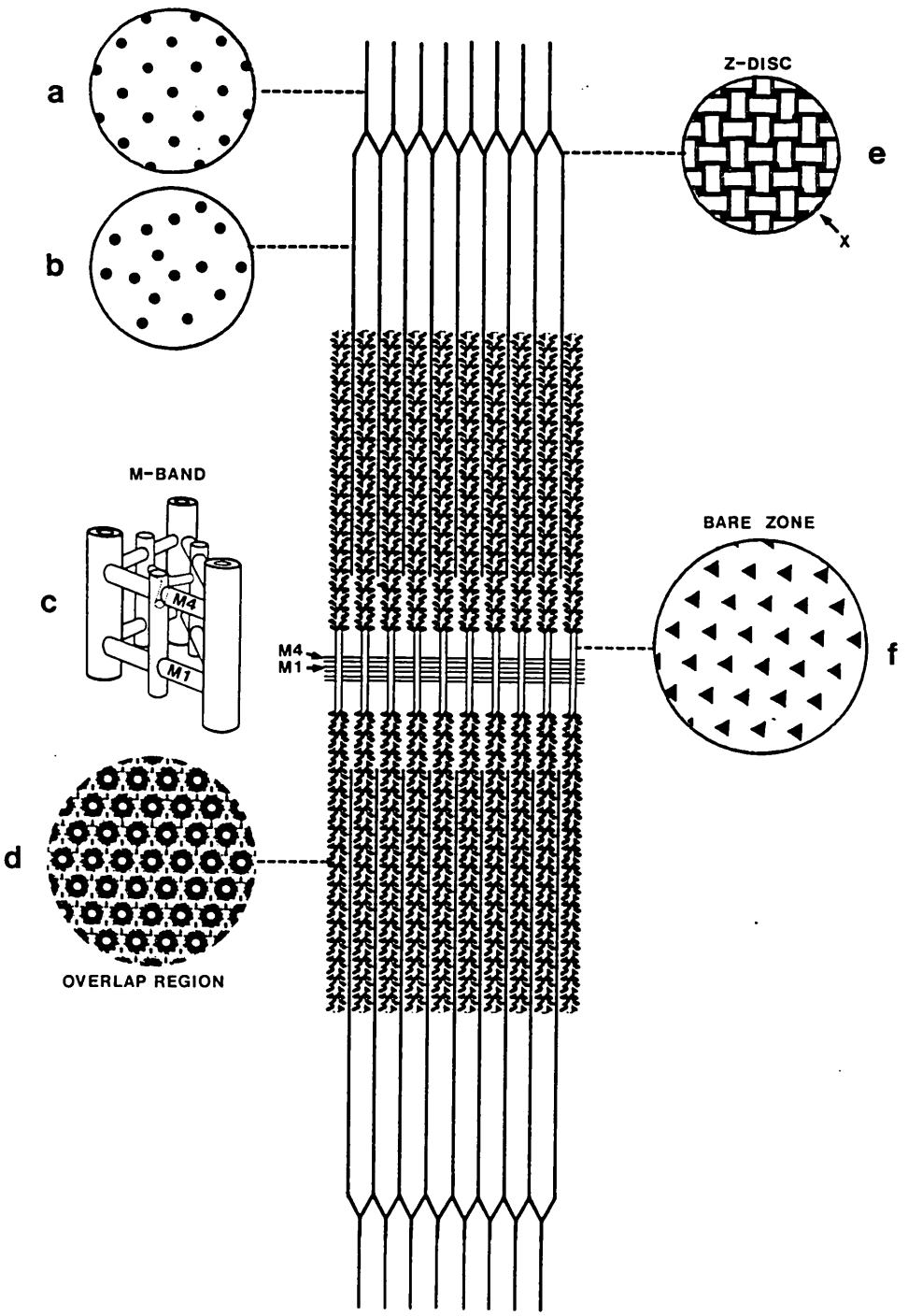


FIGURE 1.1.2 Schematic representation of the arrangement of the main structural components of the sarcomere. Spacings between the filaments in the I-band and A-band regions not to scale. The longitudinal Z-line structure corresponds schematically to a view along X in (e).

(Huxley, 1952; Elliott et al, 1963).

The sites of interaction between the two types of filaments are evident as projections or "crossbridges", projecting approximately perpendicular to the thick filament surface in longitudinal sections of fixed vertebrate muscle viewed in the electron microscope (Huxley, 1957).

1.1.3. Thin Filaments and Regulation.

The thin filaments account for about 35%wt of the myofibrillar protein and consist of two intertwined helical strands of the 41,700 molecular weight G-actin molecules. Each strand has a helical repeat of 720Å to 740Å and a subunit repeat, determined by the G-actin diameter, of 54.6Å. The two strands are displaced longitudinally by half of the subunit repeat, giving the F-actin helix an axial repeat of 360Å to 370Å containing 13 to 14 subunits separated axially by 27.5Å (Hanson and Lowy, 1963; Huxley and Brown, 1967; Figure 1.1.3). The G-actin molecule is polar (Wakabayashi et al, 1975) and confers a polarity to the actin filament (Huxley, 1963), it binds to calcium ions and non-covalently to ATP in a mole-to-mole ratio (Rees and Young, 1967; Tsuboi, 1968).

Tropomyosin molecules account for about 17%wt of the thin filament. The tropomyosin molecule comprises two intertwined α-helical polypeptide chains which form a rodlike structure 20Å in diameter and 410Å long (Cohen, 1975; Cohen et al, 1971). Tropomyosin molecules can interact by end to end polymerization (Caspar et al, 1969) and they may do so in the thin filament, possibly overlapping slightly, to form almost continuous strands lying close to the grooves on either side of the F-actin helix (Figure 1.1.3(b)). Each molecule is long enough to extend across

seven actin monomers. At every seventh actin monomer on each strand one troponin complex is localized with a periodicity of 38.5nm along the thin filament (Figure 1.1.3; Huxley and Brown, 1967). The troponin complex is composed of three well characterised proteins, troponin C, troponin I and troponin T. Each component appears to have one specialized function but all are required together with tropomyosin to make the Mg^{2+} ATPase of actomyosin sensitive to calcium ion levels greater than or equal to 10 micromolar.

When muscle is stimulated, calcium ions bind to the troponin C subunit of the troponin complex, which interacts with one or possibly two actin monomers. Any changes produced by this binding must then be transmitted to the five or six adjacent actin monomers which are potentially able to interact with myosin heads but do not interact directly with the troponin complex. If these changes are not transmitted through allosteric changes in the actin monomers, tropomyosin is seen as a likely means by which they may be. This has led to the postulated role of tropomyosin in a "steric-blocking hypothesis" for thin filament regulation.

The approximate position of attachment between the myosin head (HMMS-1) and actin, obtained from three-dimensional reconstruction of thin filaments labelled with HMMS-1, seems to be at an angle of about 30^{o} in Figure 1.1.4. Modelling of the changes in the first three actin layer lines (i.e. 37nm, 18.5nm and 12.3nm) in X-ray diffraction patterns from muscles in resting and contracting states (Huxley, 1972; Lowy, 1972; Vibert et al, 1971, 1972) has shown that the relative intensification of the 18.5 nm layer line on contraction can be accounted for if the

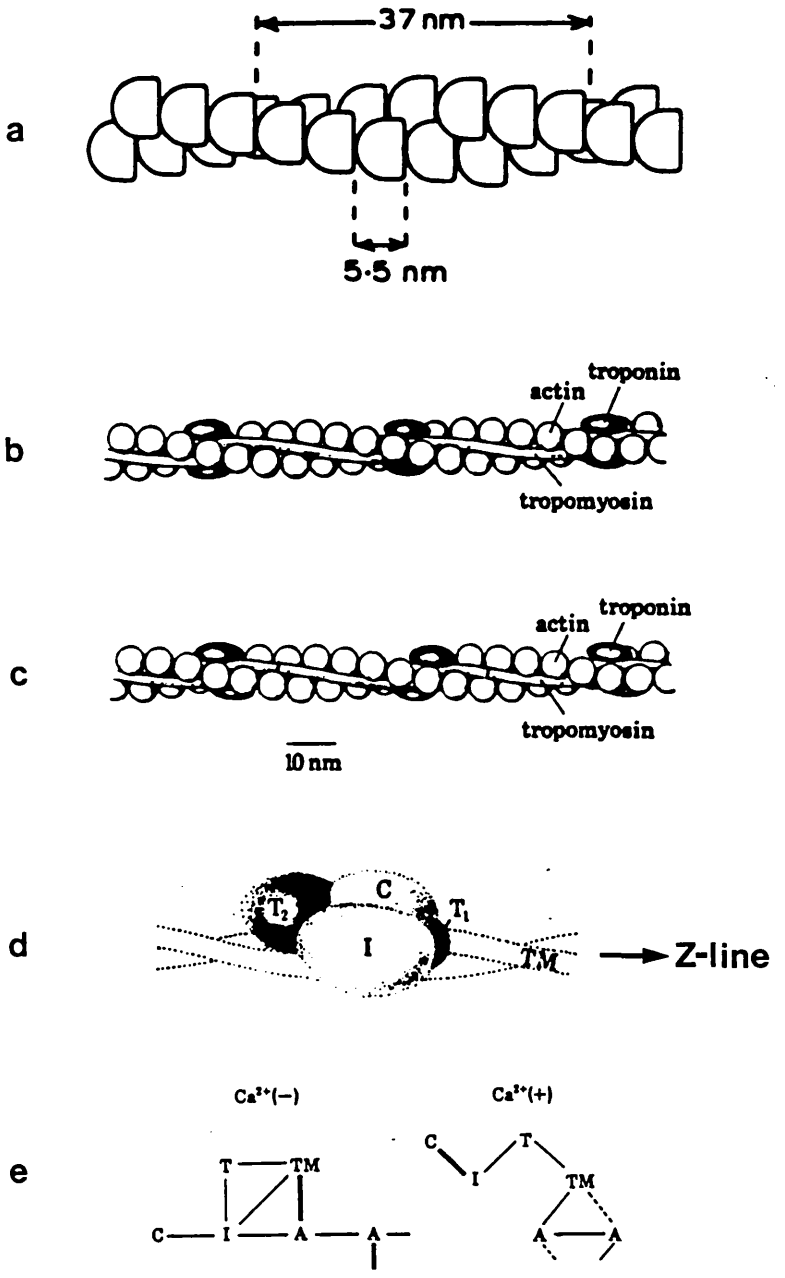


FIGURE 1.1.3 (a) Diagram of the visualised polarity of the F-actin helix (after Wakabayashi et al (1975), from Bagshaw (1982)). (b) Thin filament structure (Ebashi et al, 1969) and a revised model (c) after Ohtsuki (1974). (d) Fine location of troponin subunits (Ohtsuki, 1974). (e) Interactions among troponin subunits, tropomyosin and actin. Scheme of physiologically important interactions from Ebashi (1980). Ca(+) and Ca(-) refer to the presence and absence of calcium, respectively. C,I,T troponin C,I,T; A, actin; TM, tropomyosin; T_1 and T_2 are fragments of troponin T.(From Ebahsi, 1980)

tropomyosin moves from a resting position at $\theta = 50^{o}$ (i.e. out of the groove and blocking the myosin attachment site) to a position at $\theta = 70^{o}$, away from the myosin head binding site (Huxley, 1972; Haselgrove, 1972; Parry and Squire, 1973).

A number of in vitro studies have supported this mechanism (Hanson et al, 1972; O'Brien et al, 1971; Gillis and O'Brien, 1975). This steric blocking model was seemingly inconsistent with the analysis of Seymour and O'Brien (1980). From their interpretation of three-dimensional reconstructions of I-segments, they concluded that the polarity of the thin filaments previously assumed was incorrect and that in fact the myosin head attachment site and the tropomyosin location were on opposite sides of the strands of the actin helix.

However, from improved preparations of decorated purified actin and native thin filaments, Taylor and Amos (1981) were able to obtain higher resolution optical diffraction data from minimal dose electron micrographs of these structures. This allowed a clearer interpretation of the resulting three-dimensional reconstruction particularly nearer the thin filament axis and it re-established the possibility of a steric-blocking mechanism for thin filament regulation. The shape of HMMS-1 derived in these recontructions was shown to give a better fit to the X-ray scattering pattern observed from HMMS-1 in solution (Mendelson and Kretzschmar, 1980) and further three-dimensional reconstructions confirm the proximity of locations for tropomyosin and myosin head binding (Vibert and Craig, 1982) suggesting that individual HMMS-1 molecules may interact with both strands of the thin filament and may straddle tropomyosin molecules lying in the grooves (Amos et al, 1982).

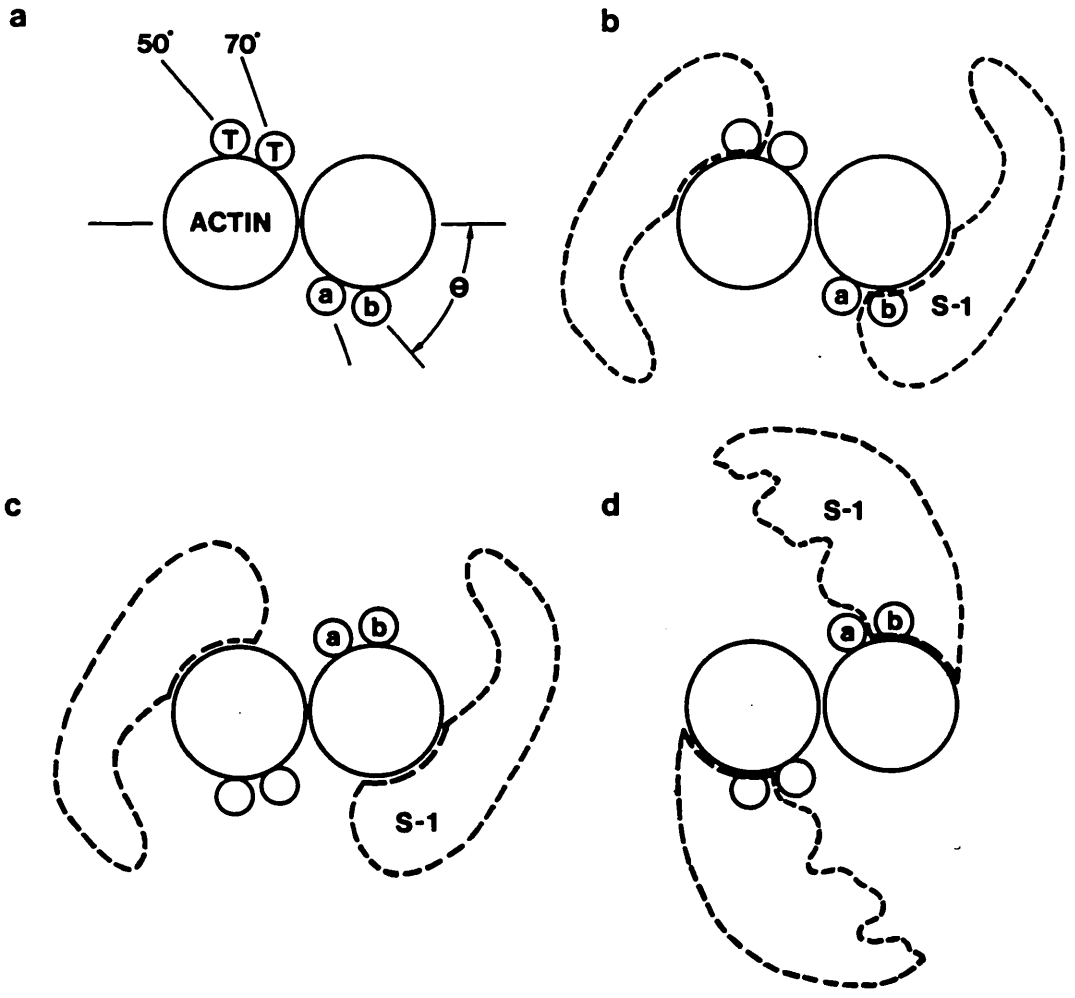


FIGURE 1.1.4 Models for the mode of attachment of the myosin head to the thin filament. (a) Positions of tropomyosin (T) in relaxed ($\theta = 50^{o}$) and contracting ($\theta = 70^{o}$) states (Huxley, 1972; Haselgrove, 1972; Parry and Squire, 1973). (b) Steric blocking model. With tropomyosin in the relaxed position 'b', the binding site for S1 is blocked. (c) S1 binding site from 3D reconstructions of I-segments (Seymour and O'Brien, 1980) (d) Relative positions of the S1 binding site and tropomyosin from decorated purified actin and native thin filaments (Taylor and Amos, 1981). (Courtesy of Dr.J.M.Squire)

It is therefore possible that steric blocking prevents interaction of part of a myosin head with one actin binding site in the absence of sufficient calcium ions in resting muscle. Thus alterations in the interaction between the subunits of the troponin complex and tropomyosin might cause the tropomyosin to roll nearer to the thin filament groove, when troponin C binds calcium in contracting muscle.

However, X-ray studies show that the crossbridges may not be poised prior to activation in close proximity to the actin binding site, waiting for the tropomyosin to move, but that they may move both radially and/or azimuthally from their regular resting arrangement on the thick filament backbone before interacting with the thin filament when the muscle contracts (Huxley, 1968; Haselgrove and Huxley, 1973; Haselgrove, 1975). That this is due to a structural change in the thick filament rather than a change in the sarcoplasm when the level of calcium ions increases has been suggested by the differences in the X-ray diffraction patterns from resting muscles and contracting muscles at no-overlap sarcomere lengths (Haselgrove, 1975). Furthermore in biochemical studies the actin-linked regulation system of tropomyosin can only suppress the ATPase activity of actomyosin by about 20 times whereas the ATPase rate of active muscle is suppressed by a factor of 1000 times to achieve the resting state of muscle. Thus myosin-linked and actin-linked regulation mechanisms may both operate in vertebrate skeletal muscle (see section 1.2.5).

1.1.4. The Contractile Cycle.

In the absence of stimulation by increased calcium ion levels the heads of the myosin molecules are not attached to

actin but hydrolyse ATP at a low rate (Figure 1.1.5(a)), being continually charged with the products of hydrolysis, ADP and inorganic phosphate, which they release very slowly. The ATPase activity of myosin is strongly inhibited by the 0.1M KCl. When the myosin heads bind to actin (Figure 1.1.5(b)), following both the binding to Troponin-C of calcium ions released from the terminal cisternae and the subsequent conformational change in the thin filament, a 200-fold increase in the ATPase rate occurs as the ATP bound to myosin heads is hydrolysed with a very rapid release of ADP and inorganic phosphate. Rapid dissociation occurs (Figure 1.1.5(d)) when $MgATP^{2-}$ is again bound to the myosin heads which are then charged for the next contractile cycle.

While the myosin heads are bound to actin conformational changes in the head and/or HMMS-2 fragment of the myosin molecule result in the displacement of the thin filaments by about 100Å relative to the thick filament towards the M-band (Figure 1.1.5(c)).

1.1.5. The Pattern of Interaction of the Actin Monomers and the Myosin Crossbridges.

It was shown by Squire (1974) that if the thin filaments are to occupy equivalent positions in the almost square (rhomboidal) Z-line lattice there are two possible ways of accommodating their approximate two-fold rotational symmetry in the Z-line square lattice. One arrangement involves identical orientations for all the filaments (Figure 1.1.6(a)) whereas in the other each filament is rotated by 90^{o} relative to its four nearest neighbours in the lattice (Figure 1.1.6(b)). Squire (1974) applied the principle of transforming the actin filaments square Z-line lattice to the hexagonal lattice in the A-band, as

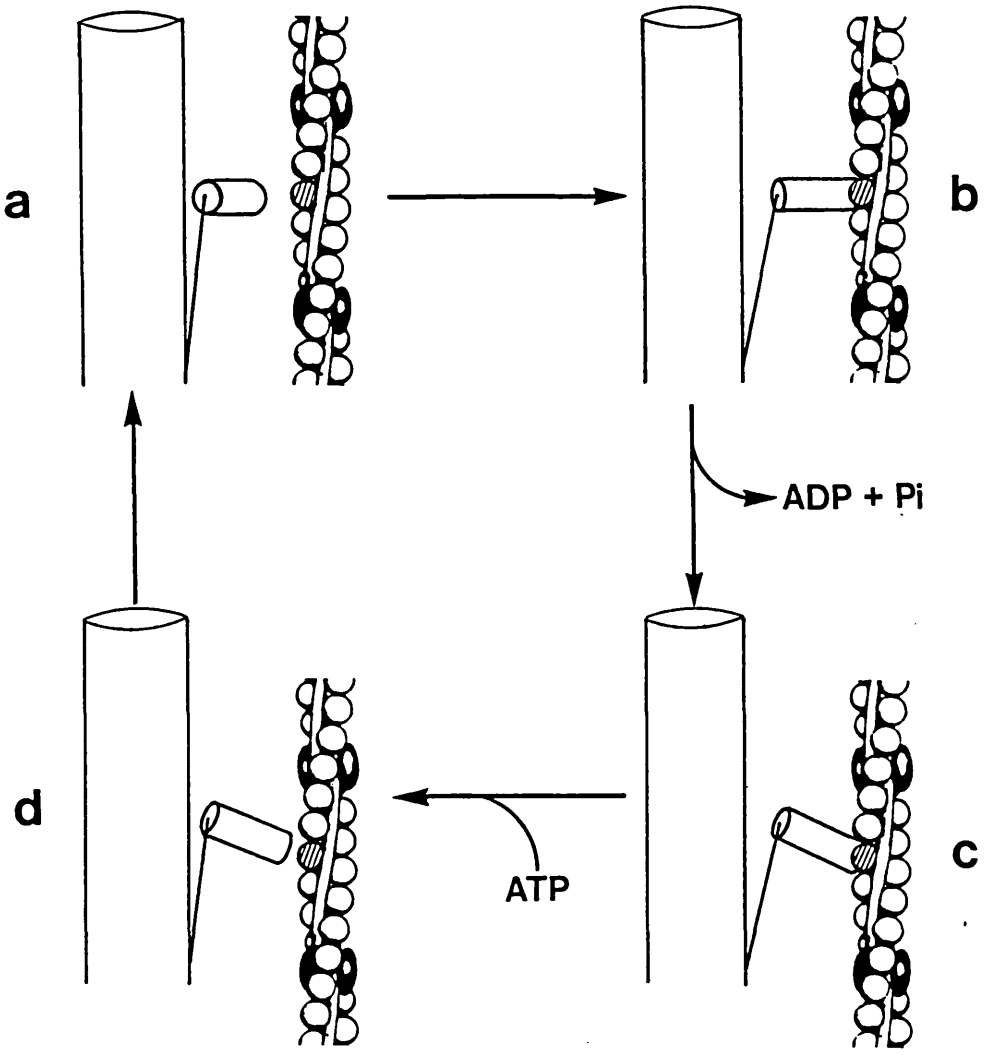


FIGURE 1.1.5 Main steps in the contractile cycle.(a) In resting muscle myosin heads hydrolyse ATP at a low rate (b) Increase in Ca^{2+} and the myosin head moves to attach to the thin filament followed by a rapid hydrolysis of ATP (c) Conformational change produces relative sliding (d) Heads detach and go through cycle again if the Ca^{2+} remains greater than about 10^{-5}M and ATP is present. Basic scheme proposed by Lymn and Taylor (1971).

suggested by Pringle (1968). By equal lateral displacements of all the filaments two possible types of hexagonal arrangement of the thin filaments in the A-band were derived (Figure 1.1.6(c) and (d)); the arrangement with identical orientations being more likely if the Z-line lattice is actually rhomboidal.

It was further proposed (Squire, 1981) that if the thin filaments are assumed to be right-handed double helices then equivalent actin monomers on the six thin filaments as seen by a single thick filament they surround, will be approximately arranged on a right-handed helix. Adjacent thin filaments in this helix are related by rotations of 60^{o} or axial shifts of one sixth of the pitch of about 720Å (Figure 1.1.6(e)).

Thus, having defined the basic structure of the thin filaments and their relative arrangement in the overlap region of the A-band, it is necessary to determine how the crossbridges are distributed about each thin filament. This distribution of crossbridges in the relaxed state will determine the pattern of interactions that the crossbridges may make with the actin monomers in the thin filaments in the active and rigor states. This distribution is determined primarily by the following three features of the A-band;

(i) The shape of the myosin molecule and the relaxed configuration of the two myosin heads.

(ii) The symmetry of the arrangement of crossbridges on the surface of the thick filament.

(iii) The arrangement of one filament relative to its neighbours in the hexagonal filament array.

This introductory chapter reviews briefly each of these features in turn. The randomness in the A-band lattices of frog

sartorius and insect flight muscles is likely to make it very difficult to establish a complete description of the relaxed three-dimensional arrangement of crossbridges as defined by the three features above. It will thus be difficult to establish unequivocally the complete cycle of events during the contraction of muscle. In contrast the simple lattice arrangement in bony fish muscles must eventually enable a better understanding of the contractile cycle.

1.2. The Myosin Molecule.

1.2.1. The Shape of the Myosin Molecule.

Early electron microscope studies of myosin molecules showed a rod-shaped molecule about 150nm long, 1.5nm to 2nm in diameter, with a globular region at one end when shadow-cast unidirectionally by the Hall mica-replication technique (Rice, 1961; Zobel and Carlsen, 1963; Huxley, 1963). Some substructure was apparent in this globular region (Zobel and Carlsen, 1963; Rice et al, 1966) but clear images of two roughly spherical subunits were only obtained when rotary shadow-casting was employed (Slayter and Lowey, 1967).

Elliott and Offer (1978) combined low temperature conditions and rotary shadow-casting to give excellent impressions of the shape and flexibilty of the myosin molecule (see section 1.2.6). The well defined attachment point of the heads to the tail permitted an accurate measurement of the sizes of these fragments. The tail length was measured to be 156nm; this compares with Lowey et al (1967) shadow-cast preparations which gave 137nm; negatively stained rod segments suggest 145nm as a minimum length (Cohen et al,1970;Harrison et al, 1971); and calculation of the length of a two chain α-helically coiled

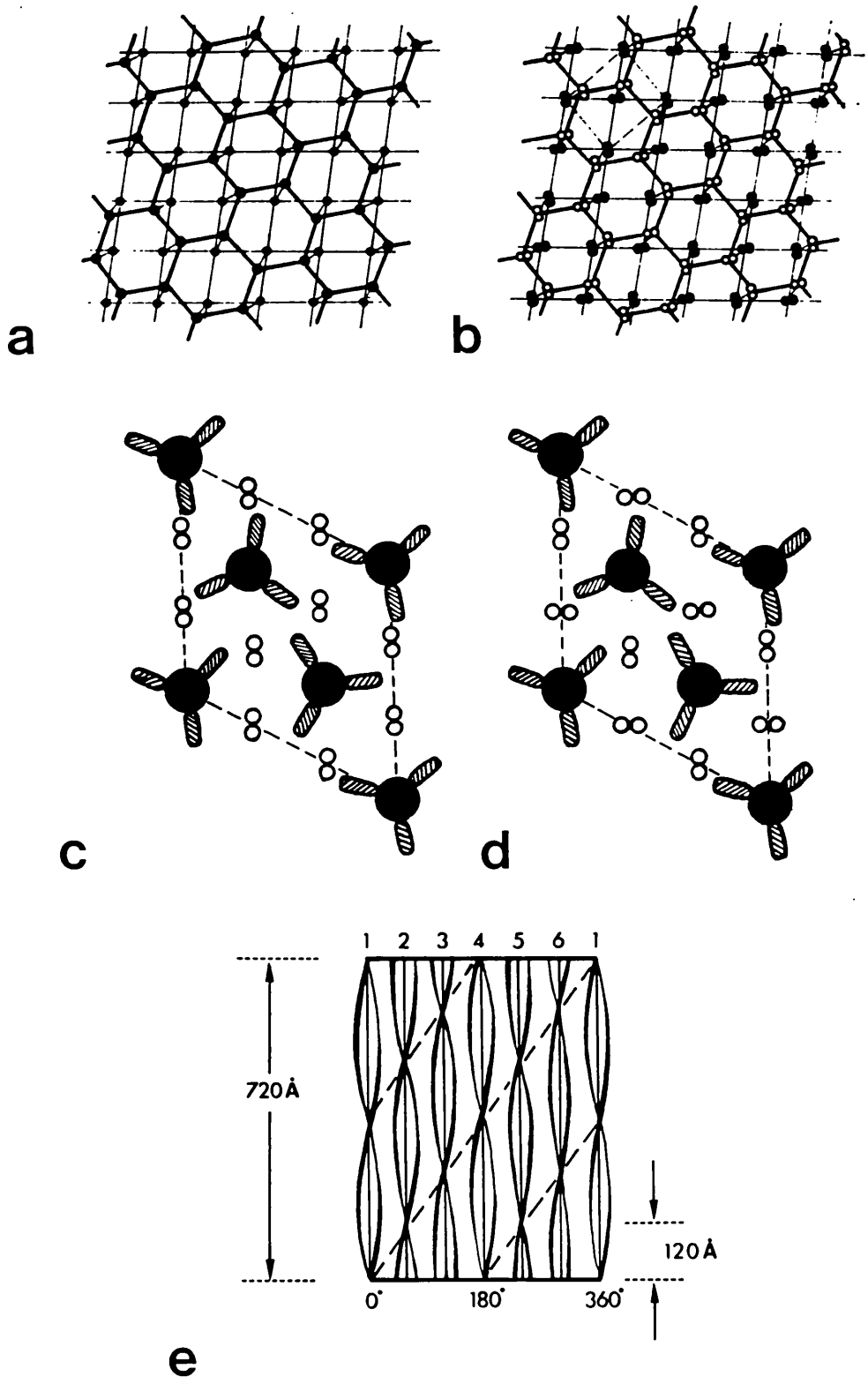


FIGURE 1.1.6 (a) and (b) are schematic representations of the transformation from the rhomboidal arrangement of thin filaments at the Z-band to the hexagonal arrangement in the A-band (after Pringle, 1968) for thin filaments identically oriented (a) and at 90° rotations in (b), and their corresponding orientations in the overlap region (c) and (d) (from Squire, 1974). (e) Diagram of the 6_2 helix of 6 thin filaments surrounding each thick filament in vertebrate muscle. A right-handed helix of thin filaments surrounds each thick filament (from Squire, 1981).

coil of molecular weight 230,000 gives a value of 150nm. Elliott and Offer (1978) observed with high frequency a sharp bend about 43nm from the head-tail junction suggesting a hinge in the HMMS-2 region of the rod, 20nm from the site where cleavage to LMM and HMM occurs.

The size of the pear-shaped heads, up to 19nm long and 4.5nm wide at their widest point, is too large to account for estimates for HMMS-1. The length of HMMS-1 from a three-dimensional analysis of F-actin decorated with HMMS-1 is about 15nm (Moore et al, 1970). Fluorescence anisotropy decay measurements of the rotational diffusion of HMMS-1 in solution indicate a prolate ellipsoid longer than 16.5nm (Mendelson et al, 1973) and Mendelson and Kretzschmar (1979) suggest the best model to fit high angle X-ray data is a ball at the end of a cylinder with an overall length of 13nm. Radii of gyration values of 3.2nm and 3.5nm from X-ray and neutron scattering measurements of HMMS-1 in solution were obtained by Kretzschmar et al (1976, 1978) and Worcester et al (unpub.) respectively.

These differences in size may be due to parts of the head adjacent to the rod being digested away during the preparation of HMMS-1 (Elliott and Offer, 1978). This is also necessary to reconcile the radius of gyration observed and that of about 5nm for Elliott and Offer's observations. If HMMS-1 represents the outer 14 to 15nm of the head, this would give the correct radius of gyration and would account for the hydrodynamic properties of HMMS-1 (Lowey et al, 1969; Yang and Wu, 1977).

Thus the shape and size of the head visualised by Elliott and Offer (1978) is consistent with other estimates, and the curvature along the head revealed by Moore et al (1970) is the

only obvious feature which remains unconfirmed.

1.2.2. Polypeptide Chain Arrangement

The myosin molecule has a molecular weight of about 500,000 (Lowey and Cohen, 1962; Dreizen et al, 1967). This is made up from two heavy polypeptide chains of molecular weight 200,000 (Gershman et al, 1969; Gazith et al, 1970) and four light chains; two "alkali" or "essential" light chains of 17,000 and 21,000 daltons and two DTNB light chains of 19,000 daltons each (Weeds and Lowey, 1971; Figure 1.2.1(a)).

Parts of the two heavy myosin chains intertwine in a coiled coil α-helical structure to form the rodlike tail of the myosin molecule (Cohen and Szent-Gyorgyi, 1957). At the globular end of the molecule the two heavy chains branch off and fold up to form the bulk of each of the two heads; two light chains residing in each head (Figure 1.2.1(a)).

1.2.3. Proteolytic Fragments of the Myosin Molecule

Brief exposure of myosin to the proteolytic enzyme trypsin (or chymotrypsin) cleaves myosin rod preferentially near the centre giving two fragments, LMM and HMM (Mihalyi and Szent-Gyorgyi, 1953; Gergely, 1953; Mihalyi and Harrington, 1959; Segal et al, 1967; Figure 1.2.1(b)).

The HMM fragments retain the enzymatic and actin binding properties of the globular myosin heads. Electron micrographs of HMM preparations show two globular subunits attached to a short rod-like tail (Lowey et al, 1969). The ATPase per mole of HMM is equal to that of the intact myosin molecule. Further exposure to trypsin cleaves the globular myosin heads (HMMS-1) from HMM (Muellerand Perry, 1961, 1962) to leave the short tail segment,

HMMS-2. HMM is soluble at low ionic strengths and HMMS-2 does not associate with itself or with LMM near neutral pH over a wide range of ionic strengths (Lowey et al, 1969). A relatively weak self-association of HMMS-2 in vivo is suggested by the formation of paracrystals with a 145Å repeat under abnormal pH conditions (i.e.near the isoelectric point; Lowey et al, 1967). This water soluble fragment has a molecular weight of 60,000, a helix content >95% and accounts for about one-third of the length of the myosin rod.

The longer LMM portion of the rod has a similarly high α-helix content to HMMS-2 (>95%, Lowey et al, 1969; Weeds and Pope, 1977), but it readily associates at low ionic strength to form filamentous or paracrystal structures. LMM represents about two-thirds of the length of myosin rod and like the rod it has a two chain coiled-coil α-helical structure of diameter about 20Å (Crick, 1953; Cohen and Holmes, 1963). Different conditions used for the proteolytic digestion of myosin produce LMM with lengths 700 to 1000Å and molecular weights 120,000 to 150,000 daltons (Lowey, 1971).

1.2.4. Properties of the Myosin Molecule

The three important characteristic properties of myosin (i.e. ATPase activity, actin binding and self-association) have been assigned to the rod and globular parts of the molecule by testing the proteolytic fragments of myosin for each of these three properties.

The two heads (HMMS-1) can be removed from the myosin molecule by digestion with papain (Figure 1.2.1(b)). The ATPase activities of this subfragment in solution or activated by actin do correspond to a first approximation to the resting and

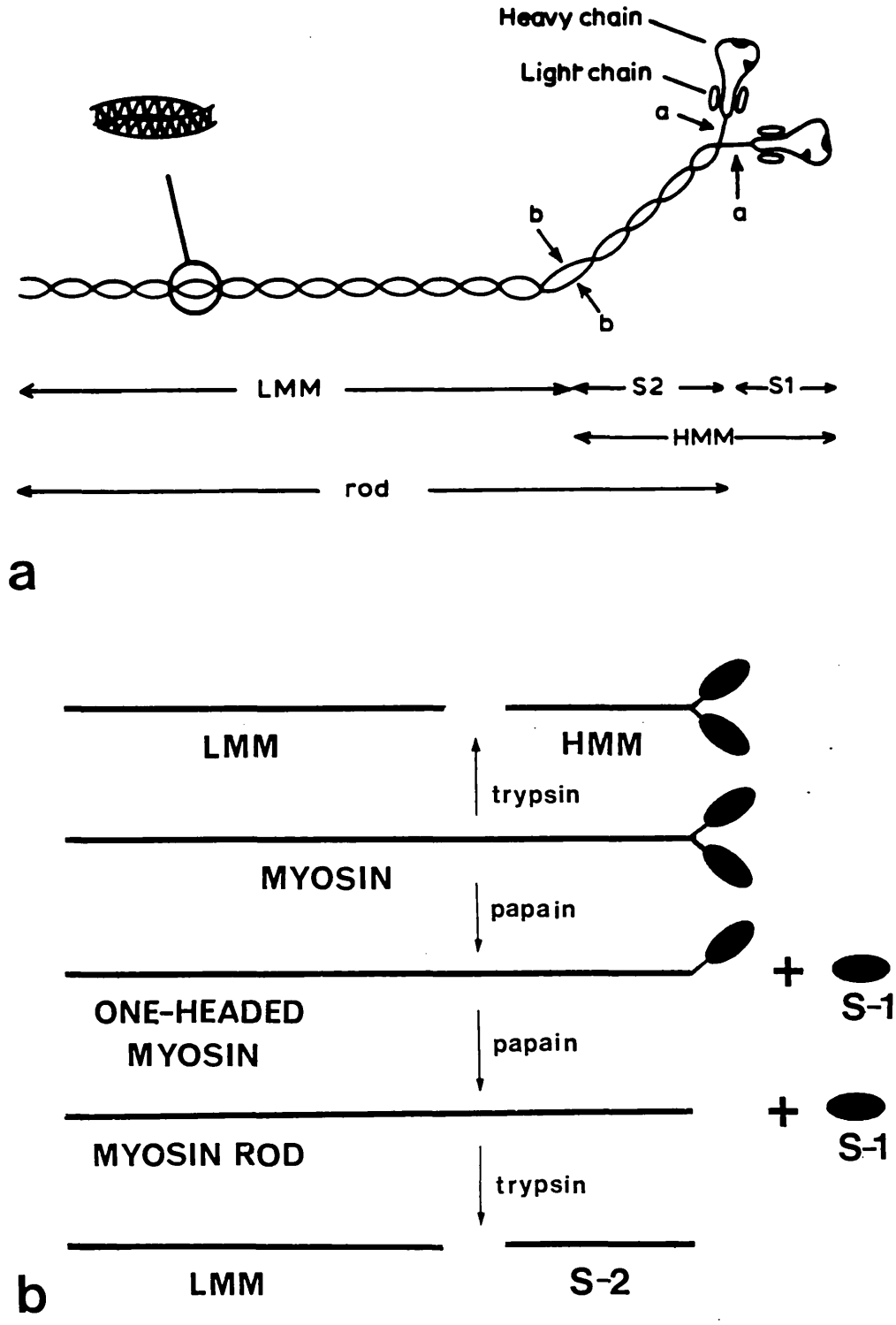


FIGURE 1.2.1 (a) The polypeptide chain arrangement in the myosin molecule. Inset is shown the coiled-coil arrangement of the myosin heavy chain in myosin rod (from Bagshaw, 1982). (b) Proteolytic fragments of the myosin molecule produced by cleavage with the enzymes papain and trypsin at positions 'a' and 'b', respectively, in (a). LMM, light meromyosin; HMM, heavy meromyosin; S-1, subfragment-1; S-2, subfragment-2.

activated rates in muscle (Ferenczi et al, 1978). With an active site concentration in muscle of 240 μmol/kg the ATPase activities of resting and isotonically contracting muscle are calculated to be < $0.002 s^{-1}$ and $6 s^{-1}$ respectively. The MgATPase of frog skeletal HMMS1 in solution at 0° C is $0.01 s^{-1}$ and it is activated by actin to $4.5 s^{-1}$.

The characteristic "decorated thin filaments" formed by the binding of HMMS-1 to F-actin have been very important in studying (i) the rigor configuration of the myosin heads, (ii) the shape of HMMS1 and (iii) what constraints there are on the binding of HMMS-1 to the thin filament. The polarity of the thin filaments and the reversal of this polarity across the Z-line were first implied by the reversal of this arrowhead appearance on either side of the Z-line in I-segments (Huxley, 1963).

1.2.5. Association of the Properties of HMMS-1 with Myosin Heavy and Light Chains

Each myosin head contains part of one heavy chain and two of the four light chains in each molecule. "Fast" and "slow" myosin heavy chains have been distinguished (Gauthier et al, 1978) in developing fast-twitch mammalian muscle (rat diaphragm). These studies show that a fibre which is fast or slow will contain predominantly fast or slow myosin heavy chains, respectively.

The light chains are distinguished into two classes by the agents which remove them from the myosin molecule. The two 19,000 dalton chains removed by DTNB (5,5'-dithiobis-(2-nitrobenzoate)) were called DTNB or "regulatory" light chains, the latter because of their similarity to light chains with a demonstrated role in molluscan thick filament regulation (Kendrick-Jones et al, 1970).

These light chains are now designated "LC2". Each myosin head contains one DTNB light chain, a stoichiometry which has been shown to be invariant in at least three fibre types; fast-twitch, cardiac and slow-twitch (Kendrick-Jones et al, 1976; Weeds, 1976).

Since the actin activated Mg ATPase activity of purified vertebrate myosin is insensitive to Ca^{2+}, there does not appear to be a direct Ca^{2+} -switch on the myosin molecule similar to that in molluscan myosins. The Ca^{2+} -binding sites on rabbit myosin are non-specific sites (Bagshaw and Reed, 1977; Bagshaw and Kendrick-Jones, 1979) and vertebrate striated muscle light chains do not restore Ca^{2+} sensitivity or the specific Ca^{2+} binding sites to desensitized scallop myosin (Sellers et al, 1980; Scholey et al, 1981).

1.2.6. Flexibility of the Myosin Molecule

The fact that the myosin rod is preferentially cleaved into LMM and HMM fragments led to conclusions from enzyme probe studies that the susceptible region was not regular α-helix (Mihalyi and Harrington, 1959). Segal et al (1967) suggested that proline residues in this region open up the structure. However the rod has been shown to be virtually 100% α-helical and to contain no proline residues (Lowey et al, 1969; Burke et al, 1973; McLachlan and Karn, 1982).

Pepe (1967) suggested a detailed packing model for the thick filament on the evidence of antibody staining which invoked a flexible hinge at the LMM/HMM junction thus enabling the head ends of the molecules to be bent away from the backbone. The latter is formed by the LMM portions of the tail (Huxley, 1963).

The small observed changes in intensity of the 143Å meridional reflection relative to off-meridional intensity and also in the spacing of this reflection, when resting muscle was either put into rigor or was actively contracting, suggested that a reorganization of the helical arrangement of crossbridges was accompanied by substantial changes in their azimuthal or radial positions (Huxley and Brown, 1967). Combined with the isolation of the soluble fragment HMMS-2 (Loweyet al, 1967) these observations were taken to mean that the insoluble LMM is bound into the core of the thick filament leaving the soluble HMMS-2 fragment of the tail and the attached heads lying close to the surface of the thick filament in resting muscle (Huxley, 1969; Figure 1.2.2(a)). This allowed the HMMS-2 rod to hinge about the trypsin-sensitive region of the tail and permitted the head carrying the ATPase and actin-binding sites to move azimuthally or radially from the surface of the thick filament to make contact with the thin filaments in rigor or contracting muscle. The axial repeat of the crossbridges is thus fixed by the packing of LMM portions of the myosin tail into the thick filament backbone. A further hinge was suggested at the junction between the heads and tail of a molecule so that with two flexible couplings the orientation of the head could be maintained as the HMMS-2 link swung out from the surface of the thick filament backbone.

The radial crossbridge movement expected from this mechanism was shown from the low-angle equatorial X-ray diagram of rigor frog and rabbit muscles (Huxley, 1968), in which about 30% of the myosin mass was deduced to have moved towards the thin filament. An analagous but smaller effect was also observed in

contracting frog muscle (Haselgrove and Huxley, 1973). The suggested "angling" of the crossbridges between the relaxed and rigor states was also consistent with the right-angled and 45°-angled crossbridges seen in electron micrographs and deduced from X-ray diagrams of glycerinated insect flight muscle (Reedy et al, 1965). Changes in interfilament spacing of 80Å effected by changes in ionic strength of muscle in rigor are also difficult to account for if the crossbridge is bound close to the thick filament surface (Rome, 1968).

Direct visualisation of flexibility at the head/tail junction (Slayter and Lowey, 1967; Elliott and Offer, 1978) and at the trypsin sensitive tail region (Elliott and Offer, 1978; Figure 1.2.2(b)) has come from studies of isolated myosin molecules. The heads appear to be able to adopt most angles independently of each other but are restricted from folding back onto the myosin tail at an angle less than 60°. This virtually universal flexibility also supports the fluorescence depolarization results of Mendelson et al (1973) and the probe studies of Thomas et al (1975). The amino acid sequences of rabbit skeletal and nematode myosin are largely known (McLachlan and Karn, 1982; Karn et al, 1982) and suggest that the N-terminal third of the myosin rod is only loosely associated with the thick filament backbone. Thus bending of the rod near the end of this region could allow the N-terminal section of the rod to swing out on a hinge during muscle contraction.

1.3. Thick Filament Structure

1.3.1. The Surface Arrangement of Crossbridges

Longitudinal sections of fresh vertebrate muscle, carefully sectioned to include only a single layer of thick and thin

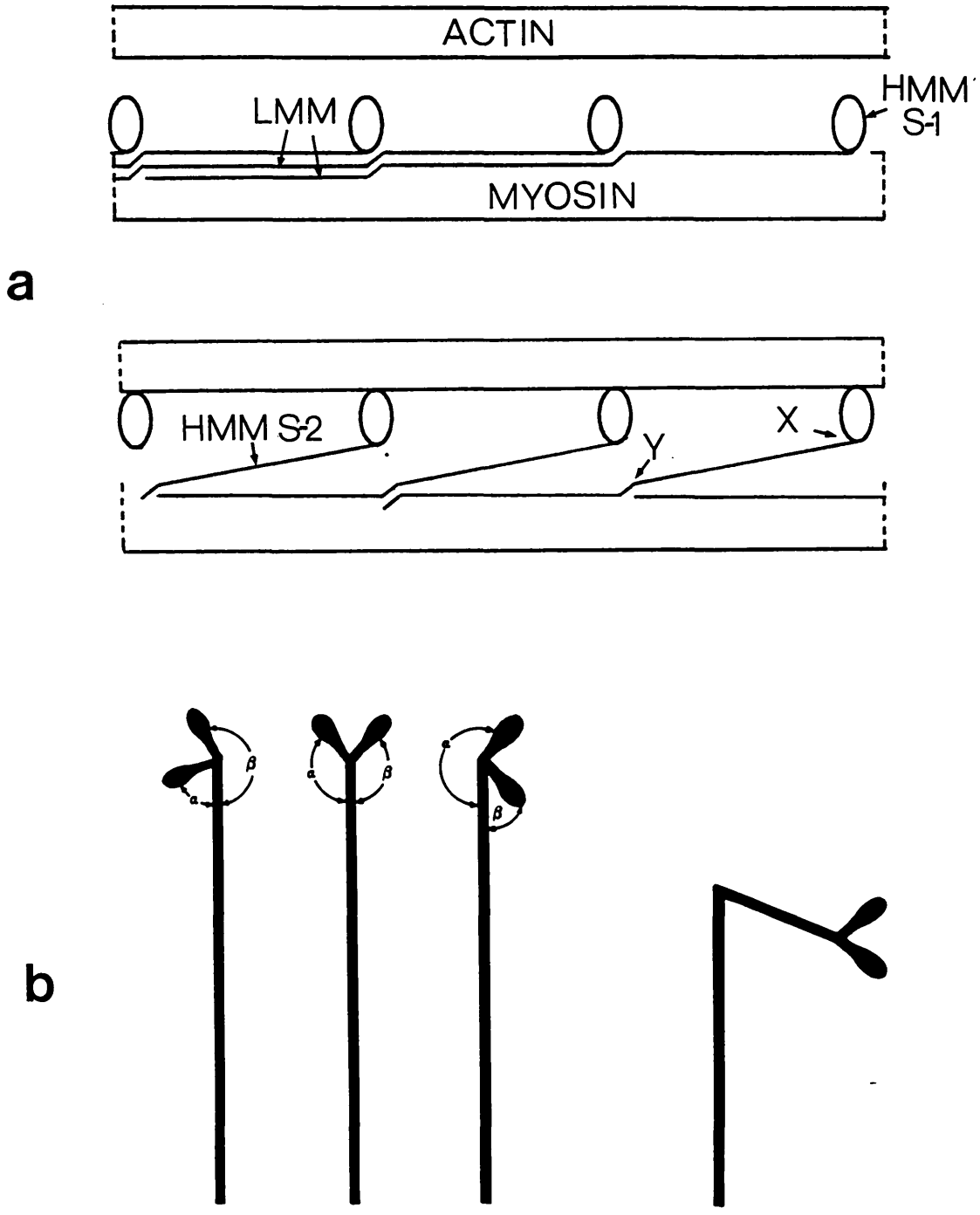


FIGURE 1.2.2 (a) Diagram of the Huxley 1969 model for the mode of movement of crossbridges to the thin filaments requiring two flexible hinges in the region of X and Y in the myosin molecule. (b) Representation of Elliott and Offer's observations (1978) of isolated myosin molecules showing directly the flexible hinges required in (a). The observed range of angles of and is about 60^{o} to 300^{o} (Courtesy of Dr.J.M.Squire).

filaments, showed projections roughly perpendicular to the surface of the thick filaments at regular intervals of about 40nm linking with neighbouring thin filaments. On average two such crossbridges occurred at each 40nm interval (Huxley, 1953). A central region devoid of these projections and about 0.15 to 0.2μm wide was seen both in these sections, in thick filaments isolated from the A-band and in synthetic filaments prepared by precipitation of purified myosin at low ionic strength (Huxley, 1963). Irregular projections occurred either side of this bare region as far as the tapered ends of the thick filament.

Huxley (1963) proposed that the polar myosin molecules were arranged on either side of the bare region with their tails pointing towards the centre of the filament, thus generating the observed bipolarity of the filament (Figure 1.3.1(a)). The tails of the myosin molecules were then considered to be packed antiparallel in the central region, parallel and regular in the centre of each half of the filament and parallel and irregularly arranged at the tapered ends of the filament.

The regularity of the crossbridges in the intact A-band has only been partly preserved in the sections of vertebrate skeletal muscle mentioned above. In isolated thick filaments, critical point dried and shadow cast (Trinick, 1973), suggestions of three or four stranded helical ordering were observed. Using the mica replication technique individual crossbridges appeared well preserved in isolated rabbit thick filaments but no order was apparent (Trinick and Elliott, 1979). Recent preparations of isolated frog thick filaments (Kensler and Stewart, 1983) analysed by optical diffraction have shown that the surface lattice of myosin crossbridges has an odd numbered rotational symmetry which

on the basis of other evidence must be threefold. A three-stranded arrangement was also concluded from measurements of the pitch angle of helical strands on thick filaments from relaxed, quick-frozen and freeze-etched rabbit psoas myofibrils (Ip and Heuser, 1983).

The important confirmation of this arrangement for vertebrate thick filaments was preceded by more detailed observations of the crossbridge arrangements in numerous invertebrate muscle thick filaments. Negatively stained insect flight muscle filaments show uniform shelves of density with a 14.5nm periodicity (Reedy and Garrett, 1977). However there was no helical ordering and no sign of the38.5nm, 24nm or 115nm repeats observed in the insect relaxed X-ray diffraction pattern. Limulus thick filaments revealed a four stranded arrangement with four crossbridges at 14.6nm levels and a helical repeat of 43.8nm (Kensler and Levine, 1982; Stewart et al, 1981). This latter result was consistent with X-ray diffraction patterns of the live muscle (Wray et al, 1974, 1975) and revealed the crossbridges as bent and extended, inclined at about 30^{o} to the helical path. Each crossbridge appeared to contain two heads of a myosin molecule.

Isolated Tarantula thick filaments also show a well defined surface array of myosin crossbridges characterized by prominent helical tracks of repeat 43nm. Preliminary analysis suggests 4-fold rotational symmetry of the crossbridge array. 4nm diameter subfilaments are also apparent in the backbone of the filament. The right-handed helical tracks of crossbridges do not appear to change hand across the bare zone (Craig and Padron, 1982; Levine et al, 1983). The rotational symmetry of scallop thick filaments

has also been shown to be 7-fold and the two myosin heads from each myosin molecule appear to be aligned almost parallel to the thick filament surface but slewed slightly from the axis so that they lie along the right-handed helical tracks of pitch 480Å (Vibert and Craig, 1983).

The first implications of helical ordering of the vertebrate crossbridge arrangement arose partly from the interpretation of the low-angle X-ray diffraction pattern from relaxed frog sartorius muscle (Huxley and Brown, 1967). Combined with earlier electron microscope observations (Huxley, 1957) the crossbridges were taken to be arranged on a 6/2 helix of subunit repeat 14.3nm and helical repeat 42.9nm, projecting about 7nm from the surface of the thick filament (Figure 1.3.2(a)). The row-line sampling of the myosin layer line pattern also indicated a three-dimensional crossbridge superlattice which was generated by rotating nearest neighbour thick filaments on a simple hexagonal lattice by 60°.

However this model predicted that there should be 200 myosin molecules in each thick filament, whereas biochemical estimates gave values closer to 300 to 400 molecules (Table 1.3.3). These would be accomodated on about 100 crossbridge levels 14.3nm apart along the thick filament length of about 1.6um (Page and Huxley, 1963).

In view of this discrepancy, it was suggested that either the 6/2 helix had two myosin molecules as a repeating unit (Huxley, 1972) or that the crossbridges were arranged on a four-stranded 12/1 helix (Squire, 1971) or a three-stranded 9/1 helix (Squire, 1972, 1973; Figure 1.3.3(b) and (c)) and that they projected further from the thick filament surface than 7nm. These

alternatives were part of a general packing scheme for myosin containing structures proposed by Squire (1971, 1972, 1973). This proposed a general relation between the diameter of cylindrical myosin filaments and their rotational symmetry. This favoured a three-stranded 9/1 helix for vertebrate thick filaments. Apart from accounting for the relaxed frog low-angle X-ray data better than the other two models (Squire, 1975; Haselgrove, 1980), this model was supported by the observations described below.

Firstly transverse sections of frog and fish muscle showed clear three-fold rotational symmetry of the thick filament backbone not only in the bare region (Franzini-Armstrong and Porter, 1964; Spiro, 1962; Huxley, 1957; Luther, 1978) but at M9 and the A-band tip of the thick filaments (Luther, 1978). In this latter case three subunits are clearly seen. In addition the M-bridges on each side of the M-band central line also show this symmetry (Luther, 1978; Luther et al, 1981). On the basis of this filament symmetry the statistical superlattice of myosin filament orientations in frog sartorius muscle and the simple lattice in fish muscle can be shown to be regularly controlled at the M-band (see later; Luther et al, 1981). Secondly rabbit psoas thick filaments exposed to very low ionic strength before contrasting with uranyl acetate appear frayed into a number of subfilaments which is generally three, and never in excess of three (Maw and Rowe, 1980).

On the basis of the packing scheme proposed by Squire , filaments with larger rotational symmetries would have larger diameters, and Limulus and Tarantula, with four-fold rotational symmetries, have diameters of 20nm (Levine et al, 1983) and 23.4nm (Kensler and Levine, 1982), respectively. This is larger

than vertebrate skeletal thick filaments which have a diameter of 14 to 15nm. Similarly for insect flight muscle since biochemical evidence indicated six myosin molecules were present at each 14.5nm level in Lethocerus thick filaments, a six-stranded 16/1 helix was proposed for the crossbridge array in insect flight muscle (Squire, 1972). It now appears that these filaments may be four-stranded (Wray, 1979) with four molecules at each 14.5nm level (Reedy et al, 1981) in accordance with other filaments which have similar diameters to those in insect flight muscle.

The helical arrangement of crossbridges in vertebrate muscle is not perfect however as revealed by "forbidden" meridional reflections in the X-ray diffraction studies of Huxley and Brown (1967). Evidence for perturbations and gaps in the crossbridge's average 14.3nm repeat sequence has come from numerous electron microscope studies of longitudinal sections.

The detailed set of transverse striations observed in A-segments (isolated assemblies of thick filaments held together at the M-line) positively stained with uranyl acetate, were concluded to be due to the LMM backbone of the filaments and the non-myosin proteins labelling it (Hanson et al,1971; O'Brien et al, 1971; Craig, 1977). However, if these segments are stained with ammonium molybdate, a series of 14.3nm-spaced stain-excluding lines about 7nm wide are seen (Craig, 1977). These show a single gap in the crossbridge sequence between the second and third crossbridge rows from the end of the A-segment. This is also seen in rabbit psoas muscle fibres made permeable by glycerination and labelled with antibody to HMMS-1 (Craig and Offer, 1976) and negatively stained cryosections of human muscle (Sjostrom amd Squire, 1977). These cryosections and A-segments (Craig, 1977)

(a)



(b) Rotational Symmetries of Helices of Crossbridges on Isolated Thick Filaments and The Thick Filament Backbone Diameters

Specimen	Rotational Symmetry	Backbone Diameter(nm)	Reference
Frog	3	15.8	Kensler & Stewart (1983)
Rabbit	3	15	Ip & Heuser (1983)
Limulus	4	23.4	Kensler & Levine (1982)
"	4	-	Stewart et al (1981)
Tarantula	4	19-20	Levine et al (1983)
"	4	-	Craig & Padron (1982)
Scallop	7	30-40	Vibert & Craig (1983)
"	-	22.5	Philpott et al (1960)

FIGURE 1.3.1 (a) The basic arrangement of the myosin tails of the myosin molecules in a thick filament to produce a bipolar structure (after Huxley, 1963). (b) The rotational symmetries determined from isolated thick filaments of vertebrate and invertebrate muscles.

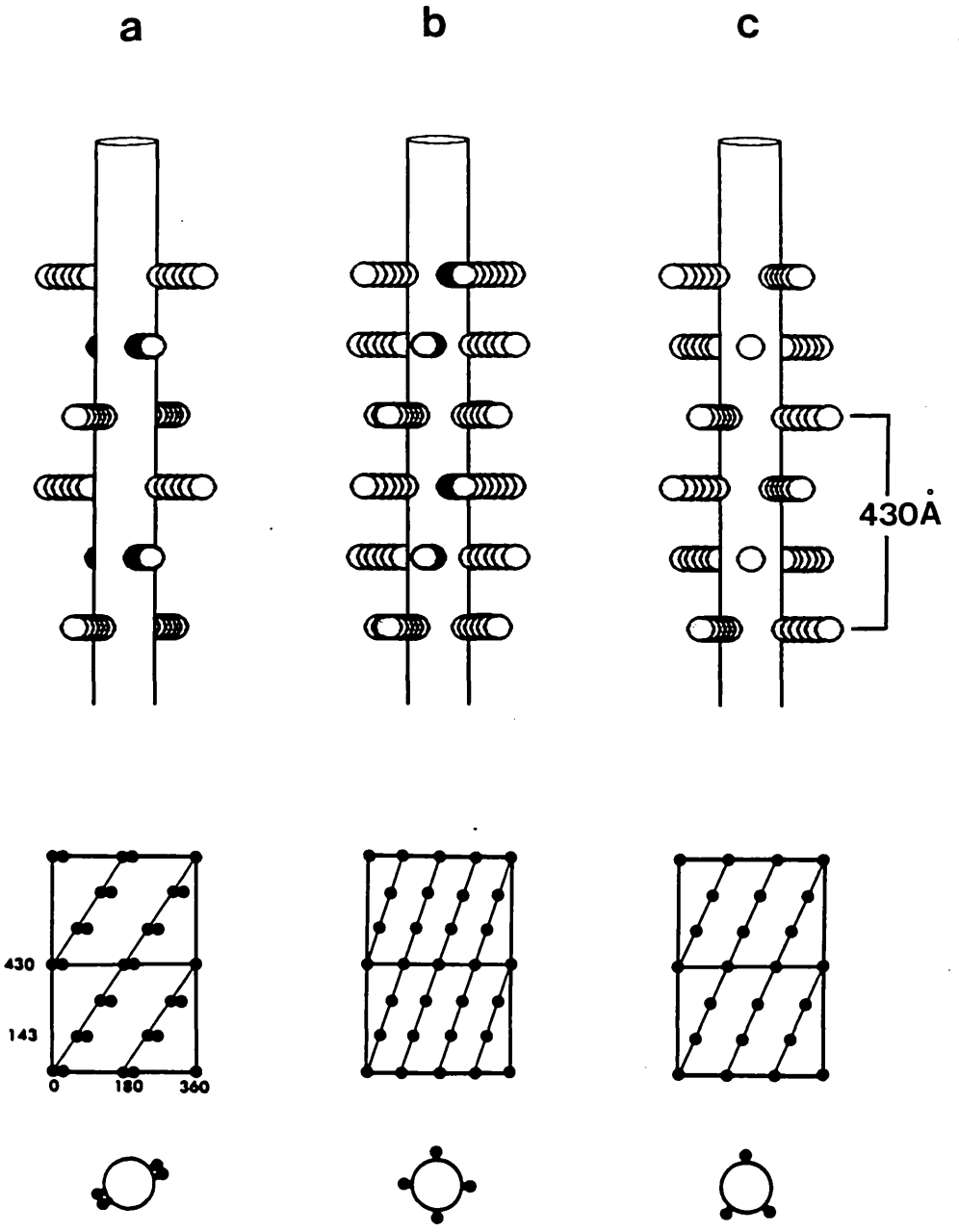


FIGURE 1.3.2 Helical symmetries proposed for the surface lattice of crossbridges in vertebrate thick filaments. (a) 6_2 helix (Huxley and Brown, 1967). (b) and (c) show the 12_4 and 9_3 helical symmetries proposed by Squire (1971, 1972, 1973). In (a), (b) and (c) the upper profile shows a perspective view of the helix (each projection corresponds to the 2 heads of one myosin molecule), the middle profile shows the corresponding radial helix net (in (a) two myosin molecules per lattice point are shown to account for the number of myosin molecules in the thick filament) and the bottom profile shows a transverse layer of one crossbridge level.

TABLE 1.3.3 The Number of Myosin Molecules At Each Crossbridge Level (N_c) in Vertebrate Skeletal Muscle Thick Filaments.

Reference	Method	N_c
Huxley and Hanson (1957)	Interference Microscopy	3.18
Huxley (1972)	Myosin concentration (170μm)	4.32
Marston and Tregear (1972)	Myosin concentration (120μm)	3.05
Tregear and Squire (1973)	Quantitative SDS gel electrophoresis	2.66
Morimoto and Harrington (1974)	SDS	3.86
Morimoto and Harrington (1974)	Density of suspension and particle counting	4.3
Potter (1974)	SDS gels	2.54
Emes and Rowe (1978)	Sedimentation	2.9
Lamvik (1978)	Filament weighing in scanning transmission electron microscope	2.7
Pepe and Drucker (1979)	SDS/PA gels and Densitometry	3.8
Borejdo and Assulin (1980)	SDS	3.0
Reedy et al (1981)	Filament weighing in STEM	2.86
Yates and Greaser (1983)	SDS gels and Amino acid analysis	2.5

also show that about the first ten rows from the bare-zone appear paired. Similar perturbations occur towards the end of the A-band where the filament taper occurs. In the central region of the bridge sequence in each half of the A-band, rows of crossbridges appear to be grouped in threes.

These observations confirm the register of crossbridge levels across the sarcomere width and the virtually unbroken sequence of rows of crossbridges between the edges of the bare-zone and the thick filament end. These preparations also permit a more accurate location of the bare region which is 149nm in A-segments (Craig, 1977); 151nm in HMMS-1-labelled myofibrils (Craig and Offer, 1976) and 160nm in cryosections (Sjöström and Squire, 1977). Sjöström and Squires measurement is from the middle of the first row of crossbridges on either side of the bare-zone whereas Craig and Offer (1976) measured from the proximal edge of these first rows, so there is no appreciable difference in these values for the bare-zone width.

1.3.2. Non-Myosin Proteins of the A-band

The presence of non-myosin proteins in the A-band, apart from the M-band,was demonstrated by Starr and Offer (1971) when the technique of gel electrophoresis in the presence of SDS was used to analyse a nominally "pure" preparation of rabbit myosin (Perry, 1955). Including the M-band proteins these non-myosin components account for about 5%wt of the thick filament. In this section the properties, locations and postulated functions of these A-band components are reviewed (Table 1.3.5).

1.3.2.A C-protein and the C-zone structure

C-protein is the most abundant of the non-myosin proteins

Table 1.3.5 .The Components of the Myofibril

Protein	*Location*	*Approx.% of total myofibrillar protein*	*MW*	*Number of polypeptide chains and chain wt.*
Myosin	Thick filaments	55	460,000	2 x 190,000(heavy chain)
				1.2 x 21,000 (A-1 light chain)
				2 x 18,000 (DTNB light chain)
				0.8 x 17,000 (A-2 light chain)
C-protein	Thick filaments(seven sites spaced about 43nm apart in each half of the A-band)	2	140,000	1 x 140,000
M-line protein	M-line†	1-2	88,000	2 x 44,000
Actin	Thin filaments	23	41,700	1 x 41,700
Tropomyosin	Thin filaments	6	70,000	2 x 35,000
Troponin	Thin filaments(at sites spaced 38.5nm apart throughout the thin filament	6	80,000	1 x 37,000 (TN-T)
				1 x 23,000 (TN-I)
				1 x 18,000 (TN-C)
α-Actinin	Z disc†	1	180,000	2 x 90,000
H-protein	Thick filaments	0.3		

†Probably other proteins are also present in the M-line and Z disc.

of the thick filament, accounting for approximately 5% of the thick filament mass or 2%wt of the myofibrillar protein. Various "isoforms" of the original "white" C-protein (Starr and Offer, 1971) have been characterised. These are red C-protein (Callaway and Bechtel, 1981; Yamamoto and Moos, 1983), X-protein (Starr et al, 1980; Starr and Offer, 1983; Yamamoto and Moos, 1983) and cardiac C-protein (Yamamoto and Moos, 1983). X-protein may be derived from red C-protein by cleavage of a short terminal segment (Yamamoto and Moos, 1983) since it is very similar to red C-protein in its elution from hydroxyapatite, its amino-acid composition and its sedimentation coefficient. The following review is concerned only with white C-protein since its characterisation has been followed with studies on its location in the A-band, its possible enzymatic properties and its interaction with the thin filaments. Biochemical studies show that white C-protein consists of a single polypeptide chain of molecular weight 160,000, probably containing 40 to 60% of β structure with the remainder random coil (Offer, 1972; Offer et al, 1973; Morimoto and Harrington, 1973). Electron microscopy of isolated C-protein molecules, combined with solution studies and low-angle neutron scattering studies, have indicated that the molecule is elongated about 350 to 400Å long and probably 20 to 30Å wide (Offer et al, 1973). Its radius of gyration from low-angle neutron scattering studies of solutions is about 125Å (Worcester et al, unpub.). The thick filament contains about 40 molecules of C-protein, but uncertainty in the precise number precludes direct correlation of the number at each of the 14 stripes with the possible rotational symmetry of the thick filament crossbridge array. There may be 37±7 molecules per thick filament i.e. 2.6 ± 0.5 at

each of the stripes according to Craig and Offer (1976a); 52 ±5 per thick filament and therefore 3.7 per stripe (Morimoto and Harrington, 1974) or 2.1 molecules per stripe if the actin to myosin ratios of Tregear and Squire (1973) are used (Craig and Offer ,1976a).

C-protein has been located by antibody labelling in the central one third of each half of the A-band

(Offer, 1972; Pepe and Drucker, 1975; Craig and Offer, 1976a) as 7 stripes separated by about 430Å. The regions extend between about 2000Å to 5000Å from the centre of the A-band. Its presence is also evident from the prominence of transverse striations at corresponding axial positions in A-segments (Hanson et al, 1971; Craig, 1977) and cryosections of human muscle (Figure 1.3.6; Sjöström and Squire, 1977).

The association of C-protein with the thick filaments in the A-band was originally indicated by the persistence of C-protein as an impurity in preparations of purified myosin. The fact that C-protein could be tagged by antibody, and the binding of the antibody near the backbone of the filament rather than between the filaments , led to the conclusion that at least part of the C-protein molecules are on the surface of the thick filament. Possible binding sites for C-protein on the thick filament have been examined by C-protein's interactions with the various proteolytic fragments of the myosin molecule.

Moos et al (1975) studied the effects of C-protein on the assembly of myosin into filaments in vitro and its interaction with low ionic strength aggregates of myosin rod and LMM. It was shown that purified myosin, free from C-protein, was capable of self-assembly and formed filaments with a 140Å repeat. If C-

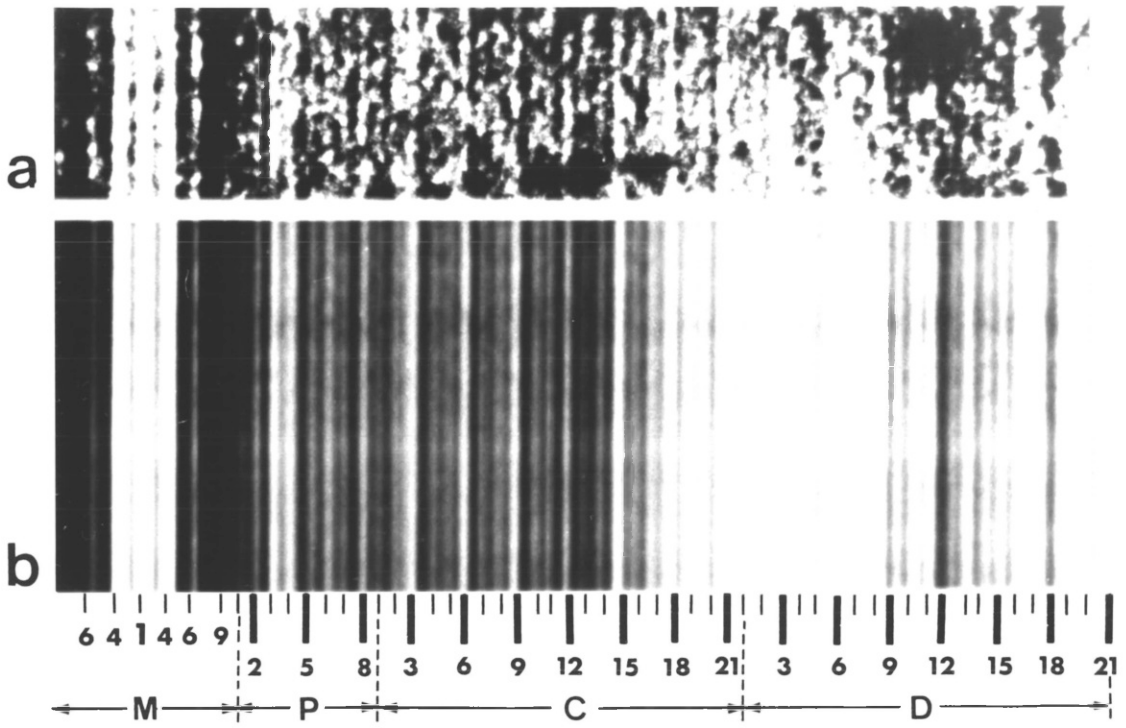


FIGURE 1.3.6 (a) Part of an electron micrograph of one half A-band of negatively stained and cryosectioned human m.tibialis anterior muscle. The fibre axis is across the page. (b) A laterally smeared image of the micrograph in (a). The nomenclature used by Sjöström and Squire (1977) for the transverse striations across the A-band is shown. The transverse striations are numbered and prefixed with a letter according to the region of the A-band. M, M-region; P, proximal zone; C, region in which "white" C-protein has been located in vertebrate muscle; D, distal zone. Magnification 297,000x. (Courtesy of Dr.J.M.Squire)

protein was added to this purified preparation in quantities four to five times more than is present in conventional myosin preparations , and in natural thick filaments (Starr and Offer, 1971; Morimoto and Harrington, 1974), the longitudinal order of the filaments is disrupted, the 140Å repeat is not visible and the filaments have a reduced and more variable diameter. With quantities of C-protein similar to that found in conventional myosin preparations or in natural thick filaments the effects are less obvious but still noticeable at the ends of the filaments.

If C-protein is added to purified myosin rod, before dialysis to low ionic strength, the large sheet-like paracrystals with a 140Å longitudinal repeat normally formed are replaced by irregular narrow filaments. In the case of the LMM fragment the formation of LMM paracrystals is not disturbed by C-protein and the C-protein forms a series of transverse stripes on the paracrystal with a longitudinal spacing identical to the principal characteristic repeat of the LMM paracrystal of 430Å.

Binding measurements at low ionic strength confirmed the strong affinity of C-protein for myosin, myosin rod and LMM. Sedimentation studies by Starr and Offer (1978) have shown separate binding sites on LMM and HMMS-2 rod fragments but no binding to the globular fragment HMMS-1.

Offer et al (1973) have shown that C-protein has no ATPase activity and no effect on the ATPase of pure myosin. It does reduce the activity of the actin-activated myosin ATPase by about half, though independent of the level of calcium ions. It does not bind calcium ions in the presence of Mg^{2+}. No evidence was found that C-protein sensitizes the thick filament to calcium

ions. This leads one to question the possible regulatory function of C-protein (Starr and Offer, 1978) in which it is envisaged to bind the S-2 rod to the thick filament surface in resting muscle, but to release the myosin heads due to calcium binding to C-protein in active muscle so that thay move away from the thick filament surface and interact with the thin filaments.

Studies of the interaction of C-protein with F-actin (Moos et al, 1978) and thin filaments (Moos, 1981) have led to the possibility that C-protein extends from the thick filament surface and interacts with the adjacent thin filaments. The binding of C-protein to the thin filaments in glycerinated rabbit psoas myofibrils was shown to be calcium regulated and switched on and off in the same range of pCa as is the myofibrillar ATPase. Thus at relaxed levels of Ca^{2+} the C-protein molecules are envisaged to be unattached to the thin filaments making it unlikely that the C-protein/actin interaction serves to stabilise the filament lattice by cross-linking between the thick and thin filaments (Moos et al, 1978). Fluorescence microscopy studies of the binding of C-protein to skeletal muscle myofibrils have shown that added C-protein only binds to the thin filaments at the same free calcium ion concentration at which the myofibrillar ATPase is activated. However, in the presence of the myosin heads, the binding of the heads to the thin filaments takes precedence over the binding of C-protein (Moos ,1981).

The role of C-protein in a vernier mechanism for controlling the precise length of the thick filament (Huxley and Brown, 1967; Squire et al, 1976) requires C-protein and myosin to have different repeats. No difference in repeat has been indicated by optical diffraction studies of antibody-labelled

muscle; by studying paracrystals of LMM labelled with C-protein or by studying A-segments (Offer, 1972; Moos, 1972; Moos et al, 1975; Pepe et al, 1975; Craig and Offer, 1976a) but none of these studies has shown unequivocally that the repeats are identical. Craig (1977) claimed from optical diffraction studies of A-segments that the repeats are identical and that the banding pattern within the C-zone shows a grouping of three crossbridge levels but no systematic change in the bands throughout the C-zone. Sjöström and Squire (1977) concluded from negatively stained cryosections that the C-protein and myosin repeats are different and that a systematic change in the striation pattern does occur along the C-zone.

1.3.2.A M-proteins and the M-band structure

M-band proteins which have been isolated and characterised are shown in Table 1.3.7. These account for 1 to 2%wt of the total myofibrillar protein and give rise to a band of high electron opacity up to 900Å wide in the centre of the A-band.

Early longitudinal sections of embedded muscle revealed within the M-band three to five stripes of high density. These were each about 40Å wide and were separated axially by about 220Å (Pepe, 1967; Knappeis and Carlsen, 1968). In transverse sections of the M-band, M-bridges appear to connect a thick filament to its six adjacent thick filaments. Pepe (1967, 1971, 1972, 1975) assumed that M-bridges at each 220Å axial level connected each thick filament to only two adjacent thick filaments, so that the hexagonal pattern of bridges resulted from overlapping layers of bridges . Knappeis and Carlsen (1968) proposed that at each M-line, each thick filament was connected to its six adjacent thick filaments and, in longitudinal and transverse sections, also

observed axially oriented M-filaments 50 to 60Å in diameter in the middle of each M-bridge and extending the M-band width. Thornell and Sjöström (1975) also identified M-filaments in longitudinal cryosections. Thin transverse sections (about 200Å) clearly support these latter abservations and are inconsistent with Pepe's model for the M-band structure (Luther and Squire, 1978, 1980; Luther et al, 1981).

Negative staining of longitudinal cryosections (Sjöström and Squire, 1977; Sjöström et al, 1981) established the fibre-type dependence of the M-band pattern and revealed two overlapping 145Å arrays of lines thought to be caused by stain excluding features on the myosin rods which pack antiparallel in this region to form the myosin filament bare zone. One pair of lines, M9 (or M9') appears stronger than the others and corresponds with fine strands of protein seen in transverse sections at the edge of the frog M-region. This protein forms thin curving bridges from each arm of a Y-shaped filament backbone. Similar structure is seen at the edge of the fish M-region, but it is difficult to distinguish M9 (or M9') from the first row of crossbridges at the proximal edge of the bare region (Luther and Squire, 1978).

A further rather prominent line occurs at M3 (and M3') about 150Å from the centre of the M-band. This does not correspond with one of the 145Å-spaced series of lines but could represent secondary M-bridges observed connecting the M-filaments to the trigonal points of the thick filament lattice (Figure 1.3.8). This M-line is more prominent in longitudinal cryosections in the 3-line (M1, M4 and M1') M-band of frog than in the 5-line (M1, M4, M6, M4' and M1') M-band of fish; the

TABLE 1.3.7 M-band Proteins

Protein	Molecular Weight	Function	Reference
Myomesin	165,000	Primarily structural	Masaki and Takaiti,1972,1974; Landon and Oriol,1975; Trinick and Lowey,1977.
Creatine kinase	40,000	Main structural component Catalyses: ATP+creatine ADP+ phosphocreatine	Walliman et al,1978. Eaton and Pepe,1972; Morimoto and Harrington,1972; Turner et al,1973.
-	165,000	Glycogen debranching enzyme	Trinick and Lowey,1977 Heizmann and Eppenberger,1978.
Glycogen phosphorylase,b	90,000	Phosphorylase activity	Eaton and Pepe,1972; Masaki and Takaiti,1972,1974; Pepe,1975;Lowey,1979.

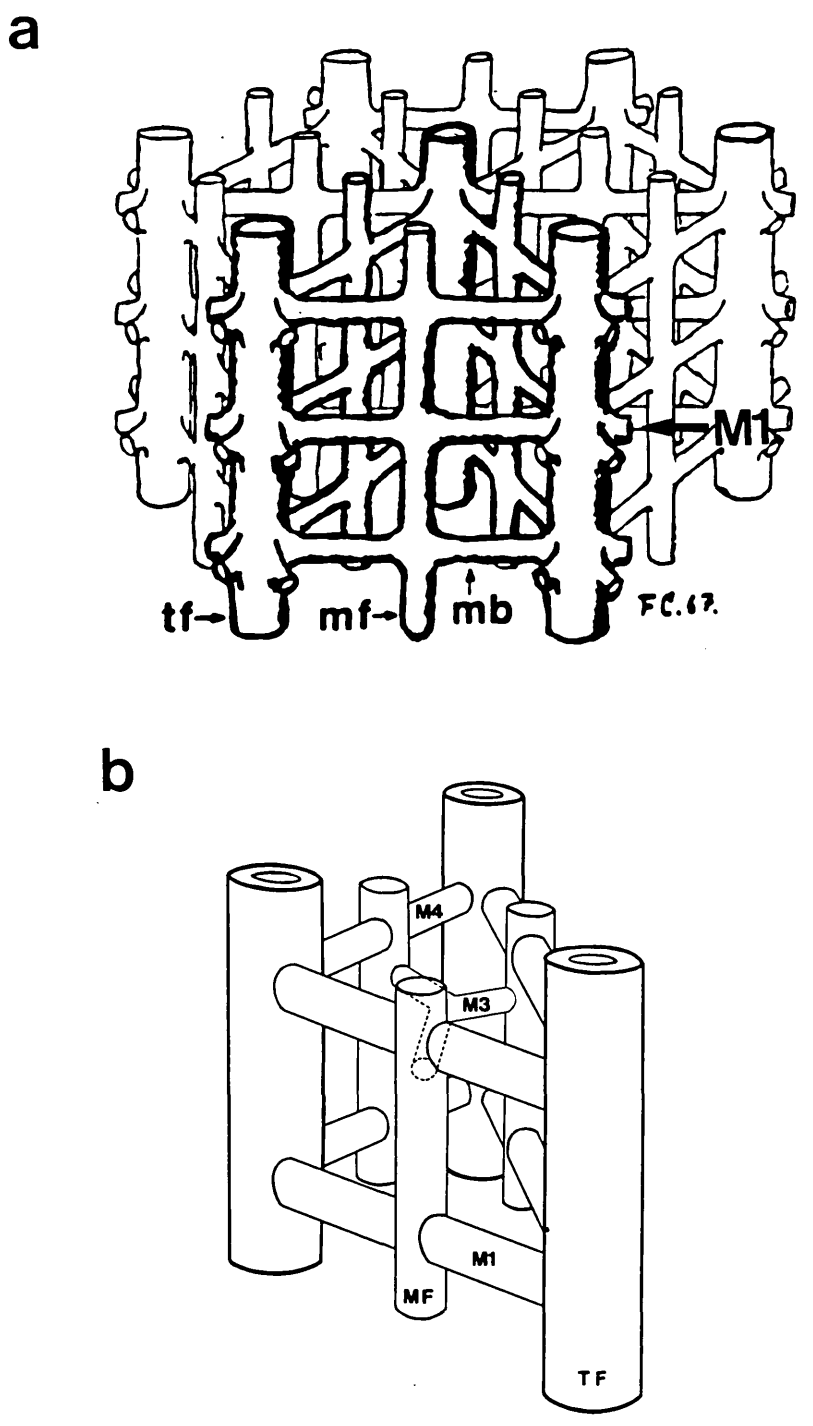


FIGURE 1.3.8 Models of the M-band structure. (a) Knappeis and Carlsen (1968). (b) Luther and Squire (1978). In (a) and (b) M1 is the central line of the M-band. The model proposed by Luther and Squire (1978) reveals bridges, M3, interconnecting minifilaments, MF. tf, thick filament; mf, minifilament; mb, minibridges. See the text for further details.

latter also shows structure between thick filaments at the M3 line (Thornell and Sjöström, 1975). The relation of the M-band structure to the lattice symmetry will be considered in section 1.5 where the lateral arrangement of filaments is considered in detail.

1.4. X-ray Diffraction From Frog Sartorius Muscle

1.4.1. Reflections Arising from the Thick Filaments

1.4.1.A. The Myosin Layer Line Pattern

The appearance of the low-angle X-ray diffraction pattern from relaxed frog sartorius muscle of a strong meridional reflection at 143Å accompanied by layer lines at 429Å (and higher orders, Figure 1.4.1) was attributed to a 6/2 helix of myosin crossbridges of pitch 429Å (Huxley and Brown,1967). The presence of meridional reflections at forbidden positions on the 2nd, 4th and 5th layer lines showed that either the helical symmetry was not perfectly obeyed by the whole crossbridge array or that some feature of the thick filament backbone has the same axial repeat as the crossbridge array's helical repeat of 429Å. Following doubt about the number of myosin molecules at each 143Å axial level, Squire (1971, 1972, 1973) considered the possibility of three-stranded 9/1 and four-stranded 12/1 helical crossbridge arrangements, the first of which is now the more likely approximate description.

Huxley and Brown (1967) carried out preliminary modelling of the intensity distribution along the first layer line and showed that all but the smaller radius side of the main peak on this layer line could be accounted for by crossbridges represented by six equally spaced scattering centres, extending from 60 to 135Å radius with their proposed helical symmetry

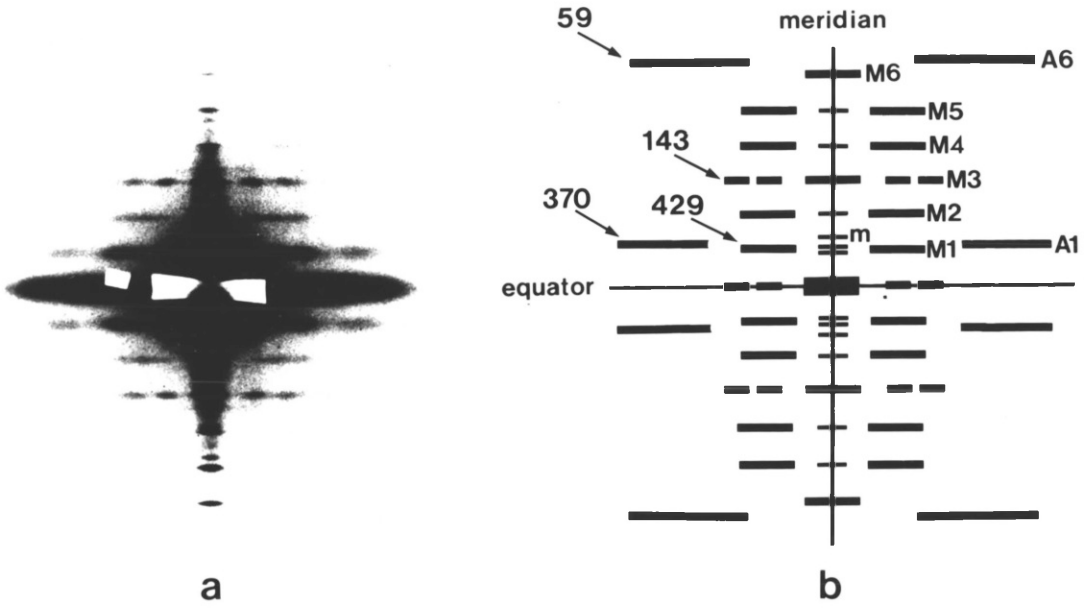


FIGURE 1.4.1 (a) Low-angle X-ray diffraction pattern from resting frog sartorius muscle (Courtesy of Dr.J.C.Haselgrove). (b) A schematic representation of the X-ray reflections in the X-ray pattern in (a). M1, M2, M3 etc. are layer lines arising from the myosin crossbridges and some of these layer lines (M1, M2, M4, M5) have "forbidden" reflections (m) along the meridian. These latter reflections indicate that the 3-fold screw symmetry of the crossbridge arrangement, which can account for the off-meridional diffraction (M1, M2 etc.) and meridional reflections on layer lines M3 and M6, may not be perfect. A1 and A6 are reflections arising from the thin filament structures, corresponding to orders of the thin filament repeat of about 370Å. A6 is not reproduced well in (a) because it is relatively much weaker than the myosin layer lines. (Courtesy of Dr.J.M.Squire)

(Figure 1.4.2(a)). Reasonable agreement between the observed and computed relative intensities of the reflections on the meridian of the third layer line and off the meridian on the first layer line was obtained. Since the thin filament surface is at a radius of about 190Å, from the thick filament axis, this suggested that the crossbridges did not extend all the way out to the thin filament surface in relaxed muscle.

Although the position of the first layer line peak is reasonably unambiguous despite the superlattice sampling, and is about $0.005Å^{-1}$, its intensity relative to the third order meridional reflection can only be said to be between the range 1:1 and 10:1 and the other layer lines 2,4 and 5 have about one quarter of the intensity of the first layer line (Haselgrove, 1975)

Squire (1975,1981) tried to distinguish between the 2,3 and 4-stranded arrangements by modelling the above data in terms of the configuration of the crossbridges arranged with one of the three symmetries (Figure 1.4.2(b)). Each HMMS-1 unit of the crossbridge was modelled by six overlapping spheres which approximated to a cylinder 140Å long and 40Å in diameter. The axes of the two cylinders in the crossbridge were parallel and 40Å apart. The whole crossbridge configuration was defined by an axial tilt (Φ in Figure 1.4.2(b)), an azimuthal rotation (slew;θ in Figure 1.4.2(b)) and radial distance, R, from the thick filament axis.

From these computations the four-stranded model at best gave poor fits both to the first layer line profile and to the layer line relative intensities, even with the crossbridges at a very large radius or high axial tilt. The two-stranded model with

only one crossbridge at each lattice point gave reasonable fits but only if the crossbridge tilt gave a projected crossbridge length of 90 to 95% of the separation between crossbridge levels. The third layer line meridional would have to increase in intensity by a factor of 3 to 5 times on activation if the crossbridge had to tilt from this resting position to one near 90° on attachment to the thin filament.

The three-stranded arrangement gave as good a fit as the two-stranded model if the crossbridges were tilted axially by about 60°. The value of the azimuthal tilt was not critical but lay in the range 75° to 105°.

The necessity for axial tilting of the crossbridges from the normal to the thick filament surface so that the projected crossbridge length onto the thick filament axis is 1/2 to 2/3 of the crossbridge repeat, found necessary for the three-stranded model, is supported by other modelling of the relaxed configuration (Figure 1.4.3; Wray et al, 1975; Haselgrove, 1980; Worcester et al, 1975).

Haselgrove (1980) recorded X-ray diffraction patterns of frog sartorius muscle stretched to reduce Bragg sampling of the myosin layer line pattern. It was found that, although, as was previously shown (Squire, 1975; Haselgrove, 1975), it is possible to model the relative intensities of the pattern with a single cylindrical rod, this cannot account for all of the features of the pattern from stretched muscles. The correlation of crossbridge radial position with the number of strands of the helix agreed with Squire's analysis and was confirmed to be fairly insensitive to the shape, size and orientation of the crossbridge. Extensive modelling of the first six myosin layer

line profiles produced a best configuration in which the two heads were tilted axially in opposite directions by 20^{o} to 40^{o} and slewed around the filament by 60^{o} to 90^{o}. The presence of such a transverse mirror plane was suggested because of the similarity in shape of the first and second layer lines (and the fourth and fifth) which was taken to indicate the two heads should point along two similar helices that rotate in opposite senses around the filament. Wray et al (1975) derived a similar transverse mirror plane for the Placopecten relaxed configuration but on the basis of very clear minima on the meridional reflections at 146Å and 73Å. However the modelling in both these cases will be considerably complicated by the possible perturbation of the crossbridge repeats in these two muscles. This is suggested by the forbidden meridional reflections in the X-ray diffraction diagram of frog sartorius muscle (Huxley and Brown, 1967) and the meridional reflections at the 3rd and 5th orders of a 290Å repeat in patterns from Pecten believed to arise from the crossbridge array (Millmann and Bennett, 1976).

Haselgrove (1980) found a similar insensitivity to the shape of the heads of the crossbridge, as in the modelling with one cylinder, provided they were sufficiently elongated. The transform of Haselgrove's best model (Figure 1.4.2(c)) was altered very little by representing the heads by curved rods approximating to the shape of the head deduced by Moore et al (1970).

1.4.1.B. Additional Meridional Reflections

The prominent 441.8Å meridional reflection from living muscle was at first attributed to some component of the thick filament with a periodicity greater than the 429Å myosin

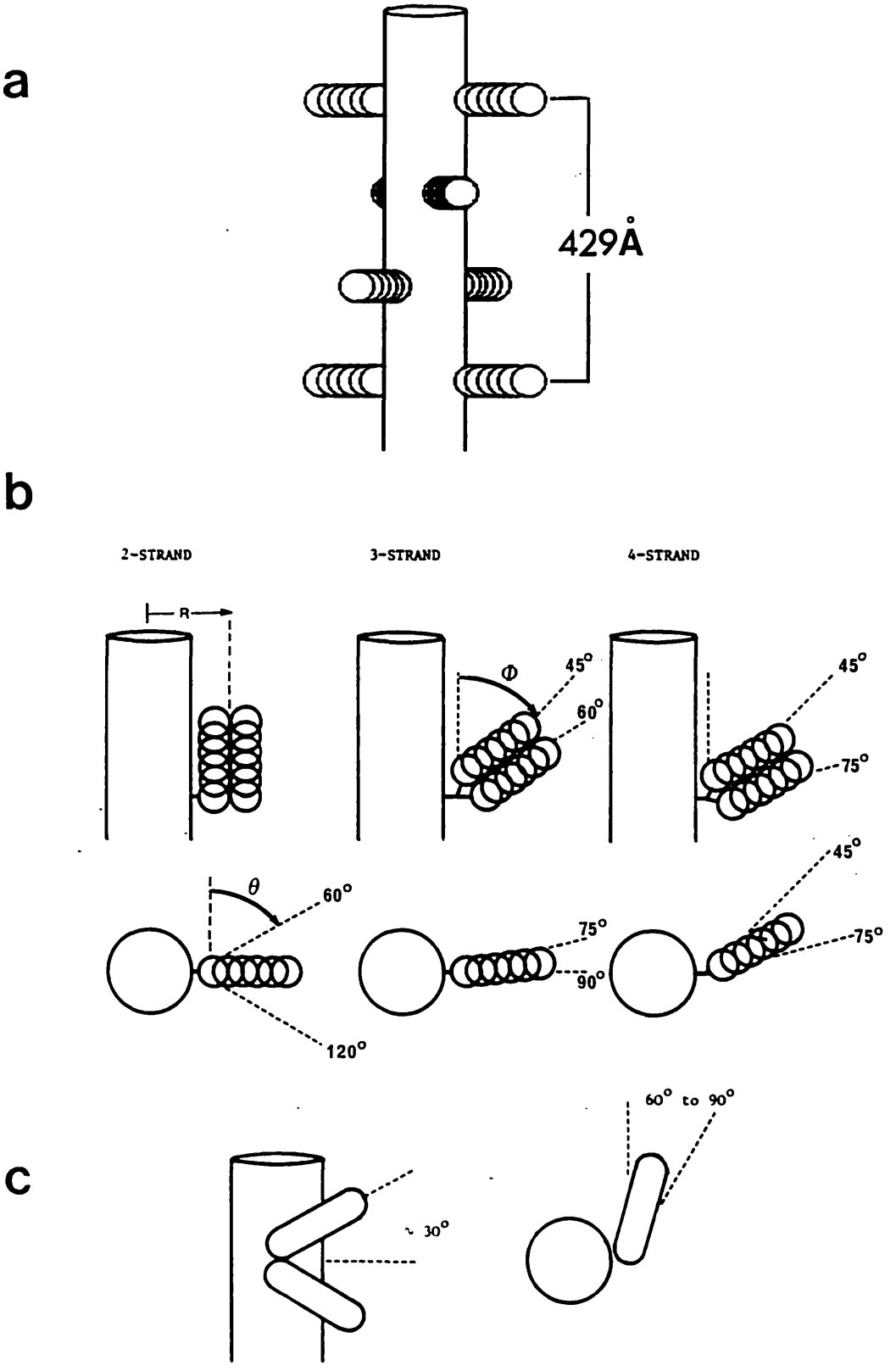


FIGURE 1.4.2 (a) Preliminary modelling of the resting crossbridge arrangement in frog sartorius muscle (Huxley and Brown, 1967) (b) Modelling by Squire (1975) for 2-,3- and 4-stranded crossbridge helices (c) Modelling by Haselgrove for a 3-stranded crossbridge helix (1980)

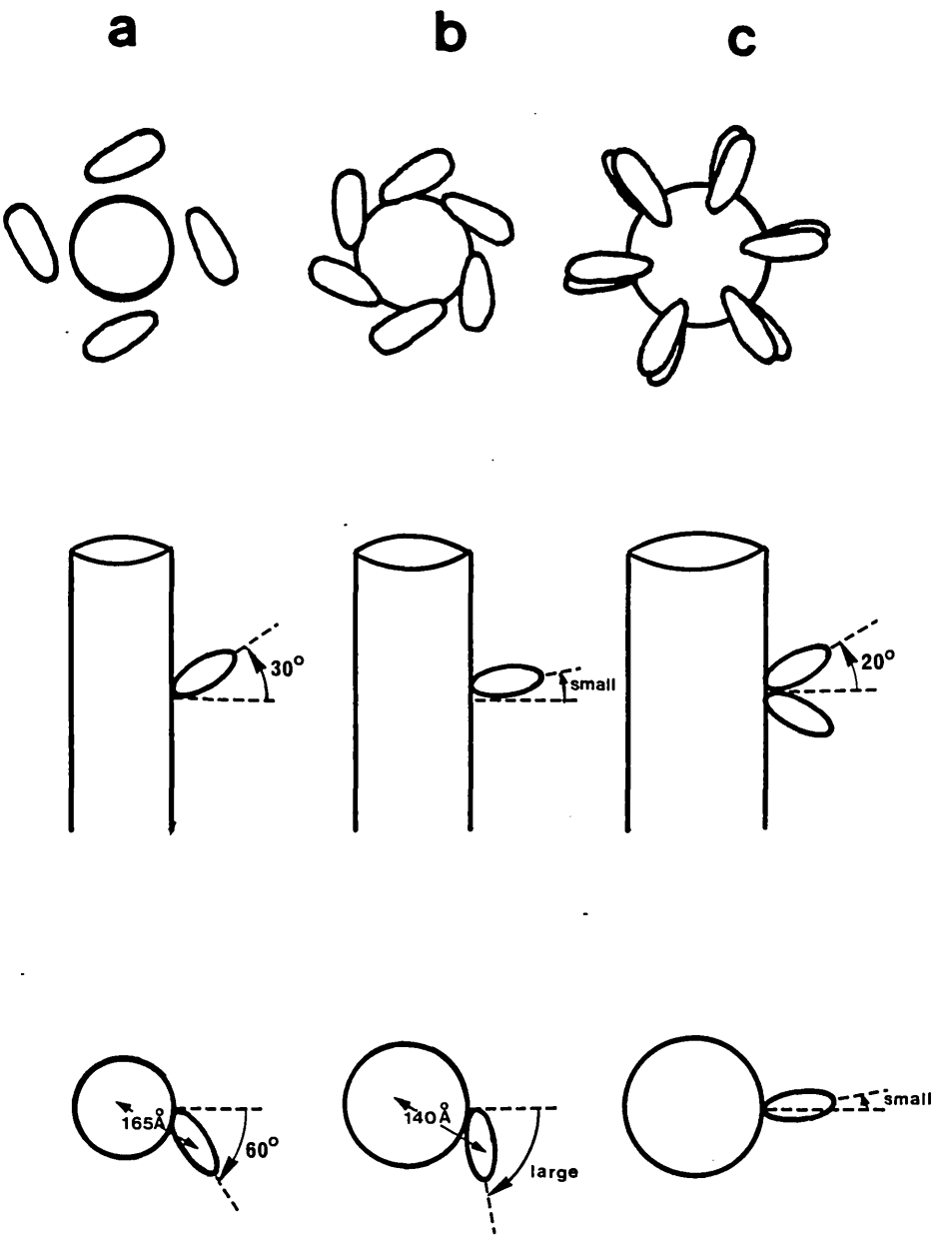


FIGURE 1.4.3 Modelling of crossbridge arrangements from X-ray diffraction patterns of glycerinated, relaxed muscles from (a) Limulus (horseshoe crab), (b) Homarus (lobster) and (c) Placopecten (scallop) (Wray et al, 1974). In (a), (b) and (c) the upper profile represents an end-on view of the crossbridge helix, the middle profile represents the approximate tilts and the bottom profile the azimuthal slews determined for each configuration. In (a) and (b) the subunits shown each represent 2 myosin heads and were modelled with twice the size of the subunit shown in (c).

periodicity (Huxley and Brown, 1967; O'Brien et al, 1971). Rome et al (1973; Rome, 1972) demonstrated that the 441.8Å and 418.4Å reflections (Huxley and Brown, 1967; Haselgrove, 1975) were enhanced by labelling glycerinated rabbit muscle with antibody to C-protein. It was then suggested that these reflections arose from a broad peak at 1/430Å, corresponding to the C-protein periodicity, being sampled by interference fringes whose separation is the inverse of the centre to centre distance of the two C-protein arrays in each half of the A-band. They demonstrated that it was not possible to explain the relative intensities of these two reflections by this simple model alone. With a C-protein periodicity of 430Å the two reflections have about equal intensity, whereas in living muscle the 442Å reflection is about three times as intense as the 418Å reflection (Haselgrove, 1975). On the other hand, with a C-protein periodicity of 440Å, the 14th order of the interference function 474Å (i.e. 14/6650) is expected to appear in the X-ray pattern with about two-thirds of the intensity of the 418Å reflection. The fact that they had incorrectly assumed a C-protein array of nine stripes, whereas it was shown that in some muscles the proximal two are not C-protein locations (Craig and Offer,1976a) making their interference function one 430Å to 440Å period too small, does not explain their results. It was suggested by Squire (1981) that a compromise is obtained if the C-protein periodicity lies between the values of 430Å and 440Å considered by Rome et al (1973). This would give an appreciable difference between the 442Å and 418Å reflections but leave the 474Å reflection very weak.

Many other sharper but weaker reflections occur between

this 400Å region and the higher angle meridional reflections from the thin filaments at about 60Å (see next section). Some of these arise from thin filament components. The whole meridional pattern shows fine sampling at the very high resolution obtained with a 2 metre long camera (Haselgrove, 1975) due to interference fringes from the two halves of the filament, which must have periodicities in the range 7,000Å to 10,000Å. It was apparent (Haselgrove, 1975) that, apart from the splitting of the 385Å and 442Å meridional reflections, the "143Å" and "215Å" reflections were also being sampled due to the separation of crossbridge regions in the A-band.

Squire (1981) has shown that all of the low-angle meridional reflections, 400Å to 100Å, from living frog sartorius muscle can be accounted for by extending this principle to the rest of the meridional pattern. The interpretation accepted the evidence for a C-protein periodicity of about 435Å (Hanson et al 1971; Sjöström and Squire, 1977) in which case the small peaks to the low-angle side of the myosin peaks at 214.3Å, 143.4Å etc. (Figure 1.4.4) could well correspond to broad successive order peaks from the C-protein array being sampled by interference fringes produced by the separation of C-zones across the A-band. In fact just those peaks expected to be enveloped by the broad C-protein peaks are seen.

1.4.2. Reflections Attributed to the Thin Filaments

1.4.2.A. The Actin Layer Lines

The X-ray reflections from the actin filament between 6Å and 59Å can be accounted for by a helical arrangement of actin monomers of the general form described in section 1.1.3 (Hanson and Lowy, 1963; Selby and Bear, 1956). Two helical strands of

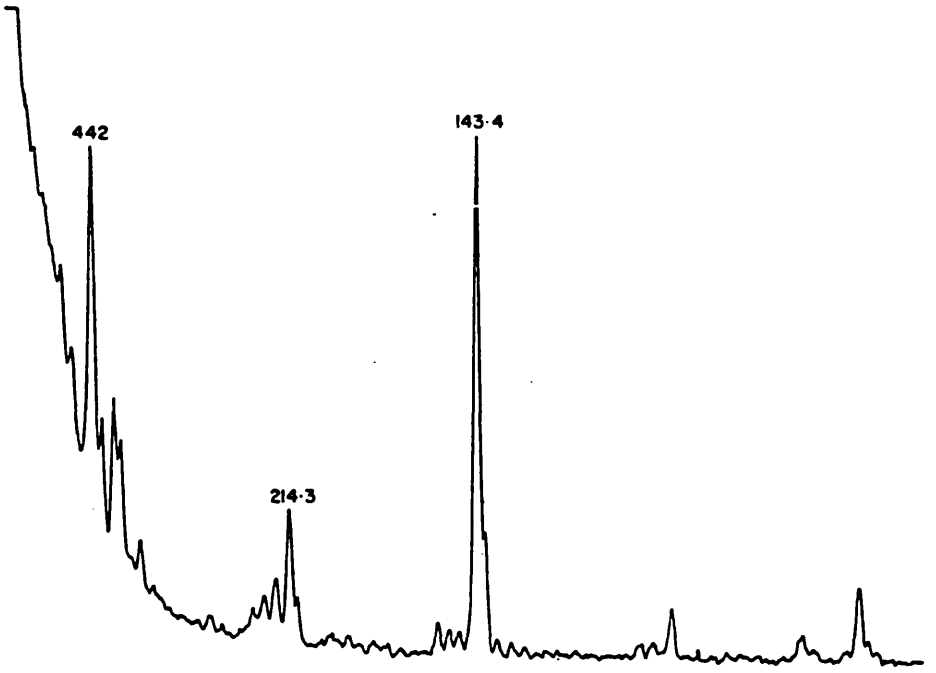


FIGURE 1.4.4 Microdensitometer trace along the meridian of an X-ray diffraction pattern from relaxed frog sartorius muscle taken on a camera with a 2-m specimen to film distance (from Haselgrove, 1975). The reflections at 442Å, 214.3Å and 143.4Å are indicated and their possible origins are discussed in the text.

subunits are wound around each other. Each helical strand has actin monomers separated axially by 54.6Å and has a helical repeat of 2 x 360Å to 2 x 370Å containing between 13 and 14 actin monomers. In this structure the subunits in one strand are displaced longitudinally relative to those of the other strand by half of the 54.6Å repeat along each strand giving a subunit repeat of 27.3Å and an axial repeat of 360 to 370Å for the actin helix. Thus the first true meridional reflection occurs at 27.3Å and there are higher orders (up to the fourth) of this period. A layer line at about 400Å was assumed to be the average of the second order from the long repeat of 720Å to 740Å and the first myosin layer line spacing of about 430Å (Vibert et al, 1972). It could not be used to obtain the helical repeat of the actin helix.

This helical repeat was derived from the separation of layer lines at 50.97Å and 59.1Å (or 59.4Å) and could not be well defined because of the axial spread in the second of these reflections. However, assuming the 50.97Å layer line spacing to be a more reliable value, integral helices with 13 or 14 subunits per turn (corresponding to genetic helices of 13 subunits in 6 turns and 28 subunits in 13 turns) predicted values of 59.5Å and 58.8Å respectively for the other layer line. This gave a range for the helical pitch of 2 x 360Å to 2 x 380Å. Since the observed value of 59.1Å was from patterns where the actin layer line was well resolved from the nearby myosin layer line the pitch was taken to be nearer to 2 x 370Å. Haselgrove (1975) obtained values of 59.5Å and 51.2Å for these prominent layer lines which yielded a helical pitch of 2 x 367Å.

1.4.2.B. Additional Meridional Reflections from the Thin Filaments

The prominent meridional reflection at 385Å was concluded to be due to a component of the thin filament (Huxley and Brown, 1967) since longitudinal electron micrographs showed stripes of about 400Å periodicity in the I-band (Pepe and Huxley, 1964; Pepe, 1966). Rome et al (1973a) confirmed directly the origin of this reflection by antibody labelling the components of the troponin complex in glycerinated rabbit muscle and observed an enhancement in the 385Å meridional X-ray reflection. This reflection appeared as a doublet at 383Å and 395Å (Huxley and Brown, 1967; Haselgrove, 1975). This splitting was attributed to interference between the two halves of the I-band (O'Brien et al, 1971; Rome et al, 1973a) and successive orders of this reflection can be accounted for in the same way (Squire, 1981).

1.4.3. The Arrangement of Crossbridges in Rigor Muscle

The myosin layer lines indexing on a 429Å repeat in resting muscle are not visible in patterns from rigor frog sartorius muscle. The myosin layer line pattern is replaced by layer lines which index on about the same helical repeat as the actin helix. These appear as two sets of low-angle reflections in that they have sharp, intense components which are orders of a repeat of 725Å close to the meridian and weak diffuse components further from the meridian with spacings consistent with an actin-like helix with a helical repeat of 725Å (Haselgrove, 1970, 1975; Huxley, 1972). The meridional reflections at 86Å, 91Å and 107Å disappear leaving the 143Å and 72Å reflections prominent and at spacings increased by about 1%. Other weaker reflections at 227Å, 212Å, 192Å, 127.5Å, 110.8Å and 101.8Å remain. These latter

reflections and the 144.8Å and 72Å reflections index on a 2315Å repeat which is 1% greater than the live muscle value of 2295Å. However this repeat of 2315Å is also six times the troponin repeat. The appearance of the 192Å and 127.5Å reflections made it more likely these arose from the thin filaments.

The general form of the X-ray diagram is attributed to the myosin crossbridges binding to the thin filaments and reorganizing their resting helical arrangement into a helical arrangement determined by the symmetry of the actin helix. The pattern has not been modelled in detail but the radial position of the outer set of layer lines was shown to be consistent with diffraction from spheres arranged in an actin-like helix at 60 to 80Å from the thick filament axis (Haselgrove, 1975). The measured spacing of the layer lines at 51Å and 59Å show no change in the axial periodicity of the actin filament on binding the myosin crossbridges (Huxley and Brown, 1967), although the first layer line spacing and the shift in the 143.4Å and 71.6Å meridional reflections indicate that a small change may have occurred in the thick filament.

1.4.4. Arrangement of Crossbridges in Active Muscle

X-ray diffraction patterns of isometrically contracting muscles show large reductions in the intensities of the low-angle myosin layer lines (Elliott et al, 1967; Huxley and Brown, 1967; Haselgrove, 1970, 1975). Time-resolved measurements (Huxley et al, 1980, 1981, 1982) of changes in the first layer line at 429Å show a reduction to 15% to 23% of the resting layer line intensity. This change occurs 5 to 10ms ahead of the onset of tension development by the muscle. Other off-meridional

reflections show a similar time-course in the change in intensity, although the residual intensity during contraction varies (i.e. to about 30% for the third layer line). The integrated intensity of the third order meridional reflection actually shows an increase and biphasic behaviour; its recovery is delayed behind tension by about 200ms on relaxation of the muscle. The increase in width of the 143Å reflection across the meridian during contraction indicated a decrease in filament alignment. The changes in intensity were interpreted as helical disordering, closely correlated with tension development, mainly in the circumferential positioning of the crossbridges.

There is no apparent change in repeat of the myosin helix according to measurements from the first layer line, although this could only be measured to an accuracy of ±5%. There is no apparent change in the spacing of the actin layer lines at 59Å or 51Å although a slight increase in the intensity of the meridional end of the 59Å layer line of about 27% (±21%) and a decrease in the outer end of this layer line of 9% (±15%) occur. An increase of about 20% also occurs in the 51Å layer line. It was shown by Parry and Squire (1973) that this increase in intensity of the 59Å and 51Å layer lines cannot be explained in terms of a change in tropomyosin arrangement about the actin helix or in the order within the thin filaments. Extra mass (HMMS-1) attaching to the actin molecules could account for these changes. A rough estimate attributed this change to HMMS-1 in contracting muscle attaching to 50% of the number of actin molecules which have HMMS-1 attached in rigor.

1.5. The Lateral Arrangement of Muscle Filaments

1.5.1. The Equatorial Diffraction Pattern

The hexagonal arrangement of thick filaments in the vertebrate muscle A-band was first suggested by low-angle equatorial X-ray diffraction of "wet" vertebrate striated muscle (Huxley, 1951, 1952, 1953). The two reflections at spacings of 450Å and 225Å were indexed as the $10\bar{1}$ and $11\bar{2}$ reflections from an hexagonal array. The double array of thick and thin filaments was confirmed by electron microscope studies of embedded transverse sections (Huxley, 1953) and longitudinal sections (Huxley,1957). It was also shown that the relative intensities of these two equatorial reflections (I_{10}/I_{11}) decreased markedly when the muscle passes into rigor with the removal of ATP from the muscle (Huxley, 1952). This was recognized as either an increase in mass at the trigonal points in the hexagonal lattice of the thick filaments or a more precise localization of the thin filaments due to some combination of the thick and thin filaments.

Elliott et al (1963) showed the systematic changes in the ratio I_{10}/I_{11} which occur as the sarcomere length is changed. This decrease in the ratio as the sarcomere length decreased was in the same direction as the rigor changes but of a smaller magnitude. It was concluded that there was no substantial change in the value of I_{10}/I_{11} for living rat and rabbit muscles when they were put into rigor by glycerination at a particular sarcomere length. More detailed observations on glycerinated rabbit psoas muscles supported this and suggested that the reported decrease in the I_{10}/I_{11} accompanying rigor (Huxley, 1953) was due to shortening of the sarcomere induced by glycerination (Rome, 1968).

Huxley (1968) confirmed his earlier observations by recording equatorial X-ray patterns from preparations of live and rigor frog sartorius and rabbit psoas muscles in which complete overlap of the thick and thin filaments was achieved. Thus any further decrease in the ratio I_{10}/I_{11} when the muscles were put into rigor could not be accounted for by shrinkage of the sarcomere as previously suggested (Rome, 1968). The appearance of transverse sections of fixed and embedded live or rigor muscles and Fourier projections using the 10 and 11 reflections were consistent with the transfer of mass from the thick to the thin filaments when the muscle passes into rigor (Huxley, 1968).

It was concluded that about 30% of the total mass of the thick filament must transfer to the thin filaments in rigor muscle, corresponding roughly to a contribution from each myosin molecule of the active end of HMM. This value for rigor muscle was confirmed by Haselgrove and Huxley (1973; 34% or 39% of the initial thick filament mass) who also studied the two main equatorial reflections during isometric contraction of frog sartorius muscles over a range of sarcomere lengths. It was shown that for resting, contracting and rigor muscles the ratio I_{10}/I_{11} depends on the sarcomere length and the state of the muscle. Fourier projections for all of these states indicated a similar movement of mass to the thin filaments in active and rigor muscle. The transfer of mass in contracting muscles was about 40% of that in rigor, which put an upper limit of 45% to 50% on the number of crossbridges instantaneously attached to thin filaments during isometric contraction.

Elliott *et al* (1967) attributed a small decrease in the ratio I_{10}/I_{11} during isometric contraction to thin filaments

becoming ordered in the hexagonal lattice along more of their length in the I-band as a result of tension generated by attached crossbridges. The decrease in I_{10}/I_{11} at complete overlap (Haselgrove and Huxley, 1973) meant the thin filaments cannot achieve the required amount of order. It was also shown that applying a load to a muscle in rigor had no affect on the equatorial intensities so that tension did not appear to be improving the alignment of thin filaments in the I-band.

Elliott et al (1967) also reported a small decrease in lattice spacing of an isometrically contracting muscle but this was shown to be due to the length of time of their X-ray exposures (Haselgrove and Huxley, 1973). The latter authors also recorded X-ray diffraction patterns from isometrically contracting muscles after they had shortened actively against a load. They showed the pattern to be dependent on the sarcomere length at which the photograph is taken and not on the sarcomere length when the muscle was first activated. Thus it was demonstrated that muscular contraction is accompanied by a sliding movement of the filaments with no appreciable change in their length.

More recent X-ray studies (Matsubara et al, 1975) and neutron scattering studies (Worcester et al, 1975) have claimed the ratio I_{10}/I_{11} for active muscle to be similar to the rigor value, on the basis that optimum activation of the crossbridges is only achieved by allowing a longer relaxation time between stimulations of the muscle. However in studies using linear position sensitive detectors to record data from optimally activated muscle (Haselgrove et al, 1976; Podolsky et al, 1976) a decrease in the absolute value of the 10 reflection of 50% (±10)

and an increase in the absolute value of the 11 reflection of 100% (±25%) occurs.

The use of electronic X-ray detectors has allowed up to seven equatorial reflections to be recorded, i.e. $10\bar{1}$, $11\bar{2}$, $20\bar{2}$, $21\bar{3}$, $30\bar{3}$, $22\bar{4}$ and $31\bar{4}$ (Lymn, 1975) from relaxed frog sartorius muscle at rest-length. This corresponds to approximately 100Å resolution. Lymn (1975) presented computed intensity data from five models (1 to 5 in Figure 1.5.1) and concluded that only models 4 and 5 with crossbridges at a large radius from the thick filament axis would account for the experimental data. He proposed that the changes observed in the ratio I_{10}/I_{11} when muscle contracts (Haselgrove and Huxley, 1973; Podolsky et al, 1976) were brought about by predominantly azimuthal movement of the crossbridges. This is contrary to previous models in which both radial and azimuthal movement were involved (Huxley and Brown, 1967: Huxley, 1968).

Lymn had rejected model 2 (Figure 1.5.1) on the basis of low calculated values for the higher order reflections. Haselgrove et al (1976) showed that this model was in fact in good agreement and thus a model with crossbridges close to the thick filament surface was consistent with Lymns observed intensities. It was also demonstrated by Fourier synthesis from five orders of this same equatorial data that a model with crossbridges at a radius less than that of the thin filaments was possible. It was noted that this analysis only served to validate the possible radial movement of crossbridges and that the types of azimuthal movement suggested by these models could not account for the large decrease in the absolute intensity of the $10\bar{1}$ reflection alone.

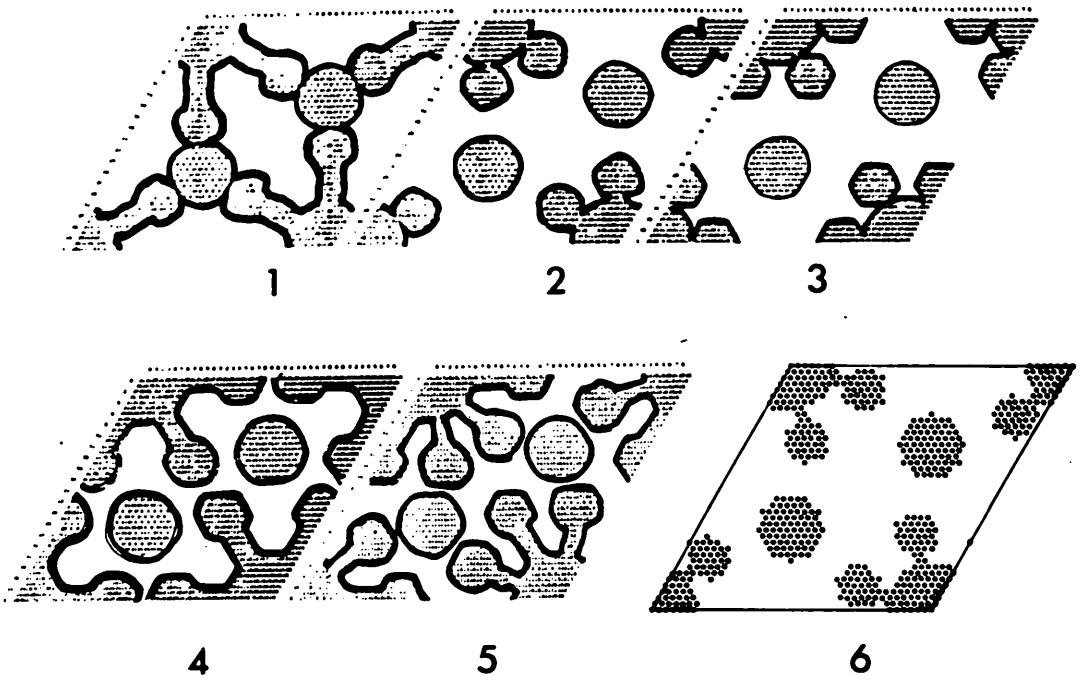


FIGURE 1.5.1 Models 1 to 5 for the hexagonal unit cell density, in the overlap region of the A-band, projected onto the equatorial plane (Lymn, 1975). The thick filaments, at the corners of the unit cell of side spacing 400Å, have a core radius of 60Å and the thin filaments at the trigonal positions of the lattice have a radius of 40Å. Each arm projecting from the thick filament core represents two myosin heads side by side to form a circular subunit. An actin to myosin ratio of 0.25 was used for the sarcomere length of 2.2μm. In models 2 and 3 the crossbridges project to 130Å radius and in models 1,4 and 5 to 180Å radius. Model 5 is for the three-stranded filament with the filament oriented so that the crossbridges lie along the 10 planes of the unit cell. In models 3 and 4 the crossbridges are slewed azimuthally by 0^{o} and by 30^{o} for models 1 and 2. Model 1 gives a ratio for I_{11}/I_{10} typical of rigor muscle and 2,3,4 and 5 give ratios typical for resting muscle. Model 6 (from Haselgrove et al., 1976) is another model similar to 2 but with the thick filaments rotated by 12^{o} and the crossbridges extended by 10Å. Each subunit in the thick filament in 6 represents an electron density of 20 arbitrary units and in the thin filament, 15 of these units. The rest of the unit cell is given zero density.

Even at the resolution of the data recorded by Lymn (1975) of about 100Å a crossbridge distribution with ninefold rotational symmetry will very likely appear as an annulus of density surrounding the thick filament (Squire, 1974). Maps from Patterson synthesis of five to seven of the recorded equatorial intensities show a featureless shelf of density surrounding the thick filaments (Squire, 1981). This can also be interpreted as hollowness of the thick filament but it is nevertheless consistent with the proposals of Squire (1974).

1.5.2.The Three-Dimensional Crossbridge Lattice in Vertebrate Skeletal Muscle

1.5.2.A Interpretation of the Myosin Layer Line Sampling in Terms of the Regular Superlattice

The row-line sampling of the myosin layer lines observed by Huxley and Brown (1967) shows that the myosin filaments are not simply in rotational register. The lattice reflections on the third layer line indexed on the same simple hexagonal lattice as the equatorial reflections but those on the first and second layer lines indexed on a hexagonal lattice of spacing $\sqrt{3}$ times that calculated from the equatorial reflections. This corresponds to a lattice defined by identical orientations of next nearest neighbour myosin filaments (Figure 1.5.2).

Since the simple lattice reflections occur on the equator each thick filament must appear identical in projection down the axis, and nearest neighbours must appear to have the same rotational orientation in the unit cell, in an end-on view of the filament lattice. The 6/2 helix of crossbridges could generate this superlattice if the second and third filaments in the unit cell were rotated by one-third of a turn and two-thirds of a turn

relative to the first filament but with all filaments having the same longitudinal register (Figure 1.5.2). Alternatively the second and third filaments can be thought of as being displaced longitudinally by one-third and two-thirds of the helical period of 429Å relative to the first filament. The lattice reflections allowed on layer lines "l" were given by the selection rules;-

$$2h + k + l = 3n$$

or $$h + 2k + 2l = 3n$$

where h, k are the indices of the superlattice unit cell.

Only reflections allowed by these selection rules were observed (Figure 1.5.3). However the real superlattice was later shown to be of a different form and to be statistical in nature.

1.5.2.B. The Statistical Superlattice

Transverse sections through the bare region of the frog sartorius muscle A-band show the three-fold rotational symmetry of the thick filament backbones most clearly. This enabled the rotational relationships between neighbouring thick filaments to be examined in detail (Luther and Squire, 1980).

An optical diffraction analysis of these electron micrographs revealed a superlattice of myosin filaments with the same shape and size as that proposed by Huxley and Brown (1967) but differing in the following respects;-

(i) The superlattice is not perfectly developed and even in very well-ordered muscle the superlattice only extends a few unit cells in any direction.

(ii) There are only two filament orientations evident 60° (or 180°) apart rather than the three invoked for a three-stranded filament to generate the superlattice by Huxley

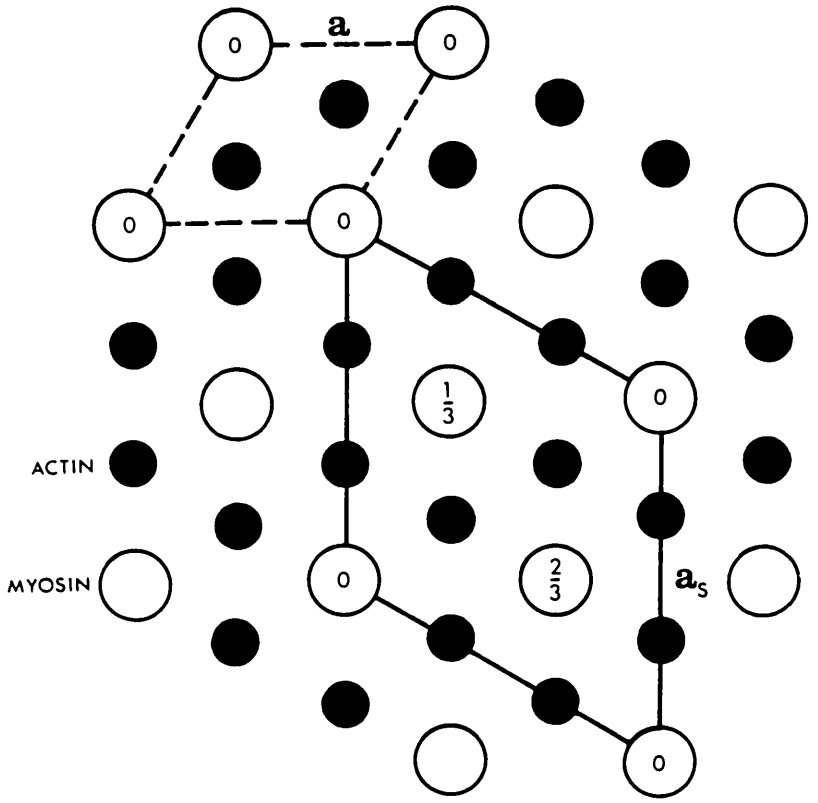


FIGURE 1.5.2 Diagram representing an end-on view of the double hexagonal lattice of thick (unfilled circles) and thin (filled circles) filaments. The simple hexagonal unit cell is shown by the broken line. The size, a_s, and shape of the superlattice is shown by the unbroken line. The numbers 0,1/2,2/3 in the unfilled circles indicate the axial positions of equivalent subunits on myosin filaments on these lattice points as a fraction of the 42.9nm repeat of the myosin filament. The crossbridge lattice generated was proposed by Huxley and Brown (1967) to account for the detailed sampling of the myosin layer lines in X-ray diffraction patterns from resting frog sartorius muscle (Courtesy of Dr.J.M.Squire).

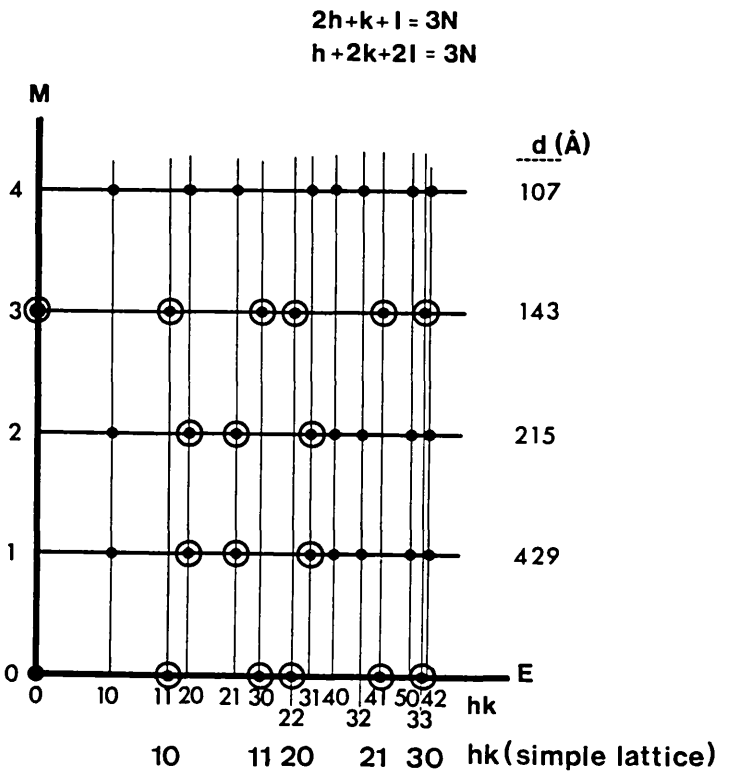


FIGURE 1.5.3 A summary of the detailed sampling (filled circles) that was predicted for the myosin layer lines (L1, L2, L3 etc.) in low-angle X-ray diffraction patterns from frog sartorius muscle on the basis of the superlattice proposed by Huxley and Brown (1967) and shown in Figure 1.5.2. This gave the selection rules shown at the top of the plot. The reflections (filled circles) observed by Huxley and Brown (1967), using X-ray cameras with good 2-dimensional resolution, are circled. The numbering below the equator, E, refers to the indexing of the reflections on the superlattice unit cell. The equivalent row-line positions for the simple lattice unit cell are shown below this (Courtesy of Dr.J.M.Squire).

and Brown.

If the crossbridge superlattice symmetry is taken to be perfectly of the Huxley and Brown type it was shown that arrangements of triangular filament profiles which exhibit randomness and just the two observed orientations are possible if these filaments have two-stranded or four-stranded crossbridge helices. This only follows if the filaments behave as rigid structures so that comparable relative orientations occur between the triangular filament profiles in the crossbridge and bare regions.

For the more likely three-stranded crossbridge helix only one arrangement of bare region triangular filament profiles places the crossbridges in the Huxley and Brown superlattice. This has three filament orientations 40^{o} apart to generate a regular bare region superlattice showing non of the randomness possible with two- and four-stranded crossbridge helices. In addition the necessary presence of three orientations in the three stranded arrangement gives an overall intensity distribution in its optical diffraction pattern which is not six-fold. However a 6-fold appearance was in fact observed in optical diffraction patterns from appropriate electron micrographs of frog sartorius muscle.

If the thick filament backbones maintain the relative rotational register apparent in the bare region , throughout the bridge region, and this backbone is simply related to the rotational orientation of the crossbridge helices, then from the observed bare region lattice it was concluded that either;

(i) The crossbridge helices are not three stranded and so two or four stranded crossbridge helices are arranged

on the regular crossbridge superlattice proposed by Huxley and Brown.

or (ii) The crossbridge helices are three-stranded and the crossbridge superlattice does not have the perfect symmetry in which adjacent filaments are rotated by 40°. Instead two rotations 60° (or 180°) apart occur.

The weight of evidence in favor of a three-stranded crossbridge helix clearly supports the second of these conclusions and with two filament orientations the bare region lattice in electron micrographs of frog sartorius muscle was shown to be defined ,with minor violations, by two "no-three-alike" rules. The first of these (Rule 1) states that no three mutually adjacent filaments in the hexagonal A-band lattice can have identical orientations; and it alone could account for the main features of the bare region appearance. The second less rigid rule (Rule 2, Luther and Squire, 1980) states that no three successive filaments along directions of the form <10> in the hexagonal A-band lattice can have identical orientations.

It was demonstrated (Luther and Squire, 1980) that the dihedral point group symmetry 32 of the myosin filament in the plane of M1 means that M-bridges from adjacent thick filaments at M1 could interact in one of two ways, termed "like" and "unlike" interactions. If "like" interactions are maximised between adjacent filaments it is possible for two out of every three mutually adjacent thick filaments to have this type of interaction. Thus Rule 1, which prevents three mutually adjacent thick filaments from having identical orientations and therefore identical interactions, follows directly from this consideration of symmetry. On the alternative assumption that "unlike" are

preferred it is then possible for every filament to have this type of interaction with its neighbouring filaments. This accounts for the simple lattice of filament orientations in the bare region of fish muscle (Franzini-Armstrong and Porter, 1964; Pepe, 1971; Luther, 1978) in which all filaments have identical orientations and presumably identical interactions exist between adjacent filaments.

The two types of M-bridge interaction predicted by this scheme were revealed at the M4 (or M4') level of M-bridges in bonyfish and frog sartorius muscles (Luther et al, 1981). In fish the M4-bridges show two types of interaction site. The bridges attach at the tips of the triangular filament backbone or at a "near-tip" site. All filaments show the same "tip/near-tip" M-bridge interactions with neighbouring filaments corresponding to the envisaged "unlike" type of interaction.

In frog sartorius muscle the predominant interaction at M4 is between two filament tips or two filament sides corresponding to the "like" interactions which give rise to Rule 1 for the generation of the superlattice. As further confirmation the same features of the bare region superlattice were evident in the actual arrangement of M-bridges at M4.

Thus the M4 M-protein interactions in fish and frog muscle account for their respective simple lattice and superlattice arrangements (Figure 1.5.4) of myosin filaments without consideration of the M1 M-protein arrangement at M1. Since all vertebrate types so far studied in longitudinal cryosections have high density at M4 and M4' (Sjöström et al,unpub.) whereas M1 may be absent (e.g. type I fibres of rat M.soleus; Sjöström and Squire, 1977) it has been suggested that M4 M-proteins are

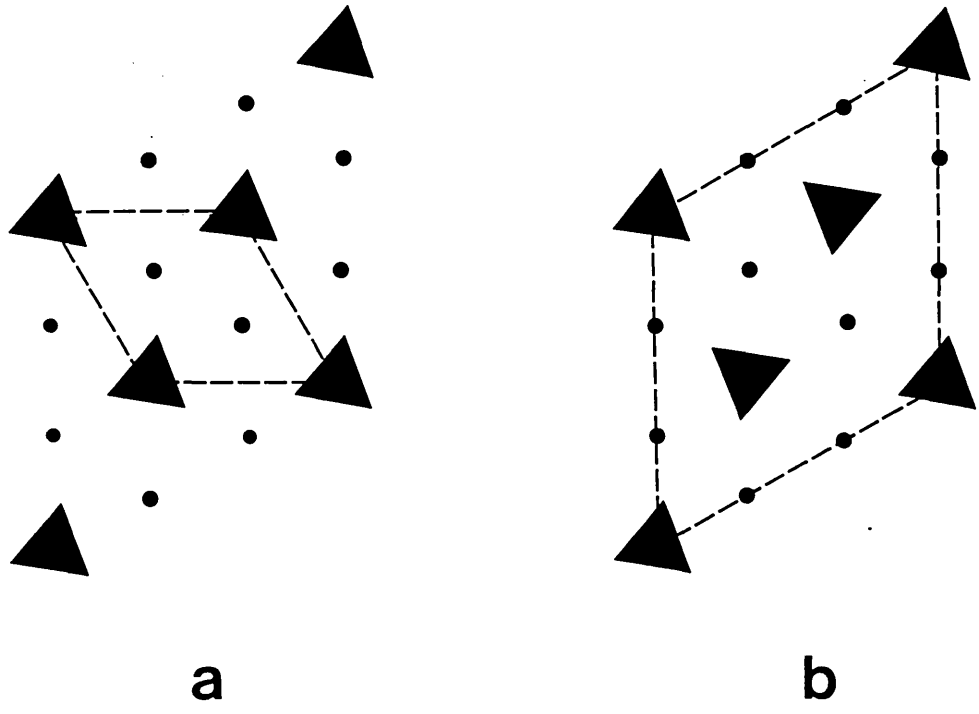


FIGURE 1.5.4 Diagram of the appearance of a transverse layer 143Å thick in the bare-zones of (a) fish muscle A-bands and (b) frog muscle A-bands. The dotted line in (a) shows the simple lattice unit cell of thick filament backbones (represented by filled triangles) in fish muscle. In (b) the superlattice unit cell is shown by a dotted line. The small filled circles represent the actin filaments (after Luther and Squire, 1980).

primarily responsible for determining the symmetry of the A-band with the M1 proteins playing a secondary role (Luther et al, 1981).

Luther et al (1981) were also able to show that the whole myosin filament has the dihedral point group symmetry 32. By studying the change in orientation of thick filament profiles across the M-band in fish muscle, the M-bridges at M4 (and M4') and the three-fold kidney-shaped profile at M6 (and M6') were shown to change "hand" across the M-band. The unique orientation of the myosin filament in the fish muscle filament lattice has also enabled three-dimensional reconstruction of the fish M-band to be carried out (Luther and Crowther, 1984; Crowther and Luther, 1984) by combining images of specimens tilted in the electron microscope (DeRosier and Klug, 1968). This reconstruction confirmed the M-band symmetry and the 32 symmetry for the myosin filament as a whole (Luther et al, 1981).

Because of this symmetry, the six M1-bridges can be considered as one set of three bridges originating from myosin tails pointing in one direction in the M-region of a thick filament and another set of three bridges originating from tails pointing in the opposite direction. If adjacent filaments interact through sets of M1-bridges from tails pointing in the same direction this corresponds to a "like" interaction and when maximised generates the superlattice (Figure 1.5.5). If adjacent thick filaments interact through sets of M1-bridges pointing in the opposite direction , corresponding to an "unlike" interaction, and these are maximised, the simple lattice is formed. Apart from this change in hand the filament profiles in frog and fish muscles also show a 40^{o} change in orientation across the M-band.

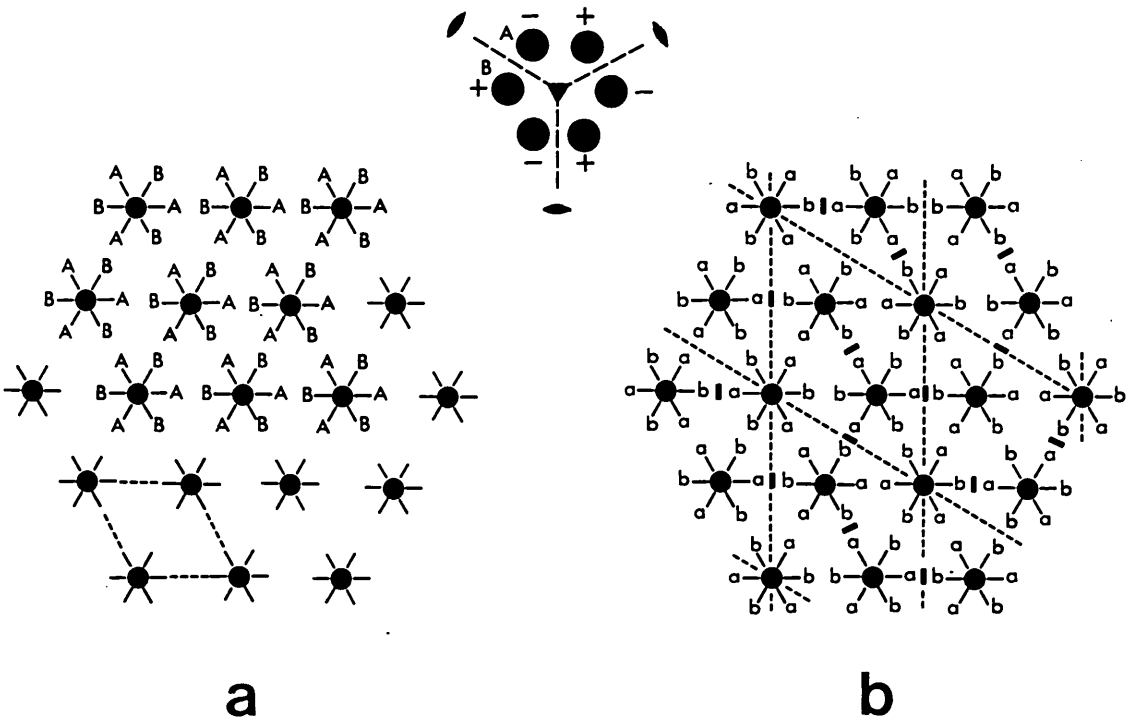


FIGURE 1.5.5 Representation of the possible relationship between the M-band structures and the relative orientations between myosin filaments in the lattices of fish (a) and frog (b) muscles. Inset is shown the 32 point group symmetry of the myosin filament, at its centre, viewed down its long axis. This symmetry for the myosin filament was predicted from an analysis of the M-band structure by Luther and Squire (1980) and eventually demonstrated by 3-D reconstruction of the fish M-band (Luther et al, 1981, 1982). (Courtesy of Drs.P.K.Luther and J.M.Squire).

Pepe (1971) obtained a value of 60° for the fish bare region.

The significance of these two types of arrangement, especially if the crossbridges are aligned in roughly the same direction indicated by the filament profiles in the bare region, i.e. 10° away from the $10\bar{1}$ rows of the hexagonal lattice, is that a pseudo-equivalence of actin environments exists. Whereas in fish muscle each of the actin filaments may be approached at one 143Å level by three crossbridges, the superlattice arrangement in frog ensures that no more than two crossbridges occur at a particular level thus allowing each crossbridge to interact with one of the two strands of the actin helix (Luther and Squire, 1980).

1.5.2.C. Reinterpretation of the Myosin Layer Line Sampling in Terms of the Statistical Superlattice

In view of the statistical crossbridge superlattice evident from the above electron microscope studies, Squire (1981) sought to reinterpret the myosin layer line sampling of the low-angle X-ray diagram from frog sartorius muscle. The argument, in brief, is as follows.

For a superlattice formed by three-stranded filaments with one of two orientations 180° apart there are no selection rules for the absence of lattice transform peaks along the layer lines. The lattice transform peaks will only be observed at positions where the rotationally averaged transform for a single myosin filament is also finite. In fact the $11\bar{2}$, $20\bar{2}$, $21\bar{3}$, $30\bar{3}$, $22\bar{4}$, $31\bar{4}$, $40\bar{4}$ and $32\bar{5}$ reflections (indexing on the 713Å superlattice unit cell) occur at least in part in the same region as the first layer line peak (Figure 1.5.6).

Each reflection will be broad because the superlattice only appears in domains a few unit cells in width and overlap of the reflections will occur to give the summation of intensities in Figure 1.5.6(c). Those reflections with a multiplicity of 12, the $21\bar{3}$, $31\bar{4}$ and $32\bar{5}$ will also have twice the weight and thus intensity of the other reflections which have a multiplicity of 6, because there are twice the number of crystal planes contributing to them.

If the first layer line peak is superimposed upon this summation three main peaks are enveloped by it which occur in exactly the same positions as those observed by Huxley and Brown (1967).

Thus no selection rules need be applied to account for the observed sampling and other features of the sampling are consistent with the statistical superlattice. For example the sampling effects are slightly different in different muscles and this could arise from different statistical populations of the two filament orientations in different muscles. The intensities and positions of the peaks are also variable (peaks were observed at up to 3% from their predicted spacings) and since the peaks on the first layer line are more diffuse than those on the equator they are not consistent with an extensive superlattice.

The two orientations of 9/1 crossbridge helices on this lattice would be expected to give superlattice peaks on the equator, but no such peaks were observed. However since the rotational symmetry of this helix is only evident from the ninth order Bessel function on the equator, this is beyond the radial distance at which even very weak equatorial peaks from the simple lattice were recorded. Thus the statistical superlattice accounts

satisfactorily for all of the X-ray diffraction data obtained so far from frog sartorius muscle.

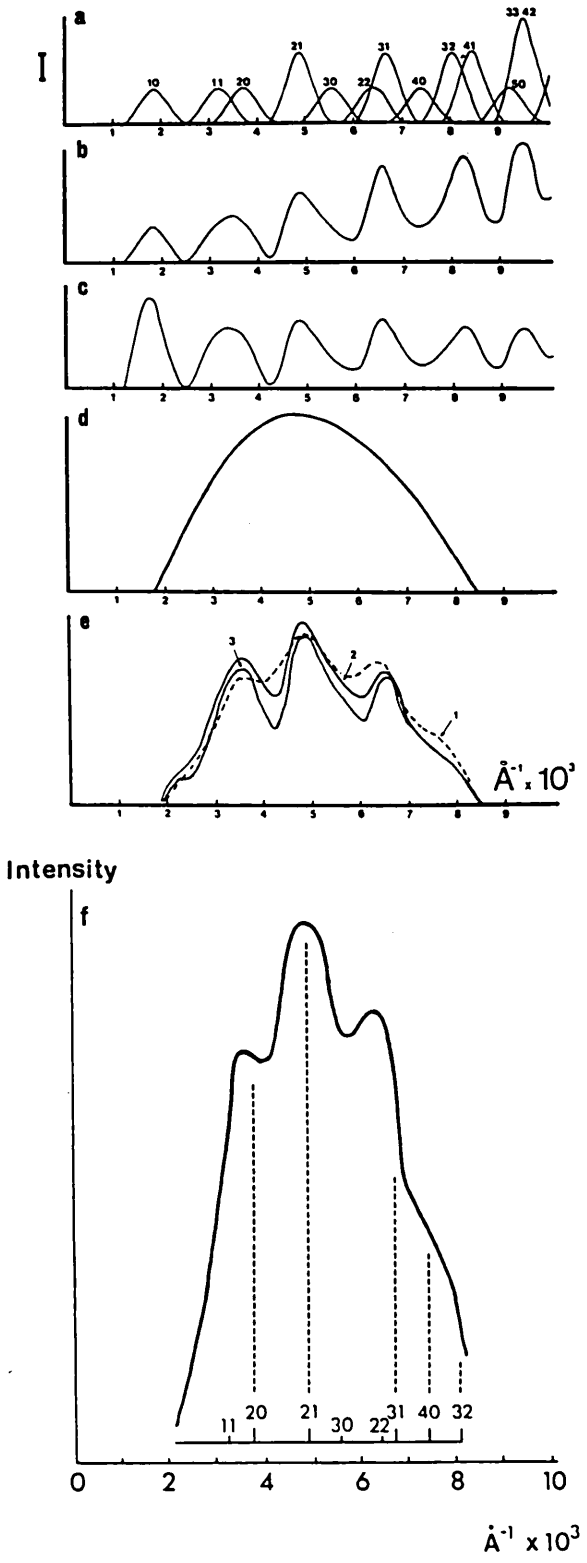


FIGURE 1.5.6 Interpretation of the first myosin layer line sampling, observed for frog sartorius muscle (Huxley and Brown (1967), in terms of the statistical superlattice. (b) The sum of the reflections in (a) from the superlattice unit cell (broadened since the superlattice is ordered over a few unit cells). (c) The result of applying the Lorentz factor to the profile in (b). (e) This is multiplied by the first layer line peak from a single myosin filament in (d), with either 50% (unbroken line) or 75% (bold line) of the unsampled filament peak in (d) added, which are compared with the observed first layer line profile (broken line and (f)). (Courtesy of Dr.J.M.Squire)

CHAPTER 2 : MATERIALS AND METHODS

2.1. DISSECTION AND ANATOMY 88

2.1.1. Dissection of Plaice Fin Muscle. 88

2.1.2. Dissection of Frog Sartorius Muscle. 89

2.1.3. Fibre Arrangement in the Plaice Fin Muscle. 99

2.1.4. Processing of the Whole Plaice Fin Muscle for Thick (15μm) sectioning. 100

2.2. OPTICAL DIFFRACTION STUDIES 104

2.2.1. Cryosectioning. 104

2.2.2. Copying of Electron Micrographs for Optical Diffraction Studies. 105

2.2.3. Optical Analysis. 106

2.2.4. Theoretical Background. 106

2.2.5. The Diffractometer Constant. 107

2.2.6. The Optical Diffractometer. 107

2.2.7. The Mask Function. 109

2.2.8. Measurement of Spacings and Relative Intensities from Optical Diffraction Patterns. 109

2.2.9. Image Analysis. 113

2.3. X-RAY STUDIES 115

2.3.1. Introduction. 115

2.3.2. The X-ray Generator. 116

2.3.3. The Curved Crystal Monochromator. 116

2.3.4. The Mirror Bender. 120

2.3.5. The 30cm Specimen to Film Camera. 124

2.3.6. The 80cm Specimen to Film Camera. 128

2.3.7. Alignment of the X-ray Camera. 129

2.3.8. Mounting the Muscles in the Specimen Cell. 132

2.3.9. Plaice Ringer Solution. 133

2.3.10. Measurement of Sarcomere Length. 136

2.3.11. Measurement of Spacings. 137

2.3.12. Determination of Reciprocal Lattice Coordinates. 137

2.3.13. Relative Intensity Measurement. 138

2.3.14. X-ray Film. 141

2.4. COMPUTER MODELLING 142

2.4.1. C-zone Modelling. 142

2.4.2. Analysis of the Equatorial Diffraction Data. 143

2.4.3. Computer Modelling of the Fish Resting Crossbridge Arrangement. 145

CHAPTER 2 : MATERIALS AND METHODS

2.1. Dissection and Anatomy.

2.1.1. Dissection of Plaice Fin muscle.

Plaice (Pleuronectes Platessa) fish were obtained from U.M.B.L.,Isle of Cumbrae. These were kept in aerated tanks in a cold room at about 4°C until the time of dissection. Since the fish were used within two to three weeks of arrival at the laboratory, and were kept at this low temperature, it was not necessary to feed them.

The sizes of the fish supplied were in the range of 6 to 10 inches in length but because the Plaice's dorsal and ventral fins each comprise about 50 fin muscles, increasing in length from the fish tail, fishes outside this range of lengths were often usable. However to obtain about a 1mm thickness of muscle, optimum for X-ray studies, dorsal fin muscles within the region of the 10th muscle from the tail end of a fish 7 to 10 inches long were used. Generally such muscles were only just long enough to give a region of parallel fibres wide enough to fill the width of the X-ray beam of 6 to 7mm in the X-ray cameras used in this work. This constraint could only be avoided in the very infrequent cases when fish larger than this were fortuitously lean.

The fish was stunned before making a first cut with a large pair of tailors scissors to destroy the fishes brain (Figure 2.1(b)). Access to the spinal channel of the fish backbone for subsequent pithing was then attained by making a second cut to remove the head.

The dorsal fin muscles were used for the sake of consistency although they were visually indistinguishable from

those of the ventral fin. These muscles are adjacent to the skin but not easily accessible by removing it. The series of muscles on the darker pigmented side of the fin could be more clearly distinguished against this dark background so these were approached from the opposite white side of the fish (Figure 2.3). The potentially most damaging stage of the dissection occurs when removing the muscles from the horizontal layer of bone/cartilage which divides the fin (Figure 2.3(b) to (c)). Each fin muscle is attached by a single tendon to the fin bone but two to five tendons of different size attach the other end of the muscle to the skin.

It was useful to support the muscle while removing the surrounding unwanted tissue by leaving the skin intact until the final stage of the dissection. The muscle was then carefully detached from the skin using a carefully blunted seeker (Figure 2.5(b) and (c)). This can be done without damaging the muscle surface (Figure 2.8). In order to mount the muscle in the cells used for X-ray studies it was preferable to trim the fin bone attachment (Figure 2.6(b),(c)). Since the tendons at this end of the muscle pass around the back of this joint, damage to them can be avoided (Figure 2.8).

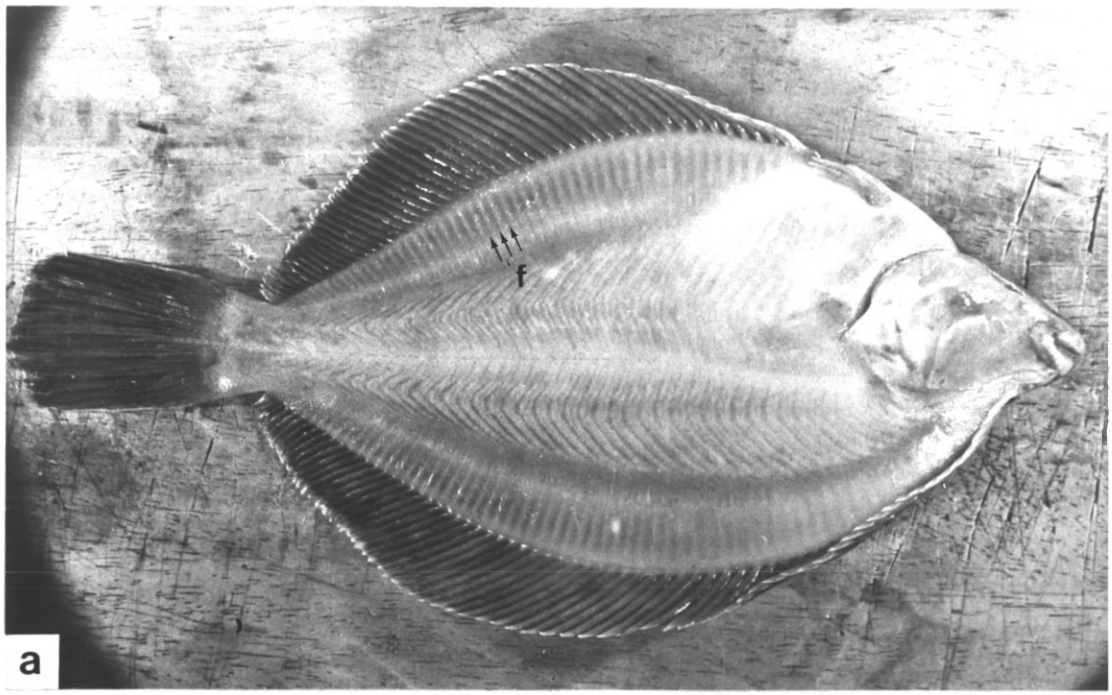
A cold fibre-optics light source was used to illuminate the dissection and cold Plaice Ringer (see 2.3.9) was frequently poured onto the preparation throughout the 45 to 60 minute duration of the dissection.

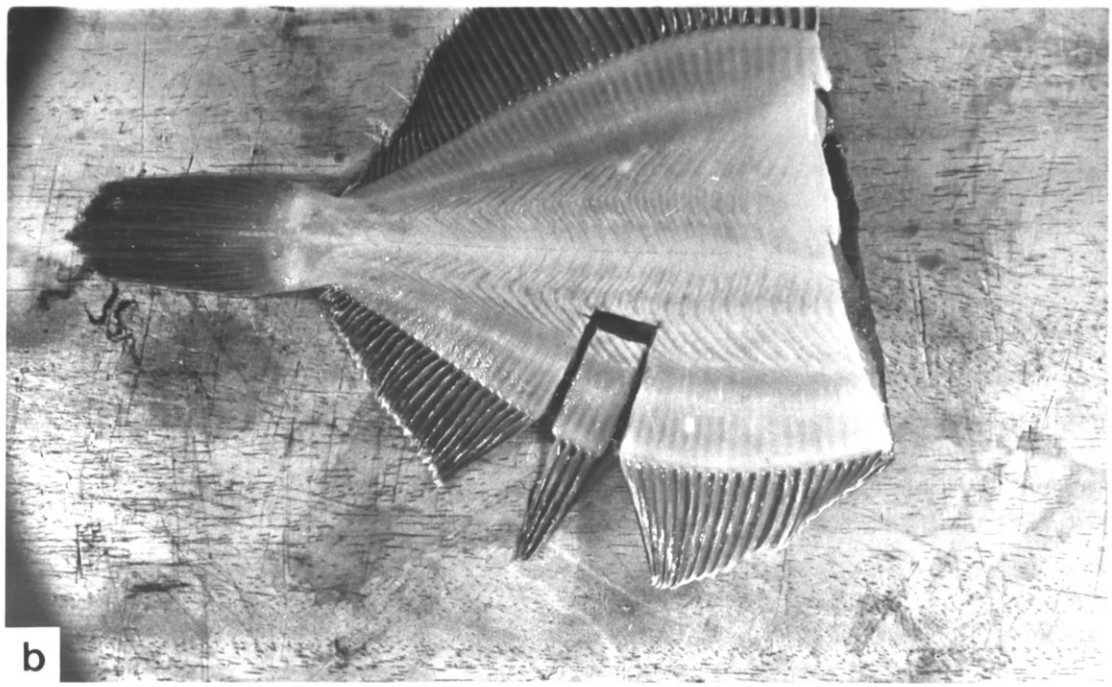
2.1.2. Dissection of Frog Sartorius Muscles.

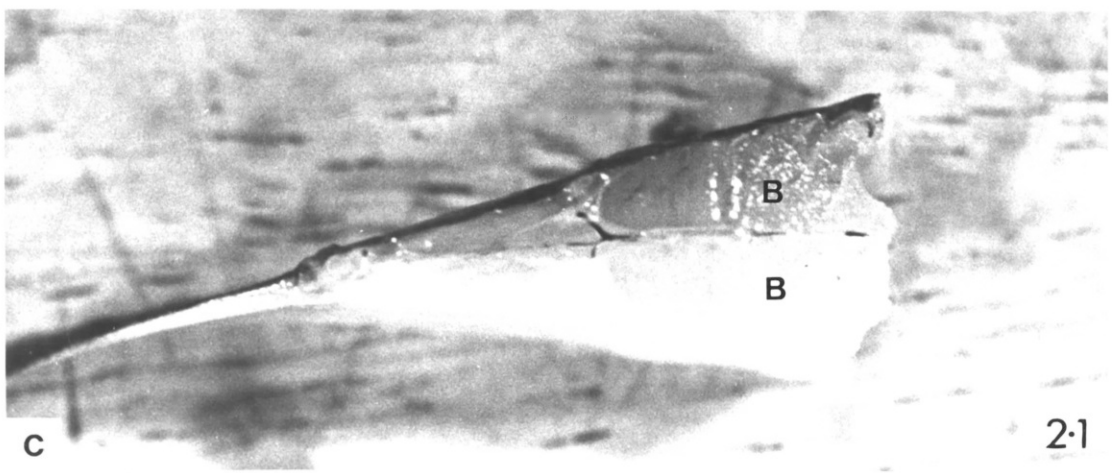
Frogs (Rana temporaria or Rana pipien) about 4" to 5" long (Phillip Harris Biological Supplies Ltd) were kept in a glass tank at room temperature and fed on crickets until the time for

FIGURES 2.1 TO 2.7 Figures 2.1 to 2.7 illustrate the dissection of the Plaice fin muscle. In Figure 2.1(a) numerous fin muscles (f) are cut from the fish including about 1cm of the body muscle (B, Figure 2.1(c)). A similar arrangement of the body and fin muscle occur either side of a layer of bone/cartilage and the dissection of the fin muscle adjacent to the darker pigmented skin is normally easier in that the translucent muscle tissue can be seen more clearly against it. In Figure 2.3(a) the muscle tissue on the opposite side of the cartilaginous layer is removed. Having removed the body muscle from the dark skin side (Figure 2.3(b)) the layer of cartilage adjacent to the muscles of interest is then pinned down (Figure 2.3(c)). With the flap of skin supporting the fin muscles held with tweezers (or better still fingers) , a scalpel blade can be passed between the surface of the muscle tissue and the surface of the skeleton. The blade surface is turned slightly downwards during this operation to avoid cutting into the muscle surface. The knife blade is taken as near to the point of attachment of the fin muscle to the fin bone (Figure 2.2(b)) as possible during this cut. The knife can then be turned downwards away from the muscle, to cut through and remove the residual cartilage layer (Figure 2.4(a)). Residual connective tissue on the surface of the fin muscles (Figure 2.4(b)) can then be simply cleared from the surface with a seeker. A particular muscle is then separated (Figure 2.4(c)) ensuring that the numerous tendons to the muscle, which attach to the skin, are not damaged. A seeker (carefully blunted) can be teased between the muscle and the skin (Figure 2.5(a) to (c)), and a "flap" of connective tissue enveloping the "skin end" of the muscle removed to produce a more usable length

of muscle (Figure 2.5(d)). The underlying skin is cut at both ends of the muscle (Figure 2.6(a)) but left protecting the lower surface of the muscle from the dissecting board surface while the bulky fin bone is trimmed (Figure 2.6(d) to (d)); Figure 2.7(a)) so that this end of the muscle can be satisfactorily tied or, as was usually the case, clamped into the specimen cell. A small hole was pierced into the flap of skin at the other end of the muscle, taking care not to disrupt the tendons, through which cotton was threaded and tied into the specimen cell.







2·1

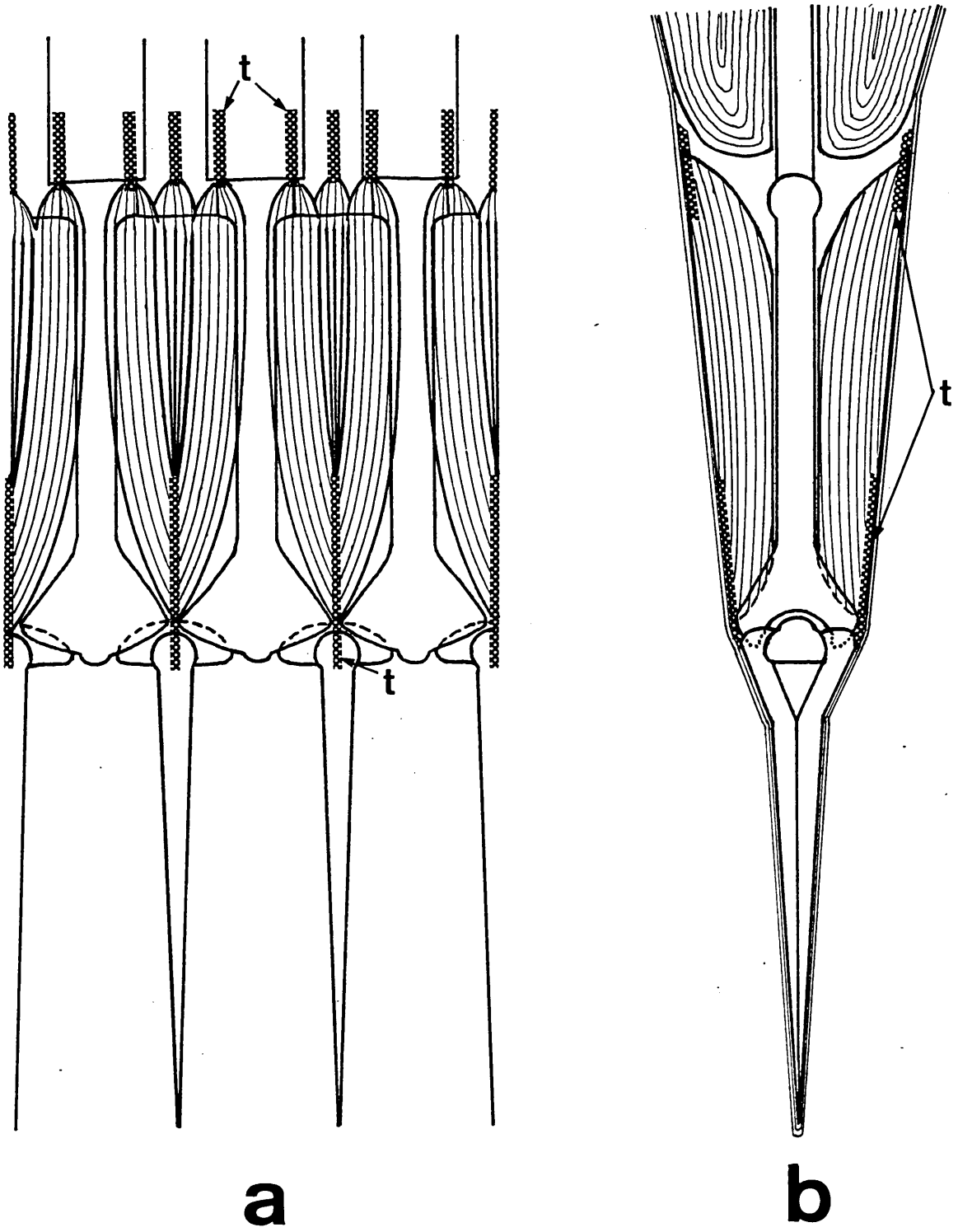
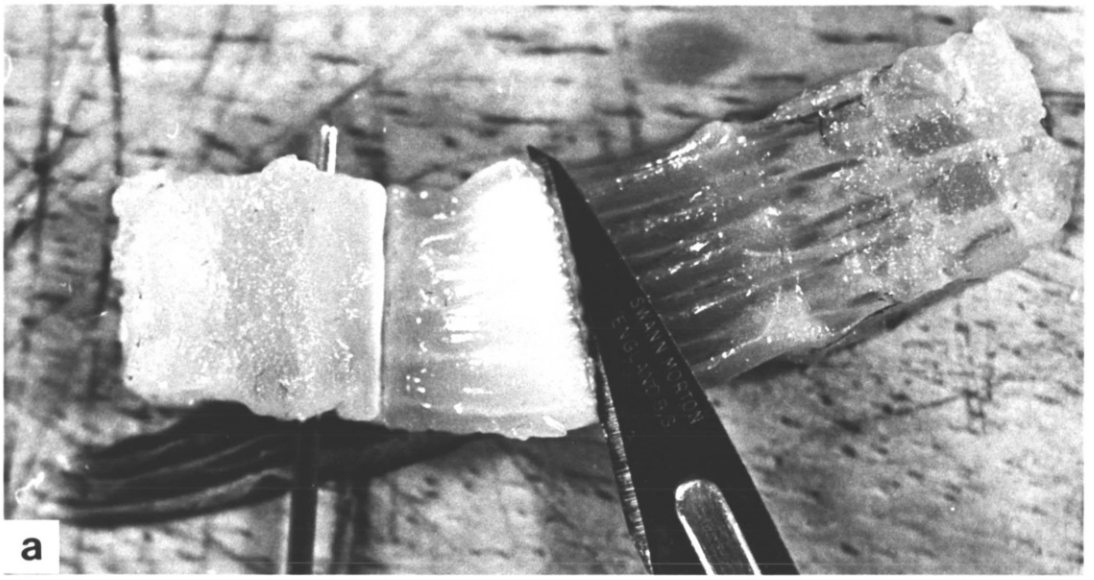
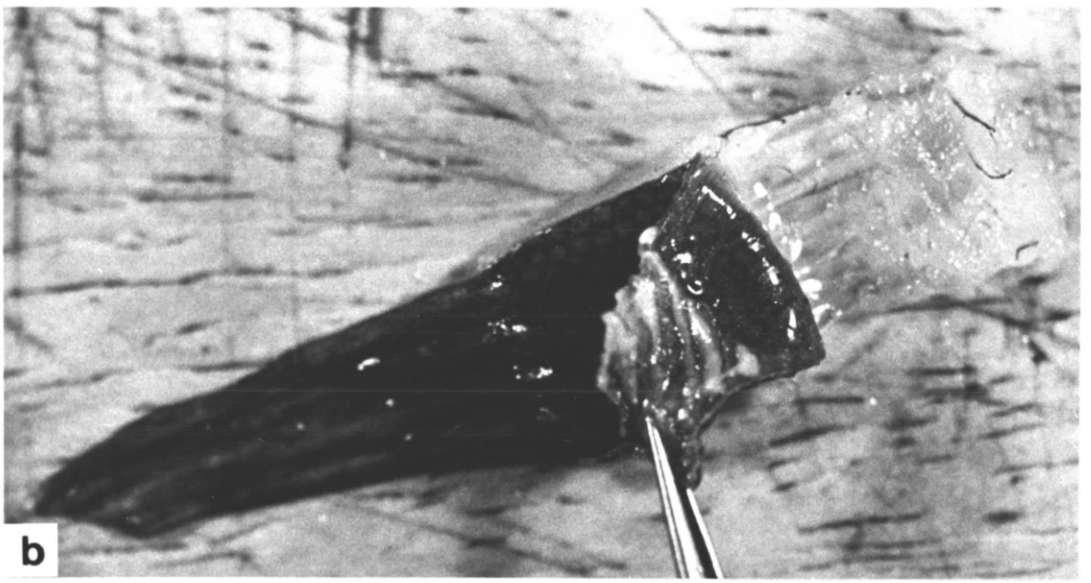
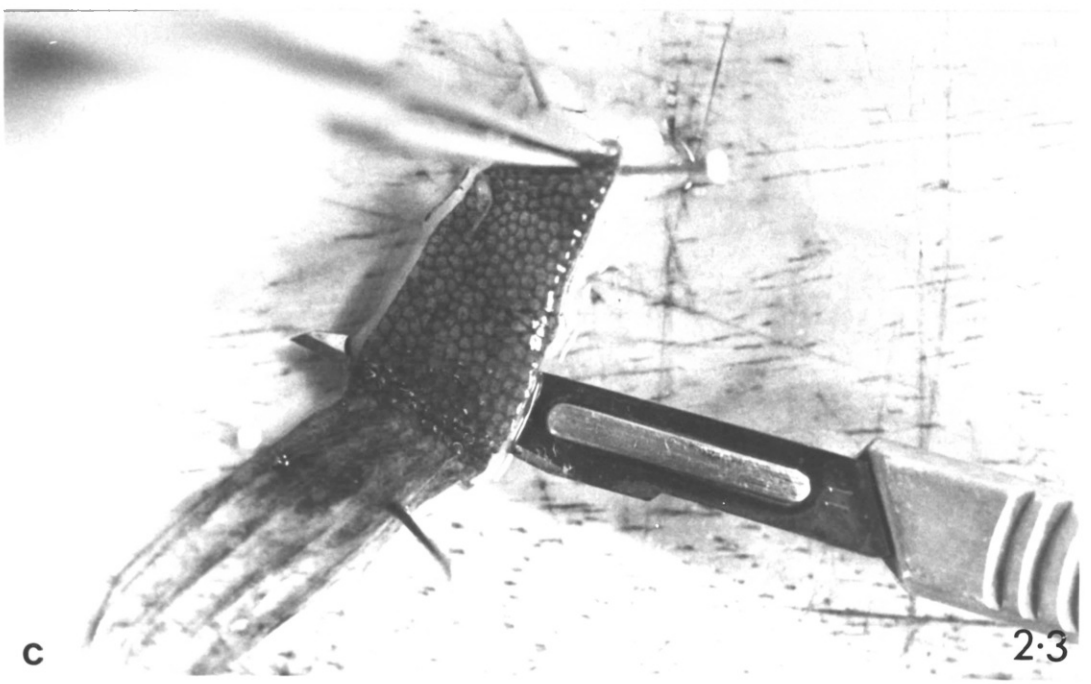


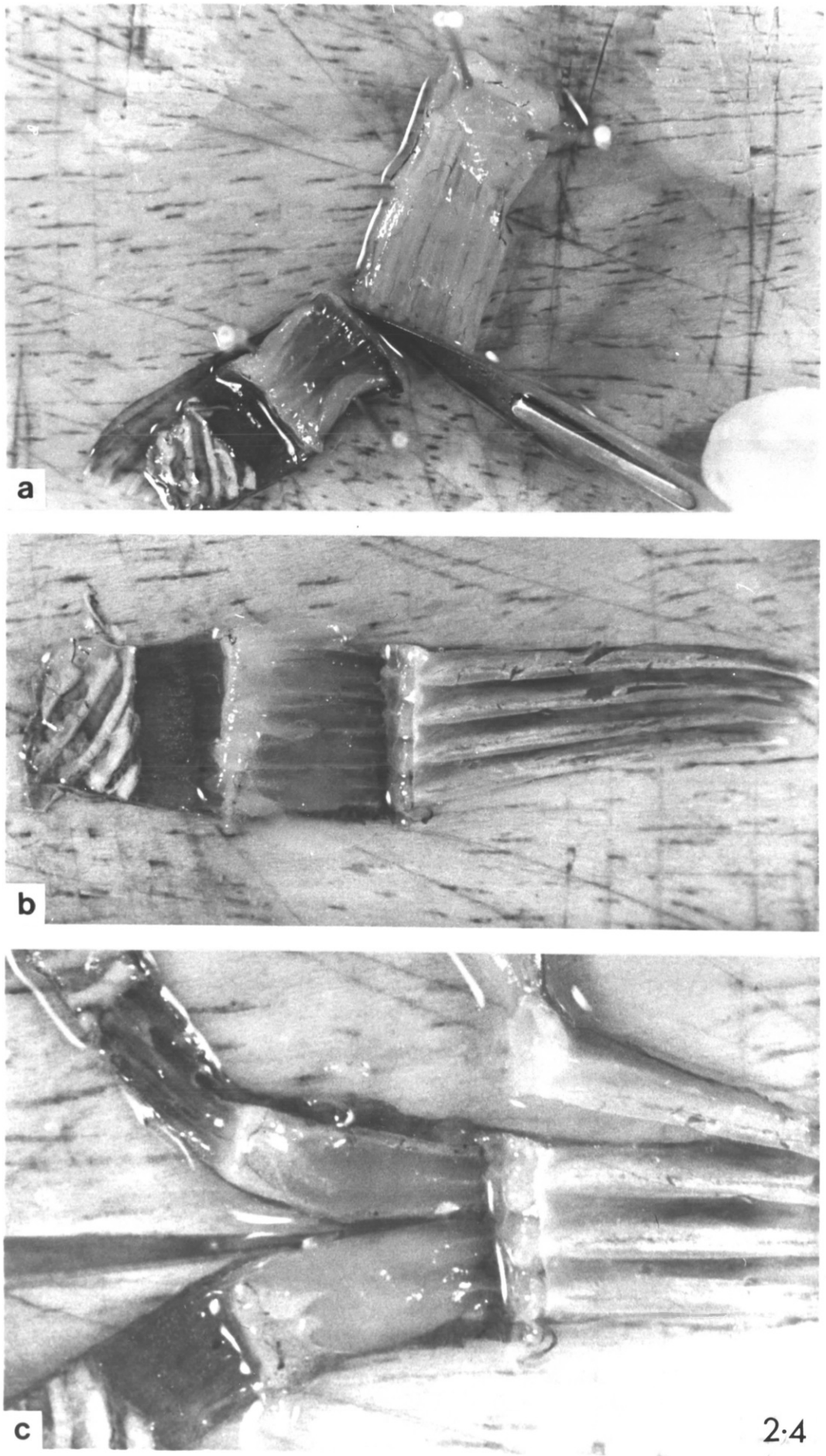
FIGURE 2.2 Diagram of the anatomy of the Plaice fin muscle showing its attachment by a narrow tendon (t) to the fin bone (f), at one end of the muscle, and by numerous tendons to the skin at the other end (b)



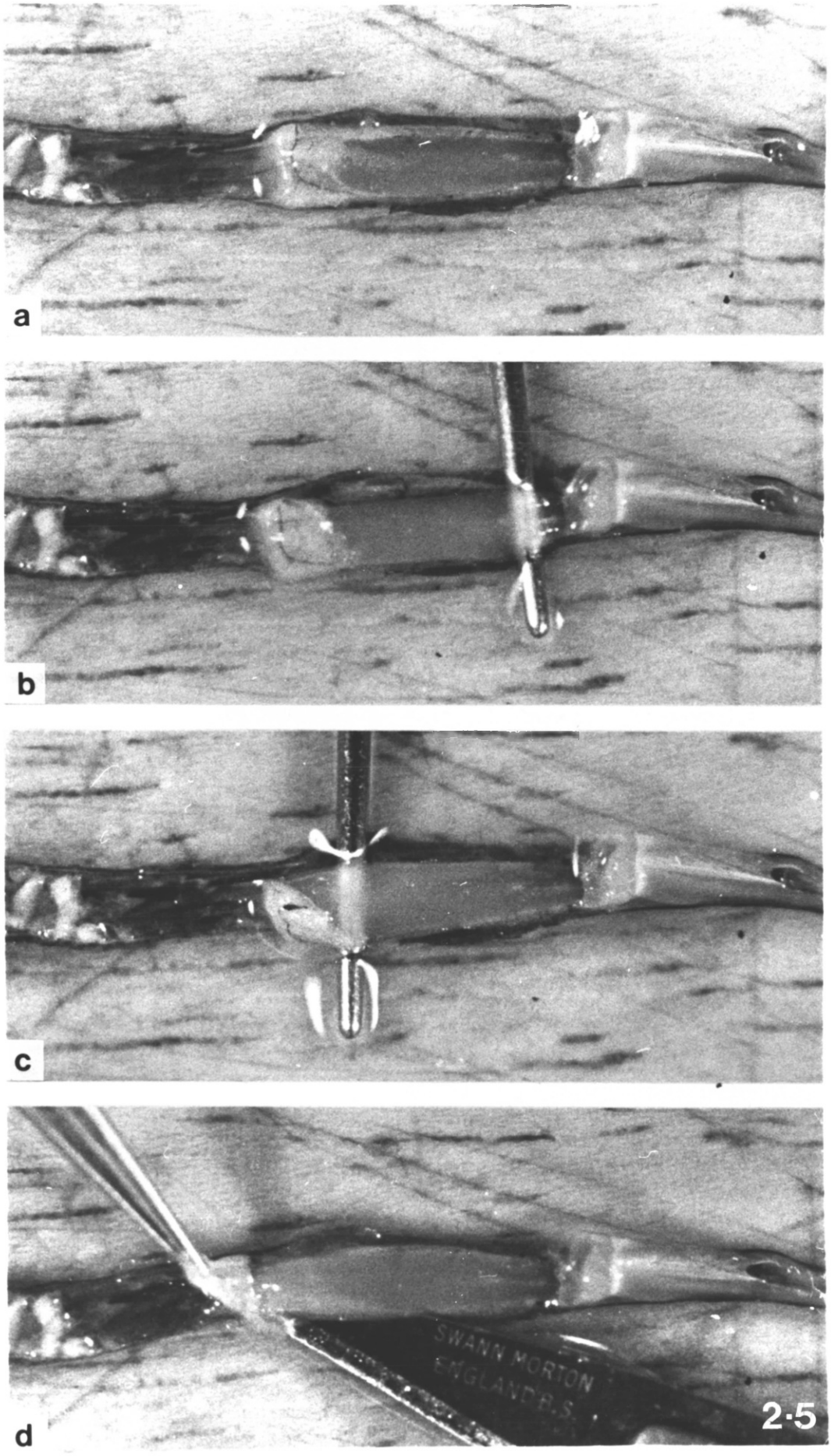


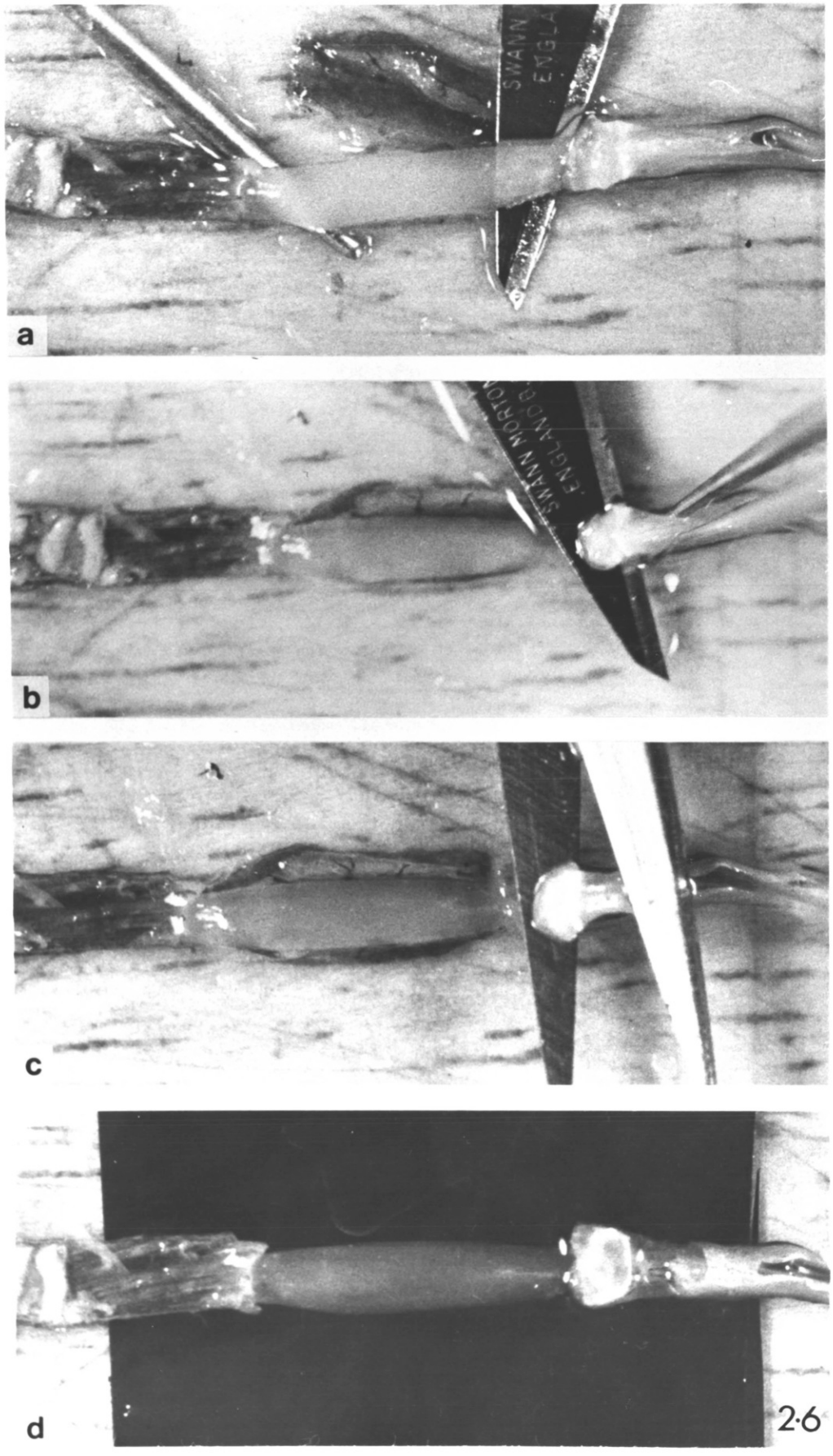


2·3

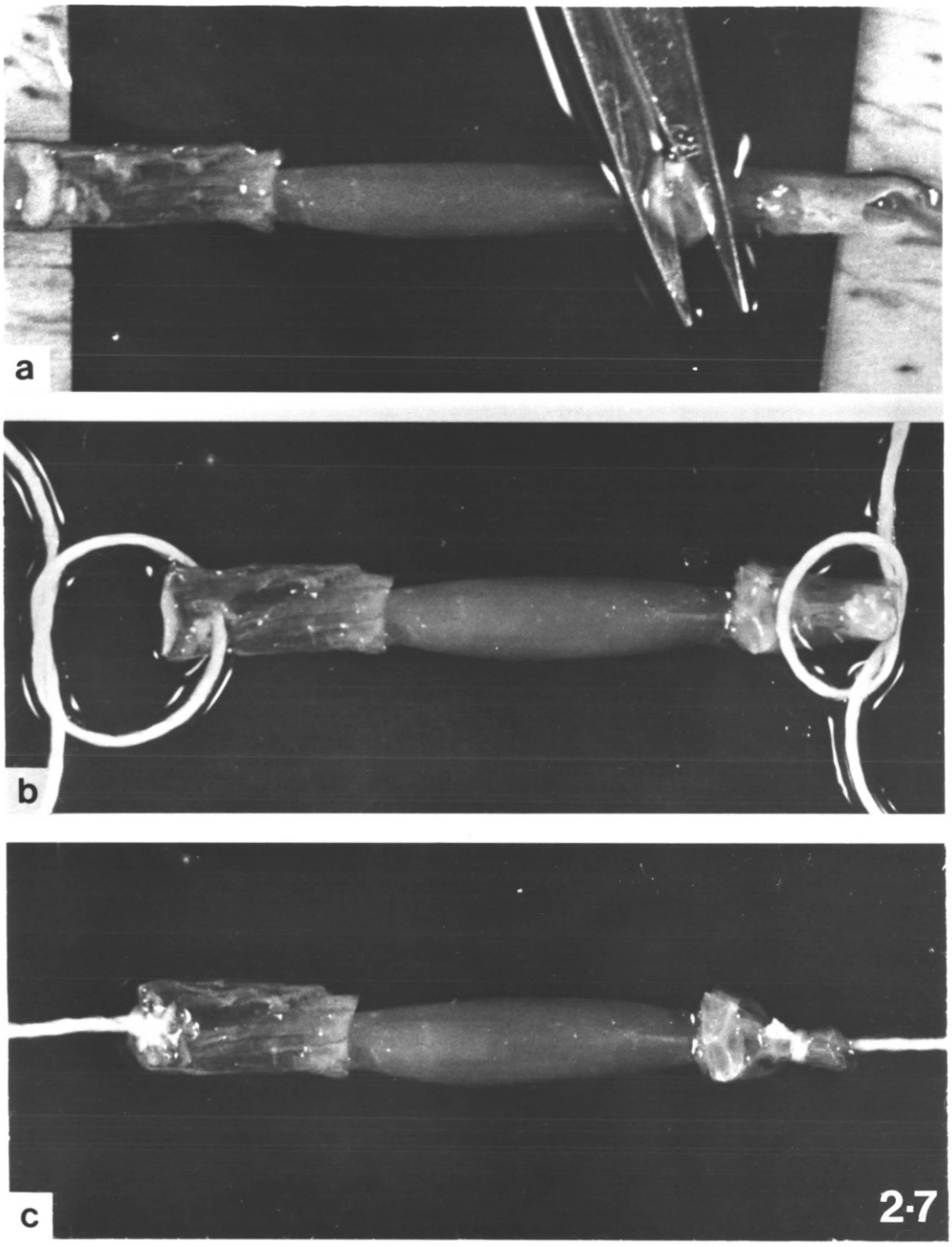


2·4


a
b
c
SWANN MORTON
ENGLAND B.S.
d
2·5



2·6


a
b
c
2·7

dissection.

Frogs were killed by decapitation after stunning them. The sartorius muscle lies adjacent to the skin, extending from the pelvic girdle to the knee joint. In contrast to the Plaice fin muscle, the skin can be easily peeled away from the surface of this muscle. Viewing through a binocular microscope, the connective tissue between the sartorius muscle and the adjacent and underlying muscles was cut. This was usually done by teasing a carefully blunted seeker between these muscles and cutting onto the seeker surface with a scalpel. This made it easier to distinguish these tissues which even under appropriate lighting conditions are sometimes not well defined. Cotton was then tied around the tibial tendon which was then severed from the bone.

2.1.3. Fibre Arrangement in the Plaice Fin Muscle.

The sartorius muscle of the frog is attached by a relatively wide tendon at the pelvic bone but the fibres converge to a narrow tibial tendon at the knee. The length of this muscle, which with the present source of frogs was 2cm to 3cm long for a thickness of about 1mm, ensures that practical X-ray beam widths in low-angle X-ray cameras can illuminate a length of the muscle in which fibres are parallel to within about 1^{o}.

The Plaice fin muscle is similarly attached by a number of flat tendons to the skin with the fibres of the muscle converging to a single narrow tendon at the fin joint. However it was apparent during dissection of this muscle that the arrangement of fibres in this latter portion of the muscle is complex thus restricting the proportion of the length of the muscle which can be used for X-ray diffraction studies.

In order to obtain a clearer picture of the arrangement of

fibres along the length of the muscle the cross-sectional appearance of the whole muscle was studied along its length. It was evident from dissection and examination of fin muscles along the entire length of the fish that the tendon arrangement at the body-end of the muscle was variable and gave rise to different numbers of segments within the whole muscle. Initially it was intended to tease the whole muscle into these segments which would then provide better specimens for X-ray diffraction studies. For this to be performed without damage to the membrane of the muscle it was clearly necessary to obtain a better understanding of the muscles anatomy.

2.1.4. Processing of the Whole Plaice Fin Muscle for Thick (15 μm) Sectioning.

Plaice fin muscles were dissected and mounted onto formers with a small amount of tension in the muscle. It was particularly important that formers were used which allowed contact of the whole muscle with the processing media for uniform preservation throughout the muscle cross-section.

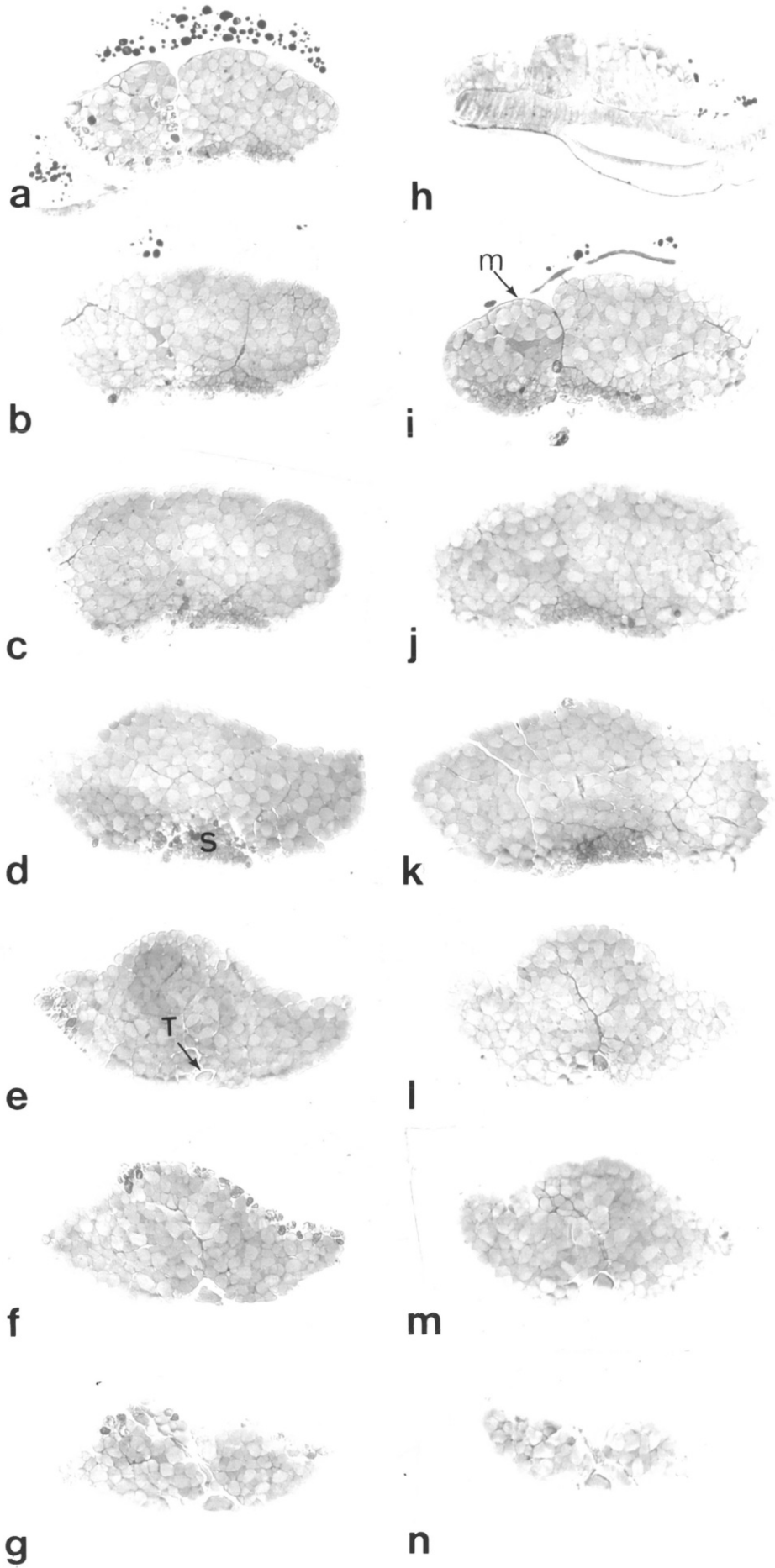
Standard electron microscopy processing and embedding procedures were used with extension of the normal times for exposure of the whole muscle to the processing media. Muscles were fixed in 2.5% glutaraldehyde solution at 4°C for 6 hours, washed in three changes of buffer (1/4, 1 and 1 hour) and fixed and post-stained in 1% osmium tetroxide for 2 hours at room temperature. The muscles were then removed from formers, rinsed for 1 hour then 7 hours in distilled water, and dehydrated in an acetone series of 25%, 65%, 95% and 100% (twice) for 1/2 hour time intervals. Following 1/2 hour exposures to 50%, 67% and 75% epon in acetone the whole muscles were infiltrated in 100% Epon

resin for 6 to 8 hours and cut into 3mm long cylindrical sections before final embedding and curing overnight.

The specimen blocks were sectioned using a Reichert microtome. Sections about 15μm thick gave satisfactory resolution of the fibre arrangement. These sections were transferred to drops of Millipore filtered deionized water on heated glass slides to stretch and flatten the sections. The excess water was partially absorbed from the slides with tissue. DPX and coverslips were finally applied to the sections which were adequately contrasted by the processing in osmium tetroxide.

Although simply staining with osmium tetroxide does give some contrast of the membrane structure ('m', Figure 2.8(i)) it was unsuccessful in trying to establish whether the segmented arrangement observed at the "body-end" of the muscle (Figure 2.8(a) to (c) and (h) to (j)) was maintained throughout the whole length of the fin muscle. Toluidine blue staining of these resin sections (and more specific staining of frozen and wax sections) was embarked upon but so far without success. It can be seen from Figure 2.8 that a tendon passes along the centre of the muscle surface, for about one quarter to one third of its length, which is adjacent to the skin ('t', Figure 2.8(e) to (g) and (l) to (n)) and attaches to a small strip of muscle ('s', Figure 2.8(d)) which has a slightly different colouration compared to the bulk of the muscle. This small portion of the whole muscle extends along the remaining length of the muscle and although this surface appears less intact than the opposite surface this may be a result of slightly different fixing characteristics of this strip. During the dissection of the muscle the surface appears smooth and undamaged on either side of the muscle.

FIGURE 2.8 Thick (15μm) sections of Plaice fin muscles. (a) to (g) and (h) to (n) show serial sections through two fin muscles at approximately 1.5mm intervals along the length of the muscle, At the "body-end" of the muscle,(a)or (h),the fibre arrangement is different in the two examples and it was apparent during the dissection that there are slight differences in the tendon arrangements at this end of the muscle along the whole length of the fish. In these sections the surface of the muscle which is uppermost in the illustration is the surface which is adjacent to the skeleton of the fish. At the end of the muscle which is attached to the fin bone ((g) or (n)) the tendon (T) can be seen to pass along the muscle to attach to a small strip of muscle (S) in (d).


a
h
b
m
i
c
j
d
S
k
T
e
l
f
m
g
n

2.2. Optical Diffraction Studies.

2.2.1. Cryosectioning.

Cryosectioning is one of the more recently developed techniques for preparing ultrathin sections of muscle or other biological tissue for electron microscopy (Sjöström et al, 1973; Thornell and Sjöström, 1975; Sjöström and Squire, 1977a). After stabilising the *in vivo* structure with a fixative the muscle tissue is frozen very rapidly to liquid nitrogen temperatures, after treatment with a cryoprotective agent or antifreeze to surpress ice crystal formation which would normally mechanically damage the tissue. The frozen muscle is then sectioned while frozen using an ultramicrotome. The ultrathin sections are then negatively stained and finally air dried before being transferred to the electron microscope.

The details of the cryosectioning method have been described fully by Sjöström and Squire (1977a). Human m. tibialis anterior tissue in a resting state was fixed for 5 to 15 minutes in 2.5% (v/v) glutaraldehyde. Cryoprotection was by treatment with glycerol 30% v/v for 30 to 60 minutes followed by rapid freezing in Freon 12 (Balzers Union Ltd) which was cooled by liquid nitrogen. Longitudinal sections from small pieces of frozen tissue were cut using the LKB cryo-kit onto a trough containing 50% glycerol or dimethylsulphoxide. The sections were negatively stained with ammonium molybdate or uranyl acetate then air dried and finally viewed in a Philips EM300 electron microscope.

2.2.2. Copying of Electron Micrographs for Optical Diffraction Analysis

Contrasty negative copies of electron micrographs of the cryosectioned A-bands were made by exposing onto Kodalith Ortho film (Kodak Ltd, type 2450). A reduced version of the electron micrograph was made since the diffractometer constant required that for a 1mm separation of diffraction spots in the optical diffraction pattern from the object, a 1mm separation of the diffracting features in the object was required.

Preparation of the copy of the electron micrograph was also subject to the following considerations;-

(i) Introducing spurious detail should be avoided during the photographic processing.

(ii) The copy must have the protein appearing clear in the film, contrasted against the opaque stain.

(iii) The copy should be "contrasty", i.e.the optical densities of the stained and unstained features must differ but to an extent in which the density profile in the original electron micrograph is not altered appreciably. It is important to ensure that the spatial frequency content of the object, and hence the higher order reflections in its optical diffraction pattern, are unaffected.

(iv) The magnification of the copy should be chosen such that the diffraction peaks have a certain minimum separation to enable the patterns to be optically filtered using masks and the spatial filtering by the reconstructing imaging lens, L_I, is reduced to a minimum.

A further problem is variation which may occur in emulsion thickness of the photographic film used to make the copy. This

would normally introduce undesirable phase variations across the laser beam wavefront. This was overcome by inserting the micrograph in an oil cell (Luther and Squire, 1978) which renders insignificant the spurious phase variation due to the emulsion.

2.2.3. Optical Analysis.

The periodicities of the stained features in the C-zones of the electron micrographs of cryosectioned human m. tibialis anterior muscle were obtained from their optical diffraction patterns and laterally smeared images as described below.

2.2.4. Theoretical Background.

If a diffraction grating with a slit separation "d" is placed at Σ_0 then beams diffracted at an angle θ from the adjacent slits (Figure 2.9) have a phase difference,

$$\delta = \frac{2\pi}{\lambda} \{ d \sin\theta \}$$

The condition for reinforcement of these diffracted beams at the transform plane, Σ_T, is that the phase difference between the beams is an even multiple (2n) of π

$$\frac{2\pi}{\lambda} \{d \sin\theta\} = 2\pi n$$

$$n\lambda = d \sin\theta$$

From Figure2.9 $\sin\theta = \sin(\tan^{-1}(D/L))$ where D is the separation of the n^{th} order spot from the optic axis of the diffractometer at $\Sigma_T$and L is the focal length of lens, L_0. Thus

$$n\lambda L = dD$$

since for small θ ; $\sin\theta = \tan\theta = \theta$. The value of the

wavelength for the laser source used is 6328Å.

2.2.5. The Diffractometer Constant

The size of the object to be used in the diffractometer, relative to that of the wavelength of the laser light source used and the dimensions of the optical bench, is an important factor in producing observable optical diffraction effects from the object which must be of a sufficient angular separation to enable optical filtering of the diffraction pattern.

The diffractometer constant, C, is a design parameter of the optical diffractometer relating the spacing of periodicities in the object, d, to the corresponding spacing of the first order diffraction peaks in the diffraction pattern;

$$C = dD = 1mm^2$$

Thus a spacing of 1mm in the object gives a 1mm separation between the first order peak and the central peak in the diffraction pattern.

2.2.6. The Optical Diffractometer

The optical diffractometer used is shown in the Figure 2.10 and illustrated in Figure 2.9(a). The laser source provides a beam of monochromatic radiation which is coherent. This fulfills the basic requirements for diffraction to occur from the object. The beam is narrow and intense but unsuitably small, approximately 1mm wide, for illuminating a region of the electron micrograph. The pinhole, p, which has a diameter of 50μm , in conjunction with the focusing lens, F, expand the beam width. The focusing lens is a short focal length microscope objective. The pinhole also cleans the beam by eliminating diffraction effects due to dust on the focusing lens.

At this stage the laser beam wavefront has been converted to a spherical front. Such a wavefront would involve crucial positioning of the object at Σ_o and so a 150cm focal length lens, L_c, collimates the beam so that a parallel beam of constant amplitude and phase across the whole aperture, M, is incident upon the object at Σ_o. The aperture M is an adjustable aperture which allows specific regions of the object to be illuminated. The plane wavefront incident upon the object becomes distorted after passing through the object and is resolved into a new set of plane wavefronts, each corresponding to a given order n = 0,±1,±2..etc., for a given spatial frequency, each travelling in a specific direction.

The long focal length objective lens, L_o which is identical to L_c with a diameter of 10cm, serves as a transform lens forming the Fraunhofer diffraction patterns of the object on the transform plane Σ_T, which is the back focal plane of L_o. In the absence of L_o the diffraction pattern would be observed on a distant screen, so L_o focuses the transform at a convenient distance from the object.

The imaging lens, L_I, projects the inverse transform of the light distributed over Σ_T (i.e. the reconstructed image) onto the image plane Σ_i. The final lens, L_p, is a microscope objective of small focal length which acts as a projector lens enlarging the reconstructed image to a more convenient size.

Those lenses which could be moved along the optical bench are indicated in Figure 2.9. This may have been necessary to focus the reconstructed image at Σ_i. A reflex camera was mounted so that it could be placed at Σ_T or Σ_i to record the diffraction pattern or the reconstructed image of the object, respectively,

onto Ilford FP4 film.

Ideal optical conditions are obtained when phase changes introduced by the lenses are identical for all beams parallel to a given direction along the optical bench. If there is a significant departure from these conditions then the most obvious effect is that a pattern without a two-fold axis of symmetry appears at Σ_1. The main causes for these aberrations are;-

(i) Defects in the lenses due either to poor quality or dust, grease..etc.

(ii) Faulty alignment of the lenses.

(iii) Departure from coherency of the illuminating system due to the quality or alignment of the pinhole.

2.2.7. The Mask Function

The presence of a rectangular aperture near the object plane means that the diffraction pattern from the object is convoluted with the diffraction pattern of the rectangular aperture, i.e. the Mask Function, in the transform plane. This mask function is particularly prominent at the central spot of the diffraction pattern and may obstruct features of interest in the diffraction pattern of the object. However the holder for the object micrograph can be rotated about the optic axis of the diffractometer thereby enabling its diffraction pattern to be rotated relative to the obstructing Mask function.

2.2.8. Measurement of Spacings and Relative Intensities from Optical Diffraction Patterns.

The spacings of meridional reflections in optical diffraction patterns were measured using a profile projector (Mitutoyotype PJ-250C). The absolute values were obtained

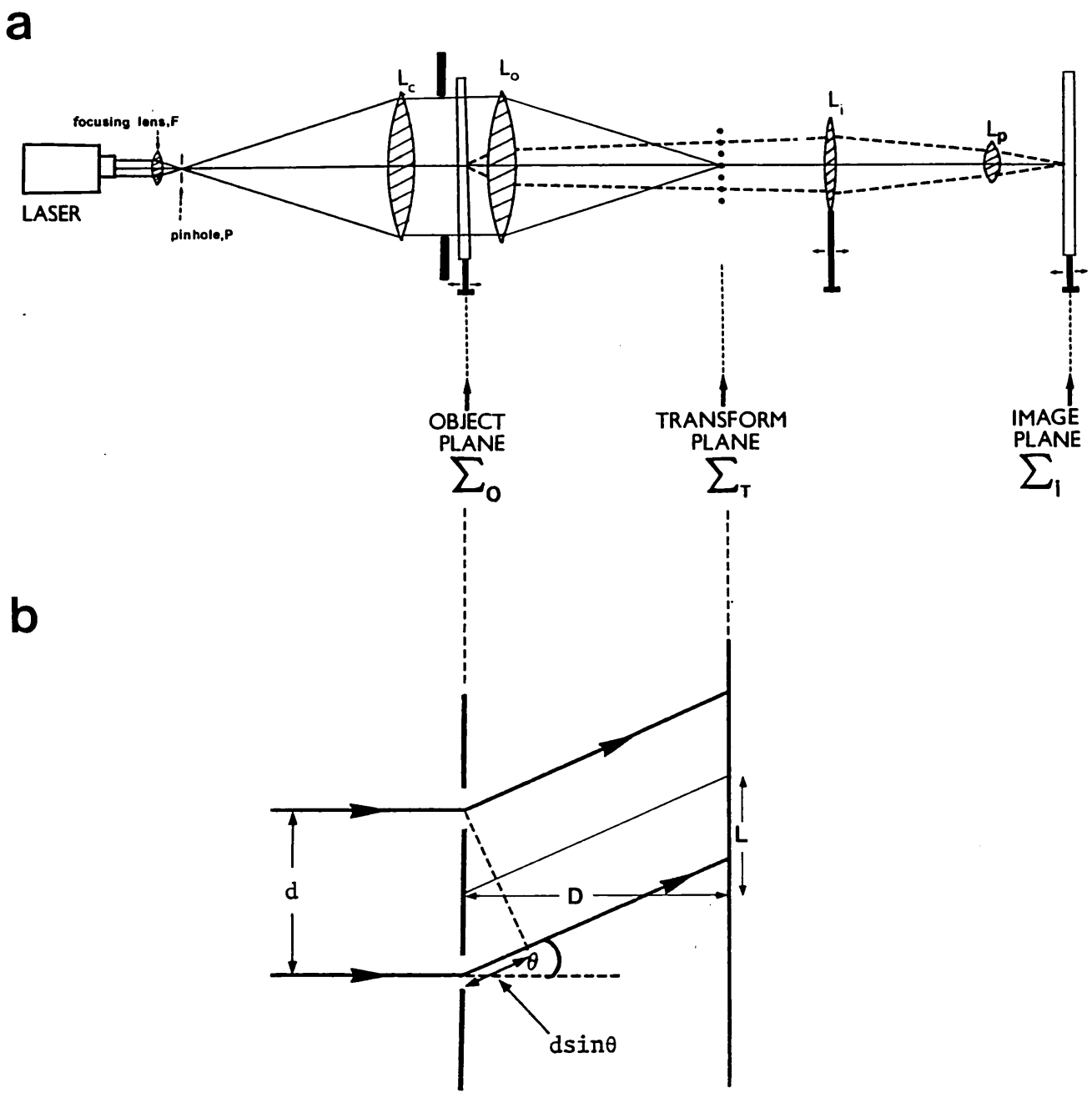


FIGURE 2.9 (a) Diagram of the optical diffractometer. The optical components are described in the text. (b) Diagram showing the path difference between two diffracted beams from a slit of separation "d" placed in the object plane, Σ_o, of the optical diffractometer.

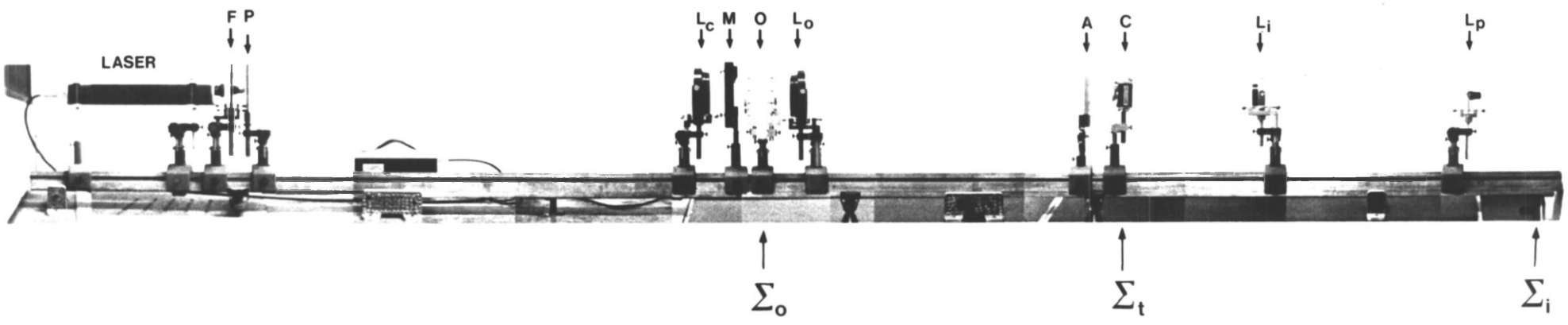


FIGURE 2.10 Photograph of the optical diffractometer. F microscope objective lens; P pinhole, 50um electron microscope aperture; L_c, L_o identical telescope objective lenses of focal length 150cm; M adjustable rectangular aperture; O oil cell (see Figure 2.11); A slide holder for masks to be incorporated into the transform plane Σ_t; C single lens reflex camera; L_i reconstructing lens; L_p microscope objective lens used as a projector lens. Σ_o, Σ_t and Σ_i refer to the object plane, transform plane and image plane respectively. These are mounted on an optical bench 5 metres long.

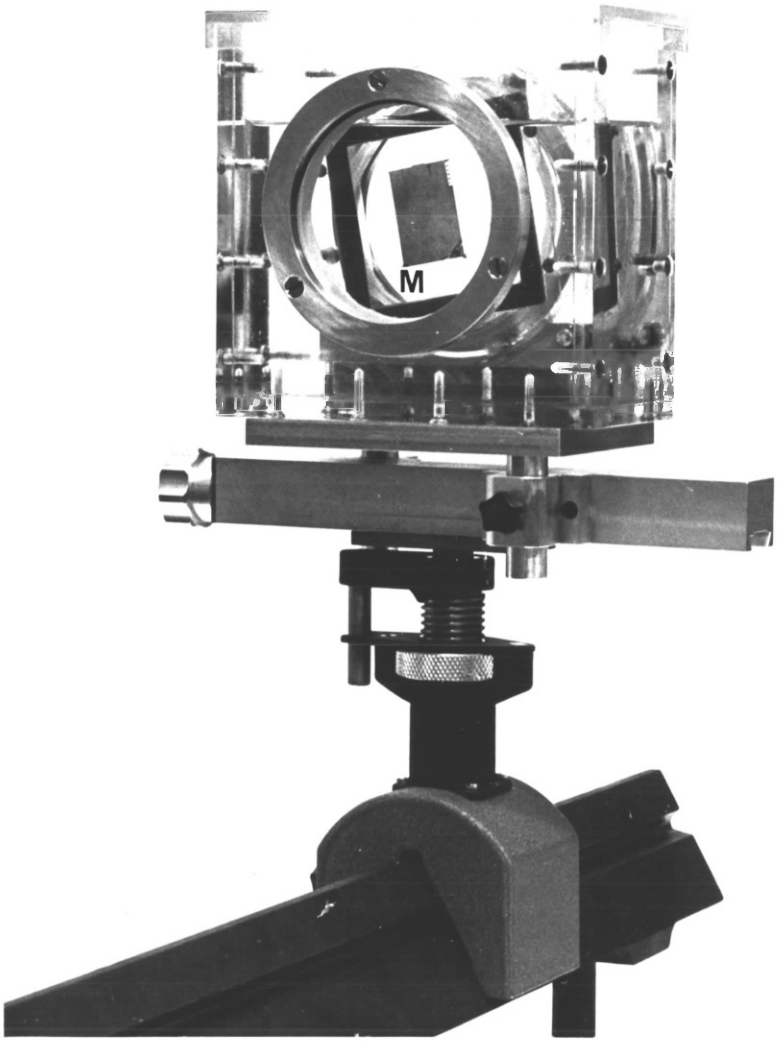


FIGURE 2.11 Photograph of the oil cell and the mounted micrograph (M).

assuming the third order meridional reflection to represent a spacing of 143Å. The meridional reflections were about 250 to 350μm wide across the meridian. By measuring individual diffraction pattern negatives up to ten times, the position of these reflections could be obtained with a 0.1% probable error (the average deviation of the measured value from the average value of the second order reflection).

Relative intensities were determined from densitometer traces of the meridian obtained from a Joyce Loebl microdensitometer (Mk IIIC) incorporating an objective magnification of 10X. An optical wedge with an optical density range of 1.5 and a linearity varying by less than 5% along its length was used. Because of the relatively fine grain of the FP4 film, compared to X-ray film, an effective axial dimension of the densitometer spot of about 15 μm presented a smooth densitometer trace providing the spot width was greater than about 25 μm. The trace background was estimated visually and relative intensities were obtained by measuring the areas under the peaks, or peak heights, and normalized using the intensity of the third order meridional reflection.

2.2.9. Image Analysis.

One-dimensional averaging (lateral smearing) of single sarcomeres across the width of the fibril was achieved in two ways.

The most reliable method involved placing the negative in the film holder of a photographic enlarger and exposing the negative onto photographic paper. During the exposure the paper was moved at a constant speed in the image plane of the enlarger in a direction parallel to the transverse striations across the

fibril in the negative, thus averaging the sarcomere stucture across the fibril width. A 2" x 9" strip of photographic paper was held flat under the glass cover of a proofprinter (Patterson Ltd) and the taped-off region of the sarcomere, which was usually one-third to one-half of the fibril width, was projected onto this paper. For good averaging it was essential that the striations in the sarcomere were straight but as much of the width of the fibril as possible was always used. It was generally found that moving the paper two or three times through the projected image gave a more uniform averaging across the width than a single scan.

The second method involved optical filtering in the optical diffractometer. A very narrow slit was introduced into the transform plane of the optical diffractometer and aligned exactly perpendicular to the transverse striations in the negative (Fraser and Millward, 1970). The narrow slit was formed by bringing together two cut edges of exposed photographic paper. The laterally smeared image was then recorded in the image plane of the optical diffractometer onto 35mm Ilford FP4 film.

The success of either method was gauged according to the uniformity of the smeared striations across the fibril width in terms of both width and density. Measurements were made of the periodicities observed in the average images either directly from film using the Mitutoyo profile projector or from microdensitometer traces of the films.

2.3.X-RAY STUDIES

2.3.1. Introduction

Two X-ray cameras with the "mirror first, monochromator second" design used and described by Huxley and Brown (1967) were used to study the axial and equatorial X-ray diffraction patterns from living Plaice fin muscle.

The shorter of these two cameras had a specimen to film distance of 30cm and was used to record the axial X-ray pattern. In order to record the layer line and row-line positions with comparable accuracy the camera and muscle were arranged to have the monochromator crystal focusing direction parallel to and then perpendicular to the muscle fibre axis respectively. The source of X-rays for this camera was an 18" rotating anode X-ray generator (Marconi-Elliott, GX-13).

The second camera had a specimen to film distance of 80cm and, with this, equatorial X-ray patterns were recorded and the absolute value of the third order meridional reflection, analagous to the 143.4Å meridional in frog sartorius muscle, was obtained for Plaice fin muscle. This camera was mounted on a 4" rotating anode generator (GX6, Marconi-Elliott).

X-rays diverging from the rotating copper anode source, S, are monochromated by Bragg reflection from a variably curved crystal monochromator, C, which then focuses the monochromatized beam of CuKα X-rays in a horizontal plane to produce a sharp vertical line focus at F (Figure 2.12). A relatively poor focus vertically is obtained by specular reflection from the surface of a single glass mirror bent in a horizontal plane at M.

Pairs of slits were placed to collimate the beam before the specimen and where it was desirable to reduce the unused X-rays

entering the X-ray camera and parasitic scatter by the mirror and crystal reflectors. The beam was enclosed in an evacuated tube between the specimen and the film position, F, to prevent scatter and loss of intensity of the diffracted X-rays by air. Evacuated chambers were also used where convenient in other regions of the camera to similarly prevent loss of X-ray intensity.

2.3.2. The X-ray Generator

The low-angle camera was set up on a GX13 X-ray generator (Elliott) comprising an 18" rotating copper anode;two diametrically opposite cathode mountings and two generator tanks capable of 4 KW output each. The bias cup to anode distance was set to obtain a standard source size of 0.1mm high (in the plane of rotation of the anode) by 1mm wide, giving a foreshoretened width of 0.1mm at a take-off angle of about 5^{o}. The maximum power loadings for both cathodes in use is 4.4KW but each cathode has an upper limit of 2.7KW. When possible the anode was biased positively by 40kV and a filament current of 60 mA used. At these settings a moderately intense low-angle myosin layer line pattern could be recorded within 24 hours.

For the camera with a specimen to film distance of 80cm the bias cup parameters for the 4" rotating anode generator were set for the same nominal source size as the GX13 generator. The bias cup to anode distance was set at 8mm for a source size of 0.1mm x 0.1mm. This generator was operated at 40kV and 25mA.

2.3.3. The Curved Crystal Monochromator

The crystal monochromators used consisted of a cylindrically bent quartz crystal, 40 x 13 x 0.3mm, with the surface cut at 3^{o} or 6^{o} to the 1120 planes. The crystals were housed in the crystal bender illustrated in Figure 2.12(b)(produced

at MRC, Hills Road, Cambridge) based on the design by Wooster et al (1949) for applying equal and opposite bending moments to the ends of the crystal.

The fundamental properties required of the curved crystal monochromator particularly for X-ray studies on muscle are as follows;

(i) It should Bragg reflect from the X-ray source only that wavelength chosen to irradiate the specimen (i.e. it should monochromate).

(ii) This monochromation should be accompanied by high intensity of reflection.

(iii) A wide angle of convergence for the reflected beam should be obtained so that diffracted X-rays from a wide region of the specimen are concentrated in a small region of the focal surface.

In order for a plane crystal to Bragg reflect the two components of the CuKα doublet from different regions of its surface, the sum of the angular width of the source (as seen from the reflecting region of the crystal) and the width of the crystal's rocking curve must be less than the difference in Bragg angles for the CuKα_1 and CuKα_2 wavelengths. When X-rays are incident upon a crystal, absorption reduces theincident intensity so that only the crystal surface contributes to the reflection. The reflectivity of the the crystals used is low (about 10%) but the crystal has a large angular aperture. A suitable crystal's mosaic spread must be matched with the angular width of the source to obtain the highest possible intensity from a plane

crystal (Witz, 1969).

Even when these conditions are fulfilled higher harmonics $\lambda/2$, $\lambda/3$ etc., of the principal wavelength are also contained in the reflected beam although being part of the white radiation their contribution is small. The second harmonic, $\lambda/2$, measures about 2% in the CuKα_1 beam reflected from two crossed quartz monochromators with an X-ray tube operated at 40kV (Witz, 1969). These shorter wavelengths can be eliminated by; lowering the tube voltage accompanied by an unfavourably considerable loss in intensity; using a reflection with a very small second-order structure factor such as (111) diamond or fluorite, though these have relatively poor elastic properties; or using a mirror in association with the crystal and setting it very close to the principal value of λ so that shorter wavelengths are not reflected. This latter method was considered although the small proportion of $\lambda/2$ meant it was not a seriously contaminating wavelength.

Some concentration of the beam intensity can be obtained by cutting the plane crystal at an angle to the diffracting planes (Fankuchen, 1937) but a significant increase in the angular width of the region of selective radiation is in practice obtained by elastically bending the crystal. Plastic bending of crystals can also have this effect but the increase in mosaic spread caused by polygonization of the crystal results in increasing contributions to the reflected beam from other unwanted wavelengths.

Simply bending a crystal, whose surface is parallel to the diffracting planes, to a cylinder of radius R and placing it tangential to the focal circle of radius R/2 introduces geometrical aberrations into the focus, F, from a point source, S

(Johann, 1931; Figure 2.13(c)). These aberrations are removed if the crystal is not placed tangential to the focal circle (Dardord, 1922; Figure 2.13(d)) so that reflecting planes of radius R intersecting the focal circle, focus the X-rays to a point; although this is at the expense of introducing further wavelength components into the reflected beam (ϕ' in Figure 2.13(d)). This however is the basic idea of the geometry suggested by DuMond and Kirkpatrick (1930) in which the crystal surface is ground to a radius R so that the diffracting lattice planes are bent to a radius of 2R. Since this arrangement only gives perfect focusing if a small source size is available, the Johann focusing conditions, in which the crystal is simply bent to form a cylindrical surface, are sufficient for the size of X-ray source used in this work. In this arrangement the source and focus are equidistant from the crystal and Guinier (1946) showed that the monochromator to focus distance could be increased without increasing the total path length of the X-ray beam (Figure 2.13(f)). This is achieved by cutting the crystal surface at an angle, δ , to the diffracting planes. Thus the source to crystal distance and crystal to focus distance are given by $2R\sin(\theta - \delta)$ and $2R\sin(\theta + \delta)$ respectively.

The values for δ of 3^{o} or 6^{o} used in this work correspond to asymmetries of 1.6 and 2.6 respectively. In order to select the $CuK\alpha_1$ line for which λ = 1.54015Å a quartz crystal in which the crystal face is parallel to the $(11\bar{2}0)$ lattice planes of d-spacing 3.34Å is used. To satisfy the Bragg condition for diffraction of the $CuK\alpha_1$ line the X-rays have to make an angle of incidence of 13^{o} $18'$ with the crystal planes.

The ideal profile for the crystal, the logarithmic spiral;

$r = e^{a\phi}$ (ϕ is the complement of the Bragg angle) was suggested by de Broglie and Lindemann (1914) and achieved practically by de Wolff (1950) (Figure 2.13(g)). All radii proceeding from the origin of the curve meet the curve at a constant angle. Thus perfect focussing is achieved, provided the source covers the caustic cross-section, by a simple bending of the crystal .The profile can be easily altered to reflect different wavelengths and larger sources can be used more efficiently.

In the present X-ray studies the simpler crystal bender produced a focus 0.1 to 0.15mm wide which gave very satisfactory resolution on cameras with a specimen to film distance of 30cm or longer. The limiting factor to the overall resolution obtainable was the quality of the focusing attainable by reflection from the glass mirror. However, unless double monochromator cameras are used, it is clearly only possible to get comparable order-to order resolution along the row-lines and layer lines, and therefore optimally accurate spacings and intensities for them, if the superior crystal focus is utilised as has been done here while also retaining the relatively large camera flux this type of camera allows.

2.3.4. The Mirror Bender

The basic construction of the mirror bender is illustrated in Figure 2.14. An optical flat rests on top of two undercut supporting rods and equal bending couples are applied at each end of the rectangular plate. The force is applied to the ends of the plate through a steel spring against which a low-geared screw is forced. Ideally the focusing element should be part of a cylinder of elliptical cross-section so that X-rays emitted from the source at one focus of the ellipse converge to a point at the

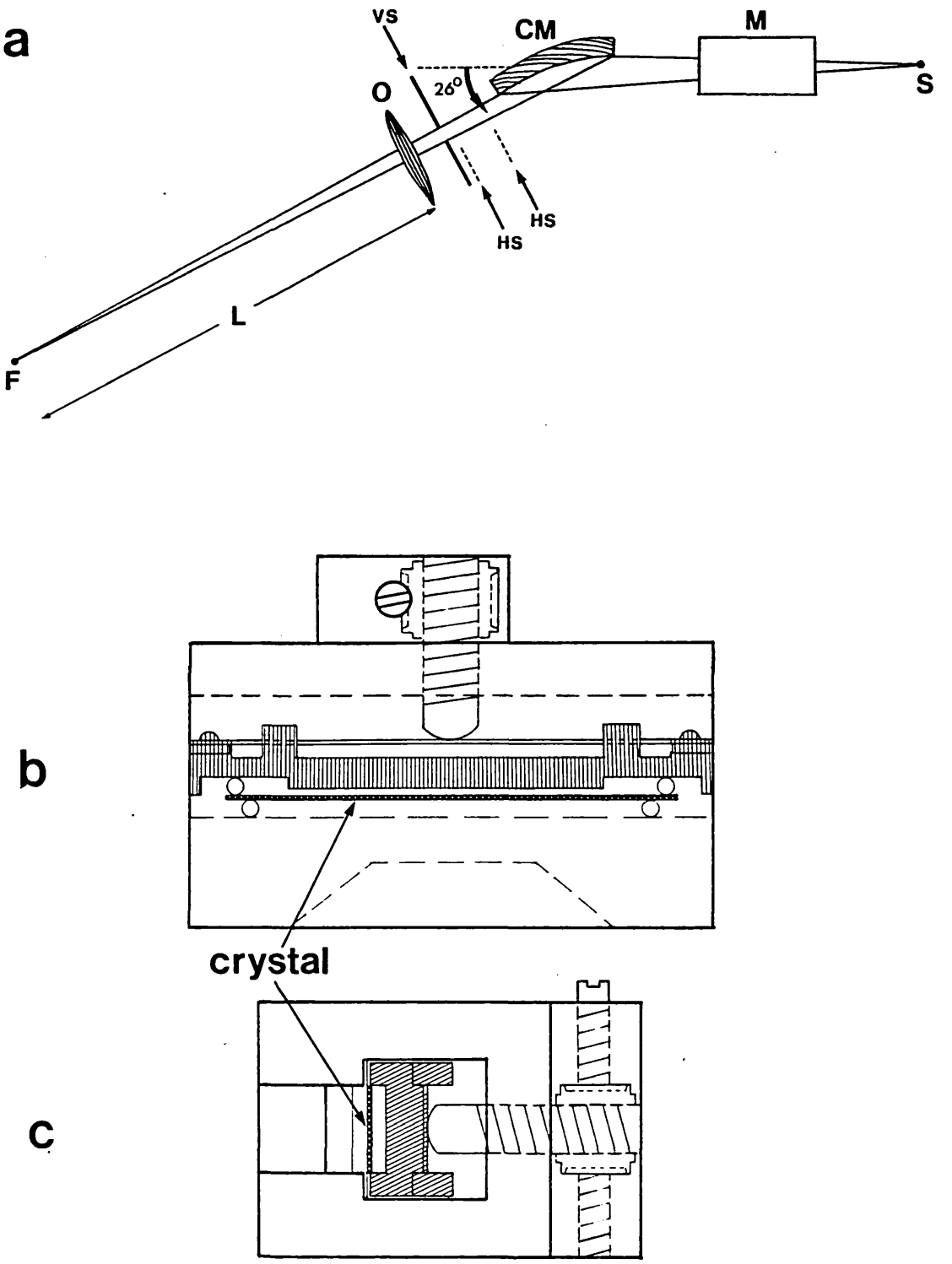


FIGURE 2.12 (a) Plan diagram showing the basic layout of the low-angle cameras used. S, source of X-rays; M, mirror bender; CM, crystal monochromator; VS and HS are vertical and horizontal slits; O is the specimen position. X-rays are focused to the point F. L is the specimen to film distance. (b) Plan view of the crystal bender (c) The crystal bender viewed along the direction of the X-ray beam.

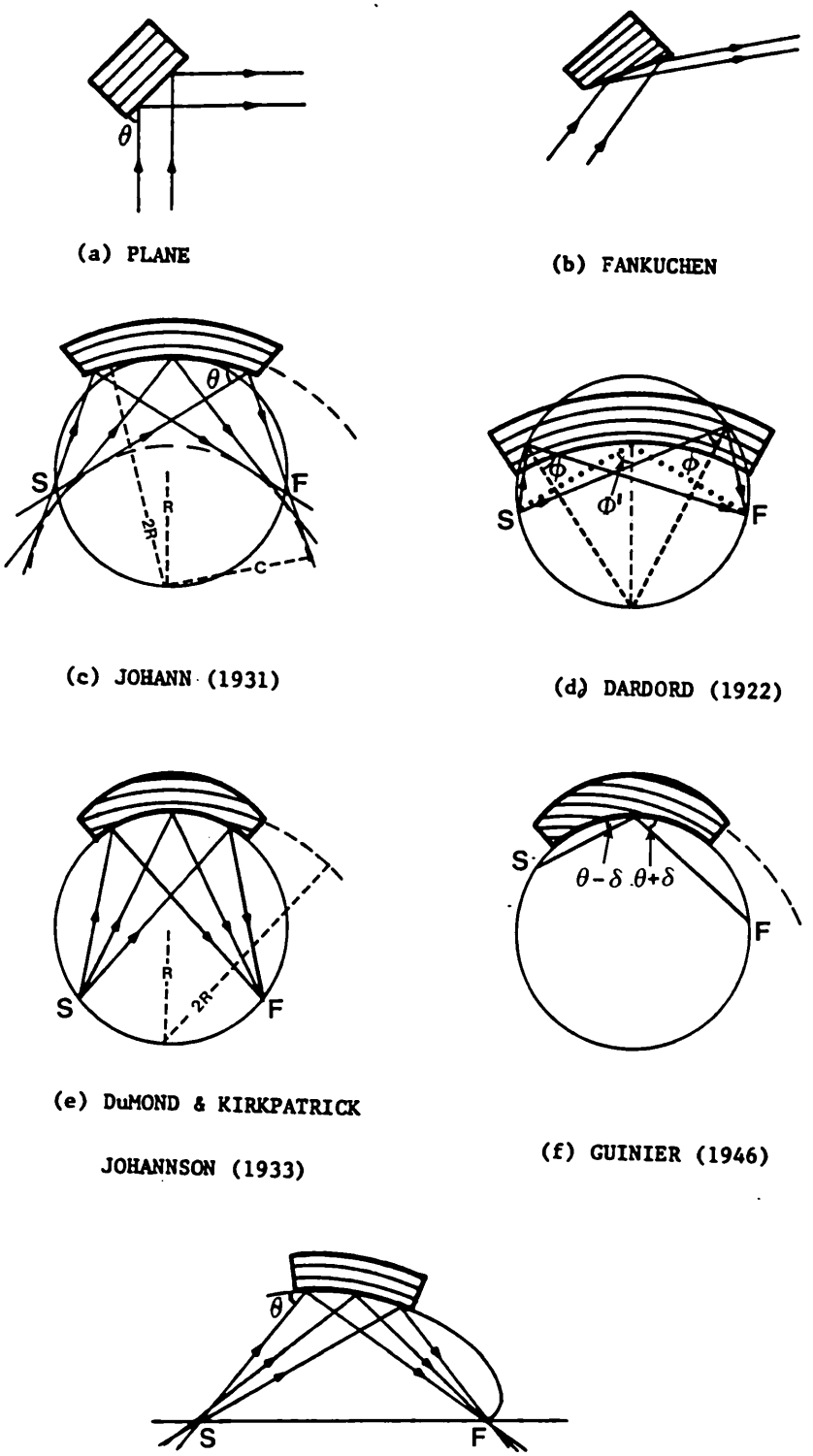


FIGURE 2.13 Developments in the design of the crystal monochromator. See text for details. S, source; F, focal point; C, caustic error circle radius; R, radius of focal circle; θ, Bragg angle; ø, complement of the Bragg angle.

other focus.

This bender enables the mirror curvature to be set such that all X-rays incident on its surface at the appropriate angle for specular reflection are brought to the focus coincident with that of the crystal monochromator. The maximum incidence angle for any appreciable reflection from the glass mirror surface is very low (about 0.25^{o}) ; the surface must therefore be very flat, to within 500Å. The mirror bender is mounted so that it can be accurately positioned relative to the X-ray beam and its curvature sensitively adjusted. Non-specularity of this reflection causes parasitic scatter from the mirror. This manifests as a diffuse halo surrounding the main reflected beam. Since this diffusely reflected radiation may be strong compared to the diffracted beams from the specimen, collimating slits (HS and VS in Figure 2.14(c)) are placed as close as possible to the specimen to minimise the extent of the parasitic scatter about the X-ray beam.

The position of the mirror from the X-ray source is determined by compromising the required vertical dimension of the X-ray focus with the proportion of the X-ray beam entering the camera to be concentrated into the focus. In the first case the ratio of the focus dimension to the effective source size is given by the ratio of the separation of the mirror and the focus, F, to the separation of the source and the mirror. This ratio increases, and likewise the vertical dimension of the focus increases, as the mirror is placed closer to the source. However the angular aperture of the mirror also increases thus reducing the necessary exposure times.

The height of the mirror is also finely adjustable. In

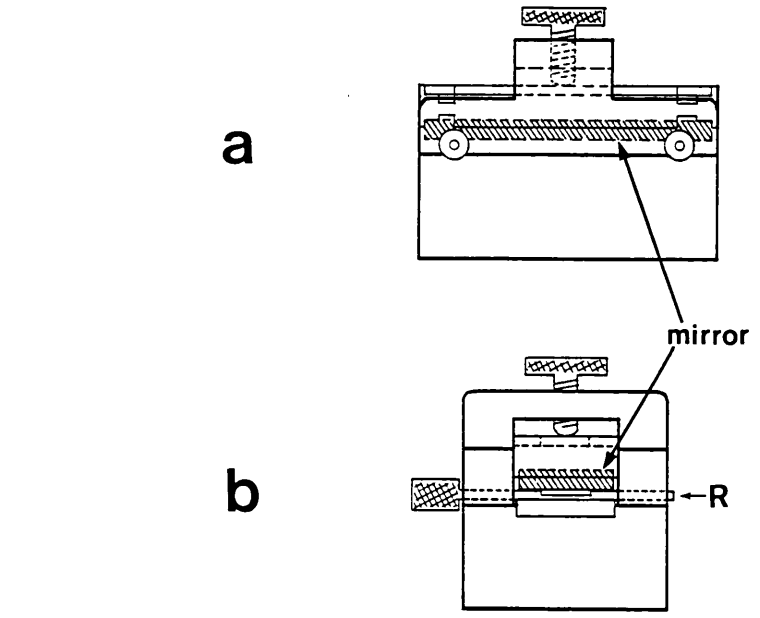
Figure 2.14(c) the reflected and unreflected parts of the beam are shown separated in the focal plane of the camera. If the reflected beam alone is used the X-ray focus has a smaller vertical dimension thus there is better resolution in this direction in the diffraction pattern. A main beam stop could be raised to block out the unrequired unreflected beam and prevent entry of unnecessary X-rays into the camera.

In situations where a shorter X-ray exposure time was more important than optimum two-dimensional resolution in the pattern the reflected and unreflected beams from the mirror could be superimposed by increasing the height of the mirror relative to the X-ray source.

2.3.5. The 30cm Specimen to Film Camera

The low-angle camera had a fixed specimen to film distance of 30cm since both the specimen cell holder and the film holder were mounted on the same cylindrical brass evacuatable pot (Figure 2.15). This unit and the first two elements of the camera, the mirror bender and crystal monochromator, were housed on two separate optical benches (PTI.Co.Ltd). The mounts for these elements comprised fine adjustments both vertically and in a horizontal plane, at right angles to the X-ray beam direction.

The specimen cell/film holder contained a pivot immediately below the specimen position so that when the lead backstop, preventing the undiffracted beam from striking the film, was moved into place, no appreciable movement of the specimen relative to the X-ray beam occurred. The lead backstop was mounted onto a strip of 50μm Mellinex film clamped to the back of the camera body. The X-ray films, in an envelope with a front window of aluminimum foil, were supported on the O-ring sealed



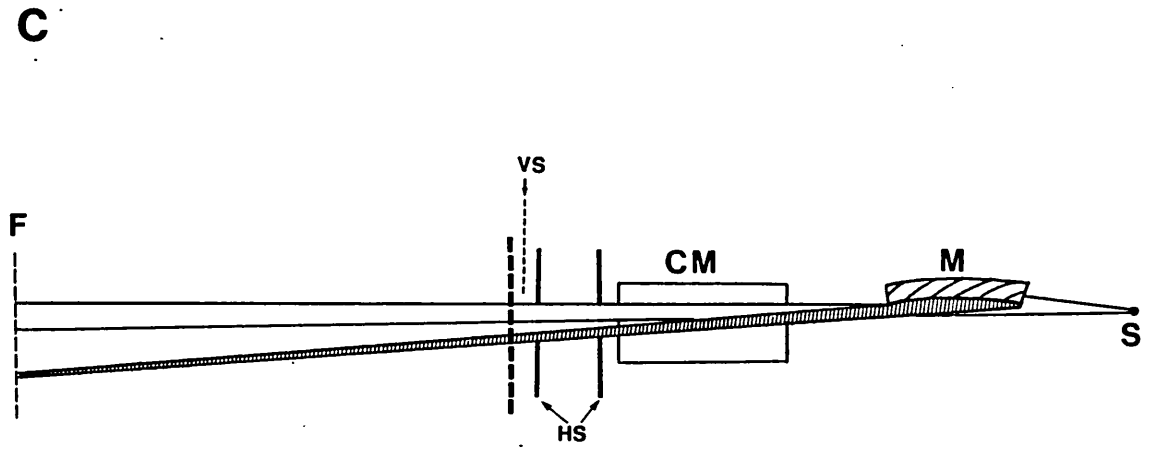


FIGURE 2.14 (a) Side view of the mirror bender. (b) View of the mirror bender along the direction of the X-ray beam showing the undercut rods, R, supporting the mirror.(c) Diagram of a side view of the X-ray camera showing the separation of the reflected (shaded region) and unreflected beams from the mirror bender (M). The vertical scale is exaggerated. M, mirror; CM, crystal monochromator; F, film plane.

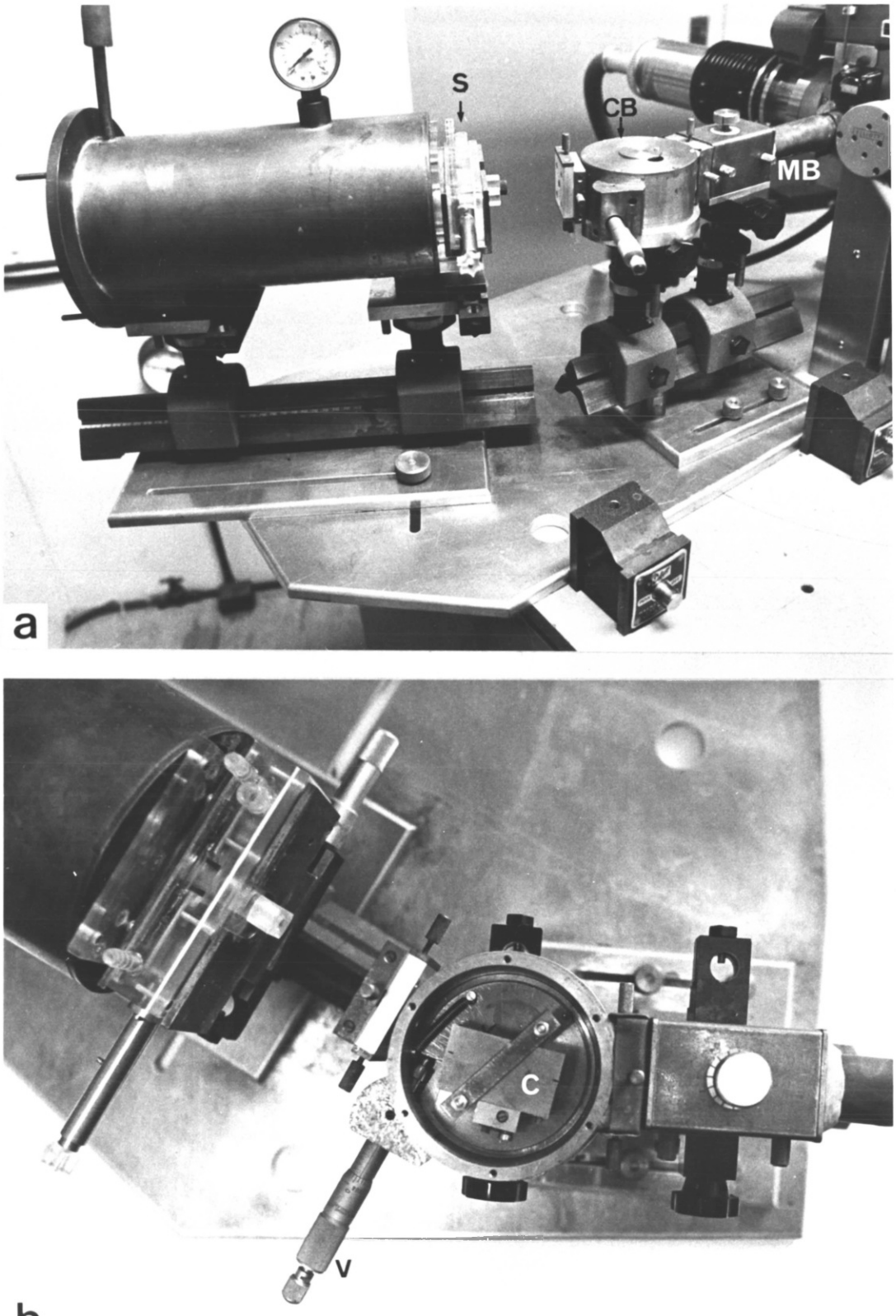


FIGURE 2.15 (a) Photograph of the X-ray camera with a 30cm specimen to film distance showing the mirror bender holder (MB), the crystal bender holder (CB) and specimen cell holder (S). (b) Plan view of the camera in (a) showing the crystal bender (C) which can be rotated in the horizontal plane by adjustment of V.

lid of the camera body.

Two camera geometries were used. In the first the muscle fibre axis was set horizontal so that optimum order-to-order resolution (and first order resolution) was obtained along the meridian of the X-ray diagram. A single glass (Spectrosil) mirror bender was placed as close as possible to the source, 11cm, it's position from the camera focus, 58cm, being determined by the crystal geometry. A vertical magnification of the 0.1mm high source of about 6 times was thus expected and in practice the focus was 0.5mm to 0.7mm high, i.e. perpendicular to the meridian. The crystal monochromator position was fixed by the 30cm specimen to film distance; the 3^{o} cut crystal it contained and the need to minimise the total length of the camera. This was placed 26cm from the X-ray source giving a 0.1mm to 0.15mm wide focus 42cm (i.e. 1.6 x 26cm) further on.

In the second arrangement the muscle fibre axis was vertical so that optimum order-to-order resolution of the row-line sampling along the myosin layer lines could be obtained by the crystal focus. However in order to retain simultaneous good order-to-order resolution between layer lines it was necessary to try to reduce the vertical magnification of the X-ray source, by the mirror, by placing it roughly midway along the camera. The crystal was rotated through 180^{o} in a vertical plane thus reversing the asymmetry so that the source-to-crystal distance was now about 1.6 times the crystal-to-focus distance. Since this latter distance could only be set to 42cm at a minimum for this particular camera the crystal had to be placed 67cm from the source and the mirror bender about 50cm from the X-ray source. Such an arrangement is not conducive to minimising the exposure

times but was unavoidable in view of the constraints of the camera and availability of crystals.

Increasing the source to mirror distance from 11cm to 50cm reduces the aperture of the camera to about one fifth compared to the previous geometry. The crystal was also now placed twice as far from the source but this is partly compensated for because in this second arrangement the crystal surface makes a larger angle ($\theta + \delta$) with the X-ray beam so that the crystal aperture is approximately given by $l\sin(\theta + \delta)/s$, where l is the crystal length and s is the crystal distance from the X-ray source.

It was still possible with this arrangement to record myosin layer line patterns, quite suitable for microdensitometry, in 13 to 20 hours to about 130Å resolution both parallel to the meridian and at right angles to it.

2.3.6. The 80cm Specimen to Film Camera

This camera was very similar in construction to the low-angle camera although the specimen cell holder and backstop/film holder were two separately mounted units.

The crystal monochromator containing a 6^{o} quartz crystal was placed about 34cm from the source producing a 0.1mm to 0.15mm wide focus 88cm further on. A single glass mirror bender was placed as close to the source as possible to maximise the X-ray flux reflected by it. The X-ray beam path was evacuated between the specimen holder and the film. With the X-ray generator operated at 40kV and 25mA, meridional patterns for calibration of the third order meridional spacing and equatorial diffraction patterns were recorded in one to two hours.

2.3.7. Alignment of The X-ray Camera

The crystal and mirror benders were mounted on the same optical bench which was aligned at a take-off angle of 4^{o} to the anode surface. The X-ray beam was firstly focused in a horizontal plane by the crystal, with the mirror absent, since its focal length is fixed by its distance from the X-ray source, y, and the angle, δ ,that the diffracting planes make with the surface of the crystal. y is equal to $2R\sin(\theta - \delta)$ where $\theta = 13^{o}\ 21'$ and the crystal to focus distance $x = 2R\sin(\theta + \delta)$. For $\delta = 3^{o}$, x/y is approximately 1.6. The crystal to focus distance and hence the specimen to film distance was minimised with the constraint that the crystal focus should enable resolution of the closely spaced $11\bar{2}$ and $20\bar{2}$ row-lines if the muscle fibre axis was mounted vertically. These row-lines are separated by approximately 0.3mm at a 30cm specimen to film distance which is approximately two times the width of the crystal focus obtained. Assuming negligible broadening of the crystal focus due mainly to disorientation of the fibre specimen this arrangement is well within the limit of resolution for these closely spaced reflections and was necessary for adequate densitometry along the layer lines.

The crystal bender was positioned on the short aligned optical bench and inclined at about 13^{o} to the X-ray beam. The bender was rotated about its vertical axis and a proportional counter, preceded by numerous layers of aluminium foil, placed at the exit of the crystal bender mount to detect the $CuK\alpha$ beam when the angle the crystal made with the beam was correct. The reflected beam appeared as a thin vertical line when viewed with a fluorescent screen at the exit of the crystal mount since only

a small region of the flat crystal was at the correct Bragg angle to the incident X-ray beam. As the crystal is rotated from this condition the reflected beam moves as the different parts of the crystal are brought to the correct angle. The crystal was then bent by adjustment of the low-geared screw until the reflected beam appeared broader (> 5 mm) and uniform as more of the length of the crystal was curved to the correct angle to the X-ray beam, for a particular fixed rotation of the bender about the vertical axis. When the correct curvature and rotation of the crystal were obtained small rotations of the crystal showed the edges of the illuminated region of the crystal moving into a reflecting position and the central region of the crystal moving away from this condition.

The CuKα_1 and CuKα_2 components of the Bragg reflected radiation could be seen to be separately reflected by the crystal at the exit of the crystal holder or at the focal position by making small rotations of the crystal bender about the vertical axis. The CuKα_1 component is approximately twice as intense as the CuKα_2 component and is easily distinguishable when viewed on fluorescent screen. A clear minima or "dip" between the α_1 and α_2 components ensured there was no simultaneous partial reflection of either λ by the crystal. Vertical slits at the entrance to the crystal enabled the angular aperture of the crystal to be limited so that approximately only the effective reflecting length of the crystal was illuminated. A proportional counter was positioned between the focus and the crystal so that the separation of CuKα_1 and CuKα_2 could be optimised with no appreciable reduction in the overall X-ray beam flux. The position of the crystal focus along the second optical bench was

finally determined by taking a series of X-ray photographs about the approximate location of the crystal focus obtained by viewing the beam with a fluorescent screen inclined to the X-ray beam. This optical bench was also aligned to ensure that the X-ray beam path was coincident with its central track.

The mirror bender was placed adjacent to the X-ray generator window and the height adjusted so that in the focal plane of the crystal both the specularly reflected beam from the mirror surface and the X-ray beam passing undeflected through the mirror bender were seen to be resolved on an inclined fluorescent screen. The undercut rods supporting the optical flat were then rotated to cut out the unreflected beam from the mirror. In order to obtain the mirror focus coincident with that of the crystal, fine adjustments of the height and curvature of the mirror were made such that the height of the focus was minimised whilst retaining maximum brightness of the reflected beam on a fluorescent screen. The brightness was used as a first guide to optimise the mirror setting which was then checked with a proportional counter by making finer adjustments about the setting obtained visually.

A set of horizontal and vertical slits mounted on the crystal holder, a few centimetres in front of the specimen position, were then adjusted as close to the beam as possible, without cutting into the beam, in order to reduce parasitic scatter from the crystal and mirror reflectors. The vertical pair of slits were adjusted by setting the edge of an inclined fluorescent screen at the edge of the X-ray beam span and closing the appropriate slit to extinguish the fluorescence. This adjustment and that of the horizontal pair of slits, which were

more critical since the beam height was 0.5mm to 1mm, were checked with a proportional counter to safegaurd actually cutting into the beam. A preliminary check on the height of the focus was carried out using a fluorescent screen with slits 0.25mm, 0.5mm and 1mm wide cut into it and then the focus was photographed.

The evacuatable chamber on which the specimen cell holder and film holder were mounted was aligned along the long optical bench so that the X-ray beam passed centrally through the cylindrical chamber. The lead backstop mounted on mellinex at the back of this chanber, just in front of the vacuum seal lid carrying the X-ray film, was then positioned to block out the X-ray beam.

2.3.8. Mounting the Muscles in the Specimen Cell

The specimen cell used on the low-angle camera is shown in Figure 2.16(a). The "bone-end" of the Plaice or frog muscles was clamped into the cell at one end and tied onto a stainless steel hook by cotton through the skin or tendon at the other. The hook formed part of a rod which could be withdrawn from the cell by fine adjustment which was necessary when setting the sarcomere length of the muscle. A large range of movement was allowed for this mechanism so that the rather short, 1cm long, Plaice fin muscles and the longer, 2cm to 3cm, frog sartorius muscles could both be accomodated in this cell. The clamp could also be rotated by $\pm 10^{o}$ around a stainless steel peg. The hook could be rotated about the muscle axis and fastened with a locking nut. These minor adjustments ensured that all muscles could be easily mounted centrally and flat in the X-ray windows of the cell.

During the X-ray exposure specimens were cooled to about

4°C and air or oxygen was bubbled through the surrounding Ringer solution in the vicinity of the X-ray window. The cell was partitioned by stainless steel plates 1/8" thick so that a coolant could be circulated through a chamber on one side of the cell thus cooling the Ringer solution in the adjoining chamber (Figure 2.17). The coolant was circulated using a Choreline low temperature thermo circulator.

Mellinex windows, 50μm thick, allowed the X-ray beam to pass through the cell with negligible absorption apart from that by the specimen. Since the Ringer solution absorbs and scatters X-rays strongly the window nearest the X-ray source could be adjusted to minimise the path of the X-ray beam through the cell, ensuring this path was never greater than about 1mm. Both X-ray windows were made just large enough to allow the incident and diffracted X-ray beams entry and exit from the cell. This produced optimally flat windows, thus minimising the X-ray beam path through the cell and facilitating the examination of the muscle specimens by laser diffraction.

X-ray windows were affixed with double-sided tape which was as stable as Araldite for this purpose and also allowed a uniform layer of adhesive to be effortlessly applied which further improved the flatness of the windows.

2.3.9. Plaice Ringer Solution

During the X-ray exposure live Plaice fin muscles were immersed in a Ringer solution derived by Cobb et al (1973). This was based on an analysis of fish blood serum and used in the composition shown in Appendix A.

Cobb et al quote a pH of 8.1 for the Ringer which is

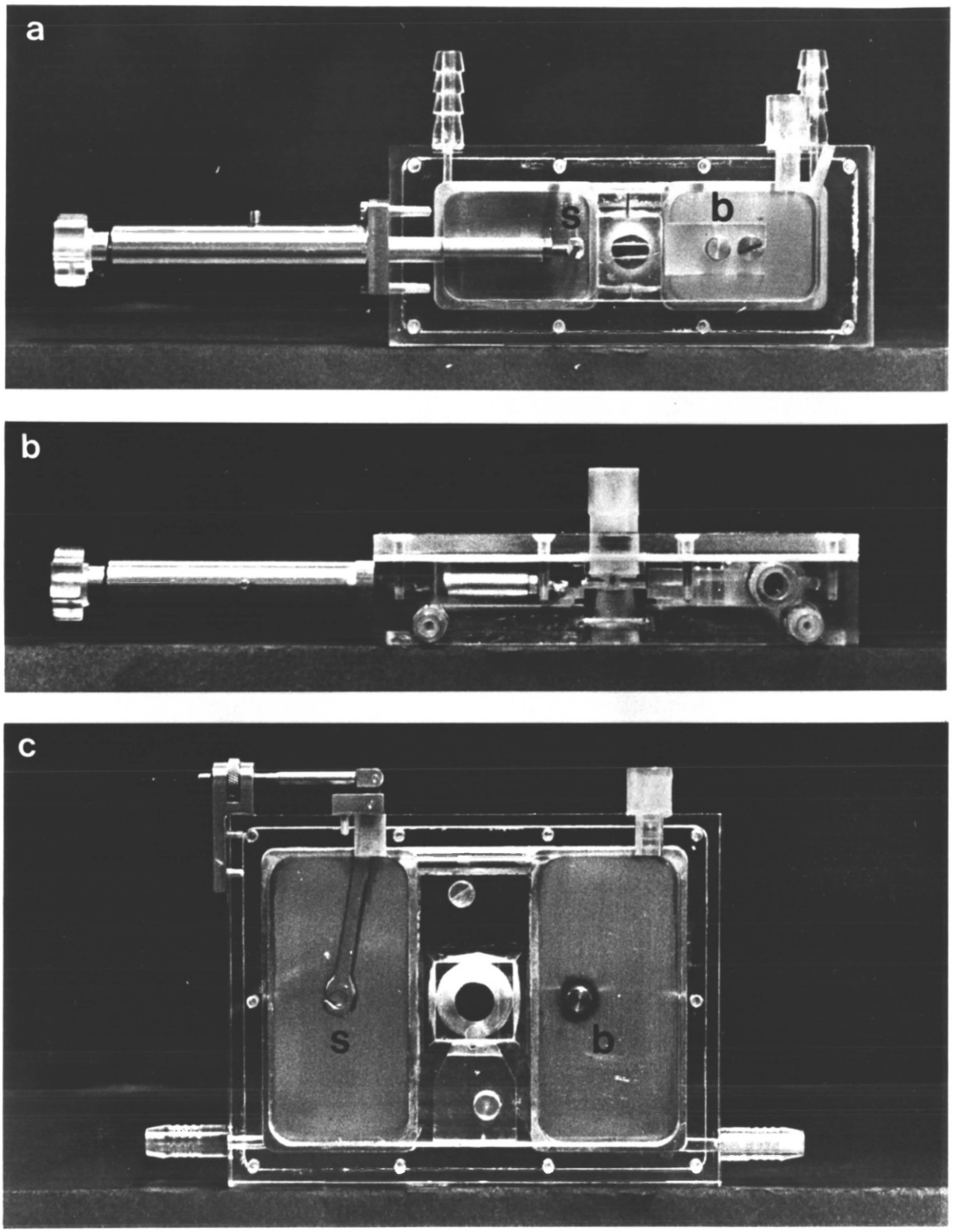


FIGURE 2.16 (a) and (b) are specimen holders used on the 30cm X-ray camera. (c) Specimen holder with a lever arrangement used on the 80cm X-ray camera. In (a) "s" is the hook to which the 'skin-end' of the muscle preparation is tied and "b" the clamp for the 'bone-end' of the muscle.

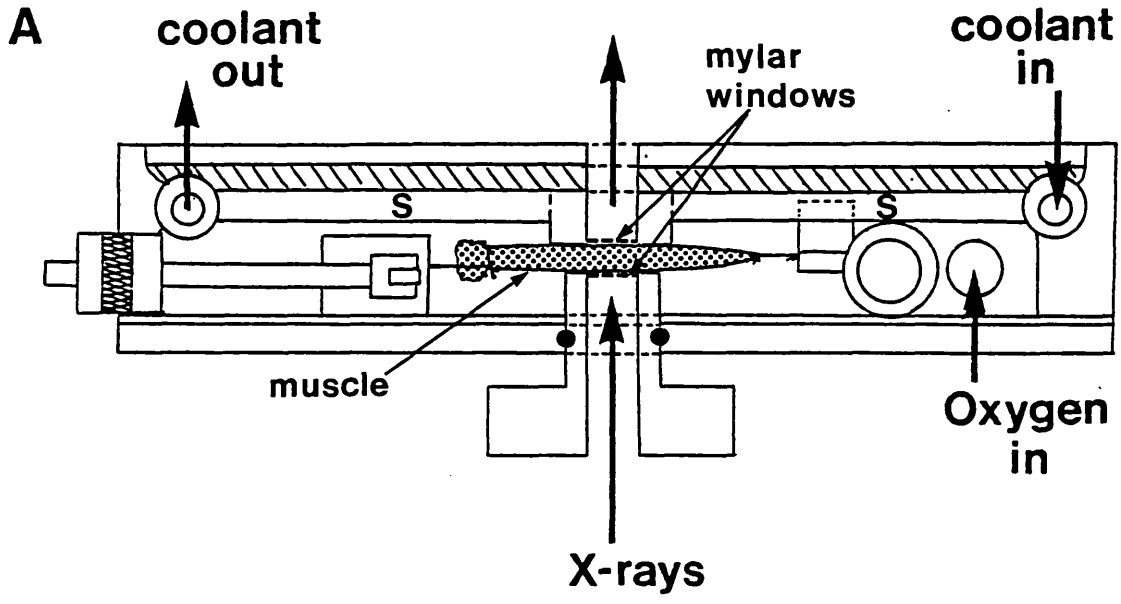


FIGURE 2.17 Schematic plan view of a specimen holder showing the cooling compartment of the cell (shaded) separated by stainless steel plates (S) from the chamber containing the Ringer solution. The mylar window nearest the X-ray source is mounted on a short perspex tube which is sealed using an O-ring into the front chamber of the cell.

unusually high (Lockwood, 1961) and the X-ray patterns were obtained making no adjustment to the pH of the Ringer from the value of 6.8 arrived at by using the above salts in boiled deionized water. Cobb et al similarly made no adjustment to the pH of the Ringer and used a value of 7.6 for their electrophysiological and electron microscopy tests on the suitability of the Ringer.

All normal methods to overcome precipitation of the calcium salt present in the quoted proportion were unsuccessful. This component was used in smaller quantities and finally omitted from the Ringer solution with no obvious deleterious effect. The effect of varying any of the other ingredients has not been investigated.

2.3.10. Measurement of Sarcomere Length

The specimen cell was mounted onto an optical bench and the central region of the X-ray window illuminated by a 1mW laser (Cooke Scientific Ltd) housed on this same optical bench. The laser diffraction pattern from the muscle sarcomere's repeat was projected onto a calibrated screen 30cm further on. The screen was calibrated using a diffraction grating with 15,000 lines per inch (corresponding to 1.63μm) and the screen was scaled by vertical lines representing 0.05μm intervals between 2 and 4μm. To ensure an accurate determination of the specimen position on this set up, the diffraction grating was placed in the specimen holder in the specimen position ensuring an accurate specimen to screen calibration.

The limitations to the accuracy of the measurement of sarcomere length concern the fibre arrangement of the muscle and the consequent difficulty in applying tension uniformly across

the muscle cross-section when loading the muscle into the specimen cell.

2.3.11. Measurement of Spacings

The spacings of reflections were measured using the Mitutoyo profile projector which projects the pattern onto a ground glass screen with a magnification of ten times. The specimen to film distance of the long (1metre) camera was measured directly while the low-angle camera was calibrated using the spacing of the third order meridional reflection, at about 144Å, which had been obtained on the long camera. These measurements were carried out for ten Plaice fin muscles then ten frog sartorius muscles on identical camera settings. The camera was reassembled and ten measurements for both types of muscle were repeated.

2.3.12. Determination of Reciprocal Lattice Coordinates.

Diffraction patterns were recorded on flat film and although diffraction at relatively low angles was being considered the errors involved in not recording onto a spherical focal surface were assessed.

The relationship between the Cartesian coordinates (x,y) of the diffraction peaks on the flat film to the angles of longitude, χ , and latitude, μ , which define the direction of the diffracted beam on the sphere of reflection (Figure 2.18) is given by $\mu = \tan^{-1}\{x/r\}$ and $\chi = \tan^{-1}\{y/\{x^2 + r^2\}^{\frac{1}{2}}\}$

where x and y are the measured coordinates of the diffraction peaks on the film and r is the measured specimen to film distance.

The magnitude of the reciprocal lattice vector, D, is given by

$$D = \frac{2\sin\theta}{\lambda} = (1/\lambda)\{[2(1 - \cos\mu\cos\chi)]^{\frac{1}{2}}\}$$

The reciprocal lattice coordinates Z and R, giving the layer-line spacings and row-line spacings 1/Z and 1/R respectively, are given by

$$Z = (1/\lambda)\sin\chi$$

$$R = (D^2 - Z^2)^{\frac{1}{2}}$$

2.3.13. Relative Intensity Measurement.

A Joyce Loebl microdensitometer (Model IIIC) was used to obtain densitometer traces from the X-ray films. This incorporated an optical wedge with a nominal optical density range of 1.5 O.D. (Wedge no. C479; actual useful range of 1.33 O.D.). Virtually all measurements of layer lines, row lines and meridional patterns could be made using this wedge and only in the case of some equatorial patterns was it necessary to use a wedge of higher range (up to 2.0 O.D.).

The axial dimension (height) of the densitometer receiving aperture was minimised to give optimum resolution. This minimum dimension was constrained by the need to integrate film grain effects. The transverse dimension (width) of the aperture was limited by the size of the diffraction peak (convoluted with the X-ray focus).

A further constraint on the size of the densitometer aperture is the error incurred if the range of optical density (D) in the field of view of the microdensitometer lens is large. The errors arise because the light transmitted by a small area of the X-ray film, I, is logarithmically related to D i.e. D =

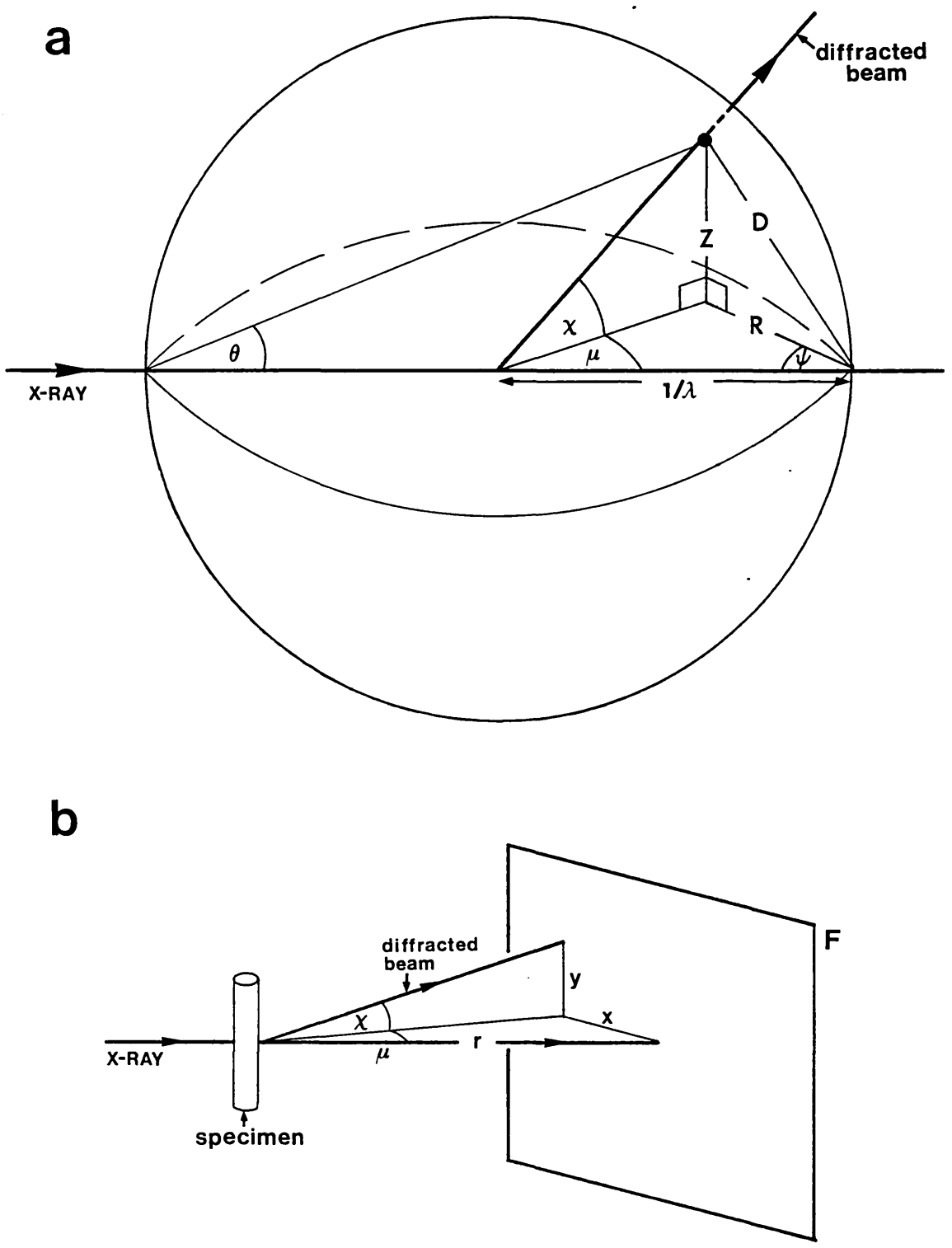


FIGURE 2.18 (a) Diagram showing how the direction of the diffracted beam is defined in terms of the reciprocal lattice coordinates in the Ewald sphere (see text). (b) Diagram showing the relationship between the coordinates (x,y) of the diffraction peak on the flat film (F) to the angles χ and μ which define the direction of the diffracted beam relative to the undeflected X-ray beam.

$\log_{10} I_o/I$ whereas D is linearly proportional to the number of X-ray quanta incident on the X-ray film, for a limited range of density. If in a region of the film the true optical density varied uniformly between 1 and 2 the true average number of X-ray quanta incident on this region is 1.5. The densitometer reading would give a value of $D = \log_{10} 1/((0.1 + 0.01)/2) = 1.26$. Wooster (1964) discusses the percentage errors in the integrated intensity given by uniformly varying density ranges in the field of view of the microdensitometer lens. These errors must be kept to around 1% to attain overall accuracy of 5% in the microdensitometer measurements which is a limit set by the sensitivity of photographic film and its processing.

Densitometer traces along meridional patterns were made with a slit height of 30μm and slit width 300μm. Since the reflections were 100 to 150μm axially and at least 500μm wide the errors due to integration were kept to a minimum. The heights of the peaks in these traces were measured and peaks either side of the pattern varied by less than 20%. Equatorial patterns were traced with a 75μm slit height and the areas under the peaks were determined. Two types of equatorial patterns were recorded. For those with a long focus dimension parallel to the meridian (i.e. 1 to 1.5mm) the slit width was up to 1000μm wide but for patterns where a near-point focus was used, the slit width was approximately the dimension of the reflection measured parallel to the meridian. In the first case, peak areas either side of the pattern varied by on average less than 15% and in the second case by less than 10%, in the case of the strong reflections (i.e. 11, 20) but up to 20% for the weaker higher order reflections which were less prominent compared to the background fluctuations.

A slit height of 75μm was used to trace the myosin layer lines off the meridian. Peak areas from the 4 quadrants of patterns which were well-resolved between layer lines (the densitometer trace being made parallel to the meridian along the appropriate row line) varied between 3% and 11% from the average value of all 4 quadrants. X-ray patterns which were recorded with better two-dimensional resolution were traced along both layer lines and row lines. Peak areas from 4 quadrants of such patterns showed an average variation of 10% from the average value. Although for the strongest reflections this variation is around 5% and up to 15 to 20% for the weakest off-meridional reflections measured.

2.3.14. X-ray Film

"CEA Reflex 25" X-ray films were used (Ceaverken) which are coated with emulsion on both sides. These were developed for 5 minutes at 20°C in DX-80 developer (Kodak Ltd.) and fixed for 10 minutes in Kodafix fixer (Kodak Ltd.), also at room temperature. Shrinkage of the film due to processing was found to be less than 0.1%. A pair of "locked" dividers were used to make indentations in X-ray films before processing and identical indentations were made in control films which were already processed and therefore transparent. No difference was found in the approximately 50mm separation of the indentation marks from either film, when measured on a device with an accuracy better than a twentieth of a millimetre. Evacuation of fresh film for up to three days also had no effect on the X-ray film dimensions.

2.4. COMPUTER MODELLING

2.4.1. C-zone Modelling

Fortran programs were written to generate the proposed density models, $\rho(x)$, of the C-zone and to calculate their continuous one-dimensional Fourier transforms, $G\{\rho(x)\}$, from the general expression;

$$G\{\rho(x)\} = \int_0^\infty \rho(x)\exp\{\frac{2\pi i x \sin\theta}{\lambda}\}dx$$

Since a finite number of elements is being considered the the integral $\int_0^\infty \rho(x)dx$ can be approximated by the summation $\sum_{x=0}^{x=\text{limit}} \rho(x)$, therefore

$$G\{\rho(x)\} = \sum_{x=0}^{x=\text{limit}} \rho(x)\{\cos[\frac{2\pi x \sin\theta}{\lambda}] + i\sin[\frac{2\pi x \sin\theta}{\lambda}]\}$$

This was computed by taking the real part of the expression and obtaining the sum of cosine terms given by;

$$A = \sum_{x=0}^{x=\text{limit}} \rho(x)\cos\{\frac{2\pi x \sin\theta}{\lambda}\}$$

Similarly the imaginary part of the expression was computed by obtaining the sum of sine terms;

$$B = \sum_{x=0}^{x=\text{limit}} \rho(x)\sin\{\frac{2\pi x \sin\theta}{\lambda}\}$$

and the final intensity was calculated as;

$$I(\theta) = A^2 + B^2$$

The computer program was set up to generate the constituent arrays to the C-zone density profile. These were then summed and the diffracted intensity $I(\theta)$ at each 0.0001 radian interval of

2θ up to 0.0125 radians, corresponding to 60Å, was computed as shown above. When computing the diffracted intensity at each θ interval in the transform the model density was sampled at 5Å intervals.

2.4.2. Analysis of the Equatorial Diffraction Data

The scheme for the analysis of equatorial diffraction data is shown in Figure 2.19. In the first stage structure amplitudes were either computed from experimental equatorial data or from simple muscle-like models described below.

The discrete Fourier transforms of models were computed in terms of an orthorhombic unit cell. The motif consists of two myosin filaments with coordinates (0,0) and (1/2,1/2), each surrounded by a shell of crossbridge density and four actin filaments with coordinates (1/2,1/6), (0,1/3), (0,2/3) and (1/2,5/6). Five equatorial reflections with indices 10, 11, 20, 21, 30 were computed, which have multiplicities of 6, 6, 6, 12 and 6 respectively. At each radius, R_{hk} in reciprocal space given by;

$$R_{hk} = \sqrt{\frac{h^2}{a^2} + \frac{k^2}{3a^2}}$$

where h,k are the equivalent indices 02,13,04,15,06 for the orthorhombic cell

the contributions to each of the 6 or 12 reflections at that radius were calculated from each of the objects in the motif in turn. The normalized contributions from the solid cylinders, representing the actin filament and myosin backbone, were given by;

$$F_{cyl}(R) = \frac{2J_1(2\pi Rr)}{(2\pi Rr)}$$

where r is the radius for the respective filament, $R = R_{hk}$

and the first order Bessel function value $J_1(2\pi Rr)$ was computed by a subroutine obtained from Dr. David Parry and checked against **Harvard Tables of Bessel Functions** and those yielded by a subroutine written by Imperial College Computing Centre.

The contribution from the shell of crossbridge density was given by the normalized scattering function for a hollow cylinder;

$$F_{shell}(R) = \frac{2[XJ_1(X) - cXJ_1(cX)]}{X^2(1 - c^2)}$$

where $c = 1 - (r_{outer} - r_{inner})/r_{outer}$

$X = 2\pi Rr_{outer}$

r_{outer}, r_{inner} are the outer and inner radii of the cylindrical shell.

The total scattering amplitude at R is then given by;

$$F(R) = \sum_j F_{cyl}(R)\exp 2\pi i(hx + ky) + \sum_j F_{shell}(R)\exp 2\pi i(hx + ky)$$

and the observed intensity is given by;

$$I_{obs} = \frac{p\,F(R)^2}{\sqrt{(h^2 + k^2/3)}}$$

which was scaled to a value of 100 for the 10 reflection. Note that the scattering amplitude is corrected by a Lorentz factor for the orthorhombic reciprocal lattice since Patterson maps and Fourier syntheses were generated in this form. However for easier comparison with other equatorial data the intensities were output using the hexagonal indices.

Patterson maps were computed from the structure amplitudes

F(R) from;

$$P(u,v) = \sum_{hk} F(R)^2 \cos(2\pi\ (hu + kv))$$

which were then scaled between 0 and 100. The Fourier synthesis from the models' structure amplitudes for the 2^4 phase combinations is then given by;

$$\rho(x,y) = \sum_{hk} P_{hk}[F(R)]\cos(2\pi\ (hx + ky))$$

where P_{hk} is one of the 16 phase combinations. Following modification of these 16 Fourier maps by the function M, Patterson maps were computed by generating their self-convolution;

$$P_{mod}(u,v) = \int_0^1\int_0^1 p(x,y)p(x+u,y+v)\mathbf{dxdy}$$

which was similarly scaled between 0 and 100.

Finally the difference map from the Patterson from the observed structure amplitudes and the modified Patterson was given by;

$$P_{diff}(u,v) = |P(u,v) - P_{mod}(u,v)|$$

and the correlation factor

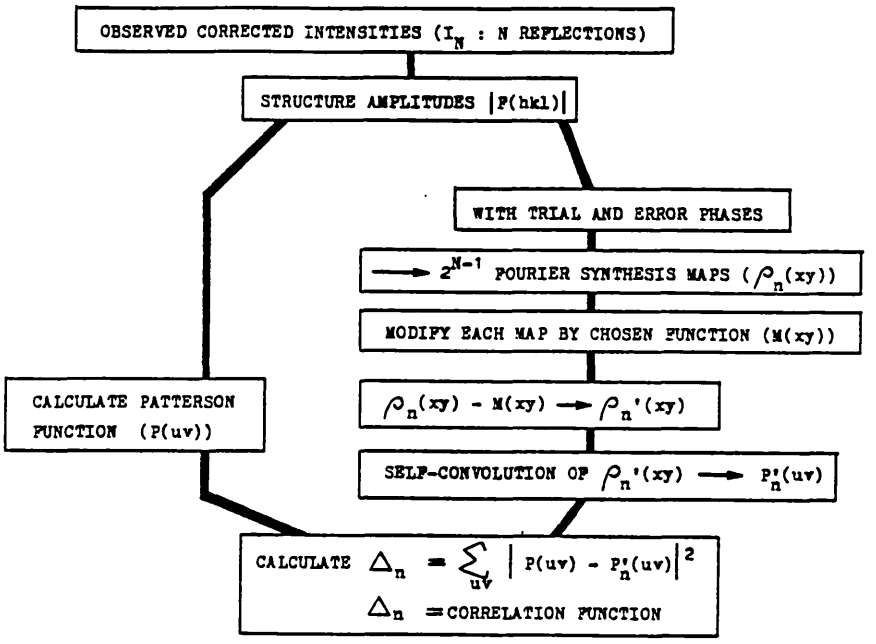
$$\Delta_n = \sum_{uv} |P(u,v) - P_{mod}(u,v)|^2$$

obtained. A very similar procedure for experimental equatorial intensity data ensued, the only difference being that amplitudes F(R) were obtained by correcting for multiplicity, p, and a simple Lorentz factor thus giving;

$$F(R) = \sqrt{\frac{I(h,k)_{obs}\sqrt{(h^2 + k^2/3)}}{p}}$$

2.4.3. Computer Modelling of the Fish Resting Crossbridge Configuration.

The computer program used to model the Plaice fin myosin



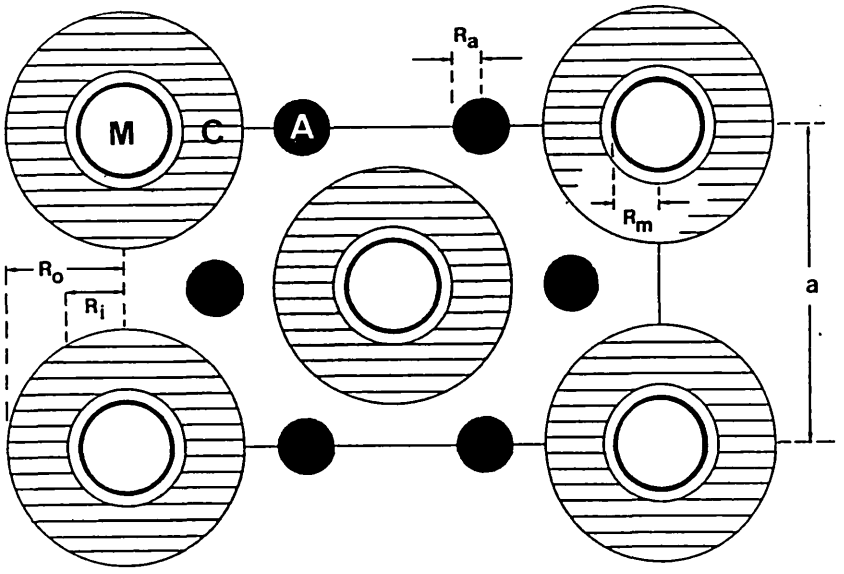


FIGURE 2.19 (a) Flow diagram of the computing procedure for the analysis of the equatorial diffraction data. (b) Diagram showing the parameters defining the end-on view of the muscle-like model structures. A, thin filament; M, thick filament; C, crossbridge annulus.

layer line pattern consisted of two main parts. The first part generated the cylindrical coordinates (R, Φ ,Z) of the spheres used to describe the shape of the myosin heads for each model configuration of the two heads. The second part computes the contribution to the diffracted intensity from each sphere defined by (R, Φ ,Z) at 12 chosen radial positions on each of the first three myosin layer lines.

The crossbridge helix was taken to have three-fold rotational symmetry. The two heads constituting the crossbridge were each described by nine spheres with the radii and separations of the model used by Offer et al (1981) (Table2.21). All configurations were repeated using a shorter model head consisting of 7 spheres, by excluding the contribution to the intensity from the inner two spheres (i.e. those at lowest radii) of each head. Since this effectively increased the radius of centre of mass of the head, the heads were placed so that the centre of the lowest radius sphere of each head was placed at radii between 50Å and 90Å (in 10Å increments) for the 7-sphere head and between 60Å and 100Å for the 9-sphere head, for all configurations.

The configuration of each head was defined by an inclination angle or tilt, β , relative to the horizontal plane (Figure 2.20(a)) and a slew angle α measured relative to the vertical plane normal to the thick filament surface at the point where the whole crossbridge makes "contact" with the surface (Figure 2.20(b)). Both heads could also be rotated about this point in a vertical plane tangential to the filament surface at this point; this rotation was called γ.

Each of the angles defining the crossbridge orientation

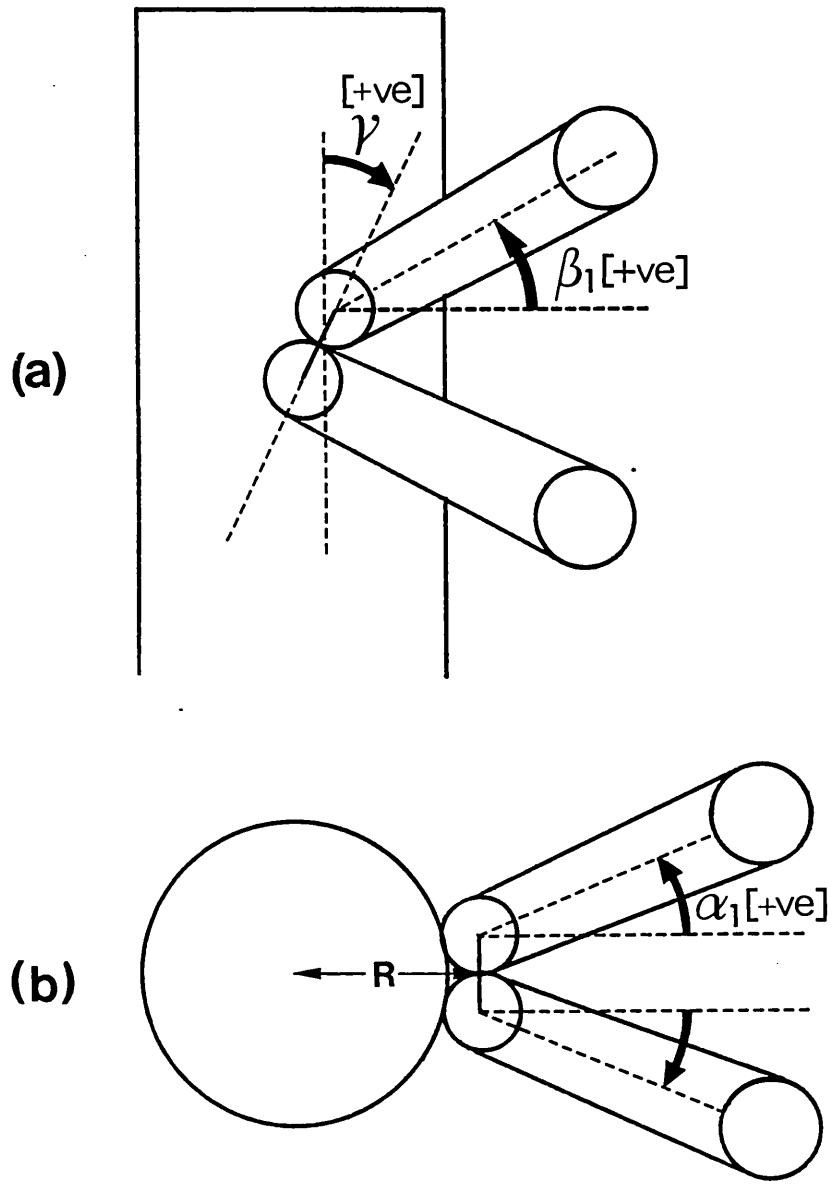


FIGURE 2.20 Diagram showing the angles α, β and γ used to define the orientation of the models of the myosin heads. (a) γ defines the rotation of the whole crossbridge in a plane tangential to the thick filament surface. β, the axial tilt, refers to the angle , measured in a vertical plane (i.e. parallel to the fibre axis), from the plane normal to the thick filament axis. (b) α, the slew, is measured in a horizontal plane, from the normal to the plane which is tangential to the thick filament surface.

TABLE 2.21 The model used to specify the shape of the myosin head by spheres.

Distance of centre of sphere from origin (Å) (Offer et al, 1981)	8	24	40	56	72	91	115	143	171
Radius of sphere (Å)	11.5	11.5	11.5	11.5	12.5	16	20	23	19
Distance of centre of sphere from first sphere (Å)	0	16	32	48	64	83	107	135	163

were incremented by 30° and for each configuration defined by β, α and γ the cylindrical coordinates (R,Φ,Z) for the 18 (or 14) spheres comprising the whole crossbridge were computed. The intensity was calculated on the first three layer lines at the observed row-line positions and intermediate row-line positions, making a total of 12 sampling points. At each sampling position, R, the contribution from the j^{th} sphere, $f_j(S)$, to the total scattering amplitude is given by

$$f_j(S) = 4\pi r_j^3 \frac{[\ \sin x - x\cos x\ ]}{x^3}$$

where $x = 2\pi r_j s$

r_j = radius of the j^{th} sphere.

$s = \sqrt{\{\ r^{*2} + (l^2/c^2)\}}$

l = layer line number

c = long-axis repeat.

These contributions, for each Bessel order n, are summed to give the scattering factor for a discontinuous helix per asymmetric unit (Cochran et al, 1952) as

$$F_c(R,\psi,\tfrac{l}{c}) = \sum_n \sum_j f_j J_n(2\pi R r_j)\exp[i\{n(\psi+\tfrac{1}{2}\pi) - n\phi_j + (2\pi l z_j/c)\}]$$

This can be rewritten (Klug et al, 1958) as

$$F(R,\psi,l/c) = \sum_n G_{n,l}(R)\exp[in(\psi + \tfrac{1}{2}\pi)]$$

$G_{n,l}(R)$ is a complex number representing the contribution of one Bessel function of order, n, to the scattering amplitude on the layer line, l, and is given by

$$G_{n,l}(R) = \sum_j f_j J_n(2\pi R r_j)\exp[i\{2\pi l z_j/c - \phi_j n\}]$$

which has a real part given by

$$A_{n,l}(R) = \sum_j f_j J_n(2\pi R r_j)\cos[2\pi l z_j/c - \phi_j n]$$

and an imaginary part given by

$$B_{n,l}(R) = \sum_j f_j J_n(2\pi R r_j)\sin[2\pi l z_j/c - \phi_j n]$$

Thus the cylindrically averaged intensity transform for an isolated molecule which is obtained by averaging $FF^*(R,\Psi,l/c)$ over Ψ (Franklin and Klug, 1955) is

$$\langle I(R,l/c)\rangle_\psi = \sum_n G_{n,l}G^*_{n,l} = \sum_n (A_{n,l} + iB_{n,l})(A_{n,l} - iB_{n,l})$$

$$\langle I(R,l/c)\rangle_\psi = \sum_{nj}\sum (A^2_{n,l} + B^2_{n,l})$$

Terms involving products of different Bessel orders are eliminated when the theoretical intensity is averaged over Ψ but, in any case, if there is no significant overlap between different Bessel orders on a particular layer line then the rotationally averaged transform outlined above will give essentially the same results as the sampled myosin filament transform given by

$$F(R_{hk},\psi_{hk},l/c) = \sum_{nJ}\sum f_j J_n(2\pi R_{hk} r_j)\exp[i\{n(\psi_{hk} + \tfrac{\pi}{2} - \phi_j) + 2\pi l z_j/c\}]$$

where $$R = (1/a)\sqrt{\{(4/3)[h^2 + k^2 + hk]\}}$$

$$\psi_{hk} = \tan^{-1}\left\{\frac{h + 2k}{h\sqrt{3}}\right\}$$

and this was found to be the case. To verify this, the individual Bessel orders on the first layer line for a number of models were computed individually. J_3 and J_{-6} on this layer line showed that the lower Bessel order term, J_3, dominated the 10, 11 and 20 row line positions, with the J_{-6} term reaching a maximum at the 21 row line position. It was only at this latter row line position that any azimuthal variation in the sampled transform was evident. Because of this small degree of interference of the main contributory Bessel orders, the cylindrically averaged transform could just be calculated at the appropriate radial position

along each layer line. However this, and the sampled myosin filament transform, were computed for all of the selected models from all of the possible configurations computed.

The observed integrated intensities were divided by the multiplicity, p, and multiplied by the simple Lorentz factor, 1/R, and then compared with the computed intensities.

The Bessel function orders, n, contributing to each layer line, l, are given for a helix with symmetry U_t as

$$l = nt + Um \qquad (m = 0, \pm 1, \pm 2, \ldots.)$$

Since each of the three strands of the crossbridge helix have the symmetry 9_1 then $l = n + 9m$

Layer lines l= 3, 6, 9 etc. from each strand of the helix correspond to the 1st, 2nd, 3rd, etc. layer lines from the three-stranded helix thus the values of n for the 1st, 2nd and 3rd layer lines are given by substituting l = 3, 6, 9 into the equation above. Thus the Bessel orders included on each layer line were; 3, -6, 12, -15 on the 1st; -3, 6, -12, 15 on the 2nd; 0, -9, 9 on the third. Higher order Bessel functions contributed very little in the regions of the transform considered.

Amplitudes were multiplied by an isotropic temperature factor to account for general disorder, given by

$$\exp(-2\pi^2 \Delta_s^2 S^2) = \exp(-\tfrac{1}{4} B S^2)$$

The inner end of the myosin head was considered to have smaller displacements than the outer end, Δ_s was therefore initially set to 2.5Å for the innermost sphere on each head and incremented by the same amount for each sphere so that the outer end had a value of 20Å. Since $\Delta_s^2 S^2 = (\Delta_x^2 x^2 + \Delta_y^2 y^2 + \Delta_z^2 z^2)$ this corresponds to a value for the root mean square isotropic displacement $\Delta_s = \Delta_x = \Delta_y = \Delta_x = 11.5$Å.

CHAPTER 3 : C-ZONE ANALYSIS

3.1. INTRODUCTION 154

3.2. OPTICAL DIFFRACTION RESULTS 157

3.2.1. Optical Diffraction Spacings. 157

3.2.2. Systematic Errors in Measurement of Spacings of the First and Second Order Peaks of the 434Å Repeat. 162

3.2.3. Relative Intensities. 167

3.3. DIRECT ANALYSIS OF LATERALLY SMEARED C-ZONE IMAGES 168

3.4. COMPUTER MODELLING OF THE C-ZONE STRUCTURE 169

3.4.1. Modelling with Box Functions. 169

3.4.2. Modelling with Gaussian Density Profiles. 175

3.4.3. Modelling with a 429Å Crossbridge Axial Repeat. 179

3.5. DISCUSSION 183

3.5.1. Summary of the Results. 183

3.5.2. The Crossbridge Array. 185

3.5.3. The Origin of the Intervening Step Density. 192

3.5.4. The Origin of the 442Å and 418Å Meridional X-ray Reflections. 193

3.5.5. The Role of C-protein in Determining the Length of the Thick Filament. 199

3.5.6. Summary. 202

CHAPTER 3 : C-ZONE ANALYSIS

3.1. Introduction.

Cryosections and A-segments have shown in most detail the pattern of transverse striations in the vertebrate muscle A-band which relate to the rows of crossbridge density and other proteins labelling the thick filaments in almost complete register across the sarcomere width. However as mentioned earlier (Chapter 1; section 1.3.2.A), studies of these different preparations report conflicting results as to the repeat of C-protein relative to myosin and on the appearance of this banding pattern particularly in the C-zone. Craig (1977) concludes that the grouping of a C-protein stripe and the two immediately proximal stripes attributed to the crossbridge levels occurs across the C-zone without change in the pattern of grouping. Sjöström and Squire (1977) however conclude that a systematic change occurs in this pattern which is consistent with different repeats for the C-protein and the axially projected myosin crossbridge arrangement.

Figure 3.1 shows a densitometer trace through the C-zone of a micrograph of a cryosectioned A-band. Visual examination of these revealed a systematic change in the staining pattern, parallel to the fibre axis, which would be expected if the prominent striations in the C-zone (C3,C6,C9..etc.; Figure 3.1.) had a different periodicity than the weaker striations (C1,C2,C4,C5,C7..etc.; Figure 3.1, Sjöström and Squire, 1977). The stain filled (dark) line to the right (distal) side of each prominent line (C3,C6,C9..etc.) is relatively strong and generally broader between striations C3 and C4 and becomes narrower and less obvious at the distal end of the C-zone,

between striations C18 and C19 for example. In addition the stain-filled line preceding each prominent line commences as a narrow line at the left (proximal) end of the C-zone between striations C2 and C3, and becomes broader and more obvious between C17 and C18.

In order to put this apparent presence of two periodicities onto a quantitative basis Sjöström and Squire measured the spacings between the sets of striations directly from micrographs. The repeat of the prominent striations C3, C6, C9, C12, C15, C18 and C21 was obtained by measuring the separations between C3 and C12, C6 and C15, C9 and C18 and then dividing each separation by three. The average value was called l_c. The repeat of the weaker lines was obtained by making similar measurements on lines C2, C5, C8, C11, C14, C17, C20 and C1, C4, C7, C10, C13, C16, C19, C21; the average value from both sets of lines was called l_m. The ratio l_c/l_m was obtained and l_c calculated assuming l_m to be the true repeat of the myosin filament, 42.9nm. The ratio l_c/l_m was 1.014(±0.006) giving l_c equal to 43.5 (±0.3)nm. Thus it was shown that the longer repeat was significantly different from l_m (at a 99.9% confidence level) and that this repeat is associated with the prominent striations C3, C6, C9, C12, C15, C18 and C21.

The purpose of the analysis described in this chapter is to extend the resolution of the optical diffraction studies of the C-zone by computer modelling the first six meridional reflections of its optical diffraction pattern which are approximate orders of a repeat of about 43nm. The features of the models are based on one-dimensionally averaged images of the cryosectioned C-zone (see Materials and Methods).

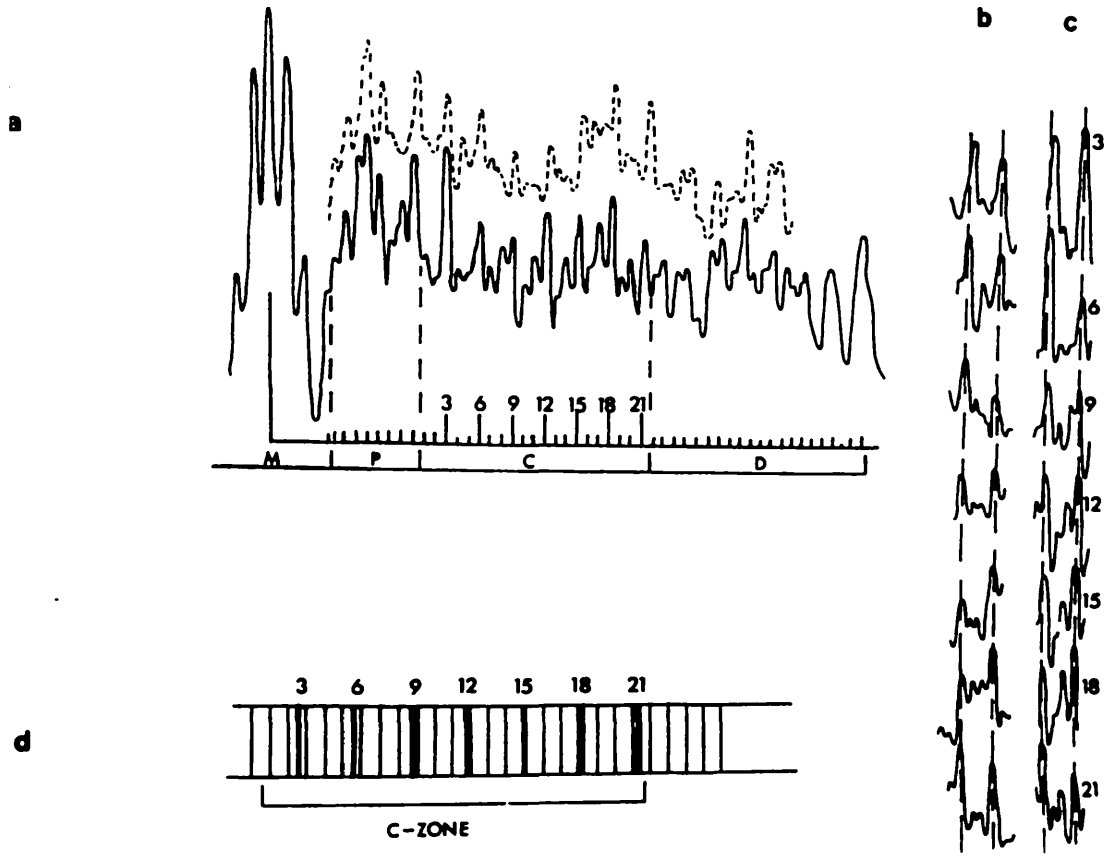


FIGURE 3.1 (a) A densitometer trace along a micrograph of the A-band of cryosectioned human m.tibialis anterior muscle (as shown in Figure 3.3). The upper (broken line) and lower traces are from opposite sides of the M-band. (b) This shows sections of the upper (broken line) trace in (a). The systematic variations in profile between each of the strong pairs of lines (3, 6, 9 etc. in the C-zone in (a)) across the C-zone are shown. Such variations are clearer in (c) which shows similar sections to (b) but for the C-zone in the lower trace in (a). (d) A diagram showing how two overlapping arrays could account for the C-zone staining profile. The broad lines (numbered 3, 6, 9 etc.) have a repeat (440Å) slightly greater than three times that of the narrow lines, which have a repeat of 143Å. This model is not intended to precisely account for the changes in profile but many features of the observed distribution are consistent with this type of arrangement (from Sjöström and Squire, 1977).

3.2. Optical Diffraction Results.

3.2.1. Optical Diffraction Spacings.

The spacings of meridional reflections were measured from optical diffraction patterns of 12 C-zones (Figure 3.2) from six different electron micrographs (Figure 3.3). Meridional reflections up to the eighth order of a repeat of about 43nm were observed and measured. The eight orders of 43nm will be referred to as reflections 1 to 8. The spacing of reflection 3 was in the range 14nm to 15nm and thus assigned the crossbridge repeat of 14.3nm for calibration purposes. Relative to this spacing, reflections 1 to 8 (Table 3.4) had measured average d-spacings of 436.3(±5.8)Å, 217.0(±0.6)Å, 143 (used for calibration), 107.3(±0.6)Å, 85.4(±0.3)Å, 71.4(±0.3)Å, 61.7Å and 53.9Å. No reliable statistics can be quoted for reflections 7 and 8.

Other less frequently seen reflections between 350Å to 380Å and at 190Å were attributed to the thin filament structures which partly or wholly overlapped the C-zones in all the micrographs studied. Sarcomere lengths were within 0.1 μm of 3.3 μm. The thin filament length in this muscle is about 1.30 to 1.35 μm. Thus between about 40% and 70% of the C-zone was overlapped by thin filaments.

Statistical analysis of the measured d spacings of reflection 1 to 6 (Table 3.5) show that reflections 4 and 6 are not significantly different from the 4th and 6th orders of a repeat of about 429Å (i.e. three times the crossbridge repeat of 143Å. Reflection 5 (85.4Å) is also very close to the 5th order of a 429Å repeat (85.8Å) but the small standard deviation results in a low level of confidence for the significance of this difference. However it is clear when reflections 4,5 and 6 are

FIGURE 3.2 Optical diffraction patterns from the C-zones of negatively stained longitudinal cryosections of human m.tib.ant. (such as those in Figure 3.3) with the fibre axis across the page. The first six orders of a repeat of about 430Å are indicated by numbered arrows. The three groups of intensity distribution, classified according to the intensities of reflections 4, 5 and 6 (i.e. I_4, I_5 and I_6) are represented by (a), (b) and (c). Shown in (a) is the optical diffraction pattern with $I_4 < I_5$ corresponding to Group I. In (b) $I_4 \geq I_5 \leq I_6$, Group II and in (c) $I_4 \geq I_5 > I_6$, Group III.

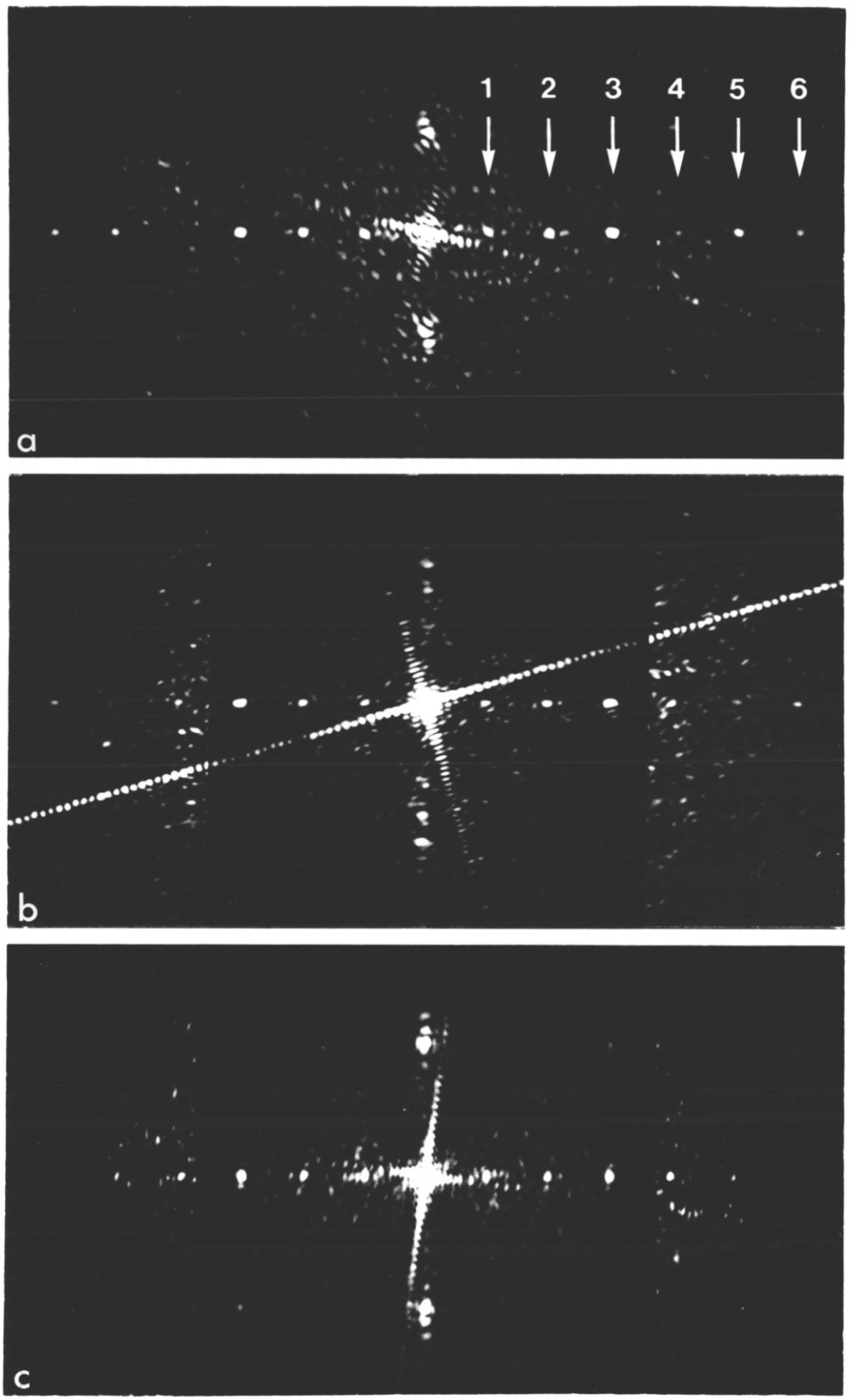
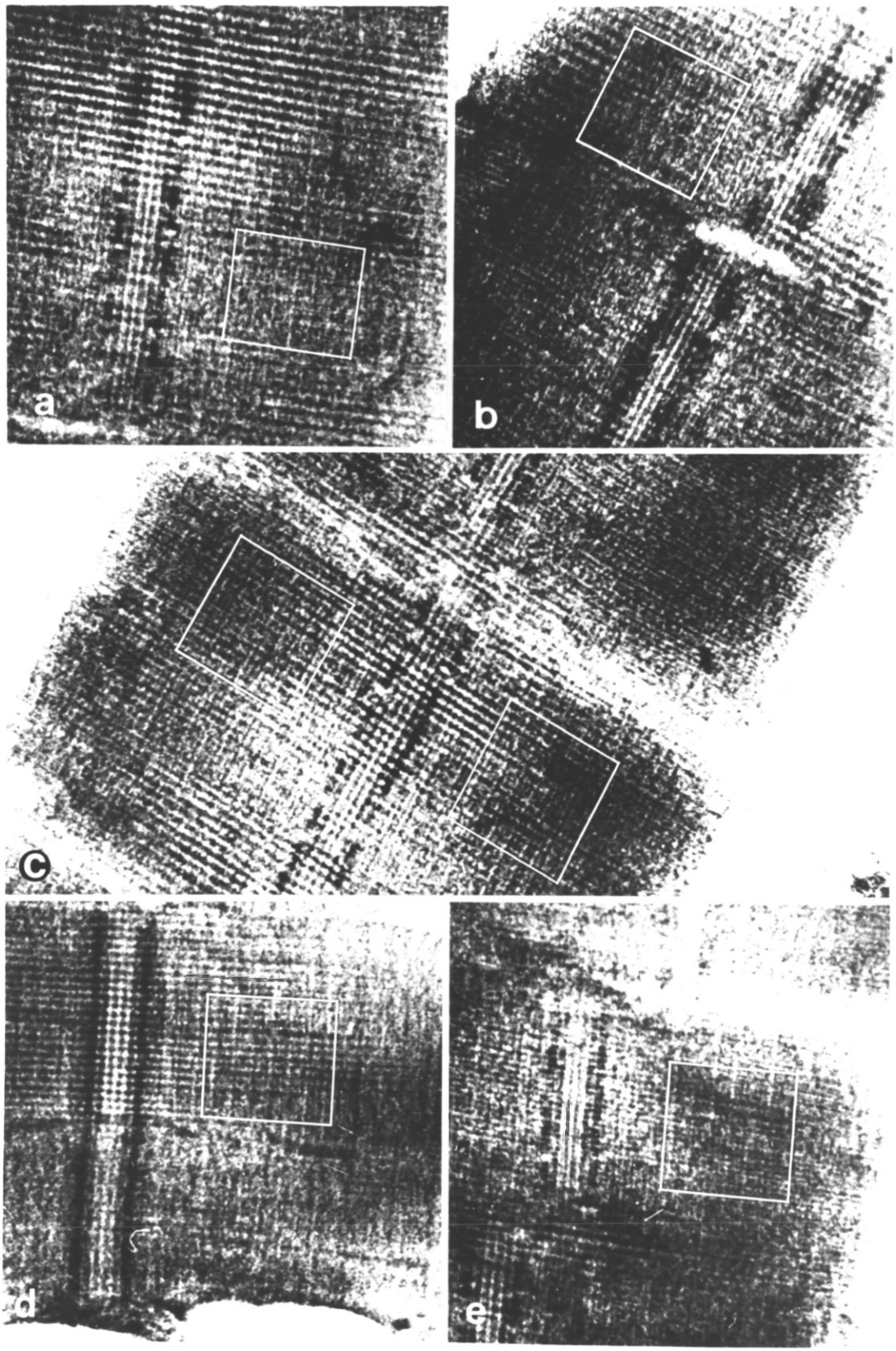


Fig 3.2

FIGURE 3.3 Parts of A-bands of negatively stained longitudinal cryosections of human m.tibialis anterior muscle showing the prominent transverse striations across the A-band. The C-zones used to produce the averages in Figure 3.6, and some of the values in Table 3.4, are indicated by the boxed regions. The consistent appearance of different sections is clearly seen. (a) and (b) have optical diffraction patterns in group I; (c) in group II, and (d) and (e) in group III. Magnification 85,000x.


a
b
c
d
e

compared with the spacing inferred from reflections 1 and 2 of 434Å (Table 3.5b) that they are unlikely to be orders of a spacing much longer than 429Å.

Measured d spacings for reflections 1 and 2 are clearly significantly different from the first and second orders of a 429Å repeat at confidence levels of about 95% and better than 99.9% respectively (Table 3.5a). It can be said with much greater confidence however that these d spacings originate from a population with a mean of about 434Å (Table 3.5b).

The large range of values for the d spacing of reflection 1 of 426 to 448Å is probably mainly due to the proximity of this peak to the mask function and interference effects displacing the peak from its true position. In the case of reflection 2 no such effects were observable which is apparent from the very low standard deviation for its measurement (i.e. 0.6Å). Despite the range of values for reflection 1 the distribution lies to the low-angle side of 429Å and accordingly at a less than 1% level of confidence it can be said to be the first order of a 429Å repeat (Table 3.5a). At a greater than 25% level of confidence it is from a population whose mean is twice the d spacing for reflection 2, 434Å (i.e. 2 x 217.0Å, Table 3.5b).

3.2.2. Systematic Errors in Measurement of the First and Second Order Peaks of the 434Å Repeat.

Since the periodicity indicated by reflections 1 and 2 is only about 1% greater than that of reflections 3,4,5 and 6 it is essential to show that this difference has not arisen from systematic errors in the analysis. The reproducibilty of measurements from the diffraction pattern of a single C-zone was estimated by;-

TABLE 3.4

Relative spacings and intensities of reflections in optical diffraction patterns from human C-zones

Group	Micrograph	d_1	I_1	d_2	I_2	d_3†	I_3	d_4	I_4	d_5	I_5	d_6	I_6	d_7	d_8
I	5641 (2)	440·0	0·4	216·8	0·7	143	1	—	vw	85·4	mw	71·1	m	—	—
	5648 (1)	426·1	0·7	217·5	0·7	143	1	106·5	0·05	85·6	0·09	71·7	0·03	61·7	53·9
	5653 (1)	429·9	0·4	217·4	0·7	143	1	107·4	vw	85·7	0·3	70·8	0·03	—	—
	Average	432·0		217·2		143		106·9		85·6		71·2			
II	5653 (2)	443·0	0·4	217·4	0·5	143	1	107·6	0·1	85·0	0·05	71·5	0·06	61·7	—
	5680 (1)	432·7	0·4	216·7	0·4	143	1	107·5	m	85·2	m	71·4	m	—	—
	(2)	436·4	0·2	215·3	0·4	143	1	107·1	mw	85·4	w	71·2	mw	—	—
	Average	437·4		216·5		143		107·4		85·2		71·4			
III	5647 (1)	432·8	0·6	216·9	0·7	143	1	—	vw	—	—	—	—	—	—
	5653 (3)	435·2	ms	217·1	ms	143	1	106·5	m	85·2	mw	71·6	w	—	—
	(4)	447·8	0·3	217·3	0·7	143	1	106·7	m	85·7	m	—	mw	—	—
	5744 (1)	436·2	0·7	217·3	0·7	143	1	108·3	0·08	—	—	—	—	—	—
	(2)	435·9	0·7	216·8	0·7	143	1	108·0	0·1	85·7	0·06	71·8	0·02	—	—
	5641 (1)	439·3	0·5	217·0	0·6	143	1	—	—	—	—	—	—	—	—
	Average	437·9		217·1		143		107·4		85·5		71·7			
Overall average		436·3		217·0		143		107·3		85·4		71·4			
s.t.d.		(5·8)		(0·6)				(0·6)		(0·3)		(0·3)			
Theoretical orders of a 429 Å repeat		429·0		214·5		143		107·2		85·8		71·5		61·2	53·6

Additional reflections were observed as follows: micrograph 5653 (2): 555·7, 378·5, 303·9, 269·5, 198·4, 195·96; micrograph 5680 (2): 379·9; micrograph 5653 (3): 367·4; micrograph 5653 (4): 378·1; micrograph 5744 (2): 355·6 and micrograph 5641 (2): 101·3.

† All spacings (d_i in ångstrom units) were calibrated using the spacing for this reflection and all intensities (I_i) were normalized using the intensity for this reflection. Each spacing measurement is the mean of about 4 to 9 independent measurements.

s, strong; w, weak; m, medium; v, very; s.t.d., standard deviation.

TABLE 3.5

Statistics of C-zone measurements

A. *%Probability that the observed spacings ($\bar{x}$) are consistent with a 429 Å repeat*

Measurement	$\bar{x}$	s	N	t	Level (%)†
1st order	436·3	5·8	12	4·2	~0·1
Twice 2nd order	434·0	1·2	12	13·8	<0·1
Direct ($429 \times I_c/I_m$)	435·0	2·6	7	5·6	~0·1
Average images ($429 \times I_c/I_m$)	432·9	2·6	6	3·5	~1

B. % *Probability that reflections 1 to 6 in Table 1 are orders of a repeat of 434 Å (twice d_2)*

Reflection	$\bar{x}$	s	u	N	t	Level (%)
1	436·3	5·8	434·0	12	1·3	>25
2	217·0	0·6	217·0	12	0	~100
3	143		Used for calibration			
4	107·3	0·6	108·5	9	5·7	<0·1
5	85·4	0·3	86·8	9	13·2	<0·1
6	71·4	0·3	72·3	8	7·9	<0·1

C. % *Probability that reflections 1 to 6 in Table 1 are orders of a repeat of 429 Å*

Reflection	$\bar{x}$	s	u	N	t	Level (%)
1	436·3	5·8	429·0	12	4·2	~0·1
2	217·0	0·6	214·5	12	13·8	<0·1
3	143		Used for calibration			
4	107·3	0·6	107·2	9	0·5	~60
5	85·4	0·3	85·8	9	3·8	~0·5
6	71·4	0·3	71·5	8	0·9	~40

Values of t were calculated using the formula $t = (\bar{x}-u)/(s/\sqrt{[N-1]})$, where $\bar{x}$ are the observed spacings with standard deviation s, u is the spacing for the postulated repeat, and N is the number of different C-zones analysed which contribute to $\bar{x}$. All spacings are in ångstrom units.

† This level indicates the % probability that the sample mean $\bar{x}$ is from a population which has a mean value u (i.e. the % probability with which the corresponding value of t will be exceeded by chance).

(i) Measuring an exposure of a diffraction pattern showing reflections 1 to 6 ten times. This gave a probable measurement error of 0.1%. This is the average deviation of the measured values from their average value for reflection 2.

(ii) Measuring different time exposures of the same diffraction pattern gave a probable error of 0.1%.

(iii) Measuring the diffraction pattern of a C-zone masked in a variety of slightly different ways gave a probable error of 0.2%. The difficulties in masking the C-zone precisely arose from the need to tilt the mask function relative to the meridional diffraction pattern (see Material and Methods, 2.2.7). In practice this tilt was minimised so that as much of the C-zone across the sarcomere width, as was well preserved, could be included in the diffraction analysis. By studying patterns at small tilts it was observed that insufficient tilt could displace the first order peak within the region of about 1/400 to 1/470Å and sometimes appear to split the reflection across the meridian. All the spacings in Table 3.4 are from patterns in which the mask function was increasingly tilted relative to the meridional diffraction until no further change in the first prominent meridional reflection was observed. This was accomplished with tilts between 10^{o} and 15^{o} which may lead to 95% or more of the actual C-zone region being included in the diffraction pattern. Since the meridional diffraction arises from structure which is periodic over a

significant length of the C-zone these small errors in defining the C-zone would not be expected to, and were not observed to, alter the meridional intensity pattern. Reflection 2, which provides much clearer evidence for the presence of a repeat of 434Å, was under these conditions placed quite satisfactorily clear of the mask function. Only in this case could the variation between the spacings from different C-zones (the average deviation of the measured values from their average value being 0.2%) be wholly accounted for.

Since the errors discussed above for reflection 2 were less for reflections 4,5 and 6, they could only possibly account for a very small part of the 1% difference in periodicities these reflections represent.

It is possible that reflections 1 and 2 represent first and second order diffraction peaks from a true periodicity of 429Å which have been shifted to their observed positions due to the unit (stripe) transform which envelopes them or due to a steep background slope underlying these reflections. Both of these artefacts would have the effect of moving the true first and second order peaks towards the centre of the pattern i.e. to higher spacings as observed. However using a stripe width representative of the observed striations at C3, C6, C9 etc., and a single repeat of 429Å for both of the arrays in the model the first order peak appeared at 1/429.3Å and the second order peak at 1/215.4Å. In order to shift these peaks to even higher spacings it was necessary to incorporate background slopes into the intensity profile about ten times the actual observed slope. This procured values of 1/432Å and 1/216.9Å.

It is therefore apparent that the two effects considered together cannot account for the observed shift of reflections 1 and 2 to the observed positions from the first and second orders of 429Å. It is fair to conclude therefore that the spacings of reflections 1 and 2 are not from a structure with a repeat of 429Å but are much more likely to come from a structure with a repeat of about 434Å. None of the spacings of reflections 3, 4, 5 and 6 are orders of a repeat of 434Å but these are very close to the 3rd, 4th, 5th and 6th orders of a repeat of 429Å. Thus the spacings of reflections 3, 4, 5 and 6 are consistent with a structure with a repeat of 429Å.

3.2.3. Relative Intensities.

The relative intensities of reflections 1 to 6 were obtained from microdensitometer traces of the meridional optical diffraction patterns (see Materials and Methods) or estimated visually from the films of these patterns (Table 3.4.). From this analysis the C-zones were grouped into three types. In all three groups the relative intensities of reflections 1, 2 and 3 followed the pattern $I1 < I2 < I3$. The average value of I2/I1 was 1.40 (±0.47) and of I3/I2 was 1.69 (±0.44). The classification of C-zones was based on the relative intensities of reflections 4, 5 and 6 and the groups were defined as follows;

Group I, $I4 < I5$

Group II, $I4 \geq I5 \leq I6$

Group III, $I4 \geq I5 > I6$

The significance of this grouping will be seen to follow from the computer modelling of these diffraction patterns.

3.3. Direct Analysis of Laterally Smeared C-zone Images

The periodicities of the transverse striations in laterally smeared C-zone images were measured directly using the same method and nomenclature as that adopted by Sjöström and Squire (1977), described in section 3.

Averaged images gave a ratio l_c/l_m equal to 1.009 (±0.006). With l_m equal to 429Å this gives l_c equal to 432.9 (±2.6)Å and thus a different periodicity is apparent which is statistically significant at a 99.9% level of confidence (Table 3.5.). As in the direct measurements of micrographs the longer repeat is also shown to be associated with the prominent striations C3,C6,C9..etc., in the C-zone.

Measurements were made of the relative separations of the weak lines in each 430 to 435Å period from laterally smeared C-zones (Figure 3.6). There are usually two such lines between each pair of prominent lines C3 to C6, C6 to C9 etc., giving three gaps which were labelled from the proximal end as a, b and c. Thus the spacings C3 to C4, C6 to C7 and so on are a, C4 to C5, C7 to C8 and so on are b, and C5 to C6, C8 to C9 and so on are c. In general it was found that b was smaller than 1/3 of a + b + c. With a + b + c approximately equal to 430Å then b was about 120 (±15)Å for Group I C-zones (see Table 3.4), about 137 (±15)Å (i.e. hardly significantly different from 1/3 of a + b + c) for Group II C-zones and about 128 (±15)Å for Group III C-zones. There was also a trend that a was greater than c although the statistics are too poor to enable one to attach any significance to this particular observation. However the low value of b strongly suggests that the repeat of the myosin crossbridge lines is not simply 143Å. It will also be seen in the computer

modelling below that it is necessary for the crossbridge lines to have a repeat of 429Å rather than 143Å in order to satisfactorily account for the optical diffraction data.

Figure 3.6(g) shows an image which is the average of the 6 smeared C-zones in Figure 3.6(a) to (f). The axial spacings of the striations in this image (Figure 3.6(g)) are very closely correlated with the average of all of the spacings taken from the 6 C-zones in Figure 3.6(a) to (f), which indicates the reproducibility of the averaging carried out and the reliability of measurements of axial spacing made from these smeared C-zones.

Attempts were made to measure the axial widths of the transverse striations in the laterally smeared C-zones (or from microdensitometer traces of them) but this was not straightforward because of difficulties in estimating the background density level. The axial widths obtained for these lines in the computer modelling were considered to be more reliable and these are discussed in the next section.

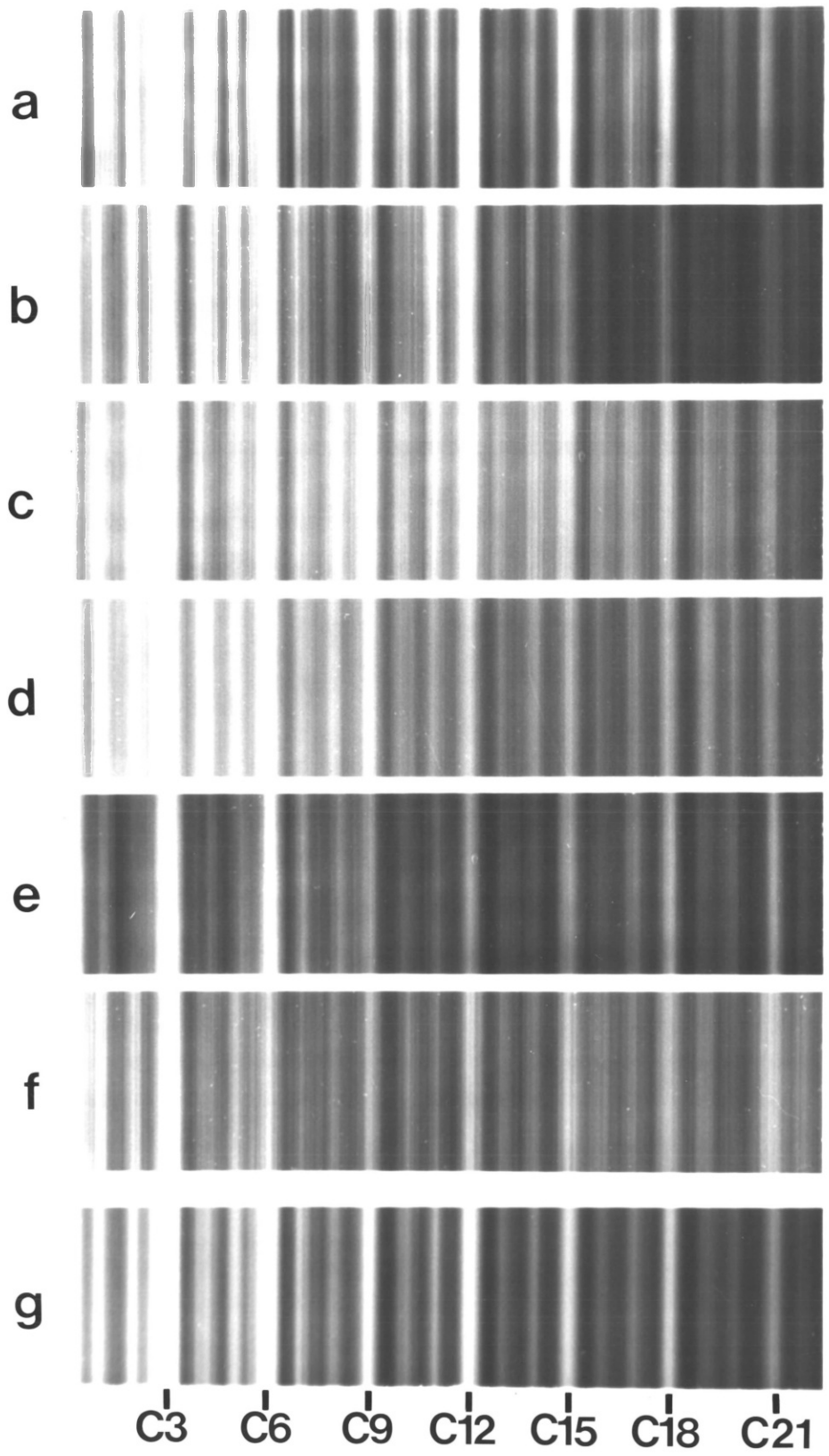
3.4. Computer Modelling Of The C-zone Structure.

3.4.1. Modelling With Box Functions.

Simple one-dimensional model density structures and their one-dimensional continuous Fourier transforms were computed to try and account for the protein density distribution within the human C-zone and the intensity distribution along the meridian of its optical diffraction pattern. The initial model comprised two one-dimensional arrays of box-functions;

(i) An array of 7 box functions with a repeat of 434Å (Figure 3.7.) was chosen to represent the larger stain excluding feature to which the prominence of lines C3,C6,C9,C12,C15,C18 and C21 was attributed.

FIGURE 3.6 Laterally smeared images ((a) to (f)) of the 6 C-zones shown as Figure 3.3 (a) to (e) respectively. These averages, and the average of all 6 images ((a) to (f)) shown in (g), were produced by the enlarger method. The strong lines C3, C6, C9 etc. are very clear in all of these averages as are the weaker (crossbridge) lines which lie between them. Similar variations in the staining profile throughout the C-zone have been made clearer by this 1-D averaging of the original electron micrographs and these variations are represented in the overall average in (g). Magnification 378,000x.


a
b
c
d
e
f
g
C3
C6
C9
C12
C15
C18
C21

(ii) An array of 19 smaller box functions with a repeat of 143Å (Figure 3.7b.) representing the weaker striations C4,C5,C7,C8...etc., which are assumed to arise from the crossbridge array.

A combination of these two arrays represented the simplest model of the C-zone structure . The heights and widths of the box functions in the two arrays could be varied and the two arrays shifted relative to each other by multiples of 5Å. The two arrays were combined to give the density model (D) and the diffracted intensity (I) of the model was computed to give the combined Fourier transform. The C-zone structure was modelled between lines C3 and C21 exclusively and the transform was calculated to include the observed reflections 1 to 6.

3.3.1. Modelling With Box Function Profiles.

The computed diffracted intensity (I) from the 434Å period box function is shown in Figure 3.7a (upper profile). The width of the box function in Figure 3.7a is 120Å. Similarly for the Fourier transform of the crossbridge array (Figure 3.7b.). The width of the box funtion in this density profile is 70Å. When the two arrays are combined to give the model for the C-zone density there will only be contributions to reflections 3 and 6 from the 143Å period array to the combined intensity profile.

Using the above components to generate realistic density profiles for the general distribution within the C-zone it is not possible to simulate the observed peak intensities or peak positions. Figure 3.8 represents the best agreement which could be achieved. The intensity profile has two main deficiences;

(i) The intensity of reflection 1 cannot be made smaller than that of reflection 2; the observed ratio of I_2/I_1

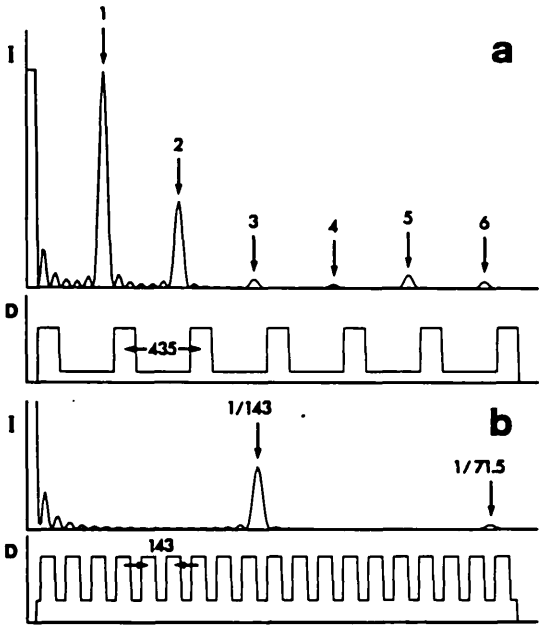


FIGURE 3.7 Density models of the C-zone staining distribution (D) and the computed intensity distributions (I). (a) Numbered arrows are used to indicate orders of the repeat of 435Å which is the repeat of the box function in the density model (D) which was taken to represent the prominent striations C3,C6,C9 etc., in the C-zone. (b) A box function with a repeat of 143Å used to represent the weaker striations due the crossbridges which have a repeat of about 1/3 of that of C3,C6 etc.

was 1.40 (±0.45).

(ii) The spacings of reflections 4 and 5 ($1/108.5\text{Å}^{-1}$ and $1/87\text{Å}^{-1}$) are determined by the larger period array whereas the observed d-spacings show that reflections 3,4,5 and 6 should be corresponding orders of 429Å (i.e. three times the crossbridge array period of 143Å) at $1/143\text{Å}^{-1}$, $1/107.2\text{Å}^{-1}$, $1/85.4\text{Å}^{-1}$ and $1/71.5\text{Å}^{-1}$ respectively.

The first of these problems can be overcome by introducing another component array into the density model, an "intervening step" density. It will be seen later that there is a case for introducing such a feature. This component was introduced as an array of broad (about 200Å wide) low density box functions placed approximately between each of the lines C3, C6, C9 ..etc., with a repeat of 434Å. A width for the box function of about 200Å was chosen so that the central maximum peak in its transform descends to zero approximately at the position of reflection 2 ($1/217\text{Å}^{-1}$) from the 434Å period array. Thus it's main contribution in the combined transform was to the first order reflection. Since each step in the intervening step array was placed roughly between density peaks in the 434Å period array, most diffracted intensity from it is out of phase with that from the 434Å array at the position of reflection 1. Here the contribution from the intervening step is subtracted from the contribution from the 434Å array.

This modification enabled the complete range of observed intensity distributions to be modelled (Figure 3.8). The range of observed intensities for reflections 1,2 and 3 could be simulated and the groups defined by $I_4 < I_5$ (Group I) and $I_4 > I_5$ (Groups

II and III) could also be accounted for by varying the height of the intervening step.

The second problem remained however that reflections 4 and 5 were almost entirely due to the first subsidiary maximum from the box function on the 434Å period array and thus had spacings of $4/434Å^{-1}$ and $5/434Å^{-1}$ rather than the observed values of $4/429Å^{-1}$ and $5/429Å^{-1}$. Some modification to the density profile was required to ensure that the transform from the 434Å period box function would not contribute to the overall pattern beyond reflection 2.

3.4.2. Modelling with Gaussian Density Profiles.

The 434Å period box function was replaced by an array of Gaussian density peaks. The width of the Gaussian peaks, defined by σ, was chosen such that the transform descended to virtually zero at $1/143Å^{-1}$. Thus the 434Å period array of the model now does not contribute to the pattern beyond reflection 2 and the modification to the density model is a realistic one since the striations in the original electron micrographs and in the contrasty copies used in the optical diffraction analysis are better represented by this profile.

The crossbridge array was similarly represented by an array of smaller Gaussian density peaks. The contribution to the overall transform from this component is not significantly altered since reflections 3 and 6 are both within the radial extent of the central zero-order peak for this component. The height of the Gaussian profile was chosen to give the same relative intensity contribution to the overall transform as that obtained in the modelling with box functions.

C-zone models including the above modifications could

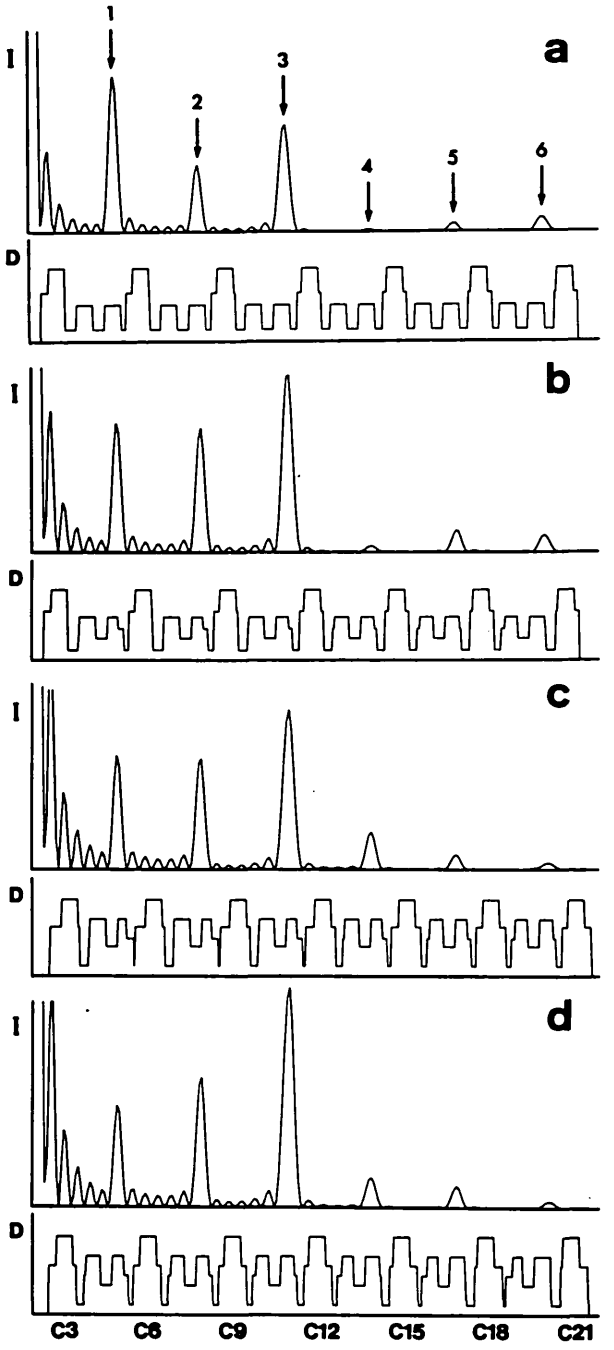


FIGURE 3.8 (a) Density models (D) have been produced by adding the two density arrays shown in Figure 3.7. In (b),(c) and (d) an additional "intervening step" box function is added which is placed midway between the prominent density peaks in (a). The heights and widths of the box functions have been varied in models (b) to (d). The C-zone density peaks in (d) have been labelled as in Figure 3.1.

clearly not generate reflections 4 and 5 and the relative intensity of reflection 1 cannot be made equal to or smaller than that of reflection 2 as is observed.

The intervening step reintroduced this time as a 429Å period box function could give reflections 4 and 5 at the observed positions of $4/429Å^{-1}$ and $5/429Å^{-1}$ if the first subsidiary maximum in its transform occurs in this region. In addition since the amplitude of the diffraction from this array at $1/429Å^{-1}$ is out of phase with that of reflection 1 (at 1/434Å) from the 434Å array it will serve to reduce the intensity of this reflection in the combined transform relative to reflections 2 and 3.

However by increasing the height of the intervening step it was not possible to produce reflections 4 and 5 with large enough relative intensities and retain the correct relative intensities for reflections 1,2 and 3. The model in Figure 3.9 shows that reflection 5 is only just evident and the relative intensities of reflections 1,2 and 3 are outside the range of the observed values. The density profile (Figure 3.9d) is also difficult to reconcile with the observed staining distribution.

Since modifying the profile shape of the repeating unit in the 434Å period array and incorporating the intervening step array with a 434Å or 429Å period array could not account for the relative intensities and spacings of reflections 4 and 5, the assumption of an exact 143Å axial repeat for the crossbridge array was considered untenable and changes in this array were considered having been suggested by measurements of the laterally smeared C-zone images.

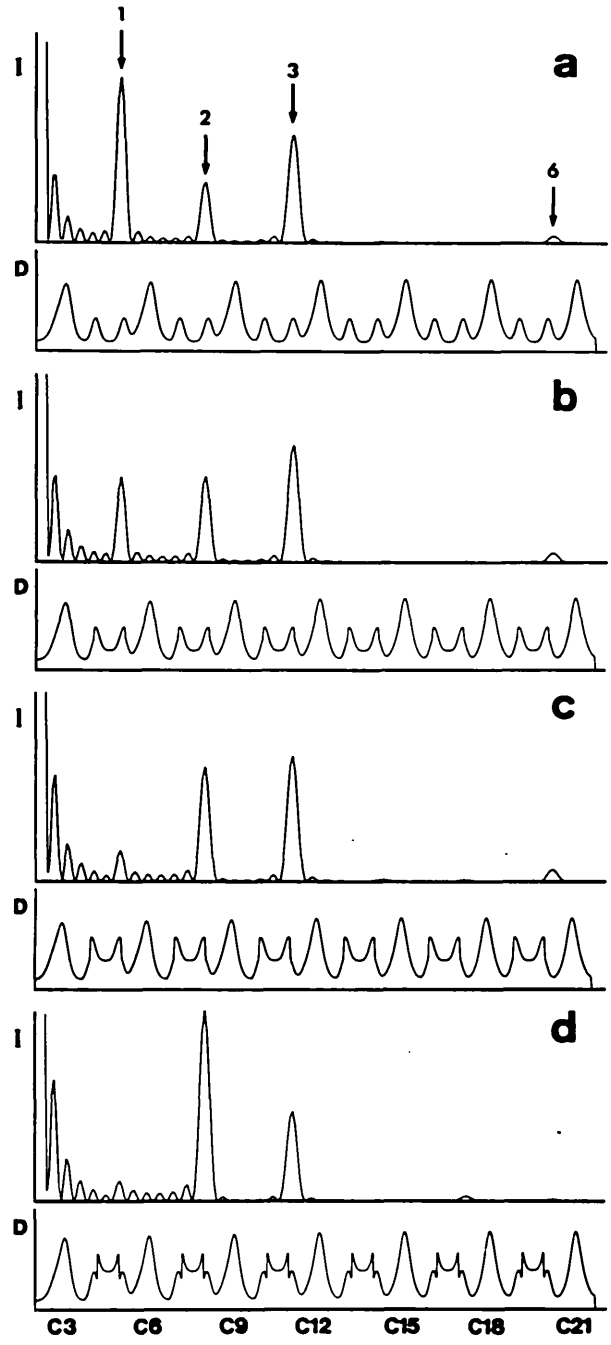


FIGURE 3.9 Density models similar to Figure 3.8 but in which the peaks C3,C6,C9 etc., and the crossbridge peaks have been replaced by Gaussian profiles of appropriate width and height. The intervening step is still present as a box function profile (see the text for further details).

3.4.3. Modelling With a 429Å Crossbridge Axial Repeat.

In the modelling so far the crossbridge array has been considered to have an exact 143Å repeat such that a = b = c = 143Å and a + b + c = 429Å (a, b and c are defined in Figure 3.10(b)). However the prominent meridional peak at 1/143Å could still be retained along with other orders of 429Å if the repeat of the crossbridge distribution was actually 429Å. This could arise due to

(i) A difference in density of successive crossbridge peaks such that every third peak had the same density or

(ii) Small perturbations of the positions of crossbridge peaks, of equivalent density, from an exact 143Å repeat such that the condition a + b + c = 429Å is still fulfilled.

Although the density variation in (i) could arise from crossbridges of equivalent size and shape appearing different in axial projection, the staining pattern in the averaged images does not show such a variation. However measurements of the spacings a, b and c from laterally smeared images suggest that a 429Å repeat could originate from (ii) above. In fact b is generally smaller than a or c. There is also a less obvious trend that a is larger than c, although interchanging these has no effect on the computed transform.

With the configuration a = 163Å, b = 113Å and c = 153Å $I_4 < I_5$ as in Group I C-zones. With a = 163Å, b = 128Å and c = 138Å then $I_4 > I_5$ as in Group II and III C-zones. The slight differences in the observed optical diffraction patterns can be accounted for by slightly different perturbations in the positions of the crossbridge density peaks. Combining crossbridge

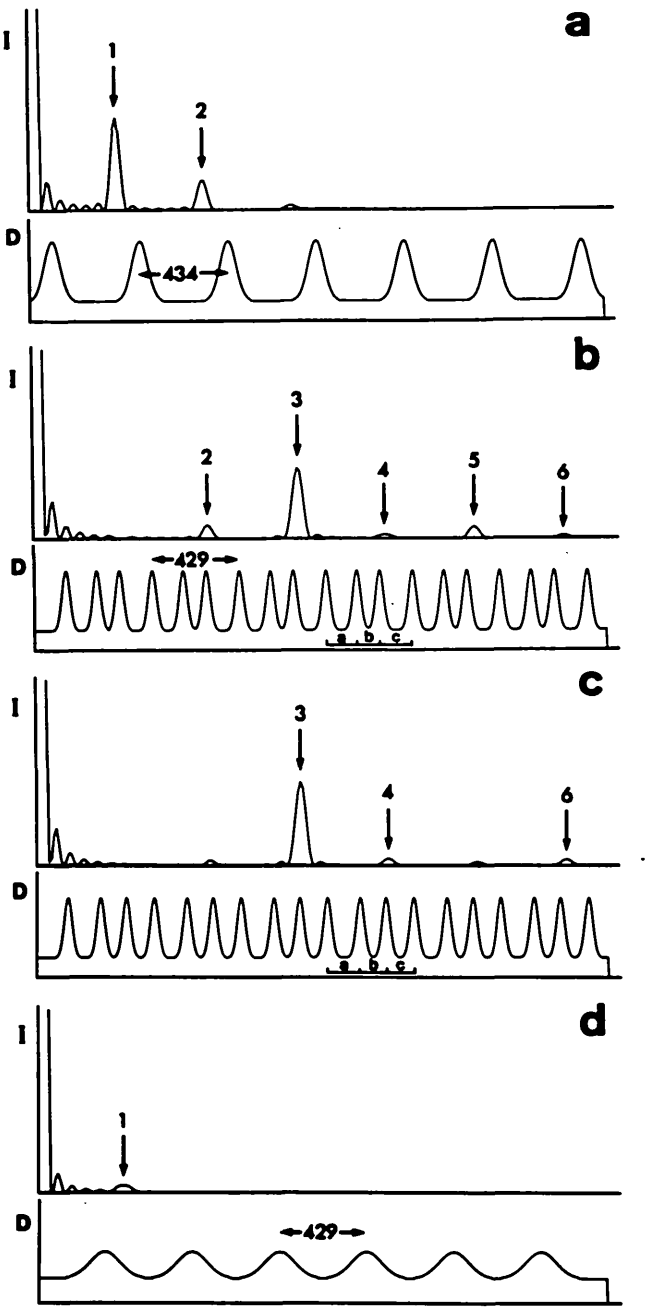


FIGURE 3.10 C-zone density models (D) and computed intensity distributions (I) in which box function profiles have been replaced by Gaussian profiles. (a) Density model for the prominent peaks C3,C6,C9 etc. (b) and (c) are density models for the crossbridge peaks but these are not equally spaced at 143Å intervals so that the true repeat of the models is 429Å. Spacings of successive crossbridge peaks are called a,b and c. The crossbridge distribution in (b) gives $I_5 > I_4$ and (c) gives $I_4 > I_5$. (d) shows the form of the intervening step density.

arrays of this form with the 434Å period array, (and an intervening step for a marginal improvement), the complete range of observed intensities and spacings of reflections 1 to 6 can be accounted for. The density models also contain features which are characteristic of the observed electron micrographs or their laterally smeared images. In Figure 3.11(a) and (b) a = 163Å, b = 113Å, c = 153Å and $I_4 < I_5$. In Figure 3.11(c) and (d) a = 163Å, b = 128Å, c = 138Å and $I_4 > I_5$.

In this latter category the crossbridge configuration giving optical diffraction patterns with $I_5 < I_6$ cannot be unambiguously classified as that shown in either Figure 3.11(a) or (c). This is because the crossbridge configuration may give $I_4 < I_5$ but limited resolution in the electron micrographs is causing the crossbridge peak unit transform being sampled at these positions to decrease rapidly from peak 4 to peak 5 to peak 6 such that the relative intensities $I_4 > I_5 > I_6$ are observed.

The C-zone density models also contain characteristic features of the staining pattern as described in section 3.1. In the observed C-zones, lines C3, C6, C9 etc., generally appear broader than C4, C5, C7, C8 etc., and in the final density models (Figure 3.11) 90% of the peak area occurs in 130Å and 80Å respectively for these two sets of striations.

The "intervening step" density was only included in the modelling as a low density, broad peak placed midway between the prominent lines C3, C6, C9 etc. and so its presence in the observed staining distribution would not be obvious. It was introduced in an ad hoc fashion to produce a small decrease in the intensity of reflection 1 in all of the models. However its presence may also explain some of the observed variation in the

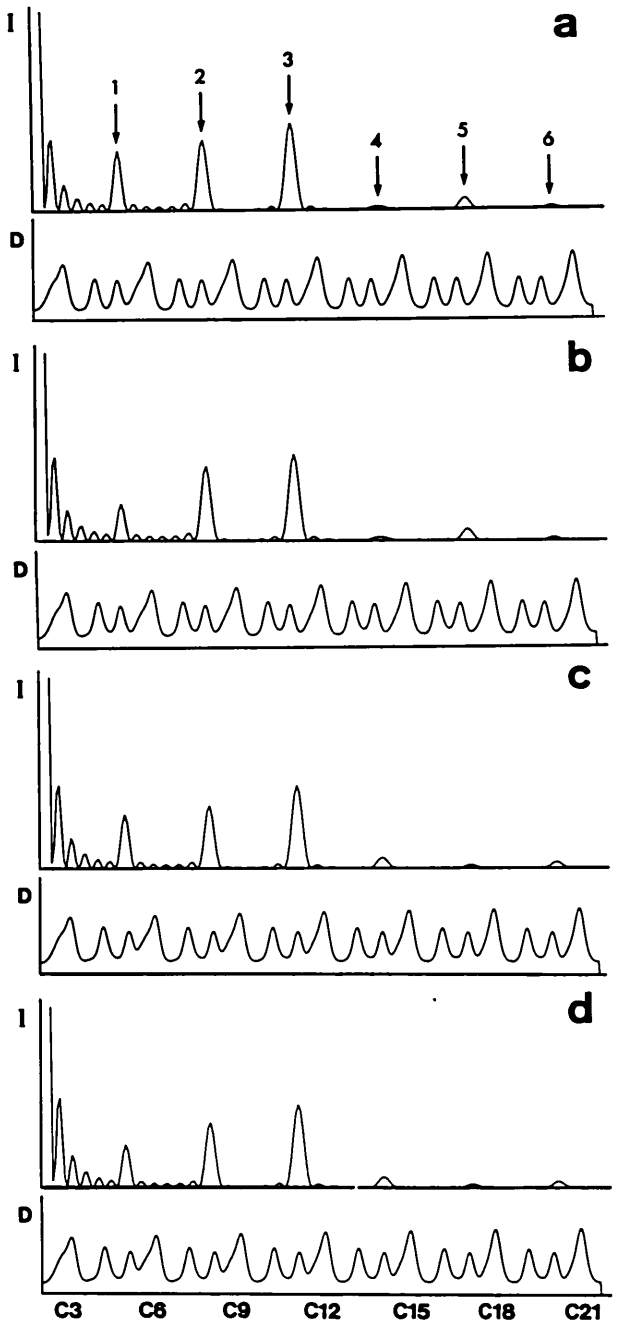


FIGURE 3.11 Full C-zone models (D) using the component density distributions in Figure 3.10. (a) and (b) correspond to Figure 3.10(b) combined with Figure 3.10(a) and two different intervening step densities. Similarly (c) and (d) correspond to similar combinations to (a) and (b) but using the crossbridge distribution in Figure 3.10(c) instead of Figure 3.10(b). The calculated intensities can generally account for the complete range of observed intensities.

spacing of reflection 1, although as discussed earlier this may be due to interference of this reflection with the mask function. In some patterns reflection 1 had a spacing less than 429Å although in the same pattern reflection 2 measured as the second order of a repeat of about 434Å. If the intervening step has a repeat of 429Å, and the density of the step is such that its contribution is greater than that from the 434Å array at the first order position (Figure 3.12), then the first order peak is shifted to spacings as low as 420Å to 400Å. This occurs because two peaks, the first orders of diffraction from the 429Å intervening step and the 434Å array, with similar profiles but slightly displaced, are interfering destructively. At the second order position the diffraction from these arrays is in phase so that a similar effect does not occur. If this is the reason for some of the variability of the spacing of reflection 1 then it would support including such a feature in all of the other models. The perturbed crossbridge arrays (which have a repeat of 429Å) also make a small contribution to the diffracted intensity at the position of reflection 1, but the density of the crossbridge peaks must be unrealistically high for the same effect described above to occur.

3.5. Discussion

3.5.1. Summary of the Results

The rigorous analysis of the human m.tibialis anterior C-zone presented here has shown that its negatively stained density distribution comprises primarily two components with axial periods which differ by approximately 1%. The component with the longer period of 434Å is most likely a non-myosin protein analogous to C-protein. The shorter, 429Å, period component most

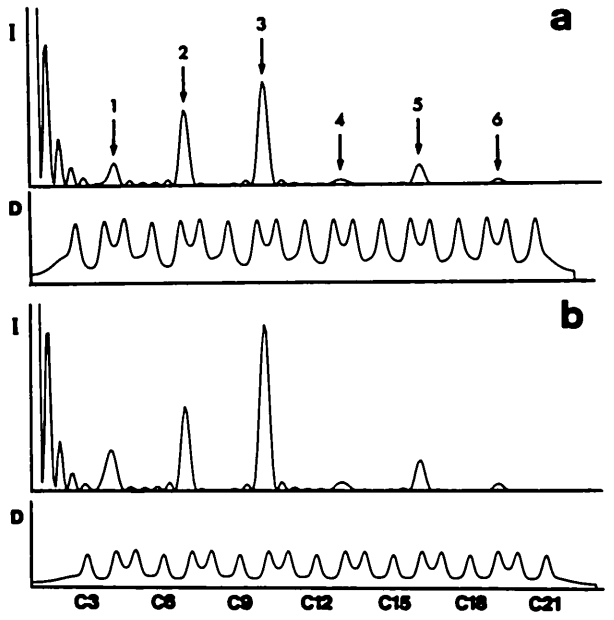


FIGURE 3.12 Models (D) such as those in Figure 3.11 but with large intervening steps. In the intensity transform (I) a considerable variation in the spacing of reflection 1 is obtained, as is occasionally observed.

likely arises from stain exclusion by the myosin crossbridges. In this preparation the three levels of crossbridges within each 429Å period are not equally spaced at 143Å intervals but show predominantly two arrangements in which crossbridge levels are systematically displaced from exact 143Å intervals.

Occasionally traces of a third periodicity of 370Å to 380Å were observed. This was attributed to thin filaments which overlapped the C-zones by varying amounts. An "intervening step" feature may also be present as a minor component of the observed staining distribution with a repeat of 429Å or 434Å.

3.5.2. The Crossbridge Array

The observed axial displacements of crossbridges from regular 143Å intervals may have occurred by a distortion of the helical arrangement of crossbridges in the living muscle resulting from the preparative procedure. However the reproducibility of the C-zone staining pattern makes this unlikely to be the predominant effect. A periodic distortion could occur by fixation induced attachment of the crossbridges to actin and indeed many of the observed crossbridge level axial separations are close to multiples of the actin helix subunit repeat of 27.5Å. The configuration in Figure 3.10(b) has a = 163Å, b =113Å, c = 153Å and in (c) a = 163Å, b = 128Å and c = 138Å. If the actin helix is considered as two strands of pitch 770Å, then , in one strand, actin monomer separations of 110Å (2 x 55Å) and 165Å (3 x 55Å) occur, whereas between neighbouring strands possible attachment sites are separated by 137.5Å (2.5 x 55Å).

Thus correspondence between the inferred crossbridge axial separations and the separations of actin monomers in one or two

strands, is obtained for two out of the three "a, b, c" values for each model. However the absence or weakness of the approximately 370Å repeat of the thin filament in the observed optical diffraction patterns and the very clear presence of a 429Å repeat suggests that, although this type of interaction with actin may possibly account for the slight differences in the crossbridge configurations observed, due to different extents of thick and thin filament overlap, it would not necessarily explain their displacement from initial regular 143Å intervals.

The presence of a 429Å crossbridge repeat in living vertebrate skeletal muscle is also supported by the appearance of "forbidden" meridional reflections in their X-ray diffraction patterns (Huxley and Brown, 1967). In vitro studies of LMM paracrytals (Bennett, 1976, 1977) also show a repeat of 3/8 of 429Å (i.e. about 160Å) from which it was concluded that myosin molecules may pack together with this stagger and may do so in the vertebrate thick filament backbone.

Figure 3.13 shows projected views of simplified three-stranded crossbridge arrangements and their optical diffraction patterns for a perfect helix (Figure 3.13(b)) and for imperfect helices in which the axial separations of crossbridge levels correspond to those in the models in Figure 3.11(a) and (b) and in Figure 3.11(c) and (d). The diffraction pattern for a perfect helix has strong meridional peaks only on layer lines $l = 3N$ ($N = 0, \pm1, \pm2$ etc.; Figure 3.13(b)). Similar prominent meridional peaks occur in the patterns of the imperfect helices but in addition there are other orders of the 429Å axial repeat. In Figure 3.13(d) $I_5 > I_4$ and the second order meridional is apparent and in Figure 3.13(f) $I_5 < I_4$ and no second order peak

is seen.

A-segments (Hanson et al, 1971; Craig, 1977) and LMM paracrystals (Hanson et al, 1971; Bennett, 1976, 1977) both give $I_5 > I_4$ and also show relatively strong 8th and 11th order peaks of the 429Å repeat. The results from LMM paracrystals suggest that the tails of the myosin molecules may pack together in the thick filament backbone with the type of axial perturbations shown in Figure 3.13(c) and the thick filament backbone staining in A-segments gives optical diffraction patterns consistent with the same type of perturbation. This may mean that other proteins absent in the preparation of LMM paracrystals do not affect the way in which the myosin tails do pack together in this central region of the thick filament. In the absence of influence from the thin filaments, the stagger between levels of crossbridges would be expected to reflect this packing of the tails. Optical diffraction patterns of A-segments stained with ammonium molybdate, in which levels of crossbridges appear well-preserved (Craig, 1977) would be the most direct way of testing whether this is so. Since such information is not yet available the relationship between the packing of the tails in the thick filament backbone and the arrangement of the crossbridge levels in living muscle must be deduced from less direct sources such as X-ray diffraction.

The pattern of "forbidden" meridional intensities in the X-ray diagram of frog sartorius muscle (Huxley and Brown, 1967) conforms to the same pattern as that discussed above. This meridional intensity is likely to be dominated by diffraction from the myosin crossbridges which project out into the sarcoplasm and so the simplest interpretation is that the

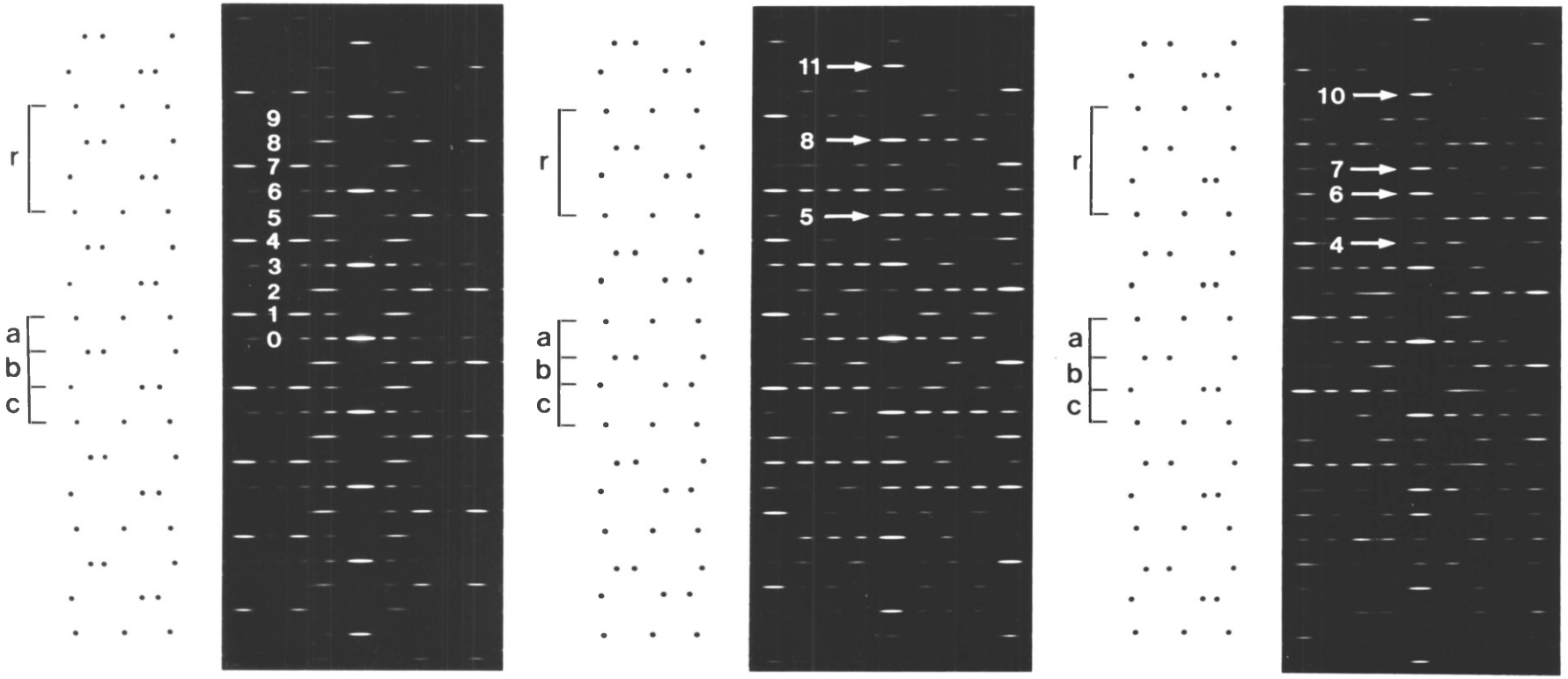
dominant axial perturbation of the crossbridges in live frog muscle is determined by the underlying packing of the LMM in the thick filament backbone, as revealed in LMM paracrystals and A-segments. This suggests that any thin filament influence of the crossbridges which is present *in vivo* does not affect the spacings between levels of crossbridges in live frog muscle. This is confirmed by the presence of the forbidden meridional reflections in very stretched muscles where the possible influence of the thin filaments is removed (Huxley, 1972; Haselgrove, 1975) although one cannot rule out other types of perturbation which do not have an axial component.

This pattern of intensity ($I_5 > I_4$) is also given by Group I C-zones (Figure 3.11(a) and (b); Figure 3.13(c)) and may thus represent a similar configuration to these preparations. In the cryosections there is also the likelihood of fixation induced attachment of the myosin heads to the thin filaments (Reedy and Garrett, 1977; Freundlich *et al*, 1980) and this would be expected to disrupt the resting arrangement of crossbridges. Therefore the other type of configuration, given by Group II C-zones, which has a relatively strong 4th order of 429Å, probably represents the effects of such a disruption for the reasons discussed below.

Time-resolved X-ray diffraction studies of frog sartorius muscles during contraction (Huxley *et al*, 1980, 1981, 1982; Yagi *et al*, 1981) have shown that considerable reductions in intensity of the forbidden meridional reflections take place, up to 5 to 10 times for the second order of 429Å i.e. 215Å, and similar changes for the fourth and fifth orders. The sixth order decreases to about 50% of its resting value (Huxley *et al*, 1982). These changes occur slightly ahead of tension development at the onset

of contraction but return to their resting values with a considerable delay behind the decay of tension on relaxation. A substantial delay is also observed for the return of the "143Å" to its resting value although its integrated intensity actually increases substantially during the peak of both tetani or twitches. It was argued above that the perturbed configuration which may exist between crossbridge levels in resting frog sartorius and human muscles (Group I; Figure 3.13(c)) would give a relatively strong fifth order forbidden meridional reflection and that the same configuration would give a stronger second order reflection than configurations in Group II, or configurations with no perturbation at all, which would give no forbidden meridional reflections (Figure 3.13(a) and (b)). Thus a change from the proposed resting configuration to one of these latter configurations during contraction would not only bring about a reduction in the forbidden meridional reflections, but would also increase the 143Å reflection during contraction (Yagi et al, 1981). The fact that there is a similar time course in the changes of these reflections, relative to tension development and decay, is also consistent with these types of rearrangements taking place. This tentatively supports the earlier assumption that the configuration in Group II (giving $I_4 > I_5 < I_6$; a = 163Å, b = 128Å; c = 138Å) is one in which the resting crossbridge perturbation has been disrupted by attachment of the crossbridges to the thin filaments. This is because the disruption caused, even by fixation induced attachment, might have a similar effect on the longitudinal rearrangement of the crossbridge levels as does the interaction of the crossbridges with the thin filaments during contraction.

FIGURE 3.13 (a), (c) and (e) show axially projected views of 3-stranded models for the vertebrate myosin crossbridge arrangement. In the model in (a) levels of crossbridges are equally spaced representing the projection of a perfect helical arrangement and therefore the spacings a, b and c are equal. Its optical diffraction pattern (b) shows meridional reflections only on layer lines numbered 3N (N = 0, ±1, ±2 etc.). The models in (c) and (e) have spacings between crossbridge levels as in Figure 3.10 (b) and (c), respectively, for the two types of axial perturbation modelled. In (c) a = 163Å, b = 113Å and c = 153Å and its optical diffraction pattern (d) has $I_5 > I_4$ (where I_N refers to the intensity of the meridional reflection on the Nth layer line). Note also that this gives a visible 2nd order meridional reflection. In (e), a = 163Å, b = 128Å and c = 138Å, $I_4 > I_5$ (f) and the second order meridional peak is relatively much weaker than in (d).


r
a
b
c
9
8
7
6
5
4
3
2
1
0
11
8
5
10
7
6
4
a
b
c
d
e
f

The small axial extent of about 80Å of the crossbridge peaks in the best models suggests that the long myosin heads (up to 190Å; Elliott and Offer, 1978) must be oriented within a small angular range (± 20° to 30°) about the perpendicular to the thick filament axis in this fixed relaxed preparation. It was pointed out by Yagi et al (1981) that the increase in the 143Å reflection predicted from the changes in perturbation discussed above would be larger than is observed and therefore a change in tilt of the crossbridges would have to occur during contraction so that the axially projected density of the crossbridges was reduced. If, in resting human muscle (as it appears to be the case in resting frog sartorius muscle (Squire, 1975; Haselgrove, 1980)) the crossbridges are oriented with a small axial tilt relative to the thick filament axis, then the required tilting of crossbridges during contraction could be accomplished by longitudinal movements of the crossbridges between this resting orientation with close to 0° tilt and the 45° tilt proposed for the end of the working stroke (Reedy et al, 1965).

3.5.3. The Origin of the Intervening Step Density.

The origin of the intervening step density depends on whether it is present with the same repeat as the prominent lines C3, C6, C9 ..etc., of about 434Å, or has a smaller repeat such as that of the crossbridge array of about 429Å. This feature was necessary in the modelling to reduce the relative intensity of reflection 1 but with a period of 429Å it could also have accounted for some of the variation in spacing of this reflection. In this case it could represent a feature of the myosin filament backbone.

In the final density models (Figure 3.11) the intervening

step could have a 434Å repeat or 429Å repeat since its contribution was in many cases small and confined to reflection 1. Even if the repeat is 434Å however it need not represent an additional protein feature associated with the C-protein peaks but could be a staining artifact as illustrated in Figure 3.14. In Figure 3.14 peaks "C" represent stain-excluding C-protein density at adjacent lines such as C3 to C6 or C6 to C9, and the likely distribution of stain between such features is shown in Figure 3.14(t). Such a piling up of stain against these peaks would be expected to occur during negative staining and its subsequent drying. If the transmission through the stain is plotted across this profile the resulting transmission profile in Figure 3.14(T) is obtained. This shows high transmission peaks where stain has been excluded by the C-protein peaks (C) between which there is a low density, broad peak similar to the intervening step ("S", Figure 3.14) used in the modelling which must have the same repeat of 434Å as that of the C-protein peaks C3, C6, C9 ..etc. If this feature has a 434Å repeat then an interesting possibility is that this step could represent protein associated with the protein at C3, C6, C9 etc. In either of these cases with a 434Å repeat, the variation in the observed spacing of reflection 1 would be considered to arise mainly from interference of this first order peak with the mask function, which is quite possible.

3.5.4. The Origin of the 442Å and 418Å Meridional X-ray Reflections.

Rome et al (1973) showed that the meridional X-ray reflections at 442.4Å and 418.4 Å (Huxley and Brown, 1967)

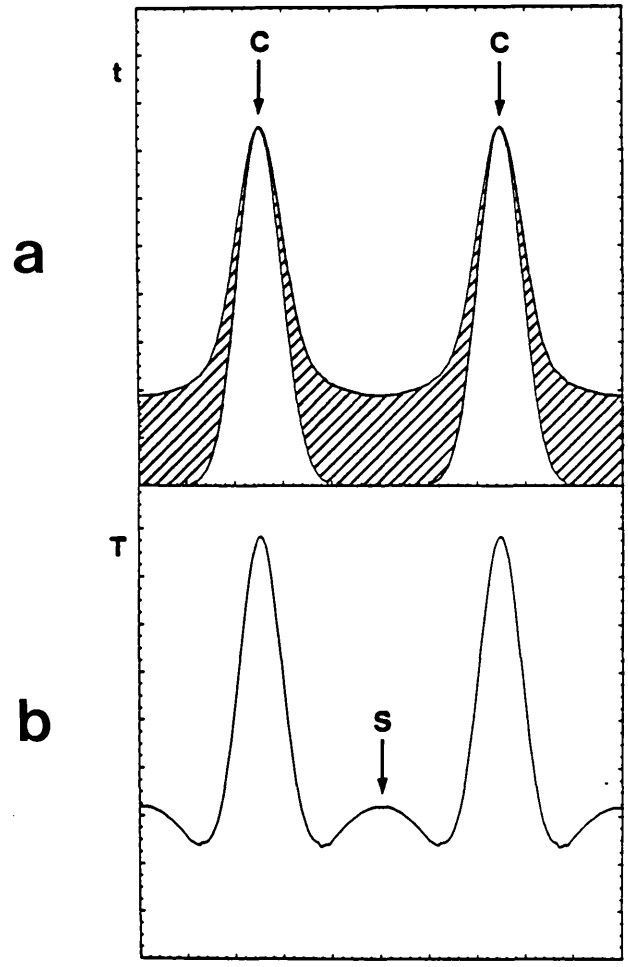


FIGURE 3.14 A possible origin of the intervening step density. In (a) successive C-protein peaks (C) are assumed to have stain (shaded) piled up against them. If the transmission is plotted as a function of position in (a) the profile in (b) is obtained. An intervening step S has been produced without introducing additional protein components to the array of C-protein peaks in (a).

originated at least partly from C-protein (see Chapter 1) which probably labels the thick filament backbone. In their modelling the C-protein was assumed to have the same 429Å repeat as the myosin crossbridge array. The first order peak in the transform of a single C-zone at $1/429Å^{-1}$ was assumed to be sampled by the 15^{th} and 16^{th} orders of an interference function of period $6650Å^{-1}$, due to the separation of two 9-line C-zones in each A-band, thus accounting for the positions of the observed meridional reflections at 442.4Å (6650/15) and 418.4Å (6650/16).

It is now known that the C-zone usually comprises only seven stripes of C-protein, the two nearest the M-band being incorrectly assigned due to a contaminant of the original antibody preparation (Craig and Offer, 1976a). The period of the interference function, L, therefore needs to be increased by one period (i.e. 434Å) so that the distance between lines C12 in the two C-zones is about 7080Å.

Figure 3.15 shows the modelling of the "400Å region" of the meridian for L = 7076Å. Each C-zone is represented by one of the final density models in Figure 3.11. In Figure 3.15(a) the first order peak from a single C-zone at $1/434Å^{-1}$ is shown and Figure 3.15(b) shows the effect of interference sampling of the intensity profile in (a) due to an interference function with L = 7076Å (i.e. the transform of the complete model in (c)). Thus the 16^{th} and 17^{th} orders of this interference function at $1/442Å^{-1}$ and $1/416Å^{-1}$ correspond approximately to the observed positions of the meridional reflections in this region. Some alteration of the positions of the interference peaks from true orders of L is expected since these peaks are sampling a C-zone first order peak (Figure 3.15(a)) with sloping sides but these shifts in position

were found to be less than 0.5%.

Figure 3.16(a) shows the calculated positions of the 16th and 17th order interference peaks for a range of L values together with the observed meridional spacings of 441.8Å and 418.4Å represented by bands with widths of the quoted uncertainty of ±0.5%. The best agreement between the observed and computed spacings occurs for L values of 7080 to 7090Å. In Figure 3.16 (b) the variation in intensity (measured peak height) of the 15th, 16th and 17th order interference peaks, for the same range of L values as in (a), when sampling the peak at $1/434Å^{-1}$ are plotted as a function of L. The values which give the best agreement with spacings correspond to a relatively low value of I_{15}, and have I_{16} markedly greater than I_{17}. Observed X-ray diffraction intensities (Haselgrove, 1975) show the 441.8Å reflection to be much stronger than at 418.4Å (17) and no reflection is observed at 474Å (15) which is very weak in the model.

The analysis by Rome et al (1973) predicted almost equal intensities for I_{16} and I_{17}. Even with the corrected value for the interference function period of 7080Å, a 429Å C-protein repeat cannot produce a more favourable I_{16}/I_{17} ratio than that in the model presented here.

This region of the X-ray meridional pattern will also receive contributions from other minor proteins in the P- and D-zones since 3 or 4 prominent stripes, with the same order of repeat as the C-protein stripes, occur in each of these zones either side of the C-zone. If the repeat of these structures is in the region of 429Å to 434Å then the effective 15-line array in each half of the A-band would give a sharper first order meridional peak compared to that in Figure 3.15(a) from a 7-line

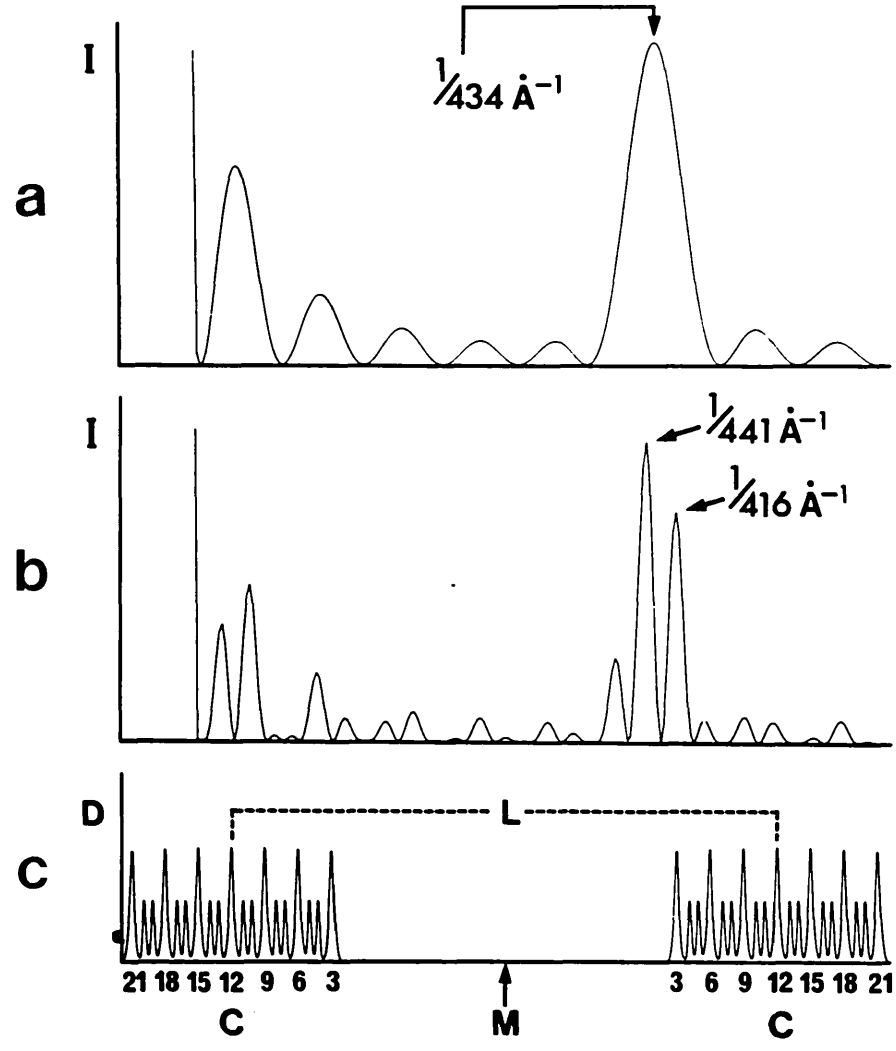


FIGURE 3.15 (a) The intensity profile of reflection 1 in the model shown as Figure 3.11 and its appearance (b) due to sampling from an interference function of spacing L = 7076Å which would correspond to the separation of the two C-zones in a single A-band as indicated in the model in (c). In (c) M denotes the centre of the M-band. For further details see the text.

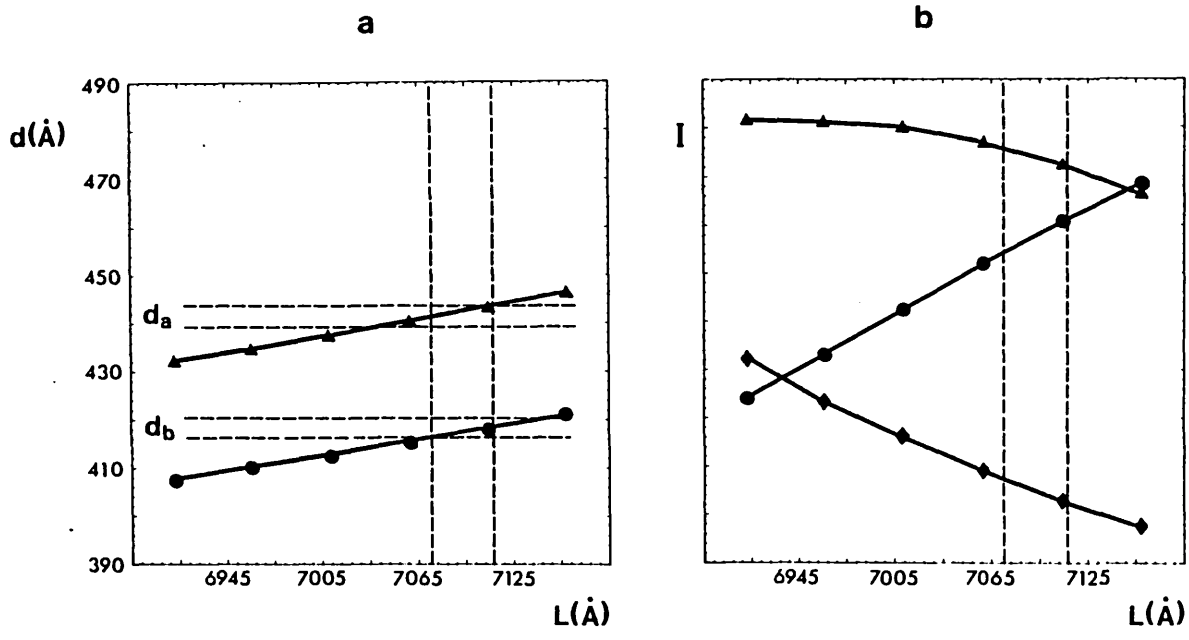


FIGURE 3.16 (a) Values of the positions of orders 16(▲) and 17(●) of the interference function L sampling reflection 1 (as in Figure 3.15) plotted as a function of L. d_a and d_b are the observed spacings of 441.8Å (+1/2%) and 418.4Å (+1/2%) (Haselgrove, 1975). (b) Intensities of orders 15(◆),16(▲) and 17(●) of the interference function of period L observed in models like that in Figure 3.15 but with different values of L.

C-zone. If this is sampled by the same interference function, L = 7080Å, then I_{17} would be further reduced relative to I_{16} and hence a better agreement with the observed ratio I_{16}/I_{17} of about 3 : 1 (Haselgrove quoted in Rome et al, 1973) is obtained. Further rigorous analysis of the P- and D-zones in these cryosections will enable this situation to be clarified. In conclusion then the 430Å to 440Å region of the meridian in X-ray diffraction patterns from frog sartorius muscle can be modelled better if, as it appears in human muscle, C-protein (or an isoform of it) is present in this muscle with a repeat of about 434Å rather than having a repeat identical to that of the myosin crossbridges (Rome et al, 1973).

3.5.5. The Role of C-protein in Determining the Length of the Thick Filament

If C-protein, or its equivalent isoform in human muscle, does have a role in regulating the length of the vertebrate thick filament, which is the only role relevant for discussion as far as these observations are concerned (in the absence of any clearly demonstrated alternative role), then such a role must be reconciled with the following observations;

(i) Optical diffraction patterns from A-segments of frog sartorius muscle (Craig, 1977) apparently show the presence of only one periodicity in the "C-zone".

(ii) C-protein on its own is unable to produce synthetic thick filaments of uniform length when added to purified myosin.

(iii) If uniformly elongated C-protein molecules are arranged along the thick filament in the form of a copolymer (Huxley and Brown, 1967) how can it give rise to stain

excluding lines less than 150Å wide.

The overall distribution of stain in A-segments (Craig, 1977; Hanson et al, 1971), stained with uranyl acetate to reveal the thick filament backbone and non-myosin proteins, is clearly quite different from the negatively stained cryosectioned material. Whereas cryosections show a generally uniform staining with a slight prominence in the staining pattern at the positions of the non-myosin proteins, the latter stripes are relatively much stronger in A-segments, particularly those stained with potassium permanganate, and would tend to dominate their diffraction patterns.

One way of reconciling the difference in periodicities observed, since it seems unlikely that the C- or X-protein would perform very different functions in the two muscles studied, is by considering the single periodicity observed in the optical diffraction patterns of A-segments to be due to the very prominent non-myosin protein stripes at approximately 43nm across the C-zone. Of course if there was no contribution at all from the staining of the crossbridges, the third order meridional reflection in the optical diffraction patterns of A-segments would be much weaker than is observed. However the third order meridional reflection from these A-segments does not appear to be as strong as the first and second order reflections in the case of rabbit psoas muscle (Craig, 1977). The situation is less clear in the case of A-segments of frog muscle since the first and second order reflections are not completely clear from the central scatter in the optical diffraction patterns. Clearly there is a need to account for both the pattern of meridional intensity and spacings, as has been done presently in the case of

cryosections, before assigning an observed periodicity in the optical diffraction pattern to a particular staining distribution in the electron micrographs.

Since self assembly of the thick filament most probably commences through the antiparallel interactions of myosin molecules in the bare-zone of the filament (Huxley, 1963) the non-myosin proteins which lie closer to the centre of the thick filament than C-protein may well be implicated in the length regulating process. Synthetic filaments formed in the presence of C-protein have tapered ends whereas in its absence the ends of the synthetic thick filaments formed by pure myosin are often blunt (Moos et al, 1975). This could be taken to mean that C-protein is responsible for the observed taper of natural thick filaments but that it requires interactions with these other non-myosin proteins before it will begin to form a copolymer of the form discussed by Huxley and Brown (1967).

Of course, a requirement of any length determining scheme in which two polymers with slightly different periodicities are involved is that the polymers are oriented with their long axes side by side. The small observed axial width of the C-protein stripes (Craig and Offer, 1976a; Craig, 1977) can only be compatible with such a scheme if the C-protein molecule has a bulky region (Squire et al, 1976) or if a considerable portion of the molecule is not stained. Until the C-protein molecule is further characterised to discount these possibilities or a clear role for it is demonstrated, then schemes of the type discussed by Squire et al (1976) are still possible.

One cannot rule out the possibility that the difference in periodicities observed here is a preparative artefact. The C-

protein repeat may be 429Å and the crossbridges may be attached to actin in the cryosections. If there was a slight shrinkage of the actin filaments relative to the thick filaments during the preparative procedure the initial crossbridge repeat may have been reduced slightly from an initial repeat of 429Å, thus generating the observed difference. There is no evidence to support this and in fact the weak presence of the approximately 380Å thin filament repeat in the optical diffraction patterns seems to suggest very little influence of the crossbridges by the thin filaments.

3.5.6. Summary

The results reported here have shown that longitudinal cryosections reveal very detailed information about the axial structure of the vertebrate A-band and this has allowed a very detailed analysis of the staining distribution in the C-zone to be carried out. In particular the following observations and conclusions have been made about the C-zone in the human muscle A-band;

(1) There are two axial periodicities, in addition to that due to actin, in the human C-zone and the larger of these peridiocities is attributed to a non-myosin protein most probably analogous to an isoform of "C-protein".

(2) The myosin crossbridges, apart from having the smaller periodicity, are arranged with a true axial repeat of 429Å rather than being equally spaced at intervals of 143Å in the C-zone.

(3) The myosin crossbridges exhibit two types of

perturbation from regularly spaced intervals.

(4) It is proposed that one of these axial perturbations (in which the grouping of crossbridge levels in each 429Å repeat has the approximate arrangement 163Å, 113Å and 153Å) represents the type of axial perturbation of the crossbridges in resting human muscle and that the pertubation in human muscle is therefore similar to that in frog muscle.

(5) The second type of perturbation, in which crossbridge levels have the approximate arrangement 163Å, 128Å and 138Å within each 429Å repeat, has been concluded to represent crossbridge levels which have been disrupted from the resting arrangement in (4) due to fixation induced attachment of the crossbridges to the thin filaments.

(6) In this fixed relaxed preparation the crossbridges are oriented with their long axes almost perpendicular to the thick filament axis.

CHAPTER 4 : ANALYSIS OF EQUATORIAL DIFFRACTION DATA

4.1. INTRODUCTION 205

4.2. COMPUTER MODELLING AND FISH EQUATORIAL X-RAY DATA 207

4.2.1. Muscle-Like Model Structures. 207

4.2.2. The Equatorial Diffraction Pattern from Vertebrate Skeletal Muscle. 212

4.3. DISCUSSION 212

4.3.1. The Equatorial Projection of Live Vertebrate Muscle Structure. 212

4.3.2. The Redistribution of Crossbridge Mass in Rigor and Active Vertebrate Muscle. 223

4.3.3. Summary. 226

CHAPTER 4 : ANALYSIS OF EQUATORIAL DIFFRACTION

4.1. Introduction

Fourier synthesis from the first two orders of equatorial X-ray diffraction from vertebrate skeletal muscle in resting, rigor or actively contracting muscle results in only one density map which is a plausible representation of the filament lattice viewed in equatorial projection. Thus at this low resolution the choice of phases to be assigned to the experimentally determined structure amplitudes for these two reflections is not ambiguous if the reasonable assumptions are made that at this resolution the equatorial projection will be centrosymmetric, thus giving phases of approximately 0^{o} or 180^{o}, and that the distribution has six-fold symmetry.

However when a higher resolution Fourier synthesis is possible a number of the Fourier synthesised density maps cannot be ruled out on the basis of established structural knowledge and these different maps imply important differences in the disposition of the myosin crossbridges in the resting state of muscle. The purpose of the work described in this Chapter is to develop a method which selects the correct combination of phases to be coupled with the experimental structure amplitudes and so determine the correct Fourier synthesis map, with no more supporting evidence about the filament arrangement than was required from the synthesis at very low resolution (i.e. using the 10 and 11 equatorial reflections).

The phase determining procedure was outlined in Chapter 2 (Materials and Methods, Figure 2.19) and is based on the structural analysis of a number of synthetic polypeptides (Squire and Elliott, 1972) with some important modifications. If a

Fourier synthesis is carried out using N observed structure amplitudes then in the case of a centrosymmetric structure 2^N density maps will be obtained if these amplitudes are computed for all possible phase combinations. Patterson functions computed by self-convoluting these N maps will be identical to the Patterson function, P(u,v), calculated from the observed structure amplitudes as follows;

$$P(u,v) = \sum_{hk} |F_{hk}|^2 \cos 2\pi(hu+kv)$$

and thus the factor, Δ_N defined by

$$\Delta_N = \sum_{uv} \left| P(u,v) - P_{\text{self convolution}}(u,v) \right|^2$$

will be zero for any combination of phases. However if the Fourier syntheses are modified by excluding density below a certain level, before forming their self-convolution, Δ_N will be non-zero and its value will reflect the differences between the self-convoluted map and the Patterson map computed from the observed amplitudes.

Squire and Elliott (1972) performed the self-convolution step in this procedure optically by approximately representing the computed Fourier syntheses by optical masks made to include the main features of the Fourier syntheses. The self-convolution produced in this way, for the phase combination most likely to be correct from the shape of the molecular transform, appeared most similar to the Patterson map computed from observed structure amplitudes. Thus their modification to the N Fourier syntheses, which amounts to excluding low-density features, conserved more of the Patterson map for what was more likely the correct phase combination than for any other combination of phases.

The critical step in the method is the form of the function, M, used to modify the Fourier synthesis and the

grounds for the type of function chosen are now considered.

The characteristic of the correct Fourier synthesis including the F(00) term(which forms the basis of other methods of phase determination where relationships have been developed between structure factors based on the assumption of positive electron density; Harker and Kasper, 1948; Karle and Hauptman, 1950; Sayre, 1952; Collins et al, 1975) is that the density should be positive throughout the unit cell with the exception of small negative excursions due to limited resolution and series termination errors.

Since the F(00) term cannot be included in the Fourier synthesis, this information is obscured. But the negative excursions in the correct Fourier synthesis should be less important in forming its self-convolution. If all possible Fourier syntheses have density below a certain "low-level" excluded this will cut off features which for the wrong phase sets are important in forming the self-convolution but only superfluous features from the correct Fourier synthesis. The self-convolution of the modified correct synthesis should be less affected by this modification than the self-convolutions of the modified incorrect Fourier synthesis.

4.2. Computer Modelling and Fish Equatorial X-ray Data

4.2.1. Muscle-Like Model Structures

Model structures, set up as described in Materials and Methods to represent the main features of the muscle filament arrangement in equatorial projection, enabled the limitations of the phase determining procedure to be assessed since the correct phase combination was of course known in all cases.

For each model, five orders of diffraction were computed

and used in the Fourier synthesis giving 2^4 possible phase combinations and therefore 16 Fourier maps (Table 4.1). The Fourier maps were modified by excluding all density below zero as a first trial function, M. The parameters for the five models are shown in Table 4.2 and the correlation factors, Δ_N, for each model for the 16 possible phase combinations are plotted in Figures 4.3 and 4.4. The following conclusions can be drawn from these Figures and the appearance of the Fourier syntheses;

(i) For all models, phase sets 9 to 16, in which the 11 reflection has a phase of 180° or -1 can be ruled out since they bear no resemblance to the original models.

(ii) The correct phase set map always has a relatively low value of Δ_N and in models 3,4 and 5 it has the lowest, excluding the maps in (i) in cases 3 and 4.

(iii) In models 1 and 2 where Δ_N is not the lowest the relative intensities of the 20, 21 and 30 reflections are small and the phase sets with lower Δ_N values than the correct map give maps containing the same essential features as the correct Fourier synthesis. These difference are not significant at the resolution of the Fourier synthesis in this analysis.

The results from applying the phase determining method to these models indicate that its success in selecting the correct phase set depends on the proportion of the total diffracted intensity contained in the higher order reflections (i.e. 20, 21 and 30). When these are relatively weak then clearly the Fourier synthesis will be dominated by the 10 and 11 reflections only. In this case phase sets 1 to 8 generate similar density maps and a narrow distribution of Δ_N values, i.e. in models 1 and 2.

TABLE 4.1 Numbering system for the 16 phase combinations for the 2^4 Fourier syntheses from the first five equatorial reflections from muscle-like model structures and live vertebrate skeletal muscle.

SET NUMBER	PHASES for reflections (HK)				
	10	11	20	21	30
1	1	1	1	1	1
2	1	1	1	1	-1
3	1	1	1	-1	1
4	1	1	1	-1	-1
5	1	1	-1	1	1
6	1	1	-1	1	-1
7	1	1	-1	-1	1
8	1	1	-1	-1	-1
9	1	-1	1	1	1
10	1	-1	1	1	-1
11	1	-1	1	-1	1
12	1	-1	1	-1	-1
13	1	-1	-1	1	1
14	1	-1	-1	1	-1
15	1	-1	-1	-1	1
16	1	-1	-1	-1	-1

TABLE 4.2 Parameters for muscle-like model structures 1 to 5. R_m and D_m refer to the radius and density of the myosin filament backbone, respectively. R_a and D_a refer to the radius and density of the thin filament, respectively. R_i, R_o and D_c describe the crossbridge annulus surrounding the myosin filament backbone and refer to the inner radius, outer radius and density of the annulus respectively.

MODEL	R_m	D_m	R_a	D_a	R_i	R_o	D_c
MODEL 1	70	9	45	7	-	-	-
MODEL 2	80	9	40	3	-	-	-
MODEL 3	50	5	45	1	-	-	-
MODEL 4	70	8.2	50	8	100	140	5.4
MODEL 5	70	8.2	50	8	70	110	7.2

The hexagonal unit cell spacing is 400Å.

R_m, R_a, R_i and R_o in Å ; D_m, D_a and D_c in arbitrary units.

The contribution of the higher order reflections is much greater in models 3 and 4 and the phase method excludes more maps in sets 1 to 8 giving the lowest correlation Δ_N for the correct map.

Model 5 gives a distribution of intensities which cannot be grouped clearly with either those of models 1 and 2 or those of models 3 and 4. However the phase method selects the correct Fourier synthesis in this case. This reveals an important feature of the method. This particular model has dense myosin and actin filaments plus a dense annulus of crossbridges surrounding each myosin filament. The overall distribution of density in the correct Fourier synthesis for this model will be less affected by the low-density cut off imposed because the relative densities of the myosin peaks, actin peaks and crossbridge annulus will remain fairly constant until the level at which the density is set to zero is quite high. This has the effect of conserving the main features of the self-convolution in particular for the correct phase combination, thus giving a lower Δ_N value for this phase set.

On the other hand Model 2 has dense myosin peaks and smaller actin peaks. In contrast to Model 5 the density cut-off imposed here would virtually exclude the actin filaments from the correct Fourier synthesis giving a marked change in its self-convolution and no selection from the phase method.

The distribution of relative intensities of the same equatorial reflections for resting frog sartorius muscle falls into the same category as models 3,4 and 5 above. It is therefore reasonable to expect a similar degree of success in selecting the correct phases for this data as in the modelling just described.

4.2.2 The Equatorial Diffraction Pattern from Vertebrate Skeletal Muscle

The result of applying the phase method to resting fish fin muscle equatorial data is shown in Figure 4.4. Phase sets 9 to 16 can once again be ruled out from the appearance of their Fourier syntheses which show no sensible peaks representing the vertebrate muscle filament arrangement.

The lowest Δ_N value anyway is obtained for phase set 5 which is marginally lower than for the Fourier synthesis given by phase set 3. These two Fourier syntheses differ distinctly from the two other plausible maps, i.e. 7 and 8, in that mass extends far from the thick filament surface to the trigonal points in the lattice where the actin filaments are located. A further preference is indicated by the selection of phase set 5 which does not show the sharp 6-fold symmetrical distribution of mass surrounding the thick filament backbone apparent for phase set 3 (Figures 4.7 to 4.9).

Very similar Fourier syntheses are obtained from resting frog sartorius equatorial data (Lymn, 1975) which emphasises the the importance of determining the phase information. As in the case of fish the phase selection method gives the lowest correlation factors for phase sets 3 and 5, map 5 giving the lowest (Figure 4.10).

4.3. Discussion

4.3.1. The Equatorial Projection of Live Vertebrate Muscle Structure

At the resolution of the equatorial data modelled here (about 130Å) it is not surprising that, despite the different crossbridge lattice symmetries in fish and frog muscles, they

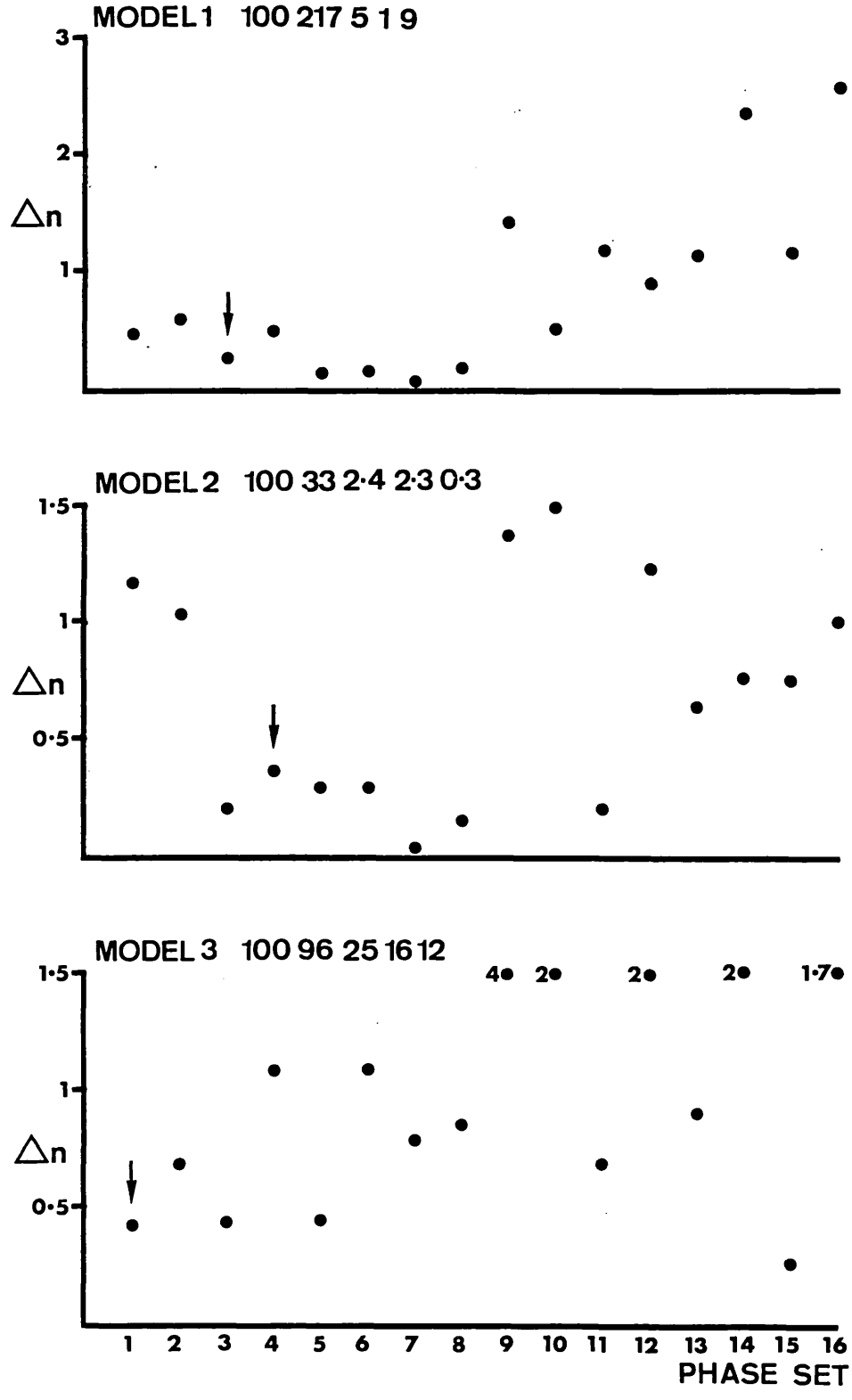


FIGURE 4.3 The correlation factor $\Delta_n = \sum_{uv} |P(u,v) - P_{mod}(u,v)|^2$ is shown plotted for each of the 16 phase sets for models 1 to 3. The computed relative intensities of the 10,11,20,21 and 30 equatorial reflections is shown at the top of each plot. The correct phase set is indicated by a vertical arrow for each model.

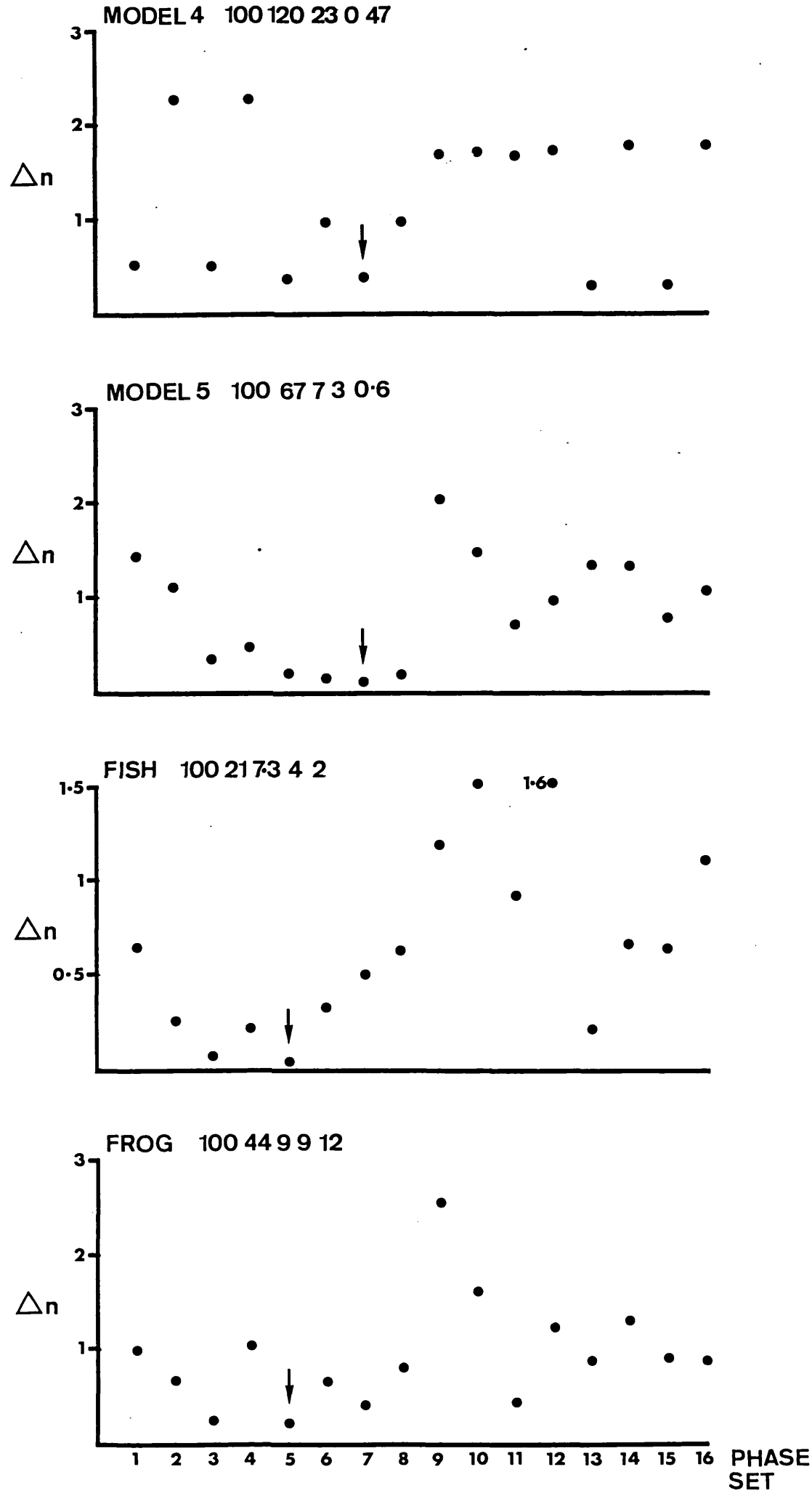

MODEL 4 100 120 23 0 47
MODEL 5 100 67 7 3 0·6
FISH 100 21 7·3 4 2
1·6
FROG 100 44 9 9 12
Δn
3
2
1
1·5
0·5
1 2 3 4 5 6 7 8 9 10 11 12 13 14 15 16
PHASE SET

FIGURE 4.4

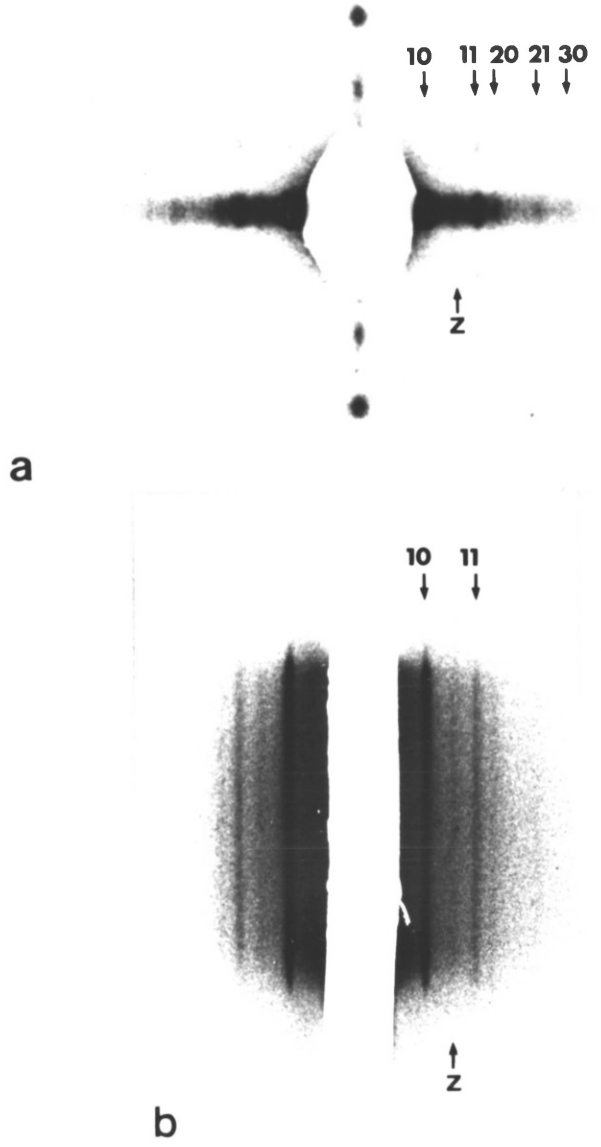


FIGURE 4.5 Equatorial X-ray diffraction patterns from live Plaice fin muscle. The muscle fibre axis is vertical, the crystal focusing direction is across the page. (a) X-ray pattern taken on a camera with a 30cm specimen to film distance. 13 hours exposure time, 30kV 50mA. (b) X-ray pattern taken on a camera with a 60cm specimen to film distance. 2 hours exposure time, 40kV 25mA. The numbered arrows indicate reflections indexed on the hexagonal lattice of thick filaments. The equatorial reflection "z" is a reflection at 1/290A attributed to the Z-line/I-band.

Table 4.6 Relative Intensities from Equatorial Diffraction Patterns of Live Plaice Fin Muscle.

	Lattice Spacing (Å)	Relative Intensities					
		10	Z*	11	20	21	30
A	473	657	-	200	113	74	-
B	473	**	50	200	75	40	16
C	472	961	-	200	66	38	22
D	-	961	50	200	70	39	19

A, equatorial intensities from row-line traces. B, equatorial intensities from layer line traces. C, equatorial intensities from "equatorial" diffraction patterns. D, average of B and C. Note that layer line traces of the equator from two-dimensionally resolved patterns (B) give very similar values to "equatorial" diffraction patterns (C). Since row-line traces of the former patterns (A) give different values, this indicates the presence of an equatorial "streak" along the equator.

** not measurable because of its proximity to the backstop. The probable error on intensity measurements is 15% or less and for the lattice spacing 1%.

* This reflection does not index on the hexagonal lattice of thick filaments of a-spacing 473Å.

should appear very similar in equatorial projection. However the Fourier syntheses eliminated by the phase method can be seen to be unlikely choices of phase for the following reasons which are independent of the distribution of crossbridges about the myosin backbone.

In Map 1 the thin filaments and the crossbridge density are far too weak. Maps 2 and 6 have thin filaments with a wide hollow centre, which is not observed. Map 7 has thin filaments with comparable density to those of the thick filament whereas they are expected to be of smaller density. Map 8 shows the myosin backbone with a wide hollow centre and although a 40Å to 50Å hollow is seen in the thick filament bare-zones of fish and frog muscles (Luther and Squire, 1978), it can easily be shown that at 130Å resolution such a feature will barely be apparent.

Phase sets 3 and 5 show similar distributions for the crossbridge density although a more uniform shell of density is apparent for phase set 5. The extent and rotational symmetry of this crossbridge density annulus will clearly depend on the symmetry of the crossbridge lattice and the crossbridge configurations in fish and frog muscles. In both cases it is very likely that crossbridges are approximately arranged on a 9/1 helix so that in equatorial projection the distribution will have at least 9-fold rotational symmetry. This will only be evident from the contribution of a 9^{th} order Bessel function on the equator, which is beyond the resolution of the Fourier synthesis considered.

Furthermore in frog sartorius muscle the two filament orientations observed in the statistical superlattice (Luther and Squire, 1980) mean that the average myosin filament will have at

least 18-fold rotational symmetry, regardless of the crossbridge configuration with respect to the thick filament surface. The presence of only one orientation of the myosin filament in the simple lattice of fish gives an approximate 9-fold rotational symmetry for the average filament, but this could appear more rotationally uniform if the two heads in each crossbridge are slewed differently around the backbone and lie side by side rather than being arranged one directly above the other along the thick filament axis. In addition any slew in one half of the A-band would be in the opposite sense to a slew in the other half of the A-band and this might have an effect if the coherence length along the filament for the equatorial reflections is large enough.

On the basis of these arguments phase set 5, which gave the lowest Δ_N values in the case of frog and fish equatorial data, is the better choice although this and phase set 3 give very similar values and both suggest a wide annulus of crossbridge density. Note that in the case of frog sartorius muscle the 6-fold symmetry of the distribution is more distinct than that in the case of fish.

The results from the phase method are encouraging so far and it will be seen in Chapter 5 that the equatorial projection of crossbridge mass obtained here for Plaice fin muscle is in good agreement with the orientation of the myosin crossbridges in resting fish muscle. There is, however, a note of caution which concerns any interpretation of the equatorial diffraction pattern from vertebrate skeletal muscle and in all previous analyses it is a point which has been overlooked.

It became apparent during this analysis that the spacing of

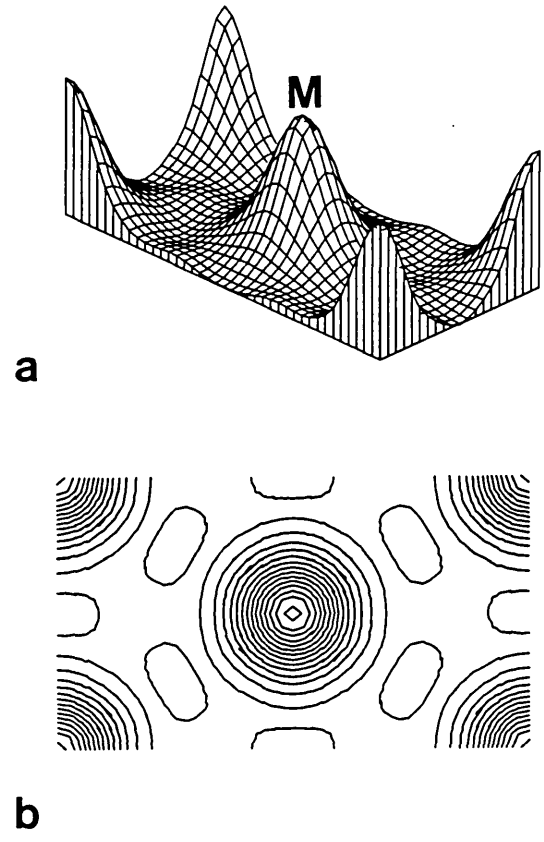


FIGURE 4.7 The Patterson map from the equatorial diffraction data in Table 4.6 from live Plaice fin muscle. (a) Surface plot (b) Contour map with 15 regularly spaced contours. M, myosin filament.

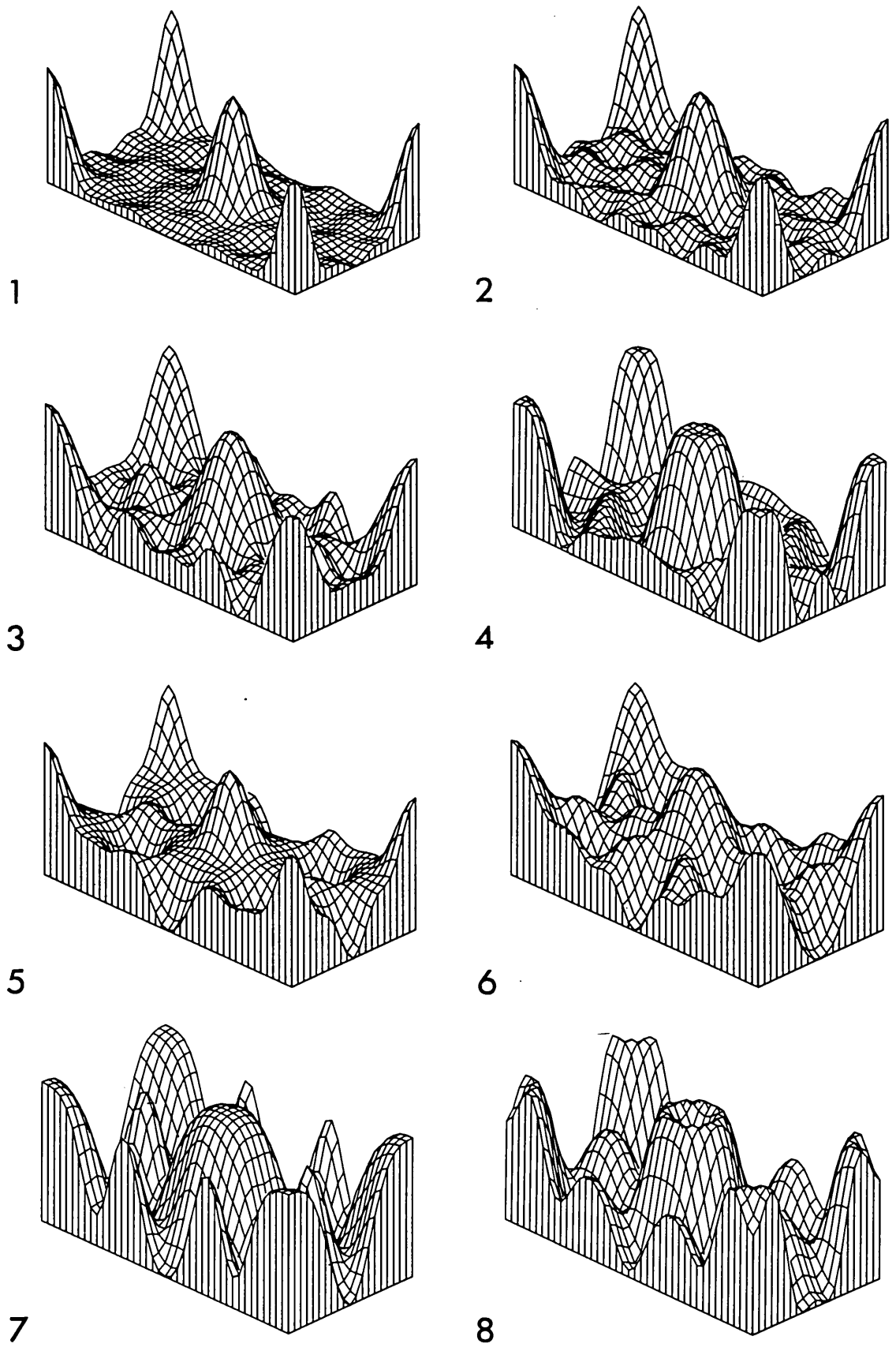
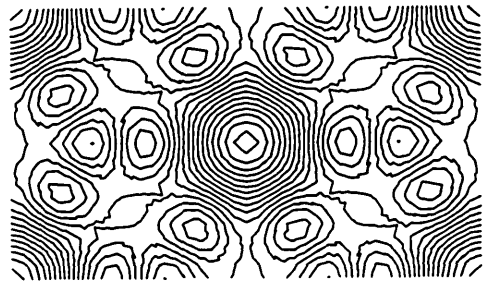
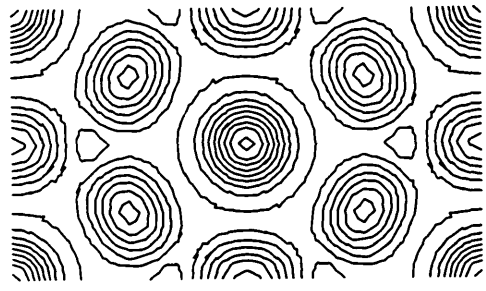


FIGURE 4.8 Surface plots of the Fourier syntheses from live Plaice fin equatorial data combined with phase sets 1 to 8. Map 5 corresponds to the phase set giving the lowest correlation factor



a



b

FIGURE 4.9 Contour maps of the Fourier syntheses in Figure 4.8 for phase sets 3 ((a)) and 5 ((b)).

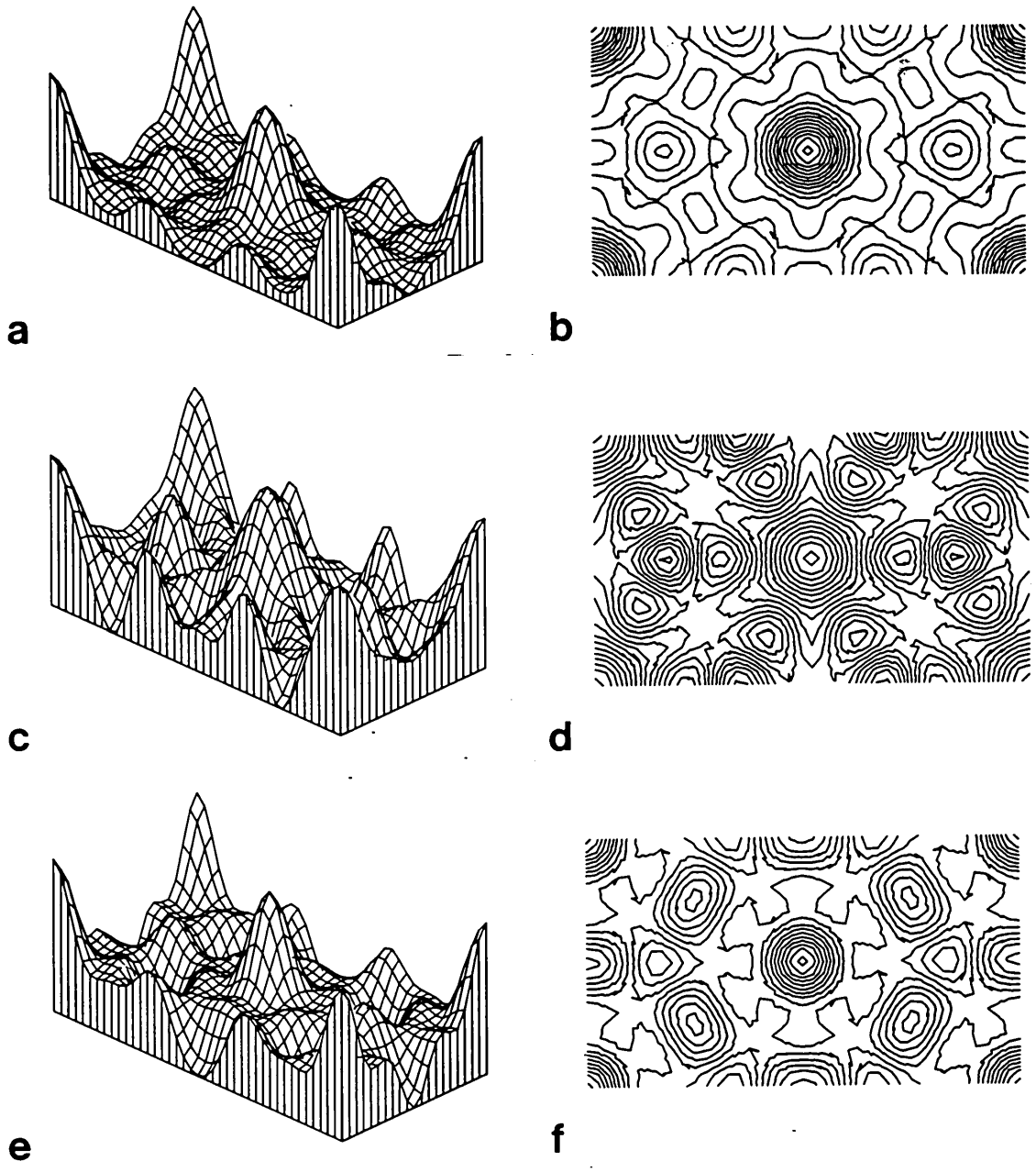


FIGURE 4.10 (a) and (b) show the Pattersom map from the first five orders of equatorial data for live frog sartorius muscle (Lymn, 1975). (c) and (d) show the Fourier synthesis for phase set 3 from the same data as in (a). (e) and (f) show the Fourier synthesis for phase set 5 from the same data.

the (11) reflection (i.e. 205Å) from the square thin filament lattice close to the Z-disc (which has a lattice spacing of 290Å and therefore gives an equatorial reflection at 1/290Å with indices (10)) corresponds exactly to the spacing of the (20) reflection (i.e. 205Å) from the lattice of thick and thin filaments in the A-band (I am very grateful to Dr.J.M.Squire for pointing this out). Thus the Z-disc and its associated thin filaments may make a small contribution to this reflection (the form of this contribution is discussed more fully in Chapter 5, section 5.6.5) which has normally been assumed to arise solely from the A-band. However the intensity of the (20) reflection could be reduced by up to one-third and phase sets 3 and 5 still had the lowest values of Δ_N, but phase set 3, which was marginally higher previously, now gave the lowest value. In the unlikely event that the contribution from the Z-disc is as much as one-half , or more, then phase set 7 always had the lowest value of Δ_N. Of course as the intensity of the (20) reflection decreases, Fourier syntheses from phase sets 3 and 7 become essentially the same in any case since they only differ in the phase of this reflection. So, although this complication is probably unimportant as far as the results presented here are concerned it will need to be overcome when refinement of this phasing procedure is carried out and when an analysis of the equatorial diffraction pattern at even higher resolution is possible.

4.3.2. The Redistribution of Crossbridge Mass in Rigor and Active Vertebrate Muscle

If the distribution of myosin crossbridges in relaxed vertebrate muscle is such that the crossbridges extend out close to the thin filaments, as proposed here, it is important to show

how the redistribution of crossbridge mass when muscle goes into rigor (Huxley, 1968) or contracts (Haselgrove and Huxley, 1973) can account for the changes in the equatorial intensity ratio, I_{10}/I_{11}, accompanying these structural changes.

Preliminary modelling of the resting equatorial diffraction data (Lymn, 1975; Haselgrove et al, 1976) could not determine whether or not the crossbridges do extend out as far as the thin filaments in resting vertebrate muscle. However because of the absolute intensity changes in the 10 and 11 reflections when a muscle contracts isometrically (Podolsky et al, 1976; Haselgrove et al, 1976) it was considered more likely that in the resting muscle the crossbridges would be contained within an annulus at a much smaller radius than the thin filaments and would move radially and azimuthally to interact with the thin filaments.

It was shown by Lymn (1978) that the intensity of the 10 and 11 reflections is substantially dependent on both the number of crossbridges attached and the distribution of attached configurations, irrespective of how far from the thick filament surface the crossbridges were in the resting state of the muscle. Computations were made for two attached configurations of the myosin heads attached to an actin helix; firstly a rigor complex type configuration with the heads tilted by about 45^{o} to the actin helix axis and secondly with the heads perpendicular to this axis. This emphasises the need to know the number of attached heads and the "average" attached configuration in accounting for changes in the equatorial intensities. Without these facts it is difficult to rule out crossbridge distributions extending as far as the thin filaments or crossbridges forming a smaller radius annulus of density around the thick filament

backbone.

Since the I_{10}/I_{11} ratio for rigor and active Plaice fin muscle is presently not well-defined it is impossible to quantitatively account for the redistribution of mass occurring from the resting state to these other states, although a similar large decrease in this ratio does occur in rigor Plaice fin muscle. Although the heads are close to perpendicular to the thin filament axis, a large contribution to the decrease in I_{10}/I_{11} will occur as the heads are tilted into a rigor configuration making a smaller angle (around 45^{o}) with the thin filament axis (Lymn, 1978). A further large contribution would be expected as the heads become "actin-centred" so that the crossbridge mass becomes aligned along the 11 planes of the hexagonal lattice.

It now appears that in rigor vertebrate muscle a large percentage of the heads are attached to the thin filaments. The changes which occur in I_{10}/I_{11} when vertebrate muscle goes into rigor were shown to be roughly equivalent to the attachment of most of the myosin heads to the thin filaments (Huxley, 1968; Haselgrove and Huxley, 1973). Enzymatic cleavage of myosin heads, firmly bound to thin filaments in rigor rabbit myofibrils and subsequent analysis of SDS gels of the myofibrils, have shown that greater than 95% of the myosin heads seem to be firmly attached to the thin filaments in rigor vertebrate muscle (Lovell et al, 1981). Studies on the orientation of paramagnetic probes attached to myosin heads in rigor myofibrils also conclude that well over 90% of the heads are attached in one configuration (Thomas and Cooke, 1980; Thomas et al, 1980) although this may be reflecting the state of the 20k domain of the myosin head which

is involved in the actin-myosin link. In addition better preserved and more detailed 3-D reconstructions of thin filaments decorated with HMMS-1 are giving an increasingly detailed picture of the geometry with which the myosin heads attach to the actin helix.

However even as the number of attached heads in rigor or contracting muscle and the precise geometry of attachment become better defined one may be in a position to model the absolute equatorial intensities but the changes from the resting state can never be truly accounted for without establishing what that resting state actually is. This has of course been the main concern of the analysis carried out in this chapter.

4.3.3 Discussion

Many algebraic relationships among structure factors for determining or refining phases exist (as mentioned earlier) which are based on the assumption of positive electron density, but such methods were developed for application to crystal structures where nearly resolved atoms are evident in a preliminary electron density map obtained by normal crystal structure analysis such as isomorphous replacement. Such methods are prohibitively expensive and in any case difficult to apply to large biological macromolecules in which the resolution of the data is usually much more limited. Collins *et al* (1975) used similar and more sophisticated modifications to the electron density map, as those used here, and from the phases and amplitudes of the modified map carried out a Fourier inversion to generate a map which was then compared with the experimentally determined Fourier. This was then refined in a normal way using the conventional reliability factor, R. This is a method for phase improvement however, rather

than phase determination.

During the course of this analysis other modifications to the Fourier maps obtained from the experimental data have been applied but none have yet been as definitive as the first simple trial function where all density below zero is set to zero. Clearly further work needs to be done to define the limitations of the phasing method. Other methods which are applicable to the problem of data with limited resolution are the maximization of entropy methods which are more suitable for dealing with imperfect data and have very recently been applied to X-ray crystallography (Collins, 1982).

These, and more sophisticated modifications included in the present procedure, will hopefully enable the phasing procedure to be developed and thus be applicable to equatorial data from other striated muscles. Clearly at the moment the method is sensitive to strong reflections but further refinement is in progress for its wider application.

CHAPTER 5 : X-RAY DIFFRACTION OF LIVE PLAICE FIN MUSCLE

5.1. INTRODUCTION 229

5.1.1. General Description. 229

5.2. THE MYOSIN LAYER LINE PATTERN 234

5.3. THE MERIDIONAL PATTERN 236

5.3.1. Reflections probably arising from the Thick Filaments. 241

5.3.2. Reflections probably arising from the Thin Filaments. 244

5.3.3. The Pitch of the Actin Helix. 244

5.4. THE ROW LINE SAMPLING OF THE MYOSIN LAYER LINES 248

5.4.1. Row-Line Spacings. 251

5.4.2. Row-Line Intensities. 251

5.5. COMPUTER MODELLING OF THE MYOSIN LAYER LINE PATTERN 252

5.5.1. The Relaxed Crossbridge Configuration. 252

5.5.2. Summary of the Modelling. 260

5.6. DISCUSSION 263

5.6.1. Summary of Differences in Plaice Fin Muscle Structure. 263

5.6.2. The Three-Dimensional Crossbridge Lattice. 272

5.6.3. The Effect of Imperfections in the Crossbridge Surface Lattice. 272

5.6.4. The Resting Crossbridge Configuration. 275

5.6.5. The Origin of the Non-indexible Equatorial Reflection. 278

5.6.6. Summary. 280

CHAPTER 5 : X-RAY DIFFRACTION STUDIES

5.1.Introduction

It was shown in chapter 1 (section 1.5) that at least in the bare regions of frog sartorius and bony fish muscle A-bands, a regular simple myosin filament lattice occurs in fish muscle whereas a statistical superlattice occurs in the case of frog sartorius. In this latter case it was also shown that the myosin layer line sampling and thus the crossbridge lattice in the resting state of the muscle were consistent with the bare region's superlattice. One of the important aims of the X-ray studies on live bony fish muscle is to see whether a similar correspondence occurs in the case of fish, in which case one unique orientation of the crossbridge helix within the simple lattice unit cell should be observed. In principle this myosin layer line pattern should be easier to interpret in terms of the rotational symmetry of the crossbridge helix and the resting crossbridge configuration.

The consequences of the different lattices in frog and fish as discussed in Chapter 1 (section 1.5.3), in terms of the opportunities for interaction of the myosin crossbridges with actin monomers in the thin filament, clearly require there to be no gross dissimilarities between the muscle structures of these two species. In the interpretation of the X-ray diagram from live Plaice fin muscle presented in this chapter, more emphasis will therefore be placed on whatever other differences are evident between the muscles of Plaice fish and frog sartorius.

5.1.1.General Description

The low-angle X-ray diagram from resting Plaice fin muscle,in common with those from other vertebrate muscles

(frog, toad and rabbit; Huxley and Brown, 1967; chicken: Matsubara 1974), is characterised by a series of layer lines with axial spacings which are orders of about 429Å arising from diffraction by the myosin crossbridges.

From the very similar shape and distribution of the meridional and off-meridional diffraction to that in the X-ray diagram of frog sartorius muscle, the same inferences can be made about the origin of these features in the X-ray diagram of Plaice fin muscle. These basic features are firstly discussed.

The same three-fold screw symmetry of the crossbridge arrangement is evident from the strong meridional reflection on the third layer line and layer lines indexing on a repeat with three times the spacing. The intensity of this reflection is about two to three times that of the strongest myosin layer line at about 429Å which is itself about one-twentieth of the strongest reflection in the pattern, the 10 equatorial reflection indexing on an hexagonal unit cell of about 473Å spacing in rest length fish muscle (Figures 5 and 5.1).

The pattern falls off towards zero intensity more rapidly at right angles to the meridian, at 80 to 60Å, than along the meridian. The limit on the meridional extent cannot be stated since these studies were limited to spacings below about 30Å. The axial breadth of the layer lines is greater than that of the third order and other meridional reflections but corresponds to diffraction from a unit of the same order of size as the thick filament length. The same inference can be made from the little apparent broadening of the meridional reflections along the meridian on cameras of 10,000Å resolution. In addition the small lateral breadth (the width across the meridian) indicates a high

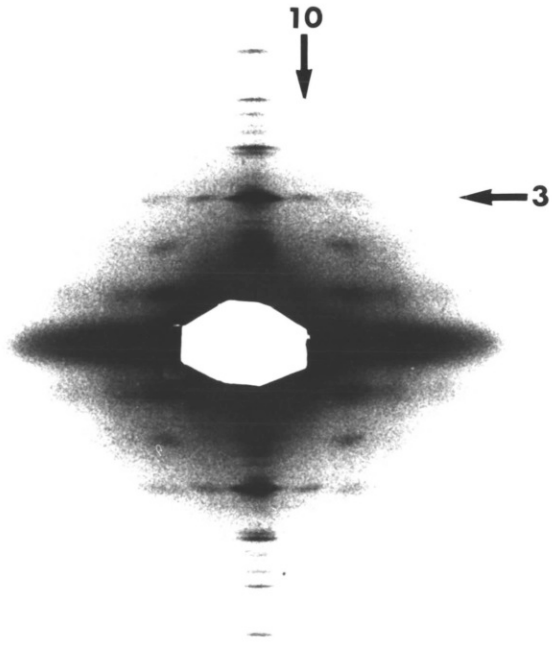
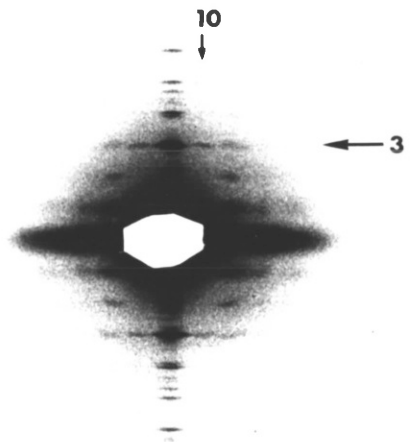
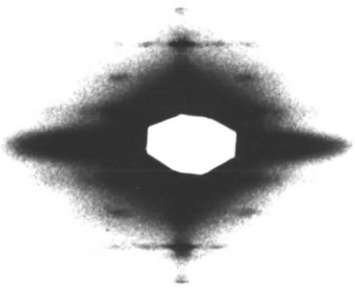


FIGURE 5 X-ray diffraction pattern from live Plaice fin muscle at rest-length taken on a camera with a 30cm specimen to film distance. The fibre axis is vertical, the crystal focusing direction is also vertical. Printed from the front film. X-ray exposure time of 40 hours at 40kV, 60mA. The vertical arrow indicates the first row-line indexed on a hexagonal lattice of a-spacing 473Å, the horizontal arrow indicates the third layer line at 1/143Å.

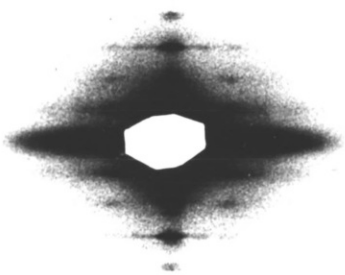
FIGURE 5.1 X-ray diffraction patterns from live Plaice fin muscle at rest-length taken on a camera with a 30cm specimen to film distance. The fibre axis is vertical, the crystal focusing direction is also vertical. Printed from the middle film in a pack of three. X-ray exposure times between 24 and 40 hours at 40kV, 50-60mA. In (a) the vertical arrow indicates the first row-line indexed on a hexagonal lattice of a-spacing 473Å, the horizontal arrow indicates the third layer line at $1/143 Å^{-1}$.



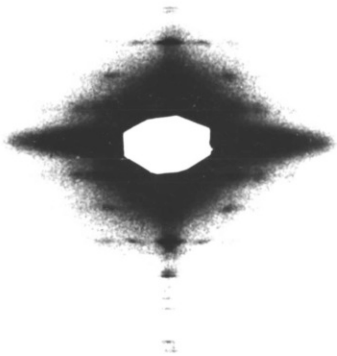
a



b



c



d

degree of lateral register of the myosin filaments across the width of the fibril. These features of the diffraction pattern, and the likely radius from the thick filament axis of the structures giving the off-meridional diffraction at the observed radial distance from the meridian (see section 5.5), indicate that diffraction from the myosin crossbridges dominates the off-meridional diffraction and that diffraction from these latter structures plus the other myofibrillar proteins dominates the meridional pattern.

5.2. The Myosin Layer Line Pattern.

The distribution of intensity along the myosin layer lines differs markedly from the well characterised distribution in frog sartorius muscle and its details are dealt with in a later section. There is a factor of about two between the most prominent layer line, the first, and the second layer line (Figures 5 and 5.1).

The layer line spacings index as the 1st, 2nd, 3rd, 4th..etc. orders of a periodicity of three times the spacing of the third order meridional reflection (Table 5.2). Absolute measurements of this latter spacing on the long camera (specimen to film distance 809.0mm) showed a single strong peak at 144.0 (± 0.1)Å. By measuring the equivalent reflection for frog sartorius muscle on precisely the same camera settings, the spacing for fish was found to be 0.1 to 0.2% less than the strongest component at this position for frog (Table 5.3).

This spacing for frog sartorius muscle is 0.6% greater than previously established values (Huxley and Brown, 1967; Haselgrove, 1975) which is equivalent to a 4mm error in

measurement of the specimen to film distance, although this is measurable to within 0.5mm or less. For the 40 patterns recorded the variation in specimen to film distance due to muscle thickness was gauged by noting the position of the adjustable window in contact with the surface of the muscle specimen in each case. The specimen to film distance over all measurements was within 0.25mm of 809.0mm.

It seemed unlikely that the difference in absolute values for the value for frog sartorius muscle could arise due to errors in measuring the specimen to film distance. Ten of these measurements from both frog sartorius and Plaice fin were made after completely realigning the X-ray camera. The second series of measurements (Table 5.3) gave statistically the same absolute spacings for each type of muscle as in the first series (Table 5.3).

The X-ray film holder was not evacuated during the X-ray exposures but shrinkage of the X-ray film (CEA Reflex 25) due to processing was found to be less than 0.1%. The 0.6% difference in spacing found for the third order meridional reflection in frog would require a shrinkage of about 0.3mm in the 47.3mm marks made on the film for this test. The observed difference for the processed and unprocessed films is no greater than the variation obtained in measuring the separation of a particular pair of indentations in the film, of about 0.05mm.

The observed difference of 0.6% for the reported values of the third order meridional reflection for frog sartorius muscle should be an obvious error using camera set-ups of the length of the order of 1 metre. Since the relative values of this meridional reflection for fish and frog muscles are more

important than this small discrepancy in absolute values, and the relative values obtained here seem reproducible, it is reasonable to have more confidence in the values obtained for this spacing from measurements on a much longer camera (Haselgrove, 1975). The observed difference was therefore attributed to systematic error and Haselgrove's considered to be a more reliable figure. Thus the third order meridional spacing in fish used for calibration has therefore been taken as 99.85% of 143.4 Å, i.e. 143.18 Å.

5.3. The Meridional Pattern.

At spacings greater than the intense 143Å reflection along the meridian, reflections are observed which are interpreted as arising from components of the thick and thin filaments. At smaller spacings the low-angle meridional diffraction pattern is dominated by reflections which index as the 4th, 5th, 6th, 8th and 11th orders of a repeat of 3 x 143.4Å (Table 5.2). The peak intensities of the prominent measurable reflections are shown in Table 5.4. These mean values are approximately represented by the meridional trace in Figure 5.5.

The meridional pattern consists of reflections of very similar character in terms of their lack of broadening along the meridian and their breadth at right angles to it. This latter feature in particular identifies these reflections with the myofibrillar proteins since the smaller fibril width of the other possible origin, that of collagen, is not consistent with the limited breadth of these observed reflections perpendicular to the meridian. Indeed in infrequent cases where tendons (constituting primarily collagen) have contributed to the overall pattern (when attempts were made to irradiate the very tip of the

TABLE 5.2 Myosin Layer Line Spacings from live Plaice Fin Muscle at Rest Length

Measured Spacing(Å)	Order of 429Å	Theoretical Spacing of order of 429Å
420.5*	1	429.0
215.6*	2	214.5
143.2**	3	143.0
106.1	4	107.2
85.7	5	85.8
71.5	6	71.5
61.5	7	61.3
53.5	8	53.6
48.0	9	47.7
38.9	11	39.0

Layer line spacings were measured along the meridian except where indicated (*). Standard deviations of 0.2Å or less apply to all measurements made along the meridian and standard deviations of 1 to 2Å for those measured off the meridian (*).

** Reflection used for calibration.

TABLE 5.3 Measurement of the Absolute Spacing of the Third Order Meridional Reflection from X-ray Patterns Recorded on an X-ray Camera with an 80cm Specimen to Film Distance.

(a) Absolute measurements of the third order meridional reflection for frog sartorius and Plaice fin muscles.

Specimen	1st measurement	2nd measurement
Plaice	144.0 (0.10)Å	144.1 (0.10)Å
Frog	144.3 (0.10)Å	144.25 (0.15)Å

(b) Shrinkage of X-ray film due to processing and evacuation.

Film	Indentation separation before processing (mm)	Indentation separation after processing (mm)
CEA	47.25 (0.03)	47.27 (0.04)
Ilford G	47.27 (0.04)	47.28 (0.02)

In (a) the 1st and 2nd measurements refer to patterns recorded after reassembling the X-ray camera. The standard deviations shown in parantheses include two measurements of all patterns. In (b) Ilford G film was evacuated for 3 days but since the film was more than one year old this may have had no effect on the shrinkage.

TABLE 5.4 Spacings and Relative Intensities of Meridional Reflections from X-ray Diffraction Patterns of Live Plaice Fin Muscle at Rest Length

Measured Spacing(Å)	Relative Intensity
497.4	0.68
440.9£	3.04
390.2	2.06
238.0	1.3
232.1	2.0
219.6	1.6
206.2	0.7
190.8	0.78
185.7*	-
171.6	-
153.3*	-
143.2	9.8
125.1*	-
109.6	0.71
106.2	1.0
98.7**	0.25
95.5	0.14
91.0	0.44
85.7	0.59
81.5	0.17
71.5	0.78
68.1	-
65.1**	-
61.5	-
59.1	-
53.7	-
50.9	-
48.0	-
39.0	-

Spacings greater than 170Å and those indicated (**) have standard deviations between 0.4 and 1Å.(£) This spacing has a standard deviation of 1.9Å. All other spacing measurements have standard deviations less than 0.2Å. The intensity measurements have a probable error between 15 and 20%.

(*) Meridional reflections seen only once

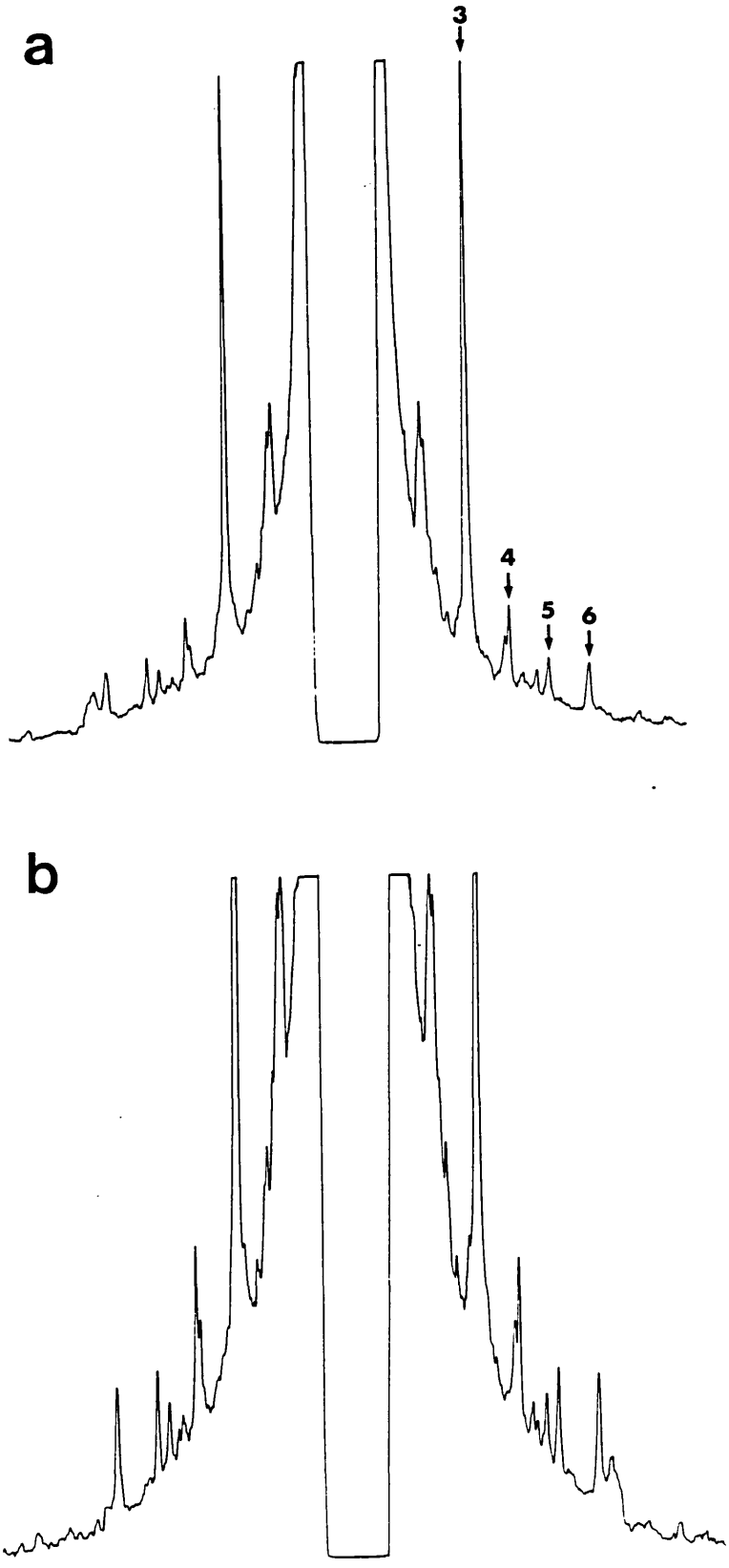


FIGURE 5.5 Microdensitometer traces of the meridian from an X-ray diffraction pattern of live Plaice fin muscle like that in Figure 5.1. (a) and (b) are from back and front films, respectively, taken from the same preparation. Meridional peaks which measure as higher orders of 429Å are arrowed 3,4,5 etc.

muscle) the difference in appearance and alignment of the reflections is quite clear.

Groups of meridional reflections appear closely spaced on medium length (30cm specimen to film distance) or longer cameras, representing diffraction from repeating units many thousands of Angstroms apart in which the diffracting structures are very precisely arranged. The possible origins of these are discussed below.

5.3.1. Reflections Probably Arising From The Thick Filaments

The most prominent reflection which does not have a spacing obviously related to that of the myosin reflections occurs at 440.9 Å. This is quite distinct from the myosin layer line at about 420Å on the long camera. This has a peak height about one-third of that of the strongest meridional reflection at 143Å.

In glycerinated rabbit muscle, reflections in this region, taken to be the 442Å and 418.4Å reflections seen in patterns from frog sartorius muscle, have been shown to be at least partly due to the C-protein component of the thick filament (Rome et al, 1973) which is closely associated with the thick filament backbone (Craig and Offer, 1976a). The presently observed meridional reflection close to this C-protein reflection has the features expected of such a component of the thick filament. These were well-established by Huxley and Brown (1967) and are briefly as follows. The small width along the meridian indicates that this component is regularly spaced probably over most of the thick filament length occupied by C-protein. The absence of appreciable broadening perpendicular to the meridian is consistent with the precise longitudinal register of this

component in filaments across the fibril width. This is to be expected from the appearance of striations due to C-protein which are continuous and straight across the fibril width (Craig and Offer, 1976a; Hanson et al, 1971; Sjostrom and Squire, 1977). On the longest camera used in this work there appears only one strong component to this reflection at 440.9Å. However this is only just clear of the central scatter (Figure 5.7(a)) and clearly requires further analysis on a camera with a 1 to 2 metre specimen to film distance.

Other meridional reflections which may be higher orders of the periodicity represented by this reflection are observed (Table 5.6). In the region of the second order of the reflection at 441Å a number of equally spaced reflections are seen at 233Å, 220Å, and 206Å on the 30cm specimen to film camera which are consecutive orders of a repeat of about 3500Å. This repeat is roughly half the separation of C-zones across the A-band and suggests that interference fringes due to this C-zone separation are partially resolved on this camera. Analogous reflections are seen in frog X-ray diagrams but a very distinct difference is the absence of a reflection at the second order position of 429Å in the meridional X-ray diagram of fish muscle. In contrast this reflection, at about 215Å, dominates this series of reflections between 240 and 200Å in frog X-ray diagrams. On longer cameras, in the case of Plaice fin muscle, reflections at 230Å and 221Å are still prominent, weaker reflections are seen at 238Å and 206Å but no second order of 429Å is apparent. Thus reflections are seen which index approximately as the 30th, 31st, 32nd and 34th orders of a repeat of about 7100Å (Figure 5.7(b)) but there is no perceptible reflection at 215Å i.e. 7100/33.

At smaller spacings than the intense 143Å reflection the high relative intensity of the 4th, 5th and 6th orders of 429Å indicate that the dominant repeat of the crossbridges is 429Å. The distribution of intensity of these "forbidden" reflections shows marked differences from the X-ray diagrams of frog sartorius muscle (Huxley and Brown,1967; Haselgrove, 1975). Although the 8th and 11th orders of 429Å are still strong, the 4th,5th and 6th orders always show the pattern $I_4 > I_5 < I_6$. The same pattern is also observed on cameras with a longer specimen to film distance. Thus the pattern of strong 2nd, 5th, 8th and 11th orders of 429Å characteristic of A-segments (Hanson et al, 1971; Craig, 1977), LMM paracrystals (Hanson et al, 1971; Bennett, 1976) and the X-ray diagram of live frog muscle (Huxley and Brown, 1967) does not occur in the X-ray diagram of live Plaice fin muscle. This may mean the perturbation of the crossbridge helix is slightly different in Plaice muscle thick filaments.

Where groups of equally spaced intervals do occur, for example between 230 and 200Å and between 98 and 81Å, the separations suggest they arise from periodicities less than about 4000Å. From this it seems unlikely, and in any case unexpected at this camera length, that interference fringes due to the separation of C-zone or crossbridge regions across the A-band can alone account for these reflections. Some of these may be due to troponin but others suggest there may be a weakly developed "beat" period of 3400 to 3500Å, which is the 8th order of 429Å and the 9th order of about 385Å. These same reflections are clearly usually even orders of the beat period and would therefore index on a repeat of about 4 x 429Å.

5.3.2. Reflections Probably Arising from the Thin Filaments

A strong meridional reflection at 390Å has been shown by the antibody labelling studies of Rome et al (1973a) to be due at least in part to troponin in other vertebrate muscles and this is the most likely origin of the 390Å reflection observed here. This was recorded on a camera with an 80cm specimen to film distance and could correspond to the mean position of an unresolved doublet at 383Å and 395Å, which is observed in the case of frog sartorius muscle. The possible second order of this reflection at 190.8Å indexes closer on a 382Å repeat and the two reflections at 98.7Å and 95.5Å are fourth orders of 395Å and 382Å respectively.

5.3.3. The Pitch of the Actin Helix

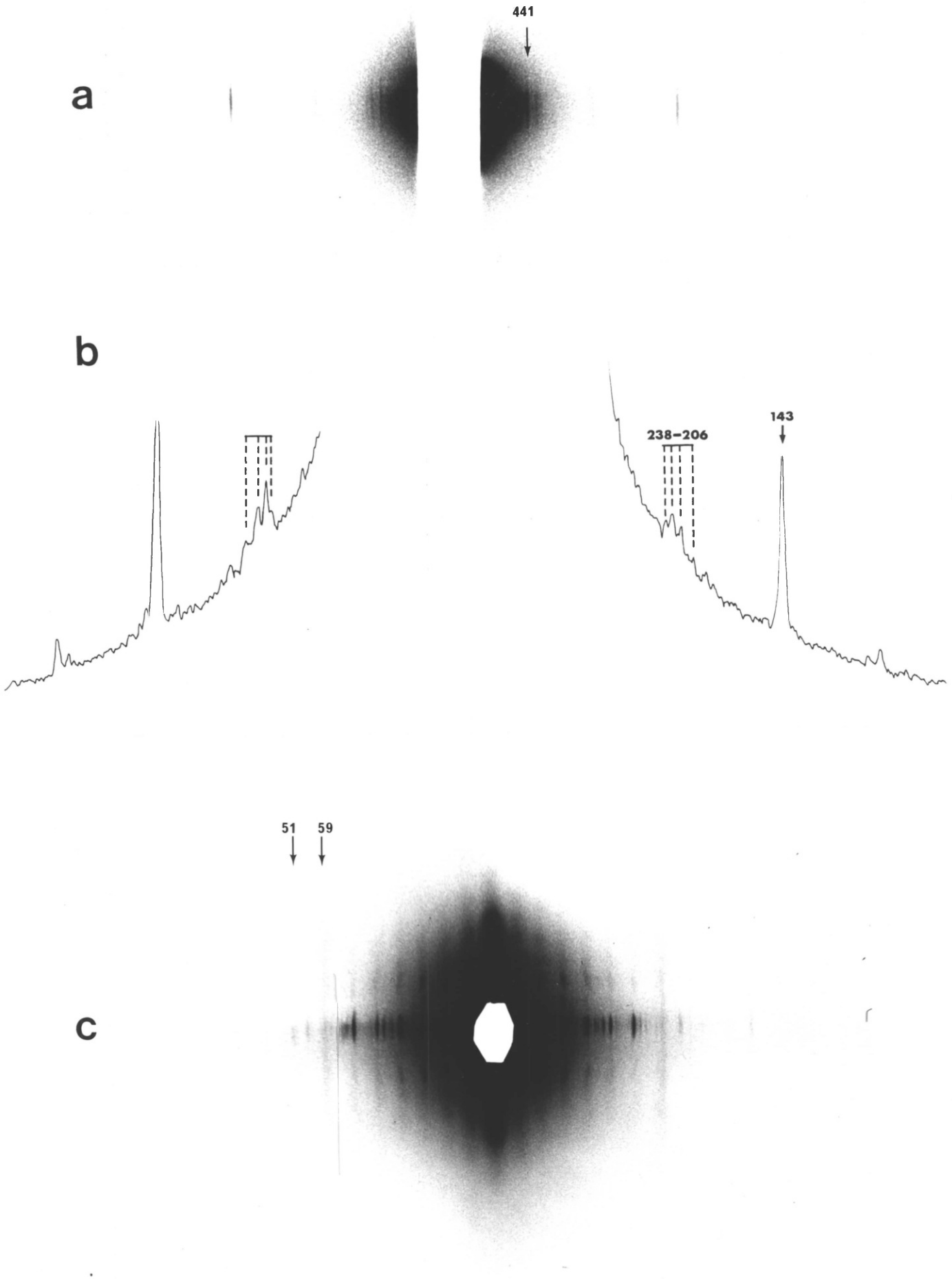
Layer lines characteristic of the actin helix occur at spacings of 59.1 (±0.17)Å and 50.9 (±0.18)Å (Figure 5.7(c)).These are in close agreement with values for analogous reflections in the low-angle X-ray diagram of frog sartorius muscle and imply that the thin filaments have a similar pitch. Values of 50.97 (±0.02)Å and 59.1 (±0.03)Å (or 59.4 (±0.05)Å) were obtained by Huxley and Brown (1967) and 51.2 (±0.5%)Å and 59.5 (±0.5%)Å by Haselgrove (1975). The spread in the measured values of these spacings is much larger in Plaice fin X-ray diagrams reflecting the difficulty in obtaining comparably well-oriented specimens. It has not been possible to improve the recording of these X-ray reflections as outlined and carried out by Huxley and Brown (1967). An accurate value for the pitch of the actin helix requires the much weaker but sharper 51Å layer line to be recorded with greater intensity and the resolution of the 59Å layer line and the nearby 61Å myosin layer line to be improved.

TABLE 5.6 The possible origins of some of the spacings of the low-angle X-ray meridional reflections from live Plaice fin muscle recorded on a camera with a 30cm specimen to film distance.

Measured Spacing(Å)	Peaks from an array of period 440Å (C-protein)	Peaks from an array of period 390Å (Troponin)	Array of period 3500Å ***	Array of period 4x429Å (1716A) **
497.4				
440.9	440.0 (1)			
390.2		390.0 (1)		
238.0				
232.1			233.3 (15)	
219.6	220.0 (2)		218.7 (16)	
206.2			205.9 (17)	
190.8		195.0 (2)	194.4 (18)	190.7 (9)
185.7			184.2 (19)	
171.6			175.0 (20)	171.6 (10)
153.3			152.2 (23)	
143.2				*143.0 (12)
125.1			125.0 (28)	122.6 (14)
109.6	110.0 (4)		109.4 (32)	
106.2				*107.2 (16)
98.7		97.5 (4)		
95.5				95.3 (18)
91.0				90.3 (19)
85.7				*85.8 (20)
81.5		78.0 (5)		81.7 (21)
71.5				*71.5 (24)
68.1				68.6 (25)
65.1		65.0 (6)		66.0 (26)
61.5				*61.3 (28)
59.1				59.2 (29)
53.7				*53.6 (32)
50.9				50.5 (34)
48.0		48.8 (8)		*47.7 (36)
39.0				39.1 (44)

* These reflections are consecutive orders of the 429Å crossbridge repeat.
** Most of these reflections index on a period of about 2 x 1716Å i.e. the 8th order of 429Å and the 9th order of 380Å.
*** This period is approximately half of the separation of C-zones across the A-band. Which in frog sartorius muscle appears to be about 7095Å (Squire, 1981).

FIGURE 5.7 (a) X-ray meridional diffraction pattern taken on the camera with an 80cm specimen to film distance. The 441Å reflection is just clear of the central scatter. (b) Densitometer trace along the meridian of a pattern such as that in (a) showing reflections in the region of the 2nd myosin layer line. The reflections with spacings of 206Å, 221Å, 232Å and 238Å are indicated by vertical broken lines. (c) X-ray diffraction pattern taken on the camera with a 30cm specimen to film distance. The fibre axis is across the page. The actin layer line with a spacing of 59Å is indicated. The 51Å actin layer line is only just visible.


441
a
b
238–206
143
51
59
c

From the separation of these layer lines, assuming them to be 6th and 7th orders of an integral helix with 13 subunits in 6 turns, a pitch of 2 x 365Å is obtained. This falls between the values of 2 x 360Å and 2 x 370Å obtained for frog sartorius muscle (Huxley and Brown, 1967). However this result can only be taken to indicate that the pitch of the actin helix is probably very similar to that in frog sartorius muscle.

5.4 Row-Line Sampling Of The Myosin Layer Line Pattern

The details of the row-line sampling of the myosin layer line pattern were studied by optimising the X-ray camera's order-to-order resolution perpendicular to the muscle fibre axis as described in Materials and Methods. Equatorial diffraction patterns from the live muscle on the long camera were also used to supplement the equatorial intensity data. Low-angle X-ray patterns at rest-length (2.45 to 2.5 micrometres) were sampled by row-lines indexing on a simple hexagonal unit cell with an inter filament spacing of 472Å (Table 5.8). Since equatorial X-ray diagrams recorded at rest length could also be indexed on a unit cell of a very similar spacing of 472Å, intensity data extracted from both sources was combined in the analysis of the row-line sampling of the equator. Firstly a general description of the layer line sampling will be given.

An extensive three-dimensional ordering of the myosin crossbridges is apparent from the sharply localized lattice reflections on the first three myosin layer lines (Figure 5.9). the extent of this ordering being particularly well demonstrated when row-lines are resolved using the crystal focus (Figure 5.9); There is no appreciable broadening of the crystal focus, suggesting that this order extends throughout the myofibril

Table 5.8 Row line Spacings from "Two-Dimensionally Resolved" X-ray Diffraction Patterns and Their Indexing on the A-band hexagonal lattice and I-band Square Lattice.

Index on 290Å Square lattice	Index on 472Å cell hexagonal lattice	Calculated Spacing	Observed Spacing
-	10	408.8	409.1
10	-	290.0	290.0
-	11	236.0	233.6
11	20	204.4	204.4
-	21	154.5	153.7
-	30	136.3	134.1

Lattice spacings were measured along the equator of the diffraction pattern from Plaice fin muscle. Hexagonal unit cell size is 472Å determined from the 204.4Å (20) equatorial reflection.
Probable error on the measurement of spacings is 0.5%.
The corresponding five row line reflections along the first layer line occurred within 0.2% of the spacing measured along the equator, as did the (10) and (11) reflections along the third and second layer lines respectively.

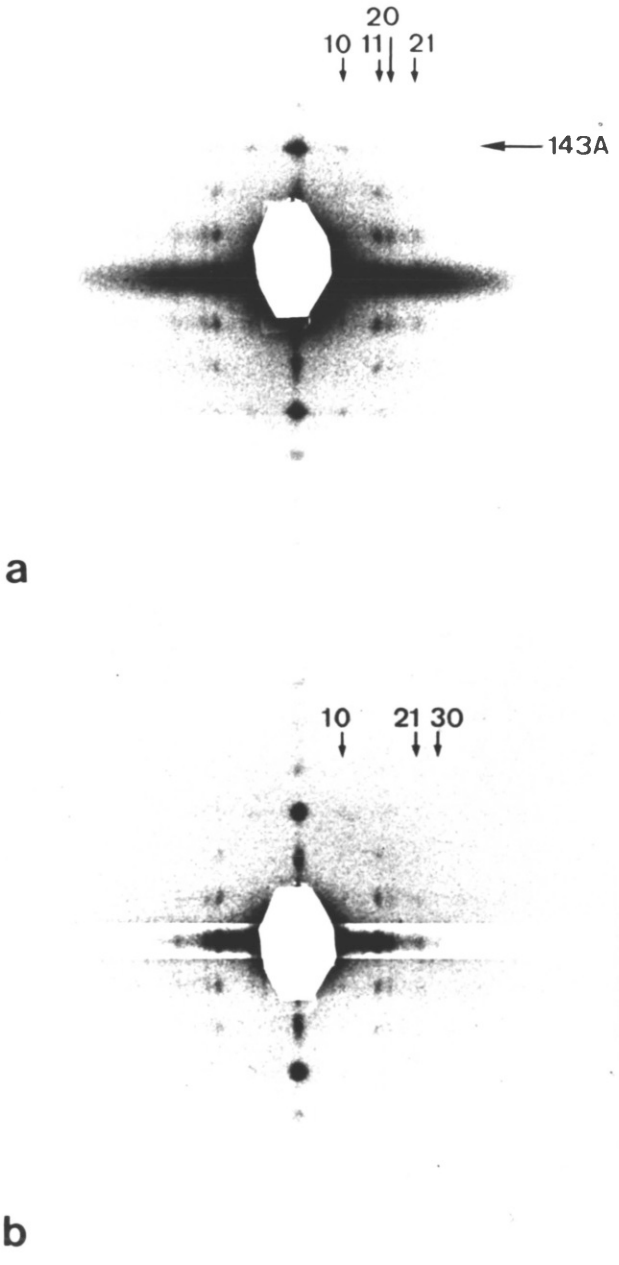


FIGURE 5.9 X-ray diffraction patterns of live Plaice fin muscle taken on a camera with a 30cm specimen to film distance. The muscle fibre axis is vertical, the crystal focusing direction is across the page. Vertical arrows indicate row-lines indexed on the hexagonal lattice of thick filaments. (a) 24 hours exposure time, 40kV 50mA. (b) 13 hours exposure time, 30kV 50mA. The equator has been printed at a shorter exposure in (b).

width. Lattice reflections for the first layer line occur on exactly the same row-lines as the equatorial reflections. Reflections on higher order layer lines occur only on those row-lines showing intensity on the equator.

5.4.1. Row Line Spacings

Accurate spacings for these row-lines were obtainable from patterns such as Figure 5.9. These row-lines agree well with row-lines indexing on a hexagonal unit cell of spacing about 472Å (Table 5.8). Measurements of the row-line spacings in the less well resolved patterns are in general agreement with the calculated spacings although the broadening of the row-lines due to the mirror focus gives an expectedly much larger probable error on these measurements. The prerequisite order-to-order resolution for the 10 and 11 row-lines is only just provided in this camera arrrangement. In addition, spacings for the 11 reflection, particularly for the first layer line, are considerably influenced to smaller spacings due to the close unresolved 20 row-line. On the second layer line the 11 reflection is relatively much stronger than the 20 reflection on this layer line and thus the row-line spacing is in very good agreement with that from the "two-dimensionally resolved" X-ray diagrams (Table 5.10).

5.4.2. Row Line Intensities

Intensity measurements were made from the 13 X-ray patterns of the most well-oriented specimens taken on a camera with a 30cm specimen to film distance. This included two of the best of those showing clear two dimensional resolution along row line and layer lines. The remainder were not as well resolved along layer lines,

particularly along the first layer line, and so measurements from them only served to confirm whether any gross errors were evident in the analysis of the two-dimensionally resolved patterns.

Since the row-line sampling of the myosin layer line pattern was clearly defined as far along the first layer line as the 30 rowline (Figure 5.11), and on the first three layer lines, collection of intensity data was limited to a resolution of about 130Å. From the two-dimensionally resolved patterns microdensitometer traces along row-lines gave an overall intensity distribution comparable with that from traces taken along layer lines, within the range of error of the microdensitometer measurements. Only along the equator of the pattern was there a sufficiently strong "streak" to give an appreciable difference between the intensities derived from row-line traces and those from a single layer line trace.

Since the 11 and 20 reflections along the first layer line of one-dimensionally resolved X-ray patterns were unresolved the values shown in Table 5.13(b) for these reflections have been weighted according to measurements on patterns with better resolution as in Table 5.13(a). This was considered to be reasonable because the ratio of the integrated intensity of the main peak (i.e. 11+20) on the first layer line of such patterns to the same row lines on the second layer line was in good agreement with the expected ratio obtained by summing the resolved component's measurements in Table 5.13(a).

5.5. Computer Modelling of the Myosin Layer Line Pattern

5.5.1. The Relaxed Crossbridge Configuration

Models were set up as described in Materials and Methods

Table 5.10 Row-line Spacing Measurements from "One-dimensionally Resolved" X-ray Patterns

Layer Line Number	Row-line Spacing(Å)		
	10	11+20	21
1	-	230.6	157.7
2	-	233.6*	-
3	417	220.6	-
4	-	216.6	-
5	-	-	-
6	242.6	-	-

Probable error on the measurements of spacings 2 - 3%

* Note that the spacing for this reflection is very close to the measurement from X-ray patterns showing essentially two-dimensional resolution (Table 5.8) in which a value of 233.6Å was obtained. Unlike the corresponding row line on the first layer line this reflection is probably not influenced to smaller spacings by the unresolved (20) reflection.

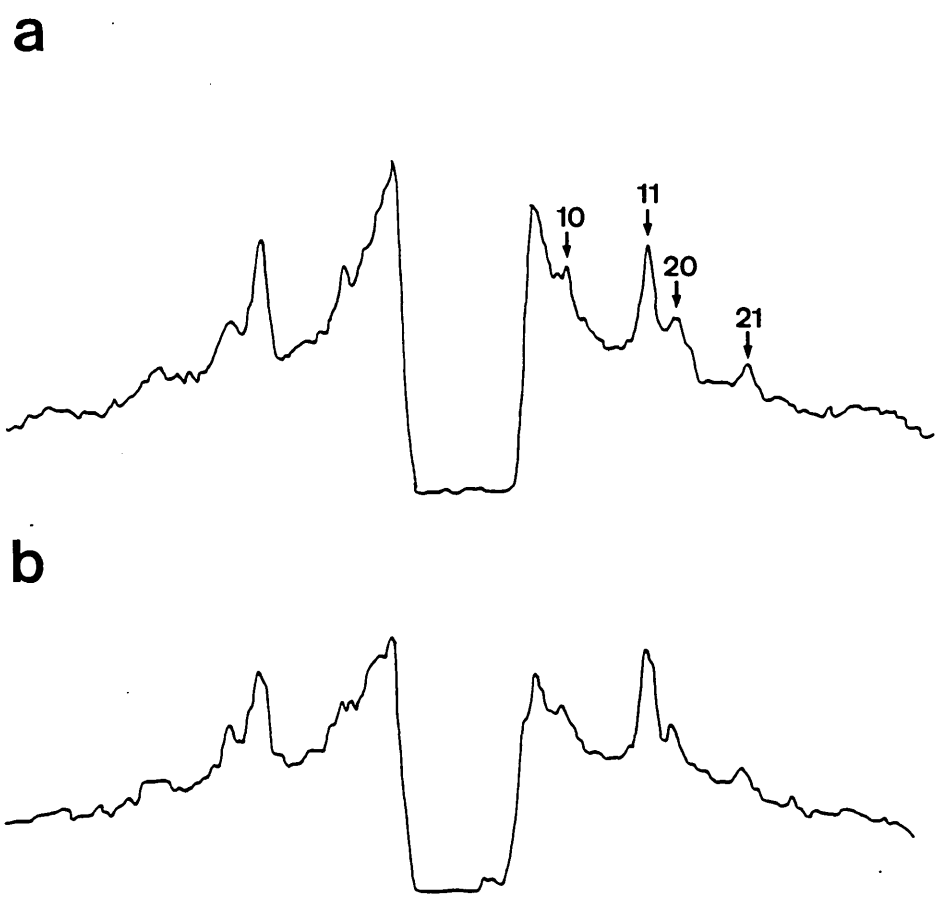


FIGURE 5.11 Microdensitometer traces of the first myosin layer line from an X-ray diffraction pattern of live Plaice fin muscle, such as that shown in Figure 5.9 with good two-dimensional resolution. (a) and (b) are traces along the first myosin layer line, corresponding to a spacing of about 430Å, from opposite sides of the equator.

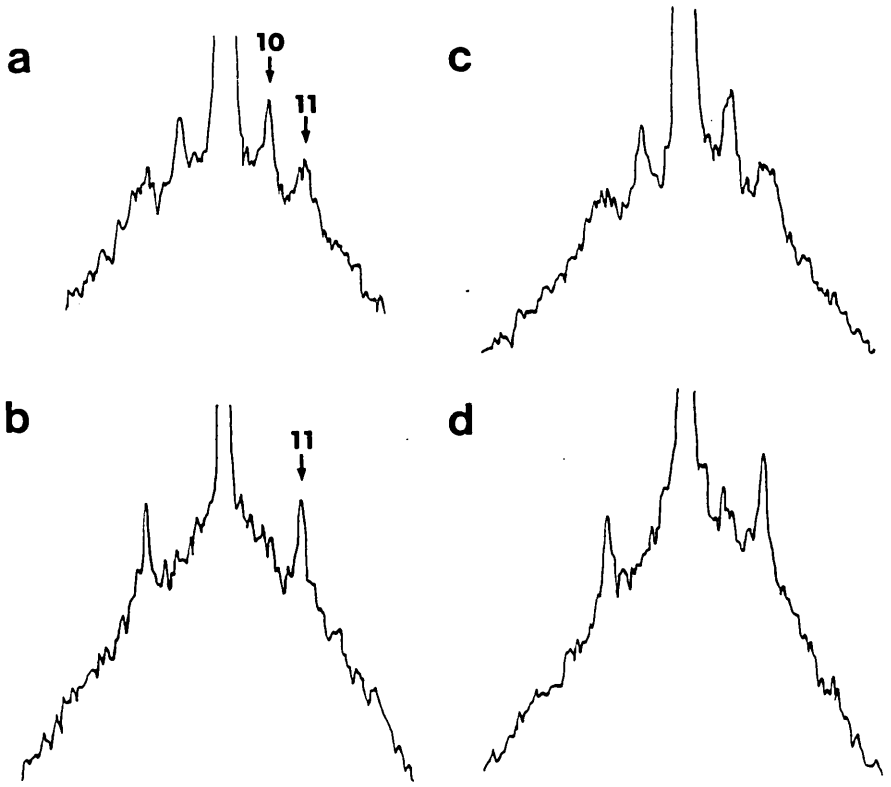


FIGURE 5.12 Microdensitometer traces of the second and third myosin layer lines (corresponding to spacings of about 215Å and 143Å respectively) from an X-ray diffraction pattern of live Plaice fin muscle such as that shown in Figure 5.9. (a) and (b) are third and second layer lines, respectively, from one side of the pattern. (c) and (d) are third and second layer lines from the opposite side of the same pattern.

Table 5.13 (a) Corrected Relative Intensities From "Two-dimensionally Resolved" X-ray Patterns

Layer Line Number	Row-line Intensities				
	10	11	20	21	30
3	7	14	3	vw	vw
2	vw	18	mw	vw	vw
1	4*	43	28	10*	3*

(b) Corrected Relative Intensities from "One-dimensionally Resolved" Patterns

Layer Line Number	Row-line Intensities		
	10	11	20
3	9	17	-
2	-	21	-
1	-	43	28

Probable error on intensity measurements is 10 to 15%. Reflections indicated (*) have probable errors of 25% to 30%. These errors include measurements made with slightly different background assumptions and values from densitometer traces along row lines and layer lines. All intensities were scaled to the (11) peak on the first layer line which was assigned a value after scaling it to the (11) equatorial reflection . This latter reflection was given an arbitrary value of 200. The observed intensities have been corrected for a simple Lorentz factor by multiplying by the reciprocal of the row line spacing. The (21) row line intensities were divided by 2 to account for the multiplicity. Further details of the intensity measurements are given in the text.

and the computed intensity data for each model then compared with the observed, corrected data shown in Table 5.13. The best fit was sought by computing the least sum of squares for each model. Ideally this sum of squares should be weighted by the square of the standard deviation for each reflection such that the minimum values of S is obtained where $S = \sum_{1}^{n} w_n \Delta_n^2$ where $w_n = 1/\sigma_n$ and Δ_n is the difference between the observed and computed quantities. However realistic standard deviations (σ_n) cannot be quoted for individual reflections (n). For values of S greater than about 400, where $\Delta_n = (I_o - I_c)$, the index $R = \sum_{1}^{n}[I_o - I_c]/\sum_{1}^{n} I_o$ is greater than 0.5 corresponding to a 50% difference, $I_o - I_c$, on all the observed reflections. Models which gave values of S less than 400 were considered further, despite this being a large margin of error, since the computer modelling serves a more useful purpose if trends in the configuration parameters can be established rather than objectively adopting the one model with the lowest value of S which will in any case be heavily dependent on assumptions made in setting up the model.

The centre of the innermost spheres of the two heads were placed at 60,70,80,90 and 100Å radii from the thick filament axis for the longer head model (9-spheres) and 50,60,70,80 and 90Å radii for the shorter head model (7-spheres). The actual radius of the inner end of the crossbridge was at this radius minus the radius of the first sphere i.e. 11.5Å. At each radius the Fourier transform was computed for all configurations of the two heads described in Materials and Methods. The same computations were carried out for a shorter myosin head by excluding the contributions to the computed intensity from the innermost spheres on each head. Using the selection criterion described

above this left about 90 models for each head shape, many of which were variations on a particular type of configuration. Around 70% to 80% of these models gave most of the strong reflections much weaker than 30% less than the observed intensity. The effect of a temperature factor on these only served to worsen the fit with the observed data. The models remaining gave conventional reliability factors, $R = \sum_1^n (|F_o| - |F_c|)/\sum_1^n F_o$, around 0.3. These remaining models and the effect of the head shape and temperature factor on them are now described. Note that the parameters shown for Models 3 and 4 below are the only parameters for these configurations giving fits which are plausible, despite the wide margin of error allowed on the observed intensities when selecting from all possible structures. The range of parameters is limited for Model 2 and most extensive for Model 1.

MODEL 1: A unique feature of this configuration, in which both heads are tilted by +30° with positive slews around the filament surface, is that it occurred with at least moderate fits over the whole range of radii, with long or short heads; the centre of gravity of the heads being brought to a radius of about 140Å by varying amounts of slew. With long heads placed with the inner end at 48.5Å radius with a small amount of slew (+0° and +30°; Figure 5.14a) the fit is very similar to that obtained if the same heads are placed at 88.5Å radius with greater slew (+60° and +90°; Figure 5.14b). If the heads are shortened only the models with 80.5Å radius give comparable fits with γ increased to 30°. A 30° difference in slew between the two heads was still required although it is difficult to distinguish to which side of the normal the two heads are placed i.e. whether the slew is -30°

and 0^{o} (Figure 5.15a) or 0^{o} and $+30^{o}$ (Figure 5.15b). If a temperature factor is applied it is only possible to retain the same degree of fit with short heads, and slightly larger γ (= 60^{o}) placed at 70.5Å radius with slews of 0^{o} and $+30^{o}$ (Figure 5.16a). If the same heads are placed 10Å further out to 80.5Å radius and slewed slightly more, by $+30^{o}$ and $+60^{o}$ (Figure 5.16b), a similar, but slightly poorer fit is obtained.

The main features of the observed diffraction pattern which are not modelled satisfactorily with this, or any other type of model, i.e. the weak 10 and 20 row-lines on the second layer line and the weak 10 row-line on the first layer line, suggest that the main peaks on these two layer lines should be less broad. This may mean that the heads should be confined to a narrower annulus of density around the thick filament backbone. This could possibly be achieved by placing the crossbridge at a larger radius with larger slews or it may be a feature of the shape of the myosin head, such as curvature, or a result of the imperfections in the surface lattice. The first possibility at least seems unlikely since large radius models with both heads slewed around the filament surface give no improvement in modelling these particular features.

MODEL 2: Configurations with the heads tilted by $+30^{o}$ and -30^{o} give similar fits to the observed data if long heads are placed at 58.5Å radius with $\gamma = 0^{o}$ and slews of 0^{o} and $+30^{o}$ (Figure 5.17a) or short heads at 90.5Å radius with $\gamma = 30^{o}$ and with no slew for both heads (Figure 5.17b). If the previous temperature factor is applied the two same configurations still give the best fits, for these tilts, with the long head model giving an improved fit on the poorly modelled second layer line.

This model fails to account well for the weak 10 row-line intensity on the first and second layer lines although most other features including the higher order reflections can be modelled.

MODEL 3: This model is similar to model 1 with long heads placed at 58.5Å radius slewed by +90° and +60° but with no tilting of the two heads (Figure 5.18a).

MODEL 4: The two heads are slewed in opposite directions (+90° and -60°) with no tilting of the two heads at 58.5Å radius (Figure 5.18b) or at a slightly larger radius of 78.5Å with more slew (+90° and -90°) and with tilts of 0° and 30° (Figure 5.18c).

5.5.2. Summary of the modelling

The following general features of the resting crossbridge configuration arise out of the computer modelling:

(1) The centre of gravity of the crossbridges (i.e. the two heads) is at a radius of about 140Å from the axis of the thick filament. This was determined by computing a Fourier synthesis from the equatorial reflections computed from a number of the best crossbridge helix models with no myosin backbone included. The Fourier synthesis thus showed an annulus of density at each of the thick filamentpeak positions in the unit cell. The peak of this annulus of density was at a radius of 140Å from the thick filament axis and was taken as the best estimate of the centre of mass of the crossbridge. Note also that the main first layer line peak in the X-ray diffraction pattern from Plaice fin reaches a maximum probably at a radial position less than $0.0043Å^{-1}$ compared to about $0.005Å^{-1}$ for the prominent first layer line peak in the case of frog sartorius muscle. If these positions are taken as rough

approximations to the relative centres of mass of the crossbridges in the two muscles then for the J_3 Bessel function argument of 4.2, for 3-fold rotational symmetry, the radius of centre of mass for fish is about 22Å greater than that for frog sartorius. Thus with a value for fish of 140Å the centre of mass for frog is about 118Å which is in reasonable agreement with values determined by previous modelling (110 to 115 Å: Squire, 1981; 120 to 130Å : Haselgrove, 1980)

(2) The tilt of the two heads is within the range ± 30°.

(3) At low resolution (i.e. at about 200Å as defined by the fit of the data out to the 20 row-line) the mass of the two heads appears to be aligned approximately along the helical strands of pitch 430Å. This can be achieved in the following ways (i) if the two heads at one lattice point are aligned along the strands both with positive slews and tilts (ii) one head from a lattice point at one level, with a positive tilt, may be placed by a head with a negative tilt from a level above (iii) at the same axial position one head of a crossbridge with a large positive slew may be placed by a head with a large negative slew from the neighbouring lattice point on the same crossbridge level.

Because of the limited resolution of the data fitted so far, there are three different ways of placing the heads in configurations to generate something approximating to the required distribution of mass. However it is of course necessary to define approximate configurational parameters of the two heads to determine a working crossbridge model. A more detailed

examination of the intensity profiles shows that there are features enabling discrimination between the models. Since some form of temperature disorder must apply to the heads, only those transforms computed with the chosen temperature factor need be discussed.

Configurations such as model 4 (Figure 5.18b and c) account well for the first layer line profile but the second layer line is too weak at the 11 peak position and too strong at radial distances beyond the 20 reflection producing a poor second layer line shape. At similar radial positions the same feature is observed for Model 2 (with tilts of $\pm 30^{o}$; Figure 5.17) but to a lesser extent with Model 1 (tilts of $+ 30^{o}$; Figure 5.16) and Model 3 (0^{o} tilt; Figure 5.18a). In choosing between Model 2 and Model 1 (or Model 3) it is clear that there are features poorly modelled in both cases and it is necessary to decide which of these are more tolerable. Both models give too strong intensity near the meridian of the first layer line profile but this is considerably stronger in the case of Model 2. The main peak position on the second layer line is at far too high a radius for Model 2 resulting in a considerably stronger 10 row-line intensity. These features, in addition to the more satisfactory weakening of the layer line profiles further along the second and third layer lines, indicate that Model 1 (or Model 3) give the better compromise on these poorly modelled features of the pattern.

The best parameters for Model 1 in the presence of a temperature factor are obtained with short heads with individual slews of 0^{o} and 30^{o} or 30^{o} and 60^{o}, with the inner end of the crossbridge at 70.5Å or 80.5Å radius (Figure 5.16(a) and (b))

respectively. The smaller slew angles give a slightly better fit. If the crossbridge is slewed further round the filament to 60° and 90° as in Model 3 no tilting of the heads is required to give comparable fits providing the longer myosin head model is used (Figure 5.18a).

Thus the best fit with a short head model is obtained with the heads making the same tilt 30° and slewed by 0° and 30° with γ= 60° at a radius of 70.5Å radius (Figure 5.16(a)), and with the longer head model the crossbridge is tilted less (0° tilt) but slewed around the filament by 60° and 90° with $\gamma = 30°$ (Figure 5.18(a)) at 58.5Å radius.

5.6. Discussion

5.6.1. Summary of Differences in Plaice Fin Muscle Structure

It has been shown that the structures of the thick and thin filaments in Plaice fin muscle are probably very similar to those in the extensively studied frog sartorius muscle at the resolution afforded by these X-ray studies.

The spacings of the actin layer lines at 59Å and 51Å imply that the actin helix has essentially the same pitch as in frog. The intensity distributions of these same layer lines indicate that there is no appreciable difference in the lateral and longitudinal register of neighbouring thin filaments. It was shown by Huxley and Brown (1967) that the observed separation of these layer lines, for frog sartorius muscle, was between that expected for integral actin helices with 13 subunits per turn (in each strand, corresponding to a genetic helix with 13 subunits in 6 turns) and 14 subunits per turn (corresponding to 28 subunits in 13 turns). The same conclusion must be reached here, although with less confidence because of the spread in measured

FIGURES 5.14 to 5.18 Representations of crossbridge helix models and their computed transforms. For each configuration discussed in the text is shown a perspective view of the crossbridge model (I), an end-on view of three crossbridge levels (II) and a bar-chart plot of the observed and computed intensity (III) on the first three myosin layer lines (L1,L2 and L3). At the five row-line positions along each layer line (10,11,20,21,30) the observed intensity is represented by a shaded bar (shown to the left of the actual observed position) and the computed intensity by a dark (filled) bar to the right. In the model representations a cylinder representing the thick filament backbone is shown with a 70Å radius for reference purposes. Intensities were scaled to the strongest peak (i.e. 11 row-line) on the first layer line. For each configuration the head model, the radius of the inner end of the heads from the thick filament axis, and the angles defining the orientation of the two heads are quoted along with any temperature disorder that has been applied. The tilt, β, and slew angle, α, are different for the two heads constituting the crossbridge and are denoted by subscripts 1 and 2 as defined in Materials and Methods. The r.m.s. displacement isotropic disorder values shown correspond to the value given for the outer sphere in each head (see Materials and Methods).

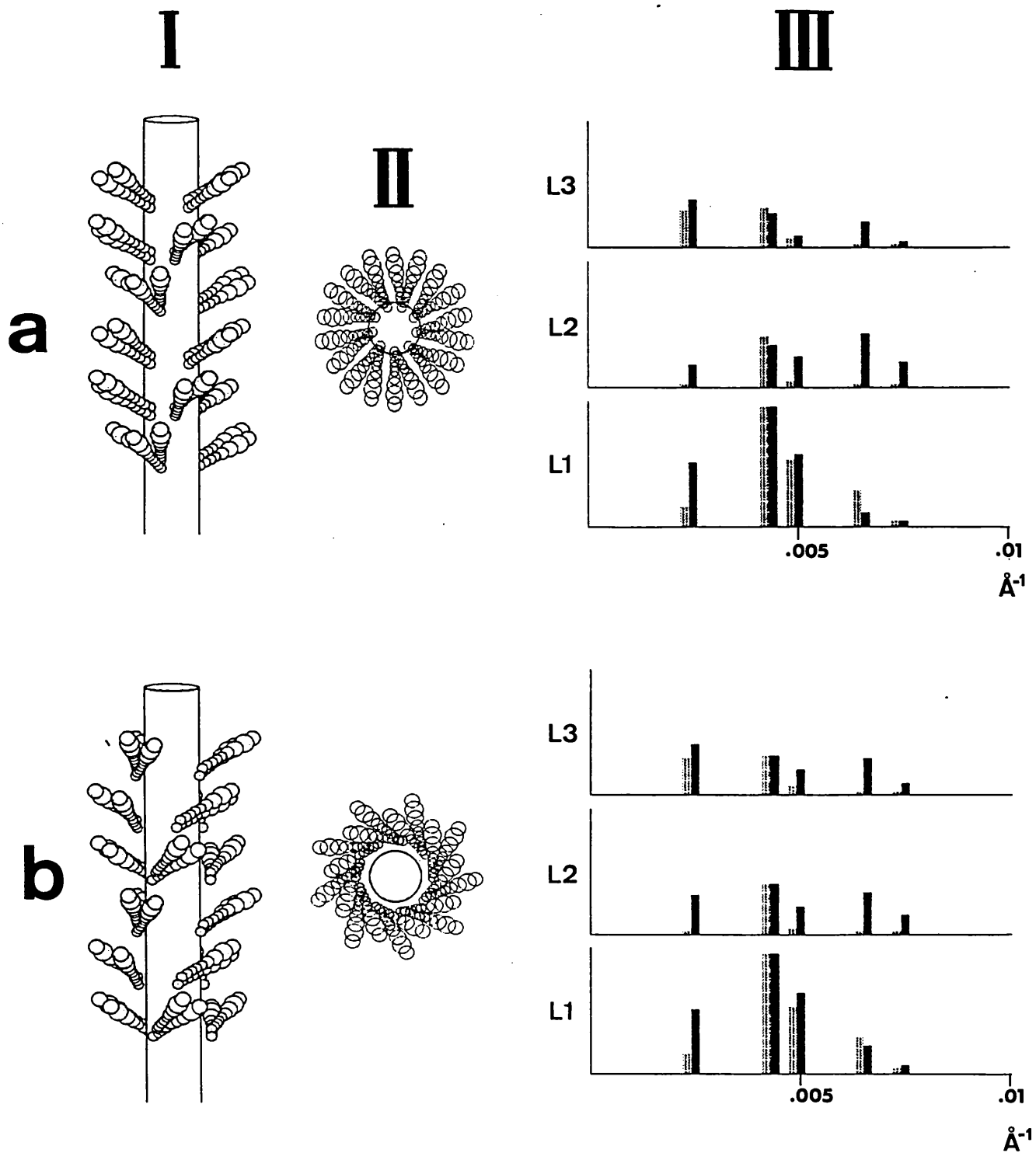


FIGURE 5.14 (a) 9-sphere head at 48.5Å radius; $\beta_1 = \beta_2 = 30^\circ$; $\alpha_1 = 30^\circ$, $\alpha_2 = 0^\circ$; $\gamma = 0^\circ$. No disorder. (b) 9-sphere head at 88.5Å radius; $\beta_1 = \beta_2 = 30^\circ$; $\alpha_1 = 60^\circ$, $\alpha_2 = 90^\circ$; $\gamma = 30^\circ$. No disorder.

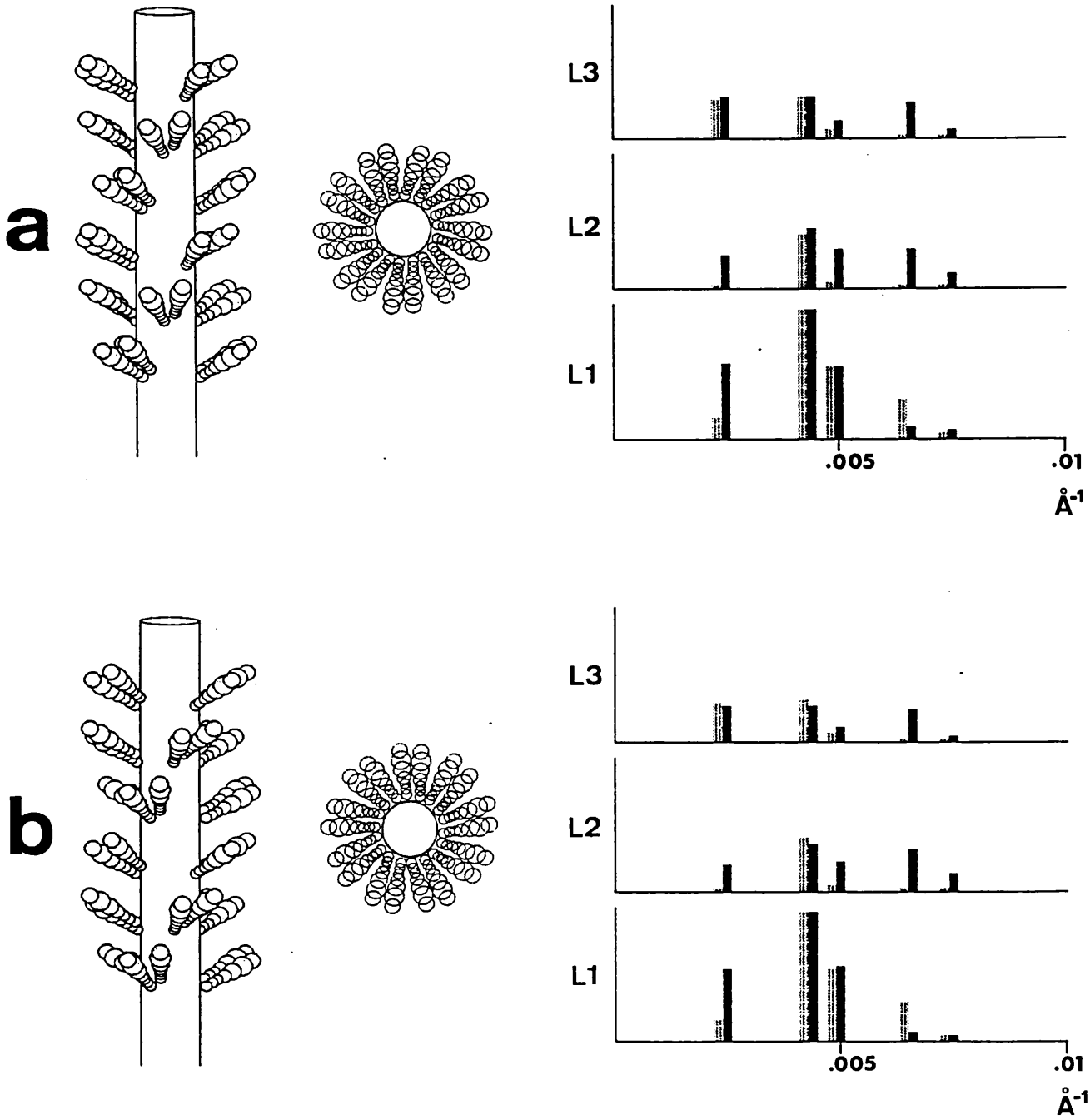


FIGURE 5.15 (a) 7-sphere head at 80.5Å radius; $\beta_1 = \beta_2 = 30^o$; $\alpha_1 = 0^o$, $\alpha_2 = -30^o$; $\gamma = 30^o$. No disorder. (b) 7-sphere head at 80.5Å radius; $\beta_1 = \beta_2 = 30^o$; $\alpha_1 = 30^o$, $\alpha_2 = 0^o$; $\gamma = 30^o$. No disorder. The inner end of the heads should be 10.5Å away from the surface of the backbone but this is only just evident in the end-on view of the models. This a computer-generated artifact.

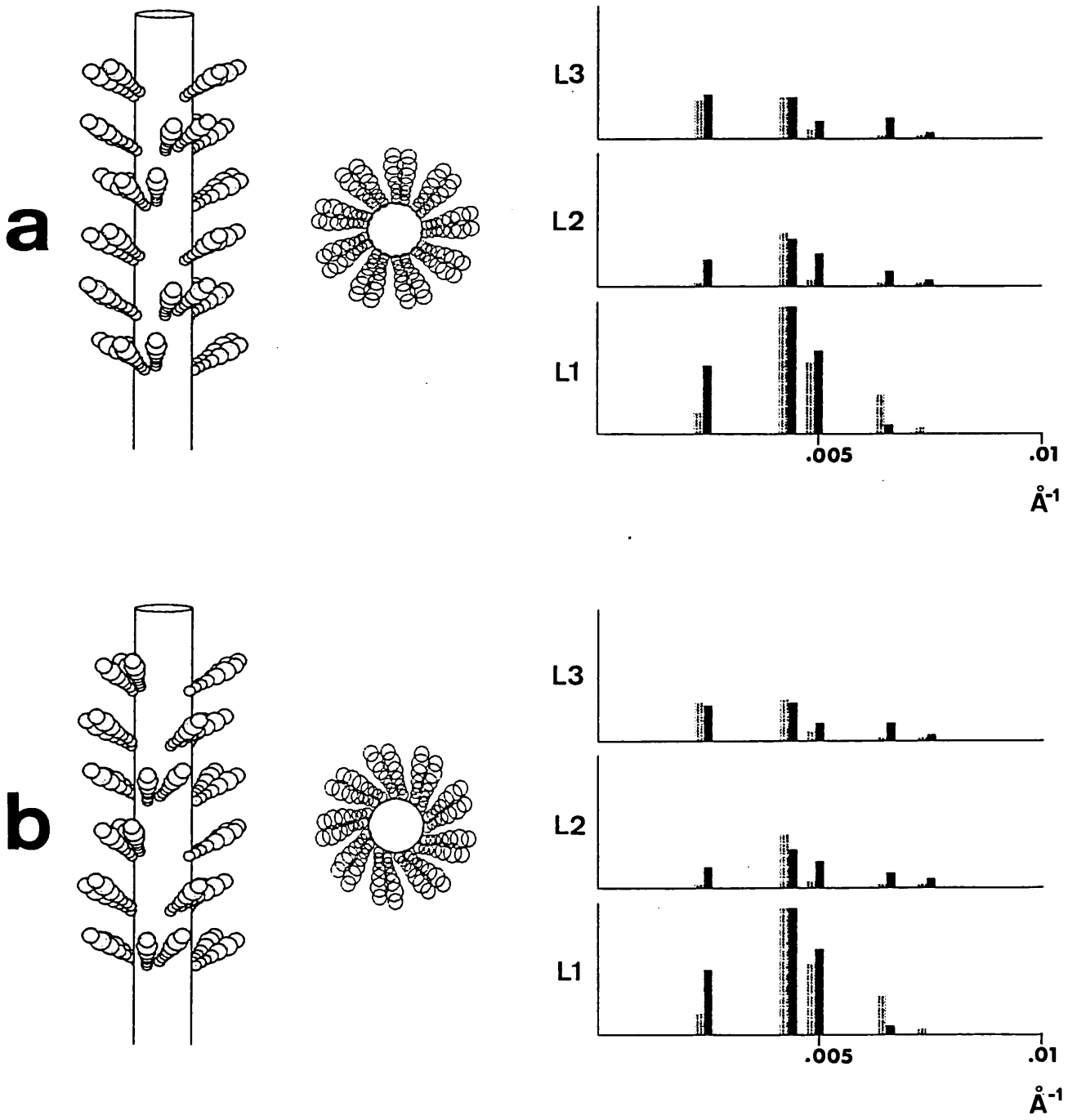


FIGURE 5.16 (a) 7-sphere head at 70.5Å radius; $\beta_1 = \beta_2 = 30^o$; $\alpha_1 = 30^o$, $\alpha_2 = 0^o$; $\gamma = 60^o$. (b) 7-sphere head at 80.5Å radius; $\beta_1 = \beta_2 = 30^o$; $\alpha_1 = 60^o$, $\alpha_2 = 30^o$; $\gamma = 60^o$. With 11.5Å r.m.s displacement isotropic disorder applied to both (a) and (b). As in Figure 5.15 in the end-on view in (b) the small gap between the backbone surface and the inner end of the heads is only just evident.

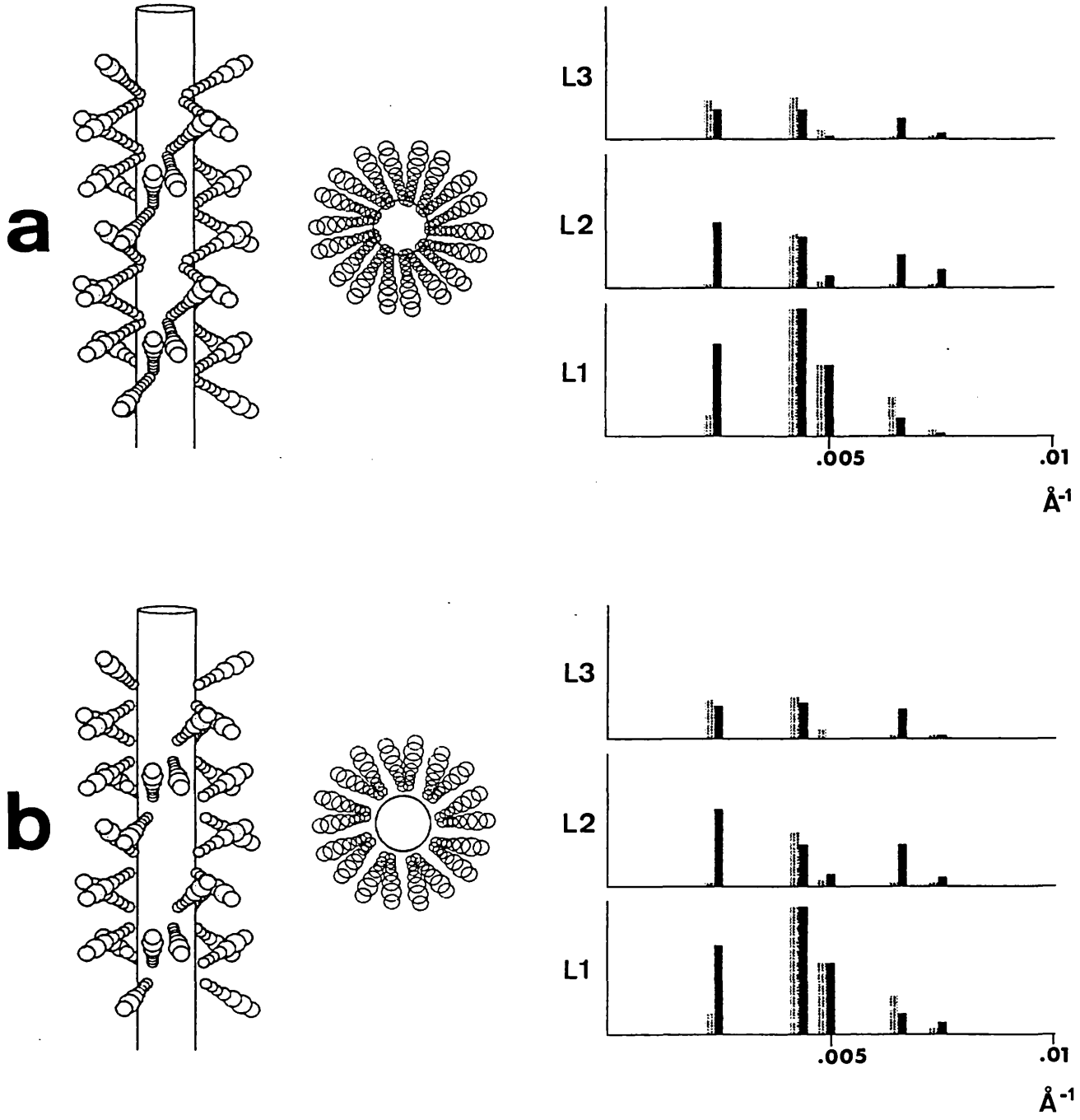


FIGURE 5.17 (a) 9-sphere head at 58.5Å radius; β_1 = 30°, β_2 = -30°; α_1 = 30°, α_2 = 0°; γ = 0°. (b) 7-sphere head at 90.5Å radius; β_1 = 30°, β_2 = -30°; $\alpha_1 = \alpha_2$ = 0°; γ = 30°. With 11.5Å r.m.s displacement isotropic disorder applied to both (a) and (b).

FIGURE 5.18 (a) 9-sphere head at 58.5Å radius; $\beta_1 = \beta_2 = 0^o$; $\alpha_1 = 90^o$, $\alpha_2 = 60^o$; $\gamma = 30^o$. (b) 9-sphere head at 58.5Å radius; $\beta_1 = \beta_2 = 0^o$; $\alpha_1 = -60^o$, $\alpha_2 = 90^o$; $\gamma = 0^o$. (c) 9-sphere head at 78.5Å radius; $\beta_1 = 0^o$, $\beta_2 = 30^o$; $\alpha_1 = 90^o$, $\alpha_2 = -90^o$; $\gamma = 30^o$. With 11.5Å r.m.s. displacement isotropic disorder applied to (a), (b) and (c).

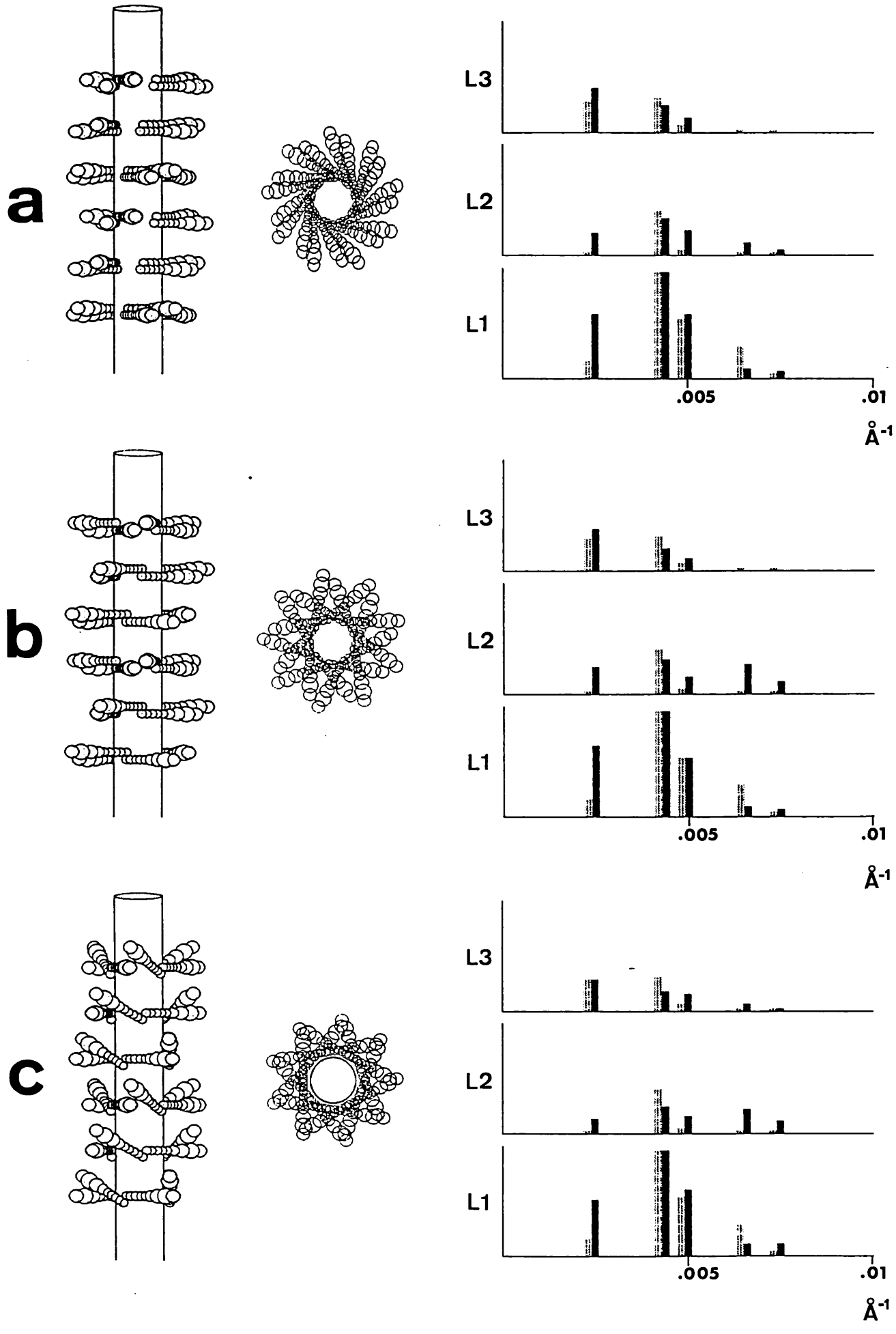


FIGURE 5.18

spacings, that the actin helix is non-integral with a pitch of about 2 x 360Å to 2 x 370Å. Studies of reconstituted thin filaments in paracrystals (O'Brien et al, 1975; Gillis and O'Brien, 1975) have shown that in high Ca^{2+} (> 10^{-5}M) the actin helix has the form of a genetic helix with 28 subunits in 13 turns. In low Ca^{2+} it forms the genetic helix with 13 subunits in 6 turns. Thus there is flexibility in the actin helix to allow slight twisting of the structure from one integral form to the other. The troponin complex is probably also present with a repeat of about 390Å.

Although the myosin crossbridges are arranged in a slightly different attitude on the thick filament surface (see later) the average repeat, as determined by the third order meridional reflection's spacing, is only about two tenths of a percentage i.e. about 0.2Å, less than that for frog sartorius muscle. Protein analogous to C- or X-protein most likely labels the thick filaments as in other vertebrate muscles with a periodicity of 441Å if the meridional spacing is taken at face value but is probably much less if interference effects are taken into account (Rome et al, 1973). Cryosections of Plaice fin muscle show a similar series of stripes across the A-band (Dr.Alan Freundlich, personal communication) to other muscles known to contain C- or X-protein (Craig and Offer, 1976a) with a periodicity of the order of 400Å.

The most marked difference is the difference in spacing of the hexagonal lattice (472Å at S = 2.4μ) at rest length compared to other vertebrates (425Å at S = 2.6μ for rabbit; 404Å at S = 2.3μ for frog; Huxley, 1968) and a correspondingly larger Z-line lattice spacing.

This increased distance between thick and thin filament surfaces has been shown to affect the orientation of the resting myosin heads in relation to the thin filaments. This is demonstrated in part by the configuration and radius of centre of mass adopted by the heads in resting muscle and possibly by the way in which crossbridge levels are perturbed from exact 143Å intervals.

5.6.2. The Three-Dimensional Crossbridge Lattice

The simple lattice row-line sampling of the Plaice fin myosin layer line pattern clearly fulfills the predictions from the studies of the bare-zone of this muscle that (i) within each myofibril the myosin filaments and therefore their crossbridge helices have a unique orientation and (ii) the crossbridge helix on each myosin filament is simply related to the backbone of the filament as observed in the bare-zone. This also gives firm support to the interpretation of the myosin layer line sampling in X-ray diagrams of frog sartorius muscle. It is very likely that the three-dimensional crossbridge lattice in frog muscle reflects the statistical superlattice of myosin filaments revealed in the bare-zone.

The consequences of this simple lattice in terms of the distribution of crossbridges surrounding each thin filament and the possible evolutionary significance compared to higher vertebrates were discussed by Luther and Squire (1980) and are briefly discussed in Chapter 6.

5.6.3. Effect of Imperfections in the Crossbridge Surface Lattice

The computations involved in trying to model realistically the configurations of the myosin heads are vast and it has not

been possible, or desirable as far as this preliminary data is concerned, to look at the effect of imperfections in the surface lattice of the crossbridges. The "forbidden" meridional reflections (Huxley and Brown,1967; Huxley et al, 1980); studies of A-segments (Craig, 1977) and the results from the cryosectioned C-zones presented in Chapter 3 are direct evidence that such imperfections are present in vertebrate muscle whether they arise from the packing of myosin molecules in the thick filament backbone, disruption of initially equally spaced crossbridge levels due to the presence of a non-myosin protein or thin filament perturbation of equally spaced levels. There is further support for such imperfections from the packing arrangements of LMM into paracrystals (Bennett, 1976).

It is difficult to predict even qualitatively just what effect these perturbations would have on these computations. However the extent to which this modelling must be modified will depend on the degree of perturbation i.e. the magnitude of the displacements of the crossbridges from an exact 143Å repeat. If only relatively small displacements are involved then the crossbridge surface lattice determined here would be expected to be a reasonable approximation to the real lattice. The reasons for believing that the crossbridge arrangement in Plaice fin muscle falls into this category are outlined below.

Two types of perturbed configurations were discussed in the modelling of the cryosectioned human C-zone. One of these, Group I, with spacings of 163Å, 113Å and 153Å within each 429Å period gave relatively strong 5th and 2nd orders of 429Å. The other type of arrangement involved significant displacement of only one of the crossbridge levels such that within each 429Å period

crossbridge levels were spaced 163Å, 128Å and 138Å apart. This configuration gave a relatively strong 4th order and much weaker 2nd order of 429Å which are both characteristics of the Plaice fin meridional pattern. Thus the axial perturbation of the crossbridge helix in Plaice fin muscle may be more like this latter configuration, similar to Group II C-zones, and therefore constitutes less disruption of the crossbridge levels from equally spaced levels.

The absence of the 215Å reflection altogether may be due to interference with a contribution from the C-protein. It was shown by Squire (1981) that a second order peak from a 7-line, 440Å period C-protein array would extend from about 237Å to 200Å. The observed reflections in this region on the meridian of frog muscle indexed as consecutive orders of about 7090Å i.e. the separation of C-zones measured across the M-band. Thus reflections at 237Å, 229Å, 221Å, 215Å, and 206Å indexed as 30th, 31st, 32nd, 33rd and 34th orders of 7090Å. The same series of reflections is seen for Plaice fin muscle on the longer camera with the exception of the 33rd order i.e. 215Å. Thus even if the there was no crossbridge contribution at 429Å/2 one would expect a contribution at this position from the C-protein. The absence of any observable reflection at this spacing suggests that the diffraction peak from the C-protein array and that from a perturbed crossbridge array have interfered destructively.

Whether or not this is the explanation for the absence of a "215Å" reflection the contribution from the crossbridges is still likely to be small from considerations of the intensity profile of this second order peak, assuming it to arise from the C-protein. The peak is centred on the 230Å and 221Å interference

peaks such that the 238Å and 206Å reflections are much weaker. From this profile it is likely that any C-protein interference peak at 215Å would have an intensity in between that of the 221Å and 206Å reflections. Thus the crossbridge contribution required to reduce this would have to be very much smaller than the relative intensity of the "215Å" reflection in frog sartorius muscle which completely dominates the series of reflections within the region of 237Å to 200Å.

5.6.4. The Resting Crossbridge Configuration

Since the three-fold rotational symmetry of the crossbridge helix was assumed to be correct, from the evidence discussed in Chapter 1, the problem of computer modelling the myosin layer line pattern was reduced to determining the orientation of the two heads of the myosin crossbridge relative to the thick filament surface. If there were well-established facts concerning the disposition of the myosin heads in living vertebrate muscle, then the most efficient way of modelling the Plaice fin layer line pattern would be to use these facts as the starting point in the modelling. Since one can assume that in the resting state just before a contractile cycle the myosin crossbridges will be surrounded by thin filaments, which may or may not influence the configuration of the crossbridges, it is the disposition of the crossbridges in the presence of the thin filaments which is of interest. For this reason the determined configuration for frog sartorius muscles which had been stretched to reduce Bragg sampling of the myosin layer lines (see Chapter 1; Haselgrove, 1980) is an unsatisfactory place to start. In the absence of this information an objective and necessarily inefficient procedure

must and has been adopted here which has the advantage of being more certain that the correct structure has not been omitted from consideration. This is only true if the initial assumptions made about the model are reasonable approximations. These assumptions include the rotational symmetry of the crossbridge helix; the surface lattice of crossbridges; the myosin head shape and size; the freedom of movement of the two heads and the temperature disorder assumed relevant for the structures.

The evidence for three-fold rotational symmetry has already been stated. It has been shown from the analysis of the forbidden meridional reflections earlier, see section 5.6.3 , that the axial perturbation of crossbridge levels is probably less marked in Plaice fin muscle. The shape of the head is based on the very clear images of isolated myosin molecules by Offer and Elliott (1978) who reported an overall length of 190Å for the myosin head (with some reservations about where the "head/tail" junction was defined) but all configurations were computed to take account of the shorter length of 140Å indicated from other sources (Moore et al, 1970; Mendelson and Kretzschmar, 1979; Mendelson et al, 1973). The range of movement of the two heads assumed about the tail has also been shown by Offer and Elliott and earlier from the study of the decay in fluorescence depolarization of labelled S1, HMM and myosin (Mendelson et al, 1973). Isolated molecules also show that the two heads are not rigidly attached to each other (Offer and Elliott, 1978) and so were given independent freedom of movement in the modelling (Thomas et al, 1975).

If the extent of Brownian rotation of the myosin heads is of the degree indicated by the electron paramagnetic resonance studies of spin-labelled heads in glycerinated muscle fibres

(Thomas et al, 1980; Thomas and Cooke, 1980) then the disorder assumed in this computer modelling is a gross underestimate. In that case any attempt to model a static configuration would be futile. However the attachment of the probe to the myosin heads in relaxed myofibrils does not leave them in a truly relaxed state in that the labelling in myofibrils does increase the myofibrillar ATPase activity in the absence of Ca^{2+} (Thomas et al, 1980). Some of the observed probe disorientation may also be due to static disorder of the heads or of the probe relative to the head (Thomas and Cooke, 1980). In addition this degree of rotational disorientation may be compatible with the relatively weak layer lines of X-ray diffraction from the glycerinated rabbit psoas muscle used in this study but it still has to be shown that such disorder exists in better ordered systems which give stronger layer line patterns such as frog sartorius or Plaice fin muscle.

So providing these assumptions are approximately valid it can be concluded that if the myosin heads in fish myosin are as long as 190Å (Offer and Elliott, 1978) the two heads in a crossbridge in resting Plaice muscle are tilted by a small amount from the perpendicular to the thick filament axis and are slewed around the surface in a transverse plane by 60^{o} to 90^{o}. If the heads are slightly shorter, about 150Å, then the crossbridges have a slightly larger axial tilt (i.e. 30^{o}) but are slewed much less in a transverse plane from the normal to the thick filament axis (i.e between 0^{o} and 30^{o}). It is not realistic at present to distinguish between the two head models from the modelling of the fish X-ray layer line data but the consequences of this type of configuration are discussed in detail in Chapter 6.

5.6.5 The Origin of the Non-indexible Equatorial Reflection

The equatorial reflection at 290Å is most likely analogous to that which has been attributed either to the I-band square lattice close to the Z-disc (Elliott et al, 1967; Huxley and Brown, 1967) , to the Z-disc itself (Davey, 1976), or to a combination of both (Yu et al, 1977). An equatorial reflection which could not be indexed on the double hexagonal array of thick and thin filaments, occurring at spacings between the 10 and 11 reflections, was first observed in resting and contracting muscle by Elliott et al (1967) and attributed by them to diffraction from the square thin filament lattice close to the Z-disc. They reported that the ratio d_z/d_{10} changed from 0.68 to 0.72 as the sarcomere changed from 2.1 to 3.6μm. Huxley and Brown (1967) also interpreted this reflection as arising from the square thin filament lattice.

Davey (1976) measured the Z-disc spacing, z, from electron micrographs of muscles over a range of sarcomere lengths, s. He found that z increased as the sarcomere length, s, decreased such that the quantity sz^2 was constant over sarcomere lengths between 2.1 and 3.0μm. Thus the cross-sectional area$_{\Lambda}^{(\text{at } s=2.5\mu m)}$ available to 2 thin filaments near the Z-disc, $\sim 11 \times 10^4 Å^2$ (i.e. $2.z^2$) was significantly less than that available in the A-band of $\sim 13 \times 10^4 Å^2$ (Rome, 1968) as noted earlier by Huxley and Brown (1967). It was concluded by Davey (1976) that the Z-disc behaved in the same manner as the A-band lattice in expanding to retain a constant volume per thin filament as the sarcomere length decreased.

Yu et al (1977) used X-ray diffraction to follow the

changes in spacing and intensity of this "Z-reflection" with sarcomere length and concluded that the ratio d_z/d_{10} varied in direct proportion to the hexagonal lattice spacing. The ratio had a constant value of 0.705 (±0.005) between sarcomere lengths 2.0 to 3.0 μm. From optical diffraction of the I-band close to the Z-disc they further concluded that only a short segment of the I-band square lattice, extending about 300Å from the edge of the Z-disc, would contribute to this Z-reflection. In view of these and Daveys electron microscope observations they took their results to mean that this X-ray reflection is dominated by diffraction from the Z-disc itself. This was supported by the roughly constant intensity of the Z-reflection over the range of sarcomere length studied and the possibly greater density of the Z-disc structure.

The observed equatorial reflection in Plaice fin muscle has the same ratio to the 10 plane spacing of 0.707 as the equatorial reflection discussed for frog above. Thus the same relationship most likely exists between the cross-sectional area available to each thin filament near the Z-disc and in the overlap region of the A-band. The larger thin filament spacing in the I-band is of course consistent with the larger A-band lattice spacing.

A consequence of this relation between the Z-line spacing and the A-band spacing is that the second order reflection from the Z-disc, corresponding to the 11 reflection from the square thin filament lattice (Figure 5.19), has precisely the same spacing (i.e. 205Å) as the 20 reflection from the hexagonal array of thick and thin filaments. Yu *et al* (1977) propose that regions of the Z-disc structure ("S" in Figure 2.19) dominate the equatorial diffraction from this region of the A-band but there

is only a limited segment, 300Å wide, either side of the Z-filament bridging structure, in which the thin filaments (possibly surrounded by a shell of protein which may be actinin) are arranged on this square lattice. A diffracting unit of this limited width ought to give considerably more broadening of the equatorial reflections parallel to the meridian than is observed. It is therefore more likely that there is a significant portion of the square thin filament lattice adjacent to the Z-disc, beyond this 300Å segment where the thin filaments appear denser, contributing to the equatorial diffraction.

Yu et al (1977) only obtained good optical diffraction in a region of the thin filament lattice about 300Å either side of the Z-disc. However in frog muscle the square lattice is approximately maintained as far as the N1-lines (i.e. 1100 to 1700Å from the centre of the Z-line; Franzini-Armstrong, 1970). The breadth of the equatorial reflection, parallel to the meridian, is therefore more consistent with diffraction coming from a more extensive region of the thin filament lattice and is unlikely to arise virtually wholly from the short segment ("S" in Figure 2.19) of the Z-line as suggested by Yu et al (1977).

The contribution of the Z-line to the equator, and therefore to the 20 reflection from the thick and thin filament lattice, will depend on whether the square lattice structures on either side of the Z-line diffract coherently or not. This is a problem which will require an extensive optical diffraction study of electron micrographs of the Z-line and further detailed examination of the equatorial X-ray diffraction pattern.

5.6.6. Summary

In summary then the following conclusions and observations

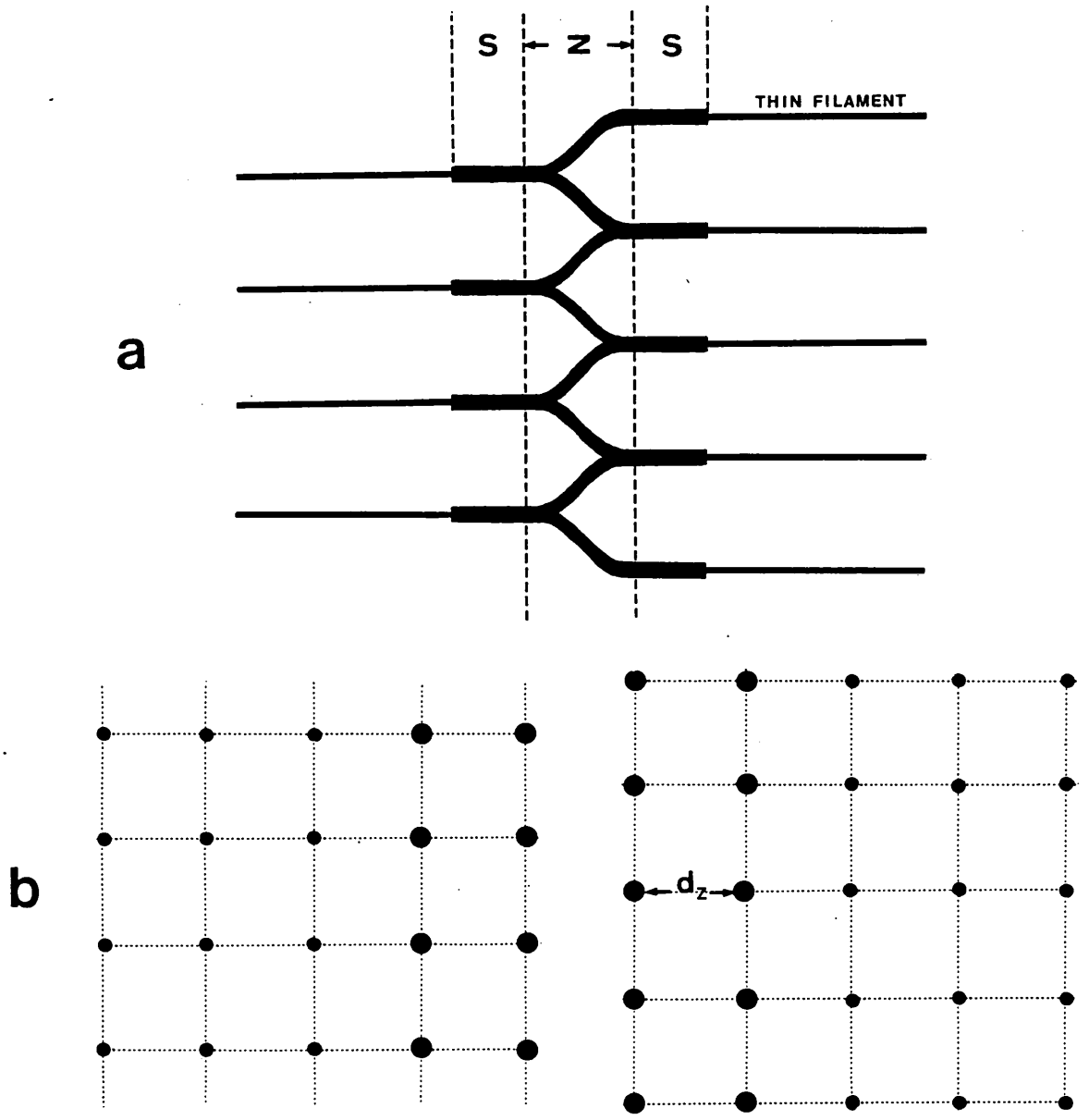


FIGURE 5.19 (a) Diagram of one type of longitudinal view of the Z-line (Chapter 1, Figure 1.1.2). The thin filaments (T) may extend as far as the region of bridging structure of the Z-line (Z), with "Z-filament" material forming a "sleeve" covering a portion of the thin filaments about 300Å long (S in (a)). (b) Diagram of the approximately square lattice formed by the thin filaments either side of the Z-disc. In the region 'S' above, the square lattice is well ordered but becomes more disordered as the distance from the Z-line increases. The square lattice is approximately maintained up to the N_1 lines in some vertebrate muscles (i.e. up to 1100Å to 1700Å from the centre of the Z-line). The square lattices either side of the region 'Z' are probably shifted relative to each other by about one half of the thin filament lattice spacing.

have been made from the X-ray studies of Plaice fin muscle;

(1) The average crossbridge repeat is about 0.2Å less than that in the thick filaments of frog muscle.

(2) There are slight differences in the specific perturbations of crossbridge levels from exact 143Å intervals compared with frog sartorius. The type of perturbation proposed for Plaice fish has only one level of crossbridges within each 429Å period displaced by up to 20Å from an exact 143Å repeat, whereas the perturbations may be slightly larger in frog.

(3) The Plaice thick filaments are labelled with a non-myosin protein with a possibly larger repeat than that of the myosin crossbridges.

(4) The myosin heads are placed at a larger radius from the thick filament axis in resting muscle, at about 140Å, compared to frog sartorius muscle probably as a consequence of the lattice spacing being about 50Å larger at rest length in Plaice fin muscle.

(5) The myosin heads are tilted between 0^{o} and 30^{o} from the normal to the thick filament axis. If the heads are 190Å long almost zero tilt is accompanied with 60^{o} to 90^{o} slew around the thick filament surface. If the heads are 40Å shorter then slightly more axial tilt, about 30^{o}, is accompanied with 0^{o} to 30^{o} slew

(6) The thin filaments have very similar helical parameters to other vertebrate thin filaments with troponin complex probably occurring at the same repeat along the thick filaments. The helix appears to be non-integral with a pitch of about 365Å.

(7) There is a single orientation of the myosin crossbridge helix within each myofibril.

(8) A second order reflection from the Z-disc/I-band at 205Å probably makes some contribution to the (20) equatorial reflection from the thick and thin filament lattice which has an identical spacing of 205Å.

(9) The diffraction from the Z-disc is likely to involve a greater portion of the thin filament length then the 300Å segment which is part of the Z-line, adjacent to the Z-bridging structure.

CHAPTER 6 : DISCUSSION

6.1. INTRODUCTION 285

6.2. The Axial Projection of the Crossbridge Arrangement. 285

6.3. The Resting Crossbridge Configuration in Vertebrate Muscle. 288

6.4. The Equatorial Projection of the Crossbridge Arrangement. 295

6.5. Future Work. 302

REFERENCES 306

APPENDIX A 322

6.1. Introduction

The optical diffraction, equatorial analysis and x-ray diffraction studies presented have been concerned in varying degrees with vertebrate myosin crossbridge arrangement. Other particular details of the vertebrate A-band structure which have arisen during these various analyses have been discussed in the relevant Chapters. The main concern of the following discussion will be see how the interpretations of these various "views" of the crossbridge arrangement correlate with a model for the resting state.

6.2. Axial Projection of the Crossbridge Arrangement

In the studies of human cryosections two types of axial perturbation of the crossbridge levels from equally spaced intervals were observed. The X-ray meridional diagram of Plaice fin muscle is consistent with one of these types of perturbation while the meridian of the frog X-ray diagram is consistent with the other. In view of these different arrangements it is pertinent to question whether the observed perturbations correspond to the packing arrangements of their constituent myosin tails in the thick filament backbone or whether this arrangement is obscured due to the interaction of crossbridges with the thin filaments.

It was stated in Chapter 3 that the pattern of forbidden meridional intensities in the X-ray diagram of live frog sartorius muscle probably reflects the axial perturbation of the myosin crossbridges and that this may be closely related to the packing of the tails of the myosin molecules in the thick filament backbone. This is also supported by the fact that the

forbidden meridional reflections are still present in X-ray diagrams from vertebrate muscles which have been stretched so that there is no overlap of the thick and thin filaments (Huxley, 1972; Haselgrove, 1975). If this is true then the different pattern of forbidden meridional reflections observed for Plaice fin muscle must mean that the crossbridge levels have a different type of axial perturbation resulting from slight differences in the underlying thick filament structure. Indeed, one would expect the thin filaments to have even less influence on the crossbridge arrangement in Plaice fin muscle since at rest length the distance between the thick and thin filament surfaces is about 33A greater than in frog sartorius muscle. This perturbation is therefore much more likely to be inherent in the structure of the Plaice fin thick filament and may be due to a difference in the packing of the myosin tails or perhaps the presence of a different isoform of C-protein displacing just one level of crossbridges from the 143Å sequence.

In the case of the human cryosections the influence of the thin filaments on the observed crossbridge levels is probably very different and much more likely to have some effect. It was shown that the two types of perturbation that occur in human cryosections both have components which are multiples of the actin subunit repeat. On this evidence alone it is not possible to say which, if either, of these perturbations is devoid of any influence from the thin filaments. The fact that these are observed in fibres showing very similar 3-line M-band structures, with M6 moderately strong, argues against these perturbations reflecting different fibre types. If the C-zones producing a strong 5th order forbidden meridional reflection (i.e. with the

perturbation 163Å, 113Å and 153Å) do represent perturbations in the human thick filament structure it is of interest to consider the possibility that frog and human thick filament structures may have evolved perturbations which are somehow advantageous over the less-marked perturbation in fish muscle. This difference may of course be simply circumstantial due to the presence of possibly different isoforms of C-protein or other non-myosin proteins.

In the same way that the statistical superlattice in frog sartorius muscle would allow a more even distribution of crossbridges around the thin filaments within each 430Å period along the thick filament, compared to the simple lattice in fish muscle , so a longitudinal rearrangement may have developed to increase the chances of near-coincidence of the actin and myosin repeats in these higher vertebrates. It was pointed out by Huxley and Brown (1967) that in view of this difference in periodicities if the crossbridges and actin monomers are matched at one point then there would usually be only two near-matches on a given actin and myosin filament per half A-band (Hanson and Huxley, 1955). This mismatch of periodicities was proposed as a possible means by which the interaction of the crossbridges and thin filaments is modulated so that a relatively steady tension could be developed in a given thin filament by the unsynchronised action of a number of crossbridges attaching to it (A.F.Huxley, 1957; Huxley, 1960).

Huxley and Brown (1967) studied the longitudinal and azimuthal positions of actin monomers in the actin helix and myosin crossbridges along the thick filament when the two filaments were placed side by side. They observed that if a

crossbridge and actin monomer were coincident at one point along the thick filament it is only after a distance of 5 x 143Å along the thick filament that an actin monomer is positioned with the correct longitudinal and azimuthal position alongside a myosin crossbridge. This implied that when the crossbridge bound to actin it would do so at intervals of 720Å and this is just the repeat obtained from the rigor muscle diffraction pattern.

In order to determine whether or not the different longitudinal perturbations observed here have any significance it will be necessary to consider the distribution of crossbridge origins around each of the actin filaments in the unit cell taking into account the simple lattice and superlattice since this will affect the azimuthal relationship between the crossbridge origins and the actin monomers. This is beyond the scope of the present work and in any case is very much determined by the rotation of each crossbridge helix within the unit cell (Section 6.4).

6.3 The Resting Crossbridge Configuration in Vertebrate Muscle

Modelling of X-ray diffraction data of living muscle is naturally less convincing as proof of the myosin crossbridge arrangement than direct visualisation of these structures in the electron microscope. With this latter method, however, the problem still remains of knowing whether the *in vivo* structure has been completely preserved although the rapid freeze fracture techniques applied to insect flight muscle (Heuser, 1983a,b; Heuser and Cooke, 1983) have the potential to greatly increase our confidence in such electron microscope images. As these methods improve in the future so the role of X-ray diffraction studies of static muscle states must become less important as a

complementary technique for determining the arrangement of crossbridges but still necessary as a stringent test of the preservation of *in vivo* structure by electron microscope methods.

In the case of Plaice fin muscle, and vertebrate muscle as a whole, electron microscope evidence to complement the modelling of the resting X-ray diffraction patterns is sparse. In order to make any sense of the resting configuration obtained here for Plaice fin muscle one is therefore resigned to (i) looking for common features in the arrangement of crossbridges in the thick filaments of other types of muscles, such as the invertebrates, which appear to have been very well preserved for electron microscope studies and (ii) reconciling the observed arrangement with less direct measures of the arrangement of the myosin crossbridges such as other X-ray studies, probe studies etc.

It has been shown that thick filaments can be isolated from invertebrate muscles, notably Limulus, which retain the overall features of the crossbridge arrangement determined from X-ray diffraction patterns of the "relaxed" (i.e. glycerinated muscle in the presence of ATP and probably also live) muscle. In the case of Limulus muscle a radius of centre of mass of the crossbridges of about 165Å was obtained from X-ray studies (Wray *et al*, 1974; 1975) which is comparable with the radius of about 155Å obtained for isolated thick filaments (Kensler and Levine, 1982; Stewart *et al*, 1981). Kensler and Levine also looked at model radial projections, incorporating model crossbridges oriented with a similar configuration to that determined from X-ray studies (i.e. with the two myosin heads in a crossbridge side by side and tilted upwards by 30^{o} and slewed azimuthally by 60^{o}) which accounted for the appearance of the negatively stained

filaments. Since the crossbridges or projections were inclined close to the 430Å helical path these isolated filaments, when shadowed, show helical stripes of density approximately following the helical path. Similar results are observed particularly for tarantula (which may be because it is phylogenetically related to Limulus) and, to some extent, scallop thick filaments (see below).

So far the same techniques have not produced as much detailed information when used to isolate frog thick filaments. The optical diffraction analysis of isolated frog thick filaments (Kensler and Stewart, 1983) showed that the phases of the principal maxima on the first layer line, either side of the meridian, differ in phase by close to 180°. This was consistent with an odd-order Bessel function and therefore an odd number of helical strands of crossbridges (i.e. three) and some evidence of helical stripes of density along the filament. More recently, freeze-fractured rabbit myofibrils have revealed similar helical stripes of density to those seen in invertebrate thick filaments (Ip and Heuser, 1983) some showing similar very clear subunit structure along the helical stripes along the filament (Cantino and Pollack, 1983). Such appearances are clearly consistent with the best configuration of crossbridges proposed here although this form of distribution could also be produced in certain cases by other models (such as Model 2, Figure 5.17).

However a further detail revealed by all the studies of invertebrate thick filaments is that two myosin heads form a subunit so that both heads appear to be inclined along right-handed helical paths of pitch 430Å or 480Å (Scallop). This arrangement is similar to the manner in which the helical stripes appear to be formed in the modelled crossbridge density of Plaice

fin muscle. It may be argued, in view of the diverse crossbridge arrangements proposed from X-ray studies of a number of crustacean muscles (Wray et al, 1975), that common features do not exist even between thick filaments of the same species. However the exceptional configuration among these crustacean muscles studied (i.e. that of Placopecten which has the two heads of a crossbridge pointing in opposite directions along the thick filament axis) is not consistent with electron microscopy of isolated thick filaments from this muscle (Vibert and Craig, 1983). These studies of scallop thick filaments reveal the very complex structure of the whole filament and their interpretation of the myosin projections is that the myosin heads in each crossbridge are parallel to each other and the whole subunit is inclined close to the helical path of pitch 480Å. This arrangement is more like that given by other isolated thick filaments which have shown detailed crossbridge structure. In the case of scallop however the same structure must be shown to be compatable with X-ray diffraction patterns of the relaxed muscle since these filaments shrink by 25% (or more) during processing which may have some effect on the disposition of the myosin heads.

If the crossbridge orientation indicated by scallop thick filaments is the same in vivo then it is exceptional in that the crossbridges are tilted very little from the axis of the thick filament. Axial tilts of 30° (or less) from the normal to the thick filament axis have been determined both for frog sartorius muscle (30° Squire, 1975; +30° and -30° Haselgrove, 1980), for the crustacean muscles and here in the case of Plaice fin muscle. In the case of scallop this difference may be functionally

significant. It has been suggested (Vibert and Craig, 1983; Flicker et al, 1981; 1983) that the alignment of the heads nearly parallel to the surface and the axis of the thick filament allows the heads at one level to interact with the light-chain containing neck regions of the myosin heads at the next level. This interaction may account for the fact that the actin-activated ATPase rates of scallop myosin increases much more rapidly with increasing Ca^{2+} concentration if the myosin is assembled into filaments (Chantler et al, 1981).

So far in this discussion an attempt has been made to present the common features in the arrangements of crossbridges on different thick filaments (such as the tendency for the myosin heads to group together and align close to the 430Å or 480Å helical paths) and to show that these same features are shown by the configuration obtained for Plaice fin muscle. The underlying assumption is that the two heads of the myosin molecule, common to all of these structures, are for some reason not completely independent of each other in the resting state of the muscle, although the ability of myosin to generate force or motion is not impaired if one head is removed. In fact single headed myosin will generate half of the tension of the intact myosin (Cooke and Franks, 1978). The Brownian motion of one head also seems to be independent of the other head (Mendelson and Cheung, 1978). It is only in superprecipitation experiments and measurements of the binding constant (Margossian and Lowey, 1973, 1978; Highsmith, 1978) that the steric constraints of the two headed myosin give lower binding constants than expected.

Other parameters of the crossbridge arrangement, such as the radius of centre of mass of the myosin heads from the thick

filament axis, are likely to be dependent on thick filament diameters and on the packing arrangement of the thick and thin filaments. Thus a comparison of these aspects of crossbridge arrangement neeeds to be restricted to muscle with similar ultrastructures. The radius of centre of mass of the crossbridges in Plaice fin muscle is about 20Å greater that that in frog sartorius muscle (Squire, 1975; R = 110 - 115Å) or 15Å greater according to Haselgrove (1980; R = 120 - 130Å). This slight difference in the observed values for R for frog sartorius is consistent with the heads leaning slightly away from the thick filament surface in preparations which were stretched to about 3.0 μm sarcomere length (Haselgrove, 1980) since this would leave a region of overlap of only about 0.3μm in each half A-band. The larger radius of centre of mass for resting Plaice fin muscle also suggests that the myosin heads lean further away from the thick filament surface to accomodate the larger distance between the thick and thin filament surfaces. In both muscles the tilt of the heads is small (i.e. less than or equal to about 30°) and the difference in radius of centre of mass is probably reflected in their being more slew of the heads (60° to 90°; Haselgrove, 1980) in the case of frog sartorius muscle. Although this configuration deduced from X-ray diagrams of frog sartorius has the two myosin heads pointing in opposite directions along the thick filament direct observations of frog thick filaments suggest the crossbridge mass is aligned along the 430Å pitch helical strands.

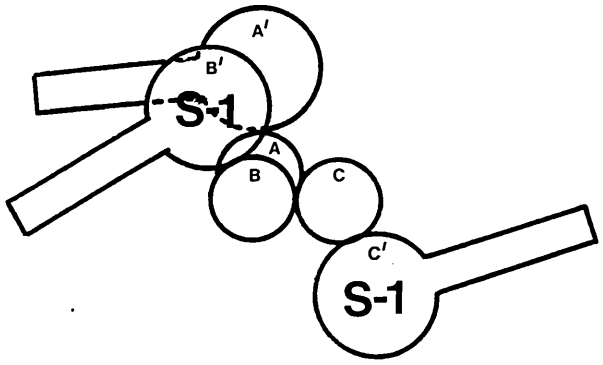
Since an attempt has been made to determine the resting orientation of the myosin heads it is important to see what restrictions this places on the initial interaction of the heads with the thin filament. If the two heads are to interact with the

same thin filament in equivalent ways this must be to adjacent (or near adjacent) subunits in the same strand of the actin filament. It was shown by Offer and Elliott (1978) that this would lead to different deformations of the two heads if the attached heads were to follow the helical symmetry of the actin helix (Figure 6.1(a)). It was pointed out that this is consistent with the binding of HMM to free F-actin filaments being smaller than expected on the basis of the binding association of $10^7 M^{-1}$ for S1 to F-actin (Margossian and Lowey, 1978). Thus the strength of binding of a second head of the HMM fragment to the actin helix appears to be reduced due to its necessary deformation.

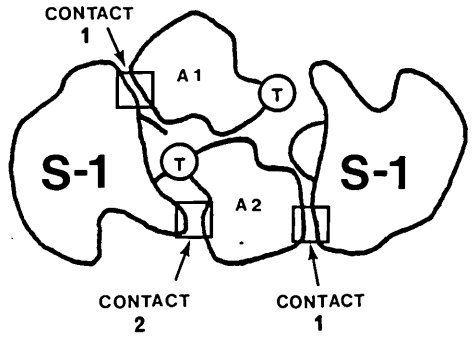
If in the resting state the crossbridges are oriented along a right-handed helix it appears, from the viewpoint of the thick filament surface, that the heads follow a helix of opposite sense to the right-handed helical strands of the neighbouring actin helix (Figure 6.1(c)). If each head of the myosin molecule were to make the type of staggered interaction indicated by recent decorated thin filaments (Amos et al, 1982) the initial interaction of the two heads with a single strand of the actin helix, if it occurs at the start of the contractile cycle, would be easier to accomplish if the heads on the thick filament surface were oriented along a helix of opposite sense (i.e. left-handed) to the helical strands which are most probably right-handed (Figure 6.1(c)). Thus from the type of resting arrangement proposed here some rearrangement of the myosin heads, such as a rotation of the whole crossbridge would be necessary for the heads to act cyclically along the same strand of a neighbouring actin helix. It seems unlikely from steric constraints in any case that the two heads of the myosin molecule will attach to the

FIGURE 6.1 (a) Ilustration of the steric constraints which weaken the binding of HMM to one strand of the thin filament. (From Offer and Elliott, 1978). Three neighbouring actin subunits are shown (A,B,C) in transverse view. Myosin heads (A',B',C') which attach at the same position on neighbouring actin subunits have their long axes separated by 26°. (b) Diagram of the reconstruction from thin filaments decorated with myosin heads (Amos et al, 1982). Two neighbouring actin monomers (A1,A2) are shown. The "comma-shaped" HMMS-1 makes contact number one with actin monomer A1 and a second contact with the next actin monomer down A2. (c) To the left is shown the radial net of the actin helix and the actin monomers which are involved in contacts 1 and 2 in (b). On the right the surface lattice of a thick filament as it would appear looking out in the direction of the thin filaments. The resting orientation of the myosin heads is shown. The two myosin heads are not aligned so that each head could make the two points of contact with the neighbouring thin filament by the crossbridge simply leaning out from the thick ilament surface without some rearrangement of the two heads occurring.

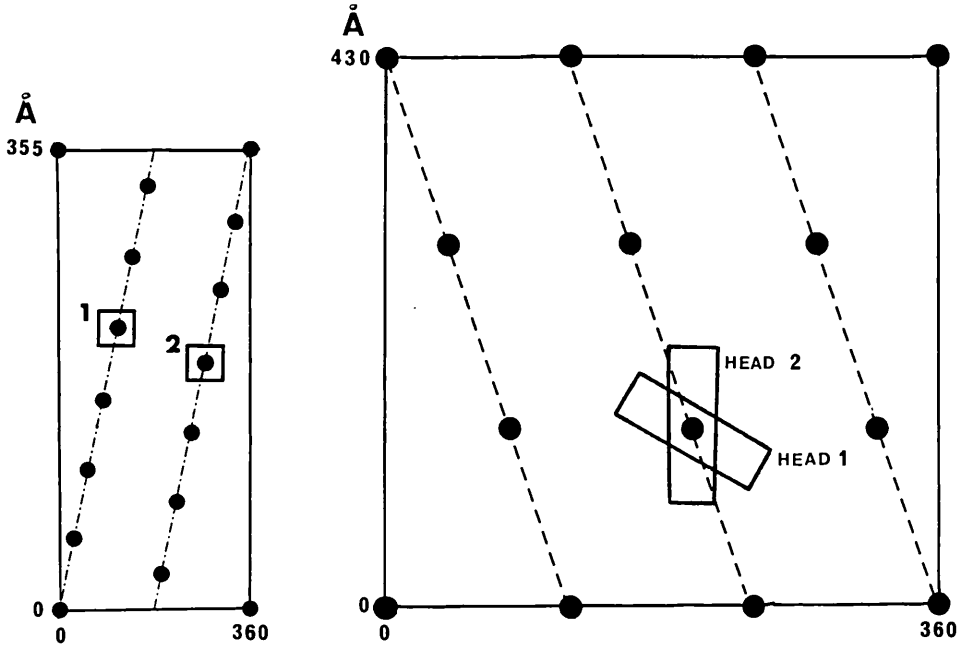
a


A'
B'
S-1
A
B
C
C'
S-1

b


CONTACT
1
A1
T
S-1
T
S-1
A2
CONTACT
2
CONTACT
1

c


Å
355
1
2
0
0
360
Å
430
HEAD 2
HEAD 1
0
0
360

same strand of the actin filament at the same instant (Offer and Elliott, 1978).

The simplest alternative type of interaction, in which both heads of the myosin molecule are involved, is for each head to make an interaction with a different thin filament as proposed by Offer and Elliott (1978). Although such interactions agree with some observations of rigor insect flight muscle (Freundlich et al, 1980) and frog sartorius muscle they do not appear to be the predominate interaction that the myosin heads make with the thin filaments. Thick sections of rigor insect flight muscle show strong lines of density connecting thick and thin filaments which is not the distribution expected if the myosin heads from each molecule attach with different thin filaments (Freundlich et al, 1980). Furthermore such a mechanism would require increasing amounts of distortion of the myosin molecule for it to operate over a range of interfilament spacings in vertebrate skeletal muscle.

The two heads are unlikely, for steric reasons, to bind to a thin filament at the same instant and seem sufficiently independent to attach and generate tension one after the other (Cooke and Franks, 1978). It is not inconsistent then that the crossbridges in the resting state should be arranged as they appear to be in Plaice fin muscle thus requiring small rearrangements of the two heads so that each head can make equivalent interactions with a neighbouring thin filament.

6.4 The Equatorial Projection of the Crossbridge Arrangement

In Chapter 4 it was proposed that the correct Fourier synthesis for living Plaice fin muscle showed a uniform shell of crossbridge density surrounding the thick filament backbone. It

was argued that such a distribution is expected on the basis of the rotational symmetry of the crossbridge arrangement in addition perhaps to some smearing out of the equatorially projected density due to the configuration the myosin heads adopt. In most of the models discussed in the analysis of the diffraction pattern of Plaice fin muscle in Chapter 5, and particularly in the best configuration, these expectations are seen to be fulfilled. In the end-on views of the best configurations the myosin heads are angularly distributed in a fairly uniform manner around the thick filament backbone.

Figure 6.2 shows the crossbridge helix models which gave the best fits to the X-ray data for the short head model (Figure 6.2(a)) and the long head model (Figure 6.2(b)), incorporated into transverse views of the overlap region. It is clear that at low resolution either type of model would give a wide annulus of crossbridge density extending out to within 10 to 20Å of the thin filaments in rest length muscle. The two models differ however in the type of movement which would be involved when the myosin heads move to attach to the the thin filaments.

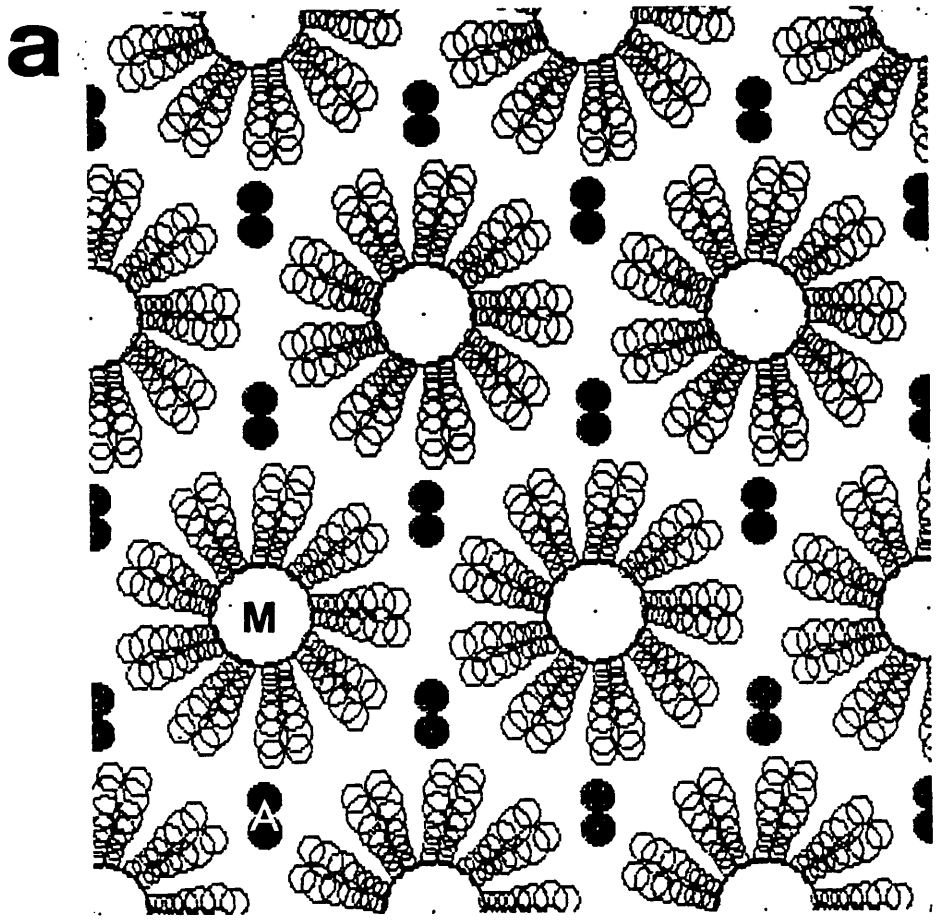
The proposed resting configuration of the myosin heads for frog sartorius muscle (Haselgrove, 1980) allows more movement away from the thick filament surface if the crossbridges were to simply swing out to attach to actin, when compared to the model which gave the marginally better fit for Plaice fin (Figure 6.2(a)). Since crosslinking studies of the myosin heads have suggested they may be close to the thick filament surface (Sutoh and Harrington, 1977), even in rigor muscle, Haselgrove suggested that the inner end of the crossbridge may move across the surface of the thick filament backbone without actually departing from

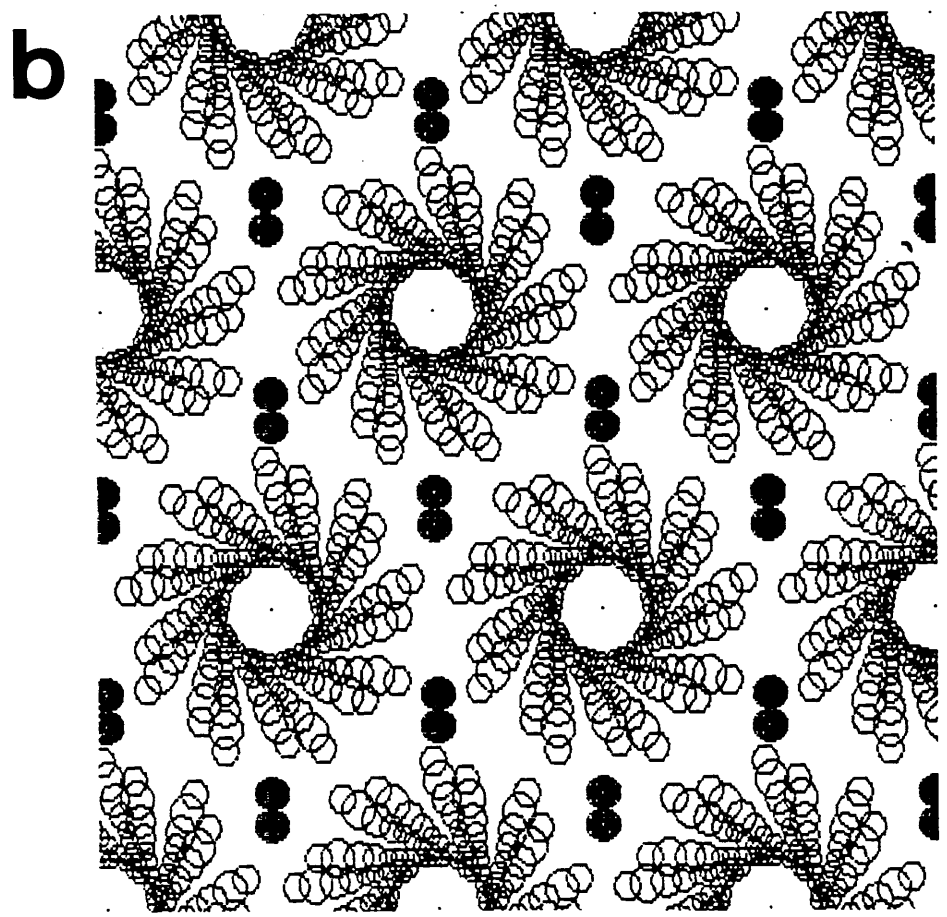
the surface. Clearly a similar type of interaction is possible with the configuration determined for Plaice fin with the longer myosin head model (Figure 6.2(b)) and similar cross-linking studies may help to confirm whether the heads have this much slew. In the case of the shorter myosin head model there is the possibility of a small amount of radial movement, since the heads are tilted axially, but it is still possible that a large contribution would arise from azimuthal movement of the heads towards the thin filaments.

On this basis it is not possible to distinguish between the models with a small and large azimuthal slew since the amount of movement in a transverse plane of the heads, required for them to interact with the thin filaments, depends both on this "resting" slew of the heads relative to the thick filament surface and on the rotation of the crossbridge helix within the unit cell. In transverse sections of the bare region the approximately triangular filament backbones were shown to point about 10^{o} relative to the 10 planes of the hexagonal lattice. It was also argued that it is necessary for the myosin heads at one crossbridge level to have this same rotation in the unit cell for there to be a pseudo-equivalent arrangement of myosin heads around the two thin filaments in the unit cell (Luther and Squire, 1980).

Apart from substantiating this idea the determination of this rotation would allow a more detailed analysis of the movement of the myosin heads towards the thin filaments. Furthermore the relation of the crossbridge helix to the backbone structure would provide important constraints for models of the thick filament structure. In order to determine this rotation

FIGURE 6.2 End-on views of crossbridge helix models which gave the best fits to the X-ray diffraction pattern from live Plaice fin muscle. The thick filament backbone is represented by an empty circle (M). The thin filaments are represented by two filled circles (A). Three levels of crossbridges are shown. The thick filament spacing represents the rest length lattice spacing in Plaice fin muscle. In (a) the short myosin heads both have 30° tilts, and are slewed by 0° and 30°. γ is equal to 60°. This crossbridge model represents the best parameters for Model 1. (b) The long heads have zero tilt and are slewed around the thick filament backbone by 60° and 90°. γ is equal to 30°. This model represents the best parameters obtained for Model 3.


a
M
A


b

from X-ray diffraction data it is clearly necessary to record the higher order reflections with much greater accuracy than has been possible here since the modelling suggests that the azimuthal variation in the myosin filament transform is only evident as far out radially as the 21 row line. This occurs mainly through the interference of the Bessel orders J_{-6} and J_{12} on the first layer line so that the intensity transform shows an 18-fold rotational symmetry.

Thus even if the difficult task of determining the rotation of the crossbridge helix within the unit cell can be accomplished there will still be some ambiguity since the intensity transform will appear identical with a 20^{o} rotation but the possibility that the crossbridge origins are aligned at a small angle to the 10 planes of the hexagonal unit cell, as it appears from the backbones of the thick filament in the bare zone, could at least be stringently tested.

6.5 Future Work

In view of the confirmation reported here that the crossbridge region of the fish A-band (like the bare-, tip- , Z-line and M-region) presents a simpler system to study, the application of low-angle X-ray diffraction, equatorial diffraction and electron microscopy techniques to this particular muscle must more readily provide a detailed pattern of the interactions that the myosin crossbridges make with the actin monomers in the intact muscle.

The 3-D reconstruction of the fish M-band (Luther and Crowther, 1984; Crowther and Luther, 1984), made possible because of the simple lattice of thick filaments in fish muscle, is

testimony of the usefulness of such an ultrastructural tool. The necessity for a simple, well-defined striated muscle system to study is highlighted all the more by the discovery that two of the most extensivley studied systems, namely those of insect flight muscle and frog sartorius muscle have elements of randomness in their thick filament lattices (Luther and Squire, 1980; Freundlich and Squire, 1983).

Clearly then the general direction of future work will be to utilise this muscle system to the full using X-ray diffraction techniques. A start has been made in this work towards determining the resting configuration of the myosin heads in this particular muscle. From a very large number of possible structures even this preliminary work has, with a moderate degree of fit, converged towards a resting arrangement which in many of its features resembles a widely accepted view of the way in which the crossbridges in resting muscle are distributed around the thick filament backbone.

With respect to improving the X-ray data from the relaxed fish muscle an application has been accepted for work on the Daresbury synchrotron source which will alleviate some of the problems of recording two-dimensionally resolved patterns with sufficiently strong intensity. The non-parallelism of the fibres in the muscle has presented some difficulties which, with the provision of a greater X-ray beam flux, can be overcome by limiting the height of the X-ray beam perpendicular to the fibre axis.

With the acquisition of more, probably higher order, data the models which have been selected from this first phase of the computer modelling for the resting crossbridge arrangement will

be further scrutinised. In particular there is a need to consider the effect of anisotropic temperature disorder since it has long been recognised (Huxley, 1969) that, circumferentially the crossbridges probably exhibit greater disorder whereas their axial positions are rather better defined. This is also apparent in resting fish muscle where the layer line intensity falls off much more rapidly at right angles to the fibre axis than along the axis.

Some of the features of the resting X-ray diffraction pattern which have been difficult to account for with any model may require modifications to the model for the myosin head shape assumed here, or the inclusion of imperfections from the perfect helical symmetry. The present studies have given some guidelines as to the axial component of the perturbations which may be firstly considered in the computer modelling. Cryosectioning of the fish A-band is also in progress (Dr. A. Freundlich, personal communication) which should allow the same detailed analysis as has been possible here in the case of human muscle; this should help to confirm the perturbations in the crossbridge array which have been deduced from the X-ray meridional pattern and many other aspects of the structure. It is also desirable that such electron microscope studies are carried out at non-overlap sarcomere lengths, so that any influence from the thin filaments is removed.

In conjunction with modelling of the layer line pattern the equatorial projection of the structure must also be shown to be consistent with the resting arrangement of crossbridges and thus modelling of the equatorial diffraction pattern will also be pursued. The possibly minor complication of the Z-line

contribution to one of the reflections from the thick and thin filament lattice is a problem which may be resolved by studying the equatorial pattern at various sarcomere lengths since the Z-line spacing and thick filament spacing will increase with decreasing sarcomere length. If the spacings change at different rates then it should be possible to resolve the contributions from the Z-line and the thick and thin filament lattice. An important point to establish in this respect is whether the thin filament lattices either side of the Z-line diffract coherently or not. Optical diffraction patterns of electron micrographs of the fish Z-line will shortly be in progress (Dr. P.Luther, personal communication) to establish how extensively ordered the thin filaments are across the Z-line.

In addition to modelling the equatorial diffraction pattern it is intended to employ more sophisticated functions in the phase determining procedure so that the very important phase information obtained from the Fourier synthesis may be correlated with phases calculated from model structures for the myosin crossbridge helix.

If it is possible to determine the azimuthal rotation of the crossbridge helix within the unit cell, from any azimuthal variation in the myosin filament transform, then the simple lattice should allow the detailed three-dimensional geometry of the crossbridge origins and the actin monomers to be established. With this information it should be possible to predict the labelling patterns the crossbridges may make with the thin filaments in the rigor and active states; predictions which should be easier to put to the test with future X-ray studies on the rigor and active states of the fish muscle.

REFERENCES

AMOS,L.A., HUXLEY, H.E., HOLMES, K.C., GOODY, R.S., and TAYLOR, K.A. (1982) Nature, 299, 467.

BAGSHAW, C.R. (1982) "Muscle Contraction", (Brammer, W.J. and Edidin, M ,eds.), Chapman and Hall, London.

BAGSHAW, C.R. and KENDRICK-JONES, J. (1979) J. Mol. Biol., 130, 317.

BAGSHAW, C.R. and REED, G.H. (1977) FEBS Lett., 81, 386.

BENNETT, P.M. (1976) Proc. 6th European Congress on Electron Microscopy, Israel (Y.Ben Shaal. ed), Vol II, 517.

BENNETT, P.M. (1977) PhD Thesis, University of London.

BOREJDO, J. and ASSULIN, O. (1980) Biochemistry, 19, 4913.

BURKE, M. HIMMELFARB, S. and HARRINGTON, W.F. (1973) Biochemistry, 12, 701.

CALLAWAY, J.E. and BECHTEL, P.J. (1981) Biochem.J., 195, 463.

CANTINO, M. and POLLACK, G.H. (1983) Biophys. J., 41, 264a.

CASPAR, D.L.D., COHEN, C., and LONGLEY, W. (1969) J. Mol. Biol., 41, 87.

CHANTLER, P.D., SELLERS, J.R. and SZENT-GYORGYI, A.G. (1981) Biochemistry, 20, 210.

COBB, J.L.S.,FOX, N.C. and SANTER, R.M. (1973) J. Fish Biol., 5, 587.

COCHRAN, W., CRICK, F.H.C. and VAND, V. (1952) Acta Cryst., 5, 581.

COHEN, C. (1975) Sci. Am., 233(5), 33.

COHEN, C., CASPAR, D.L.D., PARRY, D.A.D. and LUCAS, R.M. (1971) ,Cold Spring Harbor Symp. Quant. Biol., 36, 205.

COHEN, C and HOLMES, K.C. (1963) J. Mol. Biol., 6, 423.

COHEN, C., LOWEY, S., HARRISON, R.G., KENDRICK-JONES, J. and SZENT-GYORGYI, A.G. (1970) J. Mol. Biol., 47, 605.

COHEN, C. and SZENT-GYORGYI, A.G. (1957) J. Am. Chem. Soc., 79, 248.

COLLINS, D.M. (1982) Nature, 298, 49.

COLLINS, D.M., COTTON, F.A., HAZEN, E.E.,Jr., MEYER, E.F., Jr., and MORIMOTO, C.N. (1975) Science, 190, No.4219, 1047

COOKE,R. and FRANKS, K.E. (1978) J. Mol. Biol., 120, 361.

CRAIG, R. (1977) J. Mol. Biol., 109, 69.

CRAIG, R., and OFFER, G. (1976) J. Mol. Biol., 102, 325.

CRAIG, R., and OFFER, G. (1976a) Proc. R. Soc. Lond. B., 192, 451.

CRAIG, R. and PADRON, R. (1982) 11th European Congress on Muscle and Motility, 5-19.

CRICK, F.H.C. (1953) Acta Cryst., 6, 685.

CROWTHER, A. and LUTHER, P.K. (1984) Nature, 307, 569.

DARDORD, M.R. (1922) J. Phys. Radium, (6) 3, 218.

DAVEY, D.F. (1976) AJEBAK, 54, Pt.5, 441.

DeBROGLIE, M. and LINDEMANN, F.A. (1914) C. R. Acad. Sci. Paris, 158 ,a44

DeROSIER, D.J. and KLUG, A. (1968) Nature, 217, 130.

DeWOLFF, P.M. (1951) Selected Topics on X-ray Crystallography. Ed.J.Bouman.Amsterdam: North-Holland Publ.Co.

DREIZEN, P., GERSHMAN, L.C., TROTTA, P.P. and STRACHER, A. (1967) In "The Contractile Process" p.85, Boston: Little, Brown & Co.

DuMOND, J.W.M., and KIRKPTRICK, H.A. (1930) Rev. Sci. Instrum., 1, 88.

EATON, B.L. and PEPE, F.A. (1972) J. Cell Biol., 55, 681.

EBASHI, S. (1980) Proc. R. Soc. Lond. B., 207, 259.

EBASHI, S., OHTSUKI, I. and MIHASHI, K. (1972) Cold Spring Harbor Symp. Quant. Biol., 37, 215.

ELLIOTT, A., and OFFER, G. (1978) J. Mol. Biol., 123, 505.

ELLIOTT, G.F., LOWY, J. and MILLMAN, B.M. (1967) J. Mol. Biol., 25, 31

ELLIOTT, G.F., LOWY, J. and WORTHINGTON,C.R. (1963) J. Mol. Biol., 6, 295.

EMES, C.H. and ROWE, A.J. (1978) Biochim. Biophys. Acta, 537, 125.

FANKUCHEN, I. (1937) Nature, Lond., 139, 193.

FERENCZI, M.A., HOMSHER,E., SIMMONS, R.M. and TRENTHAM, D.R. (1978), Biochem. J., 171, 165.

FLICKER, P.F., WALLIMAN, T. and VIBERT, P.J. (1981) Biophys. J., 33, 279a.

FLICKER, P.F., WALLIMAN, T. and VIBERT, P.J. (1983) J. Mol.Biol., (in the press)

FRANKLIN, R.E. and KLUG, A. (1955) Acta Cryst., 8, 777.

FRANZINI-ARMSTRONG, C. (1970) Tissue and Cell, 2 (2), 327.

FRANZINI-ARMSTRONG, C. and PORTER, K.R. (1964) J. Cell Biol., 22, 675.

FRASER, R.D.B. and MILLWARD, G.R. (1970) J. Ultrastruct. Res., 31, 203.

FREUNDLICH, A., LUTHER, P.K. and SQUIRE, J.M. (1980) J. Mus. Res. Cell Mot., 1, 321.

FREUNDLICH, A. and SQUIRE, J.M. (1983) J. Mol. Biol., 169, 439.

GAUTHIER, G.F., LOWEY, S. and HOBBS, A.W. (1978) Nature, 274, 25.

GAZITH, J., HIMMELFARB, S. and HARRINGTON, W.F. (1970) J. Biol. Chem., 245, 15.

GERGELY, J. (1953) J. Biol. Chem., 200, 543.

GERSHMAN, L.C., STRACHER, A. and DREIZEN, P. (1969) J. Biol. Chem., 244, 2726.

GILLIS, J.M. and O'BRIEN, E.J. (1975) J. Mol. Biol., 99, 445.

GUINIER, A. (1946) C. R. Acad. Sci., Paris, 223, 31.

HANSON, J. and HUXLEY, H.E. (1953) Nature, 172, 530.

HANSON, J. and HUXLEY, H.E. (1955) Symp. Soc. Exp. Biol., 9, 228.

HANSON, J. and HUXLEY, H.E. (1957) Biochim. Biophys. Acta, 23, 250.

HANSON, J., LEDNEV, V., O'BRIEN, E.J. and BENNETT, P.M. (1972) Cold Spring Harbor Symp. Quant. Biol., 37, 311

HANSON, J. and LOWY, J. (1963) J. Mol. Biol., 6, 46.

HANSON, J., O'BRIEN, E.J., and BENNETT, P.M. (1971) J. Mol. Biol., , 58, 865.

HARKER, D. and KASPER, J.S. (1948) Acta Cryst., 1, 70.

HARRISON, R.G., LOWEY, S. and COHEN, C. (1971) J. Mol. Biol., 59, 531.

HASLEGROVE, J.C. (1970) PhD Thesis. Canbridge.

HASLEGROVE, J.C. (1972) Cold Spring Harbor Symp. Quant. Biol., 37, 341.

HASLEGROVE, J.C. (1975) J. Mol. Biol., 92, 113.

HASLEGROVE, J.C. (1980) J. Mus. Res. Cell Mot., 1, 177.

HASLEGROVE, J.C. and HUXLEY, H.E. (1973) J. Mol. Biol., 77, 549.

HASLEGROVE, J.C., STEWART, M. and HUXLEY, H.E. (1976) Nature, 261, 606.

HEIZMANN, C.W. and EPPENBERGER, H.M. (1978) J. Biol. Chem., 253, 270.

HEUSER, J.E. (1983a) J. Mol. Biol., 169, 123.

HEUSER, J.E. (1983b) J. Mol. Biol., 169, 155.

HEUSER, J.E. and COOKE, R. (1983) J. Mol. Biol., 169, 97.

HIGHSMITH, S. (1978) Biochemistry, 17, 22.

HUXLEY, A.F. (1957) Prog. in Biophys. and Biophys. Chem., 7 , p.255. Oxford : Pergammon press.

HUXLEY, A.F. and NIEDERGERKE, R. (1954) Nature, 173, 971.

HUXLEY, H.E. (1951) Discuss. Faraday Soc., 11, 148.

HUXLEY, H.E. (1952) Ph.D. Thesis, University of Cambridge, Cambridge.

HUXLEY, H.E. (1953) Biochim. Biophys. Acta, 12, 387.

HUXLEY, H.E. (1957) J. Biophys. Biochem. Cytol., 3, No.3, 631.

HUXLEY, H.E. (1960) The Cell, Vol.4 (Brachet, J. and Mirsky, E.A.,eds.), pp365-481, Academic Press, New York.

HUXLEY, H.E. (1963) J.Mol.Biol., 7, 281.

HUXLEY, H.E. (1964) Proc. Roy. Soc. Ser. B., 160, 442.

HUXLEY, H.E. (1968) J. Mol. Biol., 37, 507.

HUXLEY, H.E. (1969) Science, 164, 1356.

HUXLEY, H.E. (1972) Cold Spring Harbor Symp. Quant. Biol., 37, 361.

HUXLEY, H.E. and BROWN, W. (1967) J. Mol. Biol., 30, 383.

HUXLEY, H.E., FARUQI, A.R., BORDAS, J., KOCH, M.H.J. and MILCH, J.R. (1980) Nature, 284, 140.

HUXLEY, H.E., FARUQI, A.R., KRESS, M., BORDAS, J. and KOCH, M.H.J. (1982) J. Mol. Biol., 158, pp.637-684.

HUXLEY, H.E. and HANSON, J. (1954) Nature, 173, 973.

HUXLEY, H.E. and HANSON, J. (1957) Biochim. Biophys. Acta, 23, 229.

HUXLEY, H.E., SIMMONS, R.M., FARUQI, A.R., KRESS, M., BORDAS, J. and KOCH, M.H.J. (1981) Proc. Natl. Acad. Sci.USA, 78, No.4 , pp.2297-2301

IP, W. and HEUSER, J. (1983) J. Mol. Biol., 171, 105.

JOHANN, H.H. (1931) Z. Phys., 69, 185.

JOHANSSON, T. (1933) Z. Phys., 82, 507.

KARLE, J. and HAUPTMAN, H. (1950) Acta Cryst., 3, 181.

KARN, J., McLACHLAN, A.D. and BARNET, L. (1982) In "Control of Muscle Development" (Pearson, M. and Epstein, H., eds.) Cold Spring Harbor Colloquium.

KENDRICK-JONES, J., SZENT-GYORGYI, A.G. and LEHMAN, W. (1970) J. Mol. Biol., 54, 313.

KENDRICK-JONES, J., SZENT-KIRALYI, E.W. and SZENT-GYORGYI, A.G. , (1976) J. Mol. Biol., 104, 747.

KENSLER, R.W. and LEVINE, R.J.C. (1982) J. Cell Biol., 92, 443.

KENSLER, R.W. and STEWART, M. (1983) J. Cell Biol., 96, 1797.

KLUG, A., CRICK, F.H.C. and WYCKOFF, H.W. (1958) Acta Cryst., 11, 199.

KNAPPEIS, G.G. and CARLSEN, F. (1963) J. Cell Biol., 13, 323.

KNAPPEIS, G.G. and CARLSEN, F. (1968) J. Cell Biol., 38, 202.

KRETZSCHMAR, K.M., MENDELSON, R.A. and MORALES, M.F. (1976) Biophys. J. , 16, 126a

KRETZSCHMAR, K.M. MENDELSON, R.A. and MORALES, M.F. (1978) Biochemistry , 17, 2314.

LAMVIK, M.K. (1978) J. Mol. Biol., 122, 56.

LANDON, M.F. and ORIOL, C. (1975) Biochem. Biophys. Res. Commun., 62, 241.

LEVINE, R.J.C., KENSLER, R.W., REEDY,M.C., HOFMANN, W. and KING, H.A. (1983) J. Cell Biol., 97, 186.

LOCKWOOD, A.P.M. (1961) Comp. Biochem. Physiol., 2, 241.

LOVELL, S.J., KNIGHT, P.J. and HARRINGTON, W.F. (1981) Nature, 293, 664.

LOWY, J. (1972) Bull. Zool., 39, 119.

LOWEY,S. (1971) In " Subunits in Biological Systems", Part A (Timasheff, S.N. and Fasman, G.D. eds.), p.201, Marcek Dekker, New York.

LOWEY, S. (1979) In "Fibrous Proteins: Scientific, Industrial and Medical Aspects (Parry, D.A.D. and Creamer, L.K.,eds.), pp. 1-25. Academic Press, New York

LOWEY, S. and COHEN, C. (1962) J. Mol. Biol., 4, 293.

LOWEY, S., GOLDSTEIN, L., COHEN, C. and LUCK ,M. (1967) J. Mol. Biol., 23, 287.

LOWEY, S., SLAYTER, H.S., WEEDS, A.G. and BAKER,H. (1969) J. Mol. Biol. , 42, 1.

LUTHER, P.K. (1978) PhD Thesis. University of London.

LUTHER, P.K. and CROWTHER, A. (1984) Nature, 307, 566.

LUTHER, P.K. and SQUIRE, J.M. (1978) J. Mol. Biol., 125, 313.

LUTHER, P.K. and SQUIRE, J.M. (1980) J. Mol. Biol., 141, 409.

LUTHER, P.K., SQUIRE, J.M. and MUNRO, P.M. (1981) J. Mol. Biol., 151, 703.

LYMN, R.W. (1975) Nature, 258, 770.

LYMN, R.W. (1978) Biophys. J., 21, 93.

LYMN, R.W. and TAYLOR, E.W (1971) Biochemistry, 10, 4617.

MARGOSSIAN, S.S. and LOWEY, S. (1973) J. Mol. Biol., 74, 301.

MARGOSSIAN, S.S. and LOWEY, S. (1978) Amer. Chem. Soc., 17 (25), 5431.

MARSTON, S.B. and TREGEAR, R.T. (1972) Nature New Biol., 225, 23.

MASAKI, T. and TAKAITI, O. (1972) J. Biochem., 71, 355.

MASAKI, T. and TAKAITI, O. (1974) J. Biochem., 75, 367.

MATSUBARA, I. (1974) J. Physiol., 238, 473.

MATSUBARA, I., YAGI, N. and HASHIZUME, H. (1975) Nature, 255, 728.

MAW, M.C. and ROWE, A.J. (1980) Nature, 286, 412.

McLACHLAN, A.D. and KARN, J. (1982) Nature, 299, 226.

MENDELSON, R.A. (1982) Nature, 298, 665.

MENDELSON, R.A., MORALES, M.F. and BOTTS, J. (1973) Biochemistry, 12, 2250.

MENDELSON, R.A. and CHEUNG, P.H. (1978) Biochemistry, 17, 2139.

MENDELSON, R.A. and KRETZSCHMAR, K.M. (1979) Biophys. J., 25, 20a.

MENDELSON, R.A. and KRETZSCHMAR, K.M. (1980) Biochemistry, 19, 4103.

MEULLER, H. and PERRY, S.V. (1961) Biochem. J., 80, 217.

MEULLER, H. and PERRY, S.V. (1962) Biohem. J., 85, 431.

MIHALYI, E. and HARRINGTON, W.F. (1959) Biochim. Biophys. Acta, 36, 447.

MIHALYI, E. and SZENT-GYORGYI, A.G. (1953) J. Biol. Chem., 201, 189.

MILLMAN, B.M. and BENNETT, P.M. (1976) J. Mol. Biol., 103, 439.

MOORE, P.B., HUXLEY, H.E. and DeROSIER, D.J. (1970) J. Mol. Biol., 50, 279.

MOOS,C. (1972) Cold Spring Harbor Symp. Quant. Biol., 37, 93.

MOOS, C. (1981) J.Cell.Biol., 90, 25.

MOOS, C., MASON, C.M., BESTERMAN, J.M., FENG, I-N.M. and DUBIN, J.H. (1978) J. Mol. Biol., 124, 571.

MOOS, C., OFFER, G., STARR, R. and BENNETT, P. (1975) J. Mol. Biol., 97, 1.

MORIMOTO, K. and HARRINGTON, W.F. (1972) J. Biol. Chem., 247, 3052.

MORIMOTO, K. and HARRINGTON, W.F. (1973) J. Mol. Biol., 77, 165.

MORIMOTO, K. and HARRINGTON, W.F. (1974) J. Mol. Biol.,83, 83.

MORNET, D., BERTRAND, R., PANTEL, P., AUDEMARD, E., and KASSAB, R. (1981) Nature, 292, 301.

O'BRIEN, E.J., BENNETT, P.M. and HANSON, J. (1971) Phil. Trans. Roy. Soc. Lond. B., 261, 201.

O'BRIEN, E.J., GILLIS, J.M. and COUCH, J. (1975) J. Mol. Biol., 99, , 461.

OFFER, G. (1972) Cold Spring Harbor Symp. Quant. Biol., 37, 87.

OFFER, G., COUCH, J., O'BRIEN, E.J. and ELLIOTT, A. (1981) J. Mol. Biol., 151, 663.

OFFER, G. and ELLIOTT, A. (1978) Nature, 271, 325.

OFFER, G., MOOS, C. and STARR, R. (1973) J. Mol. Biol., 74, 653.

OHTSUKI, I. (1974) J. Biochem. (Tokyo), 75, 753.

PAGE, S. (1964) Phil. Trans. Roy. Soc. Ser. B, 160, 460.

PAGE, S. and HUXLEY, H.E. (1963) J. Cell. Biol., 19, 369.

PARRY, D. and SQUIRE, J.M. (1973) J. Mol. Biol., 75, 33.

PEPE, F.A. (1966) J. Cell. Biol., 28, 505.

PEPE, F.A. (1967) J. Mol. Biol., 27, 203.

PEPE, F.A. (1971) In "Progress in Biophysics and Molecular Biology" (eds. J.A.V.Butler and D.Noble) Vol.22, p77, Pergamon Press.

PEPE, F.A. (1972) Cold Spring Harbor Symp. Quant. Biol., 37, 97.

PEPE, F.A. (1975) J. Histochem. Cytochem., 23, No.7, 535.

PEPE, F.A. and DRUCKER, B. (1975) J. Mol. Biol., 99, 609.

PEPE, F.A. and DRUCKER, B. (1979) J. Mol. Biol., 130, 379.

PEPE, F.A., CHOWRASHI, P.K. and WACHSBERGER, P.R., (1975) Comparative Physiology - Functional Aspects of Structural Materials (Bolis, L., Maddrell, H.P. and Schmidt-Nielsen, K., eds) p.105, North Holland Publishing Co., Amsterdam.

PEPE, F.A. and HUXLEY, H.E. (1964) In "Biochemistry of Muscular Contraction", ed. by J. Gergely, p.320, Boston: Little, Brown and Company

PERRY, S.V. (1955) In "Methods in Enzymology, Vol.2 (Colowick, S.P. and Kaplan, N.O., eds.), pp.582-588, Academic Press, New York.

PHILPOTT, D.E., KAHLBROCK, M. and SZENT-GYORGYI, A.G. (1960) , J. Ultrastruct. Res., 3, 254.

PODOLSKY, R.J., St.ONGE, R., YU, L. and LYMN, R.W. (1976) Proc. Nat. Acad. Sci. USA, 73, Pt.3, 813.

POTTER, J.D. (1974) Arch. Biochem. Biophys., 162, 436.

PRINGLE,J.W.S.(1968) Aspects of Cell Motility (Miller, P.L.,ed.), pp.67-86, Cambridge University Press, Cambridge.

REEDY, M.K. and GARRETT, W.E.,Jr. (1977) In "Insect Flight Muscle" (Tregear, R.T.,ed.),pp.115-135, North-Holland, Amsterdam.

REEDY, M.K., HOLMES, K. and TREGEAR, R.T. (1965) Nature, 207, 1276.

REEDY, M.K., LEONARD, K.R., FREEMAN, R. and ARAD,T. (1981) J. Mus. Res. Cell Mot., 2, 45.

REES, M.K. and YOUNG, M. (1967) J. Biol. Chem., 242, 4449.

RICE, R.V. (1961) Biochim. Biophys. Acta, 53, 29.

RICE, R.V., BRADY, A.C., DePUE, R.H. and KELLY, R.E. (1966) Biochem. Z., 345, pp.370.

ROME, E. (1968) J. Mol. Biol., 37, 331.

ROME, E. (1972) Cold Spring Harbor Symp. Quant. Biol., 37, 331.

ROME, E.J.,HIRABAYASHI,T. and PERRY,S.V. (1973a) Nature New Biol., 244, No.135, 154.

ROME, E., OFFER, G., and PEPE, F.A. (1973) Nature New Biol., 244, 152.

SAYRE, D. (1952) Acta Cryst., 5, 60.

SCHOLEY, J.M., TAYLOR, K.A. and KENDRICK-JONES, J. (1981) Biochimie, 63, 255.

SEGAL, D.M., HIMMELFARB, S. and HARRINGTON, W.F. (1967) J. Biol.Chem., 242, 1241.

SELBY, C.C. and BEAR, R.S. (1956) J. Biophys. Biochem. Cytol., 2, 71.

SELLERS, J.R., CHANTLER, P.D. and SZENT-GYORGYI, A.G. (1980) J. Mol. Biol., 144, 223.

SEYMOUR, J. and O'BRIEN, E.J. (1980) Nature, 283, 680.

SJOSTROM, M., KIDMAN, S., LARSEN-HENRIKSON, K. and ANGQUIST, K.-A (1981) J. Histochem. Cytochem.(in press)

SJOSTROM, M. and SQUIRE, J.M. (1977) J. Mol. Biol., 109, 49.

SJOSTROM, M. and SQUIRE, J.M. (1977a) J. Microscopy, 3(3), 239.

SJOSTROM, M., THORNELL, L.E. and CEDERGREN, E. (1973) J. Microsc., 99, 193.

SLAYTER, H.S. and LOWEY, S. (1967) Proc. Nat. Acad. Sci., Wash., 58, 1611.

SPIRO, D. (1962) Trans. N. Y. Acad. Sci., 21, 879.

SQUIRE, J.M. (1971) Nature, 233, No.5320, 457.

SQUIRE, J.M. (1972) J. Mol. Biol., 72, 125.

SQUIRE, J.M. (1973) J. Mol. Biol., 77, 291.

SQUIRE, J.M. (1974) J. Mol. Biol., 90, 153.

SQUIRE, J.M. (1975) Annu. Rev. Biophys. Bioeng., 4, 137.

SQUIRE, J.M. (1981) "The Structural Basis of Muscular Contraction" (Plenum Press)

SQUIRE, J.M. and ELLIOTT, A. (1972) J. Mol. Biol., 65, 291.

SQUIRE, J.M., SJOSTROM, M., and LUTHER, P.K. (1976) 6th European Congress on Electron Microscopy.

STARR, R., BENNETT, P.M. and OFFER, G. (1980) J. Mus. Res. Cell Motil., 1, 205.

STARR, R. and OFFER, G. (1971) FEBS Lett., 15, 40.

STARR, R. and OFFER, G. (1978) Biochem. J., 171, 813.

STARR, R. and OFFER, G. (1983) J. Mol. Biol., 170, 675.

STEWART, M., KENSLER, R.W. and LEVINE, R.J.C. (1981) J. Mol. Biol., 153, 781.

SUTOH, S. and HARRINGTON, W.F. (1977) Biochemistry, 16, No.11, 2441.

TAYLOR, K.A. and AMOS, L.A. (1981) J. Mol. Biol., 147, 297.

THOMAS, D.D. and COOKE, R. (1980) Biophys. J., 32, 891.

THOMAS, D.D., ISHIWATA, S'I., SEIDEL, J.C. and GERGELY, J. (1980) Biophys. J., 32, 873.

THOMAS, D.D., SEIDEL, J.C., HYDE, J.S. and GERGELY, J. (1975) Proc. Nat. Acad. Sci. USA, 72, No.5, 1729.

THORNELL, L.-E. and SJOSTROM, M. (1975) J. Microsc., 104(3), 263.

TREGEAR, R.T. and SQUIRE, J.M. (1973) J.Mol.Biol., 77, 279.

TRINICK, J.A. (1973) Ph.D. Thesis, University of Leicester, Leicester.

TRINICK, J.A. and ELLIOTT,A. (1979) J. Mol. Biol., 131, 133.

TRINICK, J.A. and LOWEY, S. (1977) J. Mol. Biol., 113, 343.

TSUBOI, K.K. (1968) Biochim. Biophys. Acta, 160, 420.

TURNER, D.C., WALLIMAN, T. and EPPENBERGER, H.M. (1973) Proc. Nat. Acad. Sci. U.S.A., 70, 702.

VIBERT, P.J., HASELGROVE, J.C., LOWY, J. and POULSEN, F.R. (1972) J. Mol. Biol., 71, 757.

VIBERT, P.J., HASELGROVE, J.C. and POULSEN, F.R. (1971) First European Biophysics Congress, Vienna, Vol.5 (Broda, E., Locker, A. and Springer-Lederer, H., eds.), p.409 413, Verlag der Wiener Medizinischen Akademie, Vienna.

VIBERT, P. and CRAIG, R. (1982) J. Mol. Biol., 157, 299.

VIBERT, P. and CRAIG, R. (1983) J. Mol. Biol., 165, 303.

WAKABAYASHI, T., HUXLEY, H.E., AMOS, L.A. and KLUG, A. (1975) J. Mol. Biol., 93, 477.

WALLIMAN, T., PELLONI, G., TURNER, D.C. and EPPENBERGER, H.M. (1978) Proc. Nat. Acad. Sci. U.S.A., 75, 4296.

WEEDS, A.G. (1976) Eur. J. Biochem. 66, 157.

WEEDS, A.G. and LOWEY, S. (1971) J. Mol. Biol., 61, 701.

WEEDS, A.G. and POPE, P. (1977) J. Mol. Biol., 111, 129.

WITZ, J. (1969) Acta Cryst., A25, 30.

WOOSTER, W.A. (1964) Acta Cryst., 17, 878.

WOOSTER, W.A., RAMACHANDRAN, G.N. and LANG, A. (1949) Rev. Sci. Instrum., 26, 156.

WORCESTER, D.L., GILLIS, J.M., O'BRIEN, E.J. and IBEL,K. (1975) Brookhaven Symp. Biol., 27, 101.

WRAY, J. (1979) Nature, 277, 37.

WRAY, J.S., VIBERT, P.J. and COHEN, C. (1974) J. Mol. Biol., 88, 343.

WRAY, J.S., VIBERT, P.J. and COHEN, C. (1975) Nature, 257, 561.

YANG, J.T. and WU, C-S.C. (1977) Biochemistry, 16, 5785.

YAGI, N., O'BRIEN, E.J. and MATSUBARA, I. (1981) Biophys. J., 33, 121.

YAMAMOTO, K. and MOOS, C. (1983) J. Biol. Chem., 258, No.13, 8395.

YU, L.C., LYMN, R.W. and PODOLSKY, R.J. (1977) J. Mol. Biol., 115 , 455.

ZOBEL, C.R. and CARLSON, F.C. (1963) J. Mol. Biol., 7, 78.

YATES, L.D. and GREASER, M.L. (1983) J. Mol. Biol., 168, 123.

APPENDIX A

Plaice Ringer solution (Cobb et al, 1973)

	(gl^{-1})
NaCl	8.22
KCl	0.39
$MgCl_2.6H_2O$	0.23
$NaHCO_3$	0.2
$NaH_2PO_4.2H_2O$	0.28
Glucose	1.0

Reprinted from *J. Mol. Biol.* (1982) **155**, 467–494

Fine Structure of the A-band in Cryo-sections

III. Crossbridge Distribution and the Axial Structure of the Human C-zone

JOHN M. SQUIRE, JEFFREY J. HARFORD, ANN CHRISTINE EDMAN
AND MICHAEL SJÖSTRÖM

J. Mol. Biol. (1982) **155**, 467–494

Fine Structure of the A-band in Cryo-sections

III†. Crossbridge Distribution and the Axial Structure of the Human C-zone

JOHN M. SQUIRE, JEFFREY J. HARFORD

Biopolymer Group
Department of Metallurgy and Materials Science
Imperial College, London, SW7, England

ANN CHRISTINE EDMAN AND MICHAEL SJÖSTRÖM

Department of Anatomy, Umea University, Sweden

(Received 30 October 1980, and in revised form 20 November 1981)

Optical analysis of the C-zones of negatively stained cryo-sectioned A-bands from human *m. tibialis anterior* muscle, combined with computer modelling of the C-zone staining pattern, has led to the following conclusions.

(1) At a 99·9% confidence level there are two slightly different axial repeats in the C-zone. One repeat of 434 (±1·2) Å probably corresponds to the C-protein repeat, whereas the other of 429 Å (used for calibration) is probably due to myosin crossbridges.

(2) The myosin crossbridge array in (1) does not consist of crossbridge rows evenly spaced at 143 Å. The crossbridge positions are periodically shifted from such positions to give a true 429 Å crossbridge repeat.

(3) The myosin crossbridges are oriented almost perpendicular to the long axis of the muscle; the axial extent of the crossbridge profiles is less than 80 Å.

It is shown that computed model structures which explain satisfactorily the appearances of cryo-sectioned C-zones can also explain several anomalous features of published X-ray diffraction patterns from vertebrate muscle.

1. Introduction

The A-bands of vertebrate skeletal muscles are highly complex structures. Apart from the actin filaments which partly penetrate the A-band they comprise myosin filaments each of which is a bipolar assembly of myosin molecules (Huxley, 1963) and these filaments are crosslinked half-way along their length by the intricate M-band network (Knappeis & Carlsen, 1968; Luther & Squire, 1978,1980). In addition, vertebrate myosin filaments are decorated along most of their length by a series of non-myosin proteins, of which the most abundant is C-protein (Offer *et al.*, 1973).

† Paper II in this series is Sjöström & Squire (1977*a*).

0022–2836/82/080467–28 $02.00/0

© 1982 Academic Press Inc. (London) Ltd.

It has been shown convincingly (Offer, 1972: Craig & Offer, 1976: Pepe & Drucker, 1975) that C-protein is located in each half of the A-band on seven stripes separated axially by approximately 430 Å in a region termed the C-zone (Sjöström & Squire, 1977*a*). This extends from about 2300 Å to about 5000 Å from the centre of the A-band.

The backbones of the myosin filaments in the vertebrate A-band are composed mainly of the light meromyosin portions of the tails of the component myosin molecules (Huxley, 1963). The remainder of each molecule, the heavy meromyosin part, which comprises the rest of the tail (heavy meromyosin sub-fragment 2: S2) together with the two globular heads (each heavy meromyosin sub-fragment 1: S1) is located at the surface of the filament backbone. Thus, the heads (crossbridges) can interact when appropriate with the adjacent actin filaments. *In vitro* studies have shown that C-protein will interact with light meromyosin (Moos, 1972: Moos *et al.*, 1975) and with heavy meromyosin S2 (Starr & Offer, 1978), but not with heavy meromyosin S1 (Starr & Offer, 1978).

The approximately 430 Å axial separation of the C-protein stripes in the C-zone is close to the 429 Å axial repeat of the array of myosin crossbridges in the bridge region of the A-band (Huxley & Brown, 1967). Within this repeat there are three levels of crossbridges spaced about 143 Å apart. Because of the similarity of the myosin and C-protein repeats, and since light meromyosin paracrystals appear to show the same repeat before and after labelling with C-protein (Moos *et al.*, 1975), it has been suggested that C-protein labels myosin specifically on every third level of crossbridges (143 Å apart) so that the C-protein repeat is identical to three crossbridge separations of 143 Å (i.e. 429 Å). For this to occur it would appear to be necessary for the myosin filament itself to have not just a helical repeat but an inherent packing repeat of 429 Å. Otherwise it might be expected that C-protein would label every level of crossbridges to give a 143 Å C-protein repeat.

However, studies of the cryo-sectioned A-band of human muscle (Squire *et al.*, 1976; Sjöström & Squire, 1977*a*,*b*) have suggested that two axial periodicities are present in the C-zone. One, of about 143 Å, was taken to be the subunit repeat of the myosin array, while the other, of about 435 Å (not 3×143 Å), was thought to be due to the human muscle C-protein.

The possible presence of two repeats in the A-band is not a new idea. It was suggested by Huxley (Huxley, 1967; Huxley & Brown, 1967) as a possible means of regulating the length of the vertebrate thick filaments. He interpreted the meridional 442 Å X-ray reflection from frog sartorius muscle as being due to a non-myosin protein component arranged with a repeat of 442 Å. Indeed, this reflection has now been shown to be due at least in part to C-protein (Rome *et al.*, 1973). However, the latter authors interpreted the reflection as being the first order peak in the C-zone transform at a spacing of $1/429$ Å^{-1} (the same as the myosin repeat), which has been sampled at $1/442$ Å^{-1} due to an interference effect between the two C-zones in a single A-band (see Discussion). In addition, Craig (1977) has studied isolated A-segments from frog and rabbit muscles and has also concluded that the C-protein and myosin repeats are the same, and that the myosin packing repeat might be 429 Å and not 143 Å. Thus there is disagreement in previous work about the periodicity of C-protein in the vertebrate A-band, and there is uncertainty

about whether the myosin molecules in the C-zone have an intrinsic repeat of about 143 Å or about 429 Å.

Here we present a very much more rigorous analysis of the human C-zone structure than was possible earlier (Sjöström & Squire, 1977*a*) and we show beyond reasonable doubt (at a 99·9% confidence level) that at least in the cryo-sectioned human A-band, there are two different axial periods. Taking one to be about 429 Å, the larger period is about 434 Å. In addition, we have found that in this preparation there is not a simple 143 Å spaced axial distribution of myosin crossbridges within the C-zone; the crossbridge positions are periodically perturbed to give a true 429 Å myosin repeat.

2. Materials and Methods

(a) *Electron miscroscopy*

The details of the cryo-sectioning method have been described fully by Sjöström & Squire (1977*a*,*b*). Human *m. tibialis anterior* tissue in a relaxed state was briefly fixed (2·5% (v/v) glutaraldehyde, 5 to 15 min), treated with glycerol (30% (v/v) in buffer, 30 to 60 min), then rapidly frozen in Freon 12 (Balzers Union Limited) which was cooled by liquid nitrogen. Longitudinal sections from small pieces of the frozen tissue were cut using the LKB cryo-kit, onto a trough containing 50% glycerol or dimethylsulphoxide. The sections were negatively stained with ammonium molybdate or uranyl acetate, then air dried and finally viewed in a Philips EM300 electron microscope.

(b) *Image analysis*

Image analysis of contrasty negative copies of electron micrographs of the cryo-sectioned A-bands was carried out using a horizontal optical diffractometer of conventional design. The negatives were mounted in an oil cell (Luther & Squire, 1980) to avoid phase artifacts. The optical diffraction patterns of selected regions of the negatives were recorded onto 35 mm Ilford FP4 film and were measured using a Mitutoyo profile projector (type PJ-250C).

One-dimensional averaging (lateral smearing) of single sarcomeres across the width of the fibril was achieved in 2 ways. One method involved placing the negative in the film holder of a photographic enlarger and exposing the negative onto photographic paper. During the exposure the paper was moved at a constant speed in the image plane of the enlarger in a direction parallel to the transverse striations across the fibril in the negative, thus averaging the sarcomere structure across the fibril width. The second method involved introducing a very narrow slit into the transform plane of the optical diffractometer and aligning it exactly perpendicular to the transverse striations in the negative (Fraser & Millward, 1970). The narrow slit was formed by bringing together 2 cut edges of exposed photographic paper. The laterally smeared image could then be recorded in the image plane of the optical diffractometer onto 35 mm Ilford FP4 film.

Measurements were made of the periodicities observed in the original micrographs or in their averaged images either directly from film using the Mitutoyo profile projector or from microdensitometer traces of the images on film. The traces were obtained from a Joyce–Loebl double-beam microdensitometer (model IIIC).

(c) *Computer modelling*

One-dimensional Fourier transforms of a variety of models of the C-zone structure were computed and displayed using the computer complex at Imperial College, and the results were printed onto microfilm using the Calcomp plotter at the University of London Computer Centre.

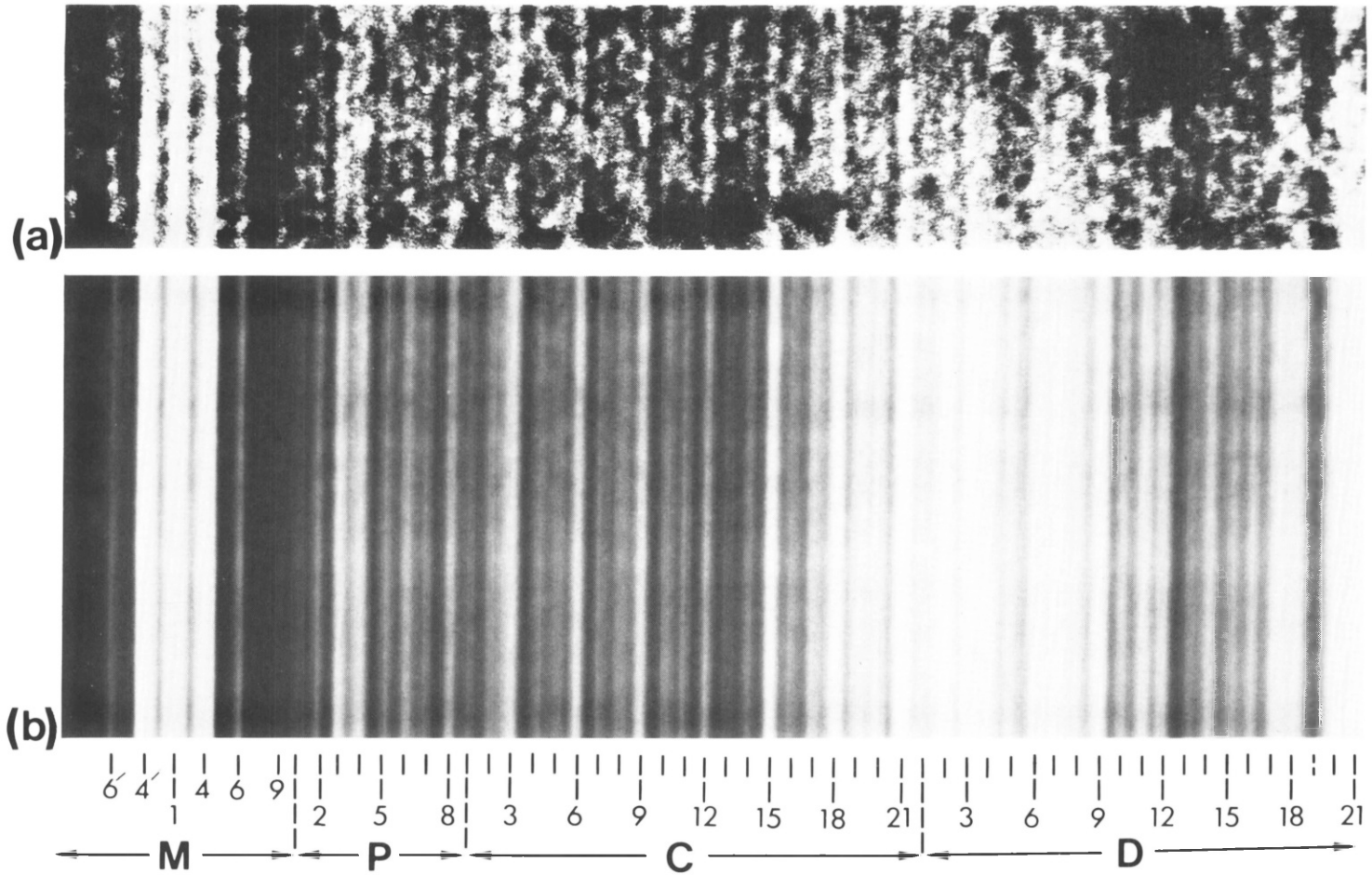


FIG. 1. Part of a negatively stained longitudinal cryo-section of human *m. tibialis anterior* showing the prominent transverse striations in the A-band (magnification 230,000 ×). These striations have been enhanced in (b) which is a laterally smeared image of (a). The various striations have been labelled as described by Sjöström & Squire (1977*a*).

3. Experimental Results

(a) *C-zones and their average images*

A detailed description of the human C-zone has already been given by Sjöström & Squire (1977*a*). Here we briefly summarize its main features in terms of a laterally averaged image not shown previously in which the structure can be seen very clearly. Figure 1(a) is part of a single cryo-sectioned A-band from human *m. tibialis anterior* showing the three clear lines of M-bridges at the left-hand end (M4', M1 and M4) and the prominent array of transverse striations which extends right up to the A-band edge at the right of the Figure. Figure 1(b) is a laterally averaged image of (a) (produced by the enlarger method, see Materials and Methods) and it shows the striations with much greater clarity than (a). As described by Sjöström & Squire (1977*a*), the A-band structure has been divided into the M-region (M), the P-zone (P, proximal), the C-zone (C) and the D-zone (D, distal). The C-zone is located centrally in Figure 1 and comprises 21 striations (white) with approximate separations 140 to 150 Å. It is clear that lines C3, C6, C9, C12, C15, C18 and C21 are much more prominent than the other lines C1, C2, C4, C5 etc. It is this variation of prominence which gives the C-zone a marked repeat of about 3×140 to 150 Å. Because of the known presence of C-protein in this part of the A-band in rabbit muscle, it is tempting to suggest that the prominent lines C3, C6, C9 etc. are associated with the presence of human C-protein in these cryo-sections. However, the analysis which follows is independent of this assumption; it will be considered again in the Discussion. What does seem to be obvious is that the basic 140 to 150 Å repeat between striations such as C1 and C2, C4 and C5, etc. probably corresponds to the separation of successive levels of myosin crossbridges along the A-band; the stain-excluding lines at C1, C2, C4, etc. are probably due primarily to the presence of the relatively bulky myosin heads.

The distribution of stain within C-zones such as that in Figure 1 has been analysed both by optical diffraction and by direct measurements as described in the following sections.

(b) *Optical diffraction analysis*

Optical diffraction patterns were recorded from 12 C-zones in six micrographs of cryo-sectioned A-bands; the micrographs being a different set from those used by Sjöström & Squire (1977*a*). Most diffraction patterns (Fig. 2) showed six orders of a repeat of about 430 to 435 Å, and in some cases the seventh and eighth orders were also seen. These orders will be called reflections 1 to 8, respectively. From absolute calibration, the third order was found to correspond to a spacing of about 140 to 150 Å and it was therefore assigned the value of 143 Å characteristic of the myosin repeat in vertebrates (Huxley & Brown, 1967). This reflection was then used to calibrate the spacings of all the other peaks. On this basis the measured average d spacings for reflections 1 to 8 (Table 1) were found to be 436·3 (±5·8) Å, 217·0 (±0·6) Å, 143 Å (used for calibration), 107·3 (±0·6) Å, 85·4 (±0·3) Å, 71·4 (±0·3) Å, 61·7 Å and 53·9 Å. No reliable statistics can be quoted for reflections 7 and 8. Occasionally additional meridional peaks, usually with spacings of about 355 to

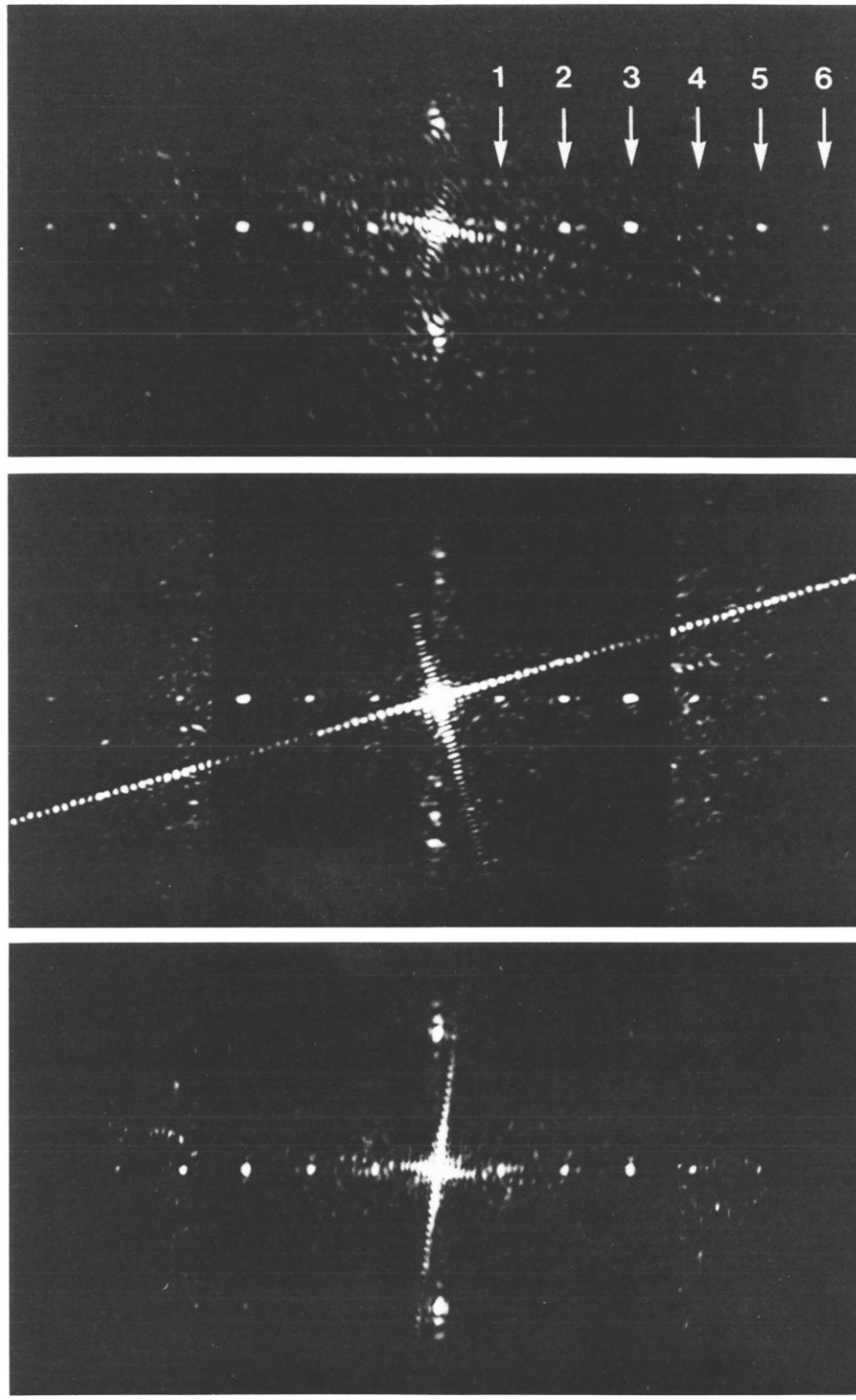


FIG. 2. Optical diffraction patterns from the C-zones of 3 micrographs like Fig. 1 (fibre axis across the page). The first 6 orders of a repeat of about 430 Å are indicated by numbered arrows.

TABLE 1

Relative spacings and intensities of reflections in optical diffraction patterns from human C-zones

Group	Micrograph	d_1	I_1	d_2	I_2	d_3†	I_3	d_4	I_4	d_5	I_5	d_6	I_6	d_7	d_8
I	5641 (2)	440·0	0·4	216·8	0·7	143	1	—	vw	85·4	mw	71·1	m	—	—
	5648 (1)	426·1	0·7	217·5	0·7	143	1	106·5	0·05	85·6	0·09	71·7	0·03	61·7	53·9
	5653 (1)	429·9	0·4	217·4	0·7	143	1	107·4	vw	85·7	0·3	70·8	0·03	—	—
	Average	432·0		217·2		143		106·9		85·6		71·2			
II	5653 (2)	443·0	0·4	217·4	0·5	143	1	107·6	0·1	85·0	0·05	71·5	0·06	61·7	—
	5680 (1)	432·7	0·4	216·7	0·4	143	1	107·5	m	85·2	m	71·4	m	—	—
	(2)	436·4	0·2	215·3	0·4	143	1	107·1	mw	85·4	w	71·2	mw	—	—
	Average	437·4		216·5		143		107·4		85·2		71·4			
III	5647 (1)	432·8	0·6	216·9	0·7	143	1	—	vw	—	—	—	—	—	—
	5653 (3)	435·2	ms	217·1	ms	143	1	106·5	m	85·2	mw	71·6	w	—	—
	(4)	447·8	0·3	217·3	0·7	143	1	106·7	m	85·7	m	—	mw	—	—
	5744 (1)	436·2	0·7	217·3	0·7	143	1	108·3	0·08	—	—	—	—	—	—
	(2)	435·9	0·7	216·8	0·7	143	1	108·0	0·1	85·7	0·06	71·8	0·02	—	—
	5641 (1)	439·3	0·5	217·0	0·6	143	1	—	—	—	—	—	—	—	—
	Average	437·9		217·1		143		107·4		85·5		71·7			
Overall average		436·3		217·0		143		107·3		85·4		71·4			
s.t.d.		(5·8)		(0·6)				(0·6)		(0·3)		(0·3)			
Theoretical orders of a 429 Å repeat		429·0		214·5		143		107·2		85·8		71·5		61·2	53·6

Additional reflections were observed as follows: micrograph 5653 (2): 555·7, 378·5, 303·9, 269·5, 198·4, 195·96; micrograph 5680 (2): 379·9; micrograph 5653 (3): 367·4; micrograph 5653 (4): 378·1; micrograph 5744 (2): 355·6 and micrograph 5641 (2): 101·3.

† All spacings (d_i in ångstrom units) were calibrated using the spacing for this reflection and all intensities (I_i) were normalized using the intensity for this reflection. Each spacing measurement is the mean of about 4 to 9 independent measurements.

s, strong; w, weak; m, medium; v, very; s.t.d., standard deviation.

380 Å, or about 190 Å, were also observed. These reflections, which could be clearly resolved from reflections 1 to 8, were assumed to be due to the structure of the actin filaments which partly or wholly overlapped the C-zones in all of the micrographs studied. In each case the sarcomere length was within 0·1 μm of 3·3 μm; the thin filament length in this muscle is about 1·30 to 1·35 μm.

TABLE 2

Statistics of C-zone measurements

A. *%Probability that the observed spacings ($\bar{x}$) are consistent with a 429 Å repeat*

Measurement	$\bar{x}$	s	N	t	Level (%)†
1st order	436·3	5·8	12	4·2	~0·1
Twice 2nd order	434·0	1·2	12	13·8	<0·1
Direct ($429 \times I_c/I_m$)	435·0	2·6	7	5·6	~0·1
Average images ($429 \times I_c/I_m$)	432·9	2·6	6	3·5	~1

B. *% Probability that reflections 1 to 6 in Table 1 are orders of a repeat of 434 Å (twice d_2)*

Reflection	$\bar{x}$	s	u	N	t	Level (%)
1	436·3	5·8	434·0	12	1·3	>25
2	217·0	0·6	217·0	12	0	~100
3	143		Used for calibration			
4	107·3	0·6	108·5	9	5·7	<0·1
5	85·4	0·3	86·8	9	13·2	<0·1
6	71·4	0·3	72·3	8	7·9	<0·1

C. *% Probability that reflections 1 to 6 in Table 1 are orders of a repeat of 429 Å*

Reflection	$\bar{x}$	s	u	N	t	Level (%)
1	436·3	5·8	429·0	12	4·2	~0·1
2	217·0	0·6	214·5	12	13·8	<0·1
3	143		Used for calibration			
4	107·3	0·6	107·2	9	0·5	~60
5	85·4	0·3	85·8	9	3·8	~0·5
6	71·4	0·3	71·5	8	0·9	~40

Values of t were calculated using the formula $t = (\bar{x}-u)/(s/\sqrt{[N-1]})$, where $\bar{x}$ are the observed spacings with standard deviation s, u is the spacing for the postulated repeat, and N is the number of different C-zones analysed which contribute to $\bar{x}$. All spacings are in ångstrom units.

† This level indicates the % probability that the sample mean $\bar{x}$ is from a population which has a mean value u (i.e. the % probability with which the corresponding value of t will be exceeded by chance).

The relative intensities of reflections 1 to 8 were estimated either visually or from microdensitometer traces (Table 1), and from this analysis the C-zones were grouped into three types. In all three groups the relative intensities (I_n) of the first three reflections (1 to 3) followed the same pattern: $I_1 < I_2 < I_3$. The average value of I_2/I_1 was 1·40 (±0·47) and of I_3/I_2 was 1·69 (±0·44). The classification of the C-zones was based on the relative intensities of reflections 4, 5 and 6 and the groups were defined as follows:

group 1, $I_4 < I_5$;

group 2, $I_4 \geq I_5 \leq I_6$;

group 3, $I_4 \geq I_5 > I_6$.

It will become clear later why this grouping is of significance.

Statistical analysis of the measured d spacings for reflections 1 to 6 (Table 2) showed that peaks 4 and 6 had spacings which were not significantly different from orders of 429 Å (3 × 143 Å). The spacing of peak 5 (85·4 Å) was also very close to an order of 429 Å (85·8 Å), but in this case the fortuitously small standard deviation in the observations (0·3 Å) made the statistics less clear cut. Nevertheless it is clear from Table 2B that this peak is very unlikely to be an order of a spacing longer than 429 Å.

On the other hand the spacing of reflection 1 was clearly different from 429 Å and the difference between the spacing of reflection 2 and 429 Å/2 was highly significant. Very similar values for the spacing of this reflection were obtained by Sjöström & Squire (1977*a*; d = 216·3 (±1·40) Å) and in the present independent analysis of a different set of micrographs (d = 217·0 (±0·6) Å). The difference between the observed values and 429 Å/2 is so significant that, at confidence levels of 99% and better than 99·9%, respectively, it can be concluded that the observed sample means do not come from a population whose mean is 429 Å/2.

The spacing of reflection 1 was much more variable than that of reflection 2. The range of best values (see below) was from about 426 Å to 448 Å. As discussed below, the proximity of this peak to the mask function and the fact that it is the least easy to measure of all the peaks probably explains some of the observed variation. However, even here there is a better than 99% probability that the observed spacings do not come from a population whose mean is 429 Å.

The estimates of the significance of the measurements summarized in Table 1 are clearly based on the assumption that the observed peaks have not been shifted from their true positions due to some form of artifact. Since the two periodicities involved (i.e. 429 Å and about 434 Å) are so close, it is clearly of importance to question what sources of systematic error there might be and what effect these might have. We therefore give below a detailed assessment of these errors.

(1) The reliability of the quoted spacings clearly depends critically on the reproducibility of measurements from a single C-zone. We have tested this by: (i) measuring individual diffraction pattern negatives up to ten times (the average deviation of the measured value from their average value gives a probable error of 0·1% for reflection 2); (ii) by measuring diffraction patterns from the same C-zone

which were recorded with different exposure times (0·1% probable error); (iii) by measuring patterns from a single C-zone that has been masked in a variety of slightly different ways (0·2% probable error). Only in this latter case (as discussed in (2), below) was the variation in measurement comparable with the differences in spacings which occur in patterns from different C-zones (the average deviation of the measured values from their average value being 0·2%).

(2) The optical diffraction patterns in Figure 2 clearly show the presence of the central cross of intensity (mask function) due to the shape of the area of micrograph that has been used. We have found that this mask function can affect the apparent spacing of reflection 1 unless precautions are taken. In particular, if the mask function is not sufficiently tilted to the meridian of the C-zone pattern (horizontal in Fig. 2) then the apparent spacing of reflection 1 can vary from as little as 1/400 $Å^{-1}$ to as much as 1/470 $Å^{-1}$, and sometimes may be split along the meridian: all these effects being attributable to interference with the mask function. Increasing the tilt of the mask function greatly reduces this problem and the spacings listed in Table 1 are those obtained from patterns with the mask functions at relatively large tilts. Note, however, that too much tilt is also undesirable since it is then difficult to mask an area which can sensibly be considered as only comprising the C-zone.

Fortunately reflection 2 is sufficiently far from the mask function that no interference effect has been observed. It is principally the spacing of this reflection on which we have based our conclusions from the optical diffraction analysis.

(3) During the modelling of the C-zones which we discuss later, we became aware that the positions of reflections 1 and 2 depend on the shape of the underlying transform that is being sampled. This in turn depends on the width of the peaks C3, C6, C9 etc. However, we have found that using models containing density peaks close to the observed width (see the following section) the apparent shifts of reflections 1 and 2 are very small. Giving the whole C-zone a single repeat of 429 Å, then reflection 1 was observed at 1/429·3 $Å^{-1}$ and reflection 2 at 1/215·4 $Å^{-1}$, not nearly enough of a shift to explain our observations.

(4) The positions of reflections 1 and 2 could in theory be further shifted towards the origin (i.e. to longer spacings) if they are superimposed on a steeply sloping background intensity which starts high near to the centre of the diffraction pattern. However, model calculations have shown that only by the addition of backgrounds with over ten times the observed slope to models such as those discussed in (3) (which already produce small peak shifts) could these peaks be shifted to about the right spacings (actually to 1/432 $Å^{-1}$ and 1/216·9 $Å^{-1}$). We conclude that the observed background has a negligible effect on our measurements.

To summarize this section it is fair to conclude, in the light of the control experiments that we have done, that the spacings of reflections 1 and 2 are not from a structure with a 429 Å repeat; the spacings are consistent with the hypothesis (Table 1) that they come from a periodicity of about 434 Å (twice the spacing of reflection 2). Similarly the spacings of reflections 3, 4, 5 and 6 are consistent with these peaks being orders of a 429 Å repeat. None of them is an order of the 434 Å repeat.

(c) *Direct analysis of micrographs and their average images*

Sjöström & Squire (1977*a*) previously suggested that the two different repeats in the human C-zone were probably due to a difference between the spacing of the prominent lines, C3, C6, C9 etc. and the spacing of the weaker lines (C1, C4, C7, etc. or C2, C5, C8 etc.). Such a difference in spacing was thought to account for some of the changes in appearance between successive pairs of prominent lines (C3 to C6, C6 to C9, C9 to 12 and so on) which can be seen clearly both in the original micrographs (Fig. 1(a) and Fig. 3) and in their laterally averaged images (Fig. 1(b) and Fig. 4). Figure 4 shows six laterally averaged C-zones together with the average of all six, and it can be seen that despite some variation there is a systematic change in structure through the C-zone. For example, C3 always appears relatively broad and tends to be flanked by a dark (stain-filled) line on its distal side and a lighter line on its proximal side. Similarly the gaps between C15 and C18 (i.e. C15 to C16, C16 to C17 and C17 to C18) tend to be fairly uniform and C20 to C21 seems to be wider than C19 to C20 which always appears relatively narrow.

Assuming that the presence of actin has a minor effect (but not a negligible one†; see also Discussion, one would expect slightly different actin overlaps in the different sarcomeres shown in Figure 4 and therefore different actin effects if they occur) then the observed variation through the C-zone must mean that there is not a simple repeat of 429 Å through the C-zone.

In order to put this qualitative argument onto a quantitative basis we have carried out direct measurements of the separations of the various striations in the C-zone, either using the original micrographs or their average images or using microdensitometer traces from these micrographs or their averages. In order to optimize both the accuracy and the significance of the measurements, the position of each striation was only used once in the quoted average. The average spacing of the prominent lines was obtained by measuring the positions of the six most well-defined of the seven lines and taking, for example, the intervals C3 to C12, C6 to C15, C9 to C18, dividing these by three and averaging the result. The measurement obtained was called I_c. Similarly the repeats of the weaker lines (C1, C2 etc.) were obtained by making similar measurements on the series of lines C1, C4, C7, C10, C13, C16 and C19 and on the series C2, C5, C8, C11, C14, C17, C20. The averaged repeats of these two series, thought to be due to the myosin crossbridges, was termed I_m.

Direct measurements from micrographs gave a value I_c/I_m of 1·014 (±0·006). Thus if I_m is 429 Å, I_c is 435 (±3) Å. The averaged images of a different set of micrographs gave a ratio I_c/I_m equal to 1·009 (±0·006). Here, if I_m is 429 Å, I_c is 432·9 (±2·6) Å. As in the optical diffraction analysis these results show that at a high confidence level (about 99·9%; Table 2), there is a periodicity present which is different from 429 Å. The direct analysis has shown in addition that the longer of

† Note that in the analysis of the C-zone diffraction patterns given later the structure of the thin filaments, especially the effect of the relatively massive 385 Å-spaced troponin subunits, can be separated very readily from that of the myosin filaments, since the two filaments give rise to different sets of diffraction peaks. The peaks which are clearly due to the thin filaments, and which, in any case, were always relatively weak, were not included in the analysis of the optical diffraction patterns. Thus the myosin filament structure alone was modelled.

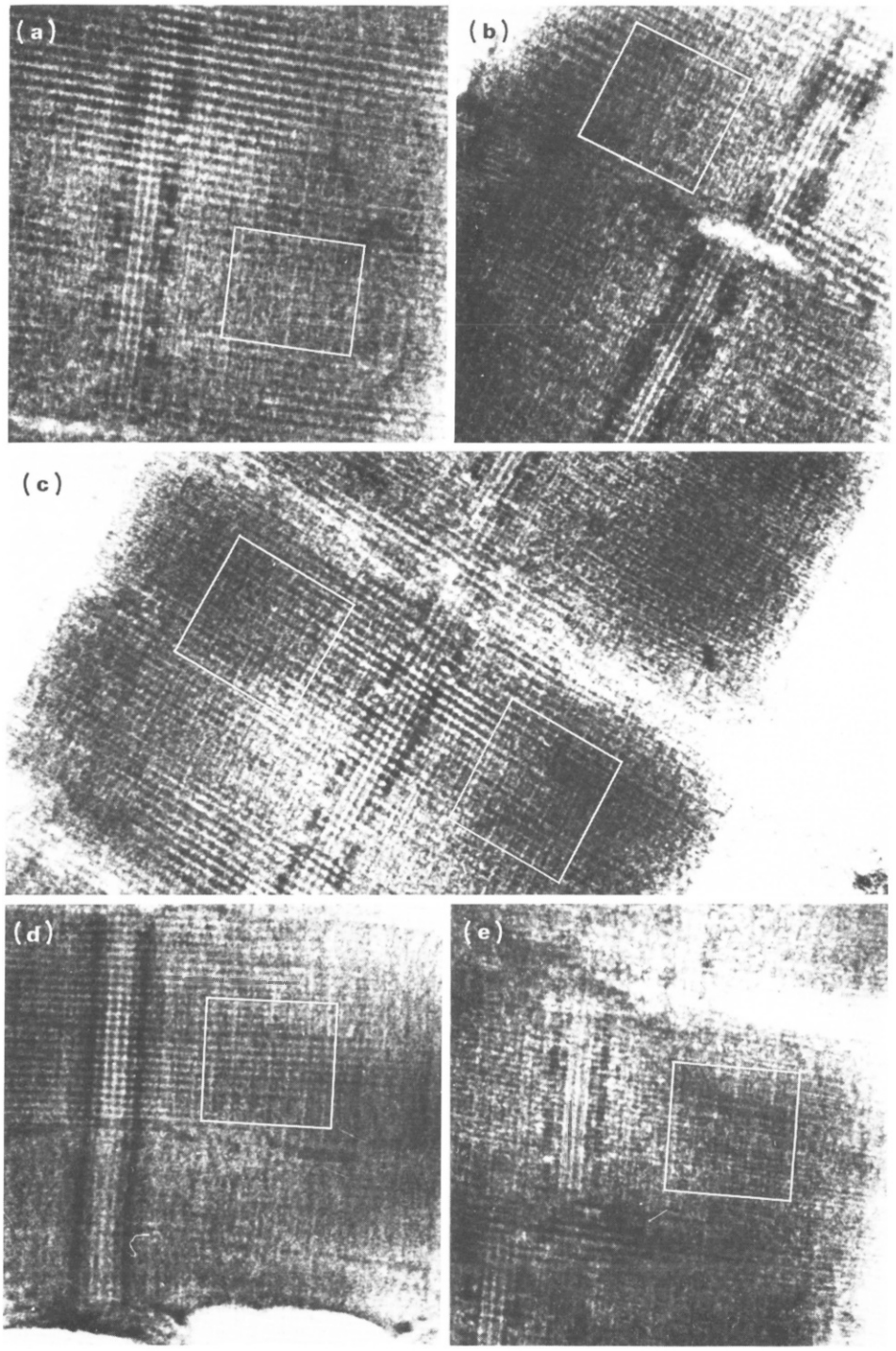


FIG. 3. Longitudinal negatively stained cryo-sections of human *m. tibialis anterior* showing the C-zones which were used to produce the averages in Fig. 4 and some of the values in Table 1. The general order in the sarcomere and the consistent appearances of different sections are clearly seen (magnification 74,000 ×). (a) and (b) Have optical diffraction patterns in group I; (c) in group II, and (d) and (e) in group III.

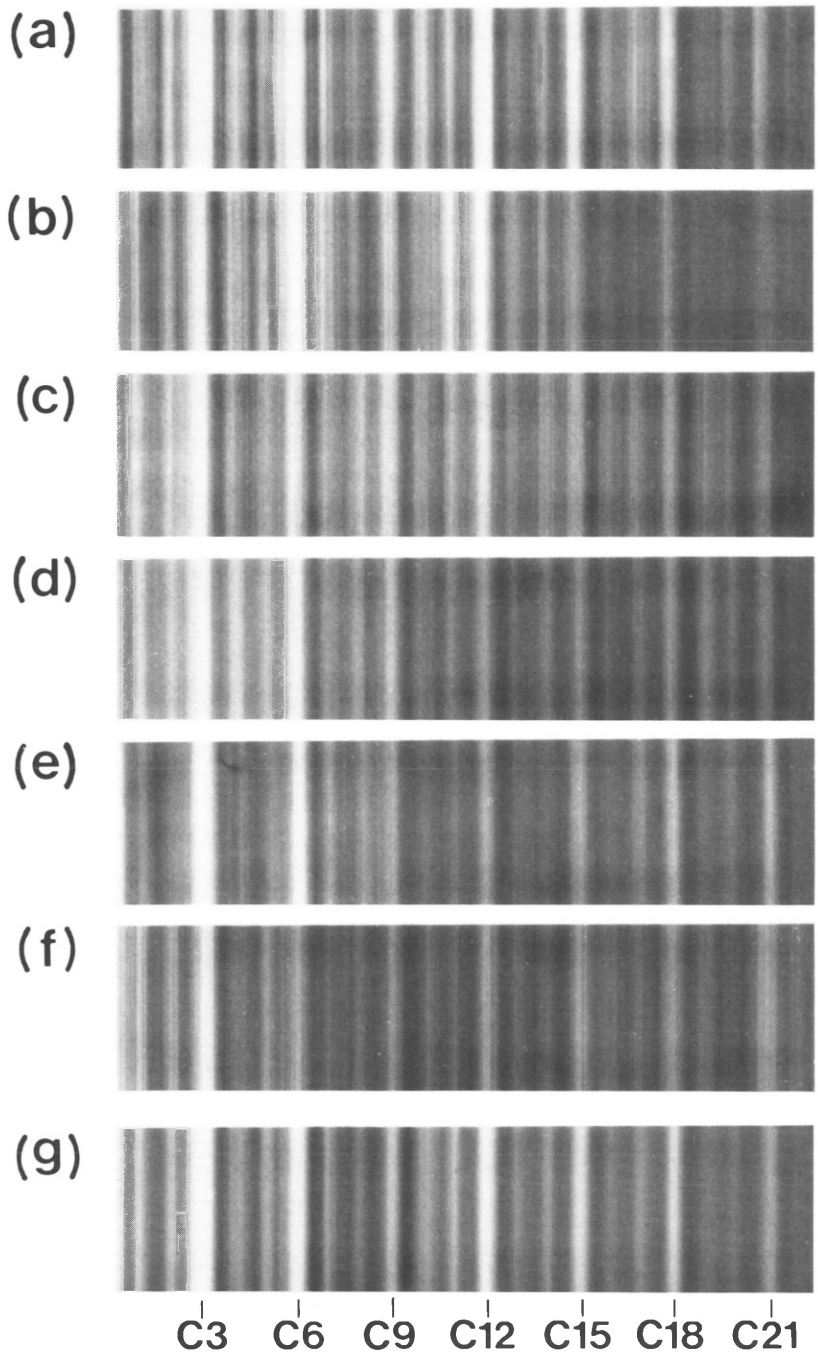


FIG. 4. Laterally averaged images ((a) to (f)) of the 6 C-zones shown as Fig. 3 ((a) to (e), respectively). All averages were produced by the enlarger method. All of these averages have themselves been averaged to give (g). The strong lines C3, C6 etc. are very clear in all averages as are the weaker (crossbridge) lines which lie between them. Similar variations in profile through the C-zone can be followed in all these images (magnification 311,000 ×).

the two periodicities is associated with the prominent striations C3, C6, C9, C12, C15, C18 and C21.

We have also measured the relative separations of the weak lines in each 430 to 435 Å period. The gaps between the prominent lines were labelled from the proximal end as *a*, *b* and *c*. Thus, the spacings C3 to C4, C6 to C7 and so on are *a*, C4 to C5, C7 to C8 and so on are *b*, and C5 to C6, C8 to C9 and so on are *c*. We found a trend such that the spacing *b* was usually lower than 1/3 of $a+b+c$. Taking $a+b+c$ to equal approximately 430 Å then *b* was found to be about 120 (± 15) Å for group I C-zones (see Table 1), about 137 (± 15) Å for group II C-zones (barely significant) and about 128 (± 15) Å for group III C-zones. There is also a trend such that *a* is usually greater than *c* but the statistics are too poor in this case to attach a great deal of weight to the observation. Nevertheless, the low value of *b* strongly suggests that the repeat of the myosin crossbridges is not a simple one of 143 Å. As shown in the modelling below, the optical diffraction results also suggest that there is an approximate crossbridge repeat of 429 Å rather than 143 Å.

Finally, an attempt has been made to estimate directly from micrographs and microdensitometer traces the axial widths of the lines in the C-zone. However, this was found to be by no means straightforward because of the uncertainty in placing the background density levels in microdensitometer traces. For this reason estimates obtained from modelling the observed optical diffraction patterns were considered to be much more reliable. These values are discussed in the following section.

(d) *Computer modelling of the C-zone structure*

We have attempted to account both for the general distribution of density within the human C-zones and for the intensity distributions in their optical diffraction patterns (ignoring the thin filament diffraction peaks) in terms of simple model structures. Initially the models comprised a series of density peaks (box functions in Fig. 5(a): lower diagram) on a repeat of 434 Å combined with a series of density peaks (Fig. 5(b)) with a 143 Å repeat. Clearly the density profile in Figure 5(a) was intended to represent the prominent striations C3, C6 etc. in the C-zone and the profile in Figure 5(b) represented the 143 Å spaced crossbridge array. These two density profiles when added together would represent the simplest possible model of the C-zone discussed briefly by Sjöström & Squire (1977*a*).

Computer programs were written to generate the two components of the model separately. In each component the widths, separations and relative heights of the density peaks could be altered. In addition, the two arrays could be shifted axially relative to each other by multiples of 5 Å. The two profiles were then added and in each case the Fourier transform of the resulting density profile was calculated. In Figure 5 the repeating features in each array are box functions, but as shown below Gaussian profiles were found to be more realistic. Note finally that all of the models that are presented represent the C-zones from line C3 to line C21 inclusive.

The computed Fourier transforms shown above the density profiles in Figure 5(a) and (b) illustrate some of the properties of the models. In Figure 5(a) reflections 1 to 3 lie within the central maximum of the Fourier transform of a single box function.

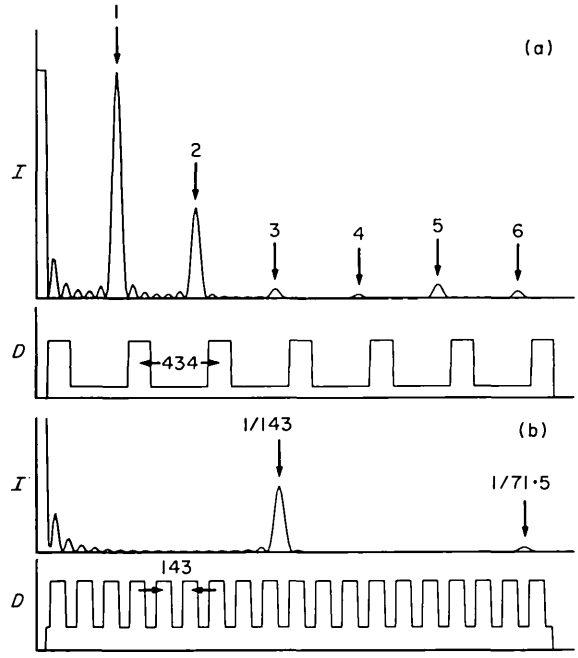


FIG. 5. C-zone density models (D) and the computed intensity distributions (I) in their diffraction patterns. (a) Box function model for the prominent C-zone striations C3, C6 etc. on a 434 Å repeat; and (b) box function model for the 143 Å spaced crossbridge peaks. Arrowed peaks in (a) show reflections 1 to 6 described in the text. Note that the slight slopes on the sides of the box functions in (a) and (b) are a computer-generated artifact which did not affect the computations.

The first minimum is close to reflection 4 and the first subsidiary maximum is near to reflections 5 and 6. Only these six reflections were considered in the modelling. By altering the width of the box function or by giving these density peaks a different shape the relative intensities of these six reflections will change in a unique and predictable fashion.

Likewise in Figure 5(b), the Fourier transform of the 143 Å spaced array contributes peaks only at 1/143 $Å^{-1}$ and at 1/71·5 $Å^{-1}$. These would correspond to reflections 3 and 6 of the Fourier transform of the combined density profile. Once again the relative intensities of the peaks at 1/143 $Å^{-1}$ and 1/71·5 $Å^{-1}$ can be altered by adjusting the width or the shape of the peaks in the density profile. Similarly, for given shapes of the density peaks, their relative heights in the two arrays will determine the relative contributions of the two constituent Fourier transforms to the final intensity profile from the total density distribution.

The choice of an appropriate model can be deduced from the observed density profile in Figures 1 and 4 and the optical diffraction patterns in Figure 2 in the following way. We have shown that reflections 1 and 2 are associated with a different repeat (434 Å) from reflections 3, 4, 5 and 6 (429 Å). The high density peaks spaced at 434 Å therefore contribute strongly to reflections 1 and 2 and negligibly

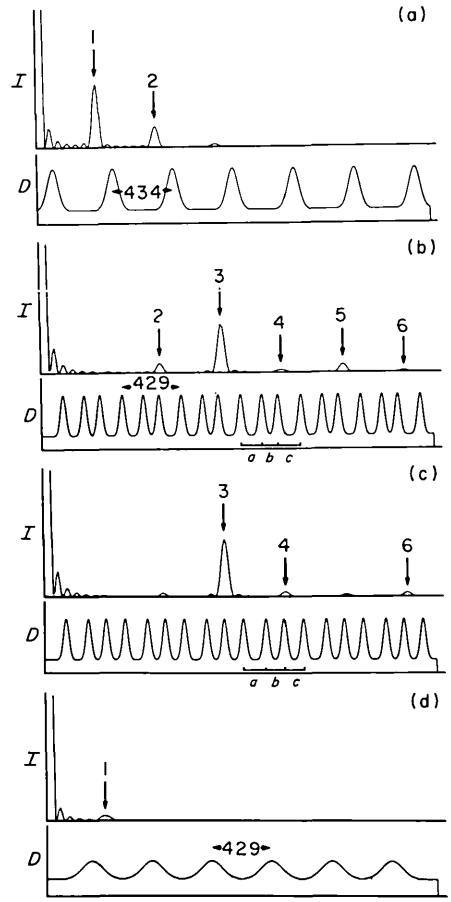


FIG. 6. The components of C-zone models containing crossbridge arrays with a true repeat of 429 Å. Spacings of successive crossbridge positions are called *a*, *b* and *c*. (d) The form of the intervening step density. (b) and (c) Two different crossbridge distributions for which $I_5 > I_4$ (b) and $I_4 > I_5$ (c). (a) The density profile and computed intensity for the prominent peaks C3, C6 etc. (*D*, density; *I*, intensity, as in Fig. 5).

to the other peaks. Figure 5(a) shows that a box function of about the right width can explain the spacings of reflections 1 and 2, but it also gives a significant subsidiary maximum near to peaks 3, 4, 5 and 6, all of which would in this case relate to the 434 Å repeat. Since the observed diffraction patterns show no trace of this spacing beyond reflection 2 the shape of the profile must be modified such that peaks 3, 4, 5 and 6 become negligibly small. This can be done by giving the prominent peaks C3, C6 etc. a Gaussian profile (Fig. 6(a)) since the transform from such a function has a central maximum with no subsidiary peaks.

Similarly a crossbridge model such as that in Figure 5(b) gives rise to peaks 3 and 6 but not to 4 and 5. This is because the model has a 143 Å repeat of which peaks 3 and 6 are the first and second orders. The extra peaks which are the fourth and fifth

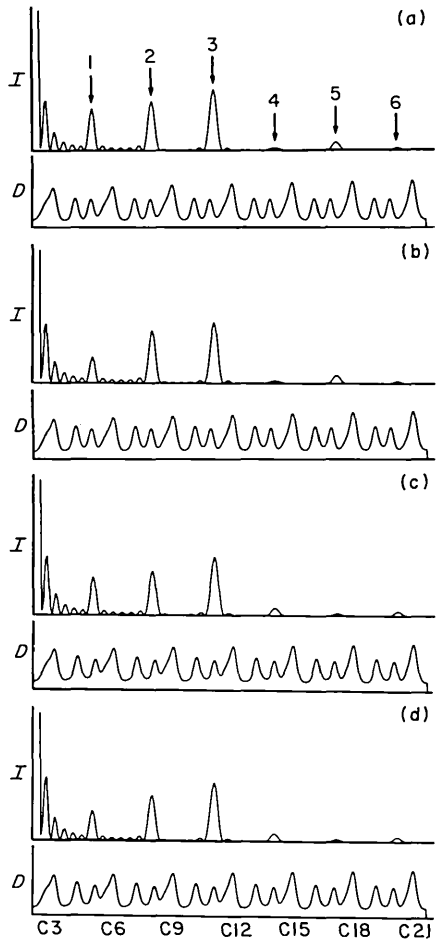


FIG. 7. Full C-zone models (D) using the component density distributions in Fig. 6. (a) and (b) Correspond to Fig. 6(b) combined with Fig. 6(a) and 2 different intervening step densities. Similarly (c) and (d) correspond to similar combinations to (a) and (b) but using Fig. 6(c) instead of Fig. 6(b). The calculated intensities (I) are generally very similar to the observed values (Fig. 2 and Table 1).

orders of 429 Å clearly require the crossbridge distribution to have a true repeat of 429 Å, not 143 Å. *A priori* this could be achieved by giving successive crossbridge profiles different densities, but this seems an unlikely possibility, since as far as is known all the crossbridges are identical in size and shape. In any case our measurements of the a, b and c spacings in the C-zone micrographs suggest that what is needed is a perturbation in the *positions* of the crossbridge peaks. An added complication is that slight variations occur in the observed diffraction patterns such that $I_4 < I_5$ in group I (Table 1) and $I_4 \geq I_5$ in groups II and III. Slightly different crossbridge distributions are required to account for these intensity differences; a feature which is implied by our direct measurements of a, b and c in the three cases. Figure 6(b) and (c) shows two possible crossbridge distributions in

each of which the individual density peaks have been given Gaussian profiles. In (b), $a = 153$ Å, $b = 113$ Å, $c = 163$ Å and $I_5 > I_4$, and in (c), $a = 163$ Å, $b = 128$ Å, $c = 138$ Å and $I_4 > I_5$. Thus, the relative intensities I_4 and I_5 may be determined by altering slightly the perturbations in the crossbridge array. Addition of the crossbridge arrays in Figure 6(b) and (c) to an array of Gaussian density peaks with a 434 Å repeat, as in Figure 6(a), gives total profiles and their Fourier transforms as in Figure 7, and these agree well with the observations. However, in order to optimize the models and give a marginally improved fit between the observed and computed intensities for reflections 1 and 2, it was found necessary to introduce an additional low density Gaussian peak with either a 429 Å or a 434 Å repeat as in Figure 6(d). The significance of this extra peak (the intervening step) is considered later.

The profiles in Figure 7 and their computed transforms show a very good fit with the range of observed intensities either with $I_5 > I_4$ (Fig. 7(a) and (b)) or with $I_5 < I_4$ (Fig. 7(c) and (d)). In all cases the spacings of all the reflections agree well with the observed values (Table 1), and the density profiles show the characteristic features of the original micrographs. In particular the values of b in the best models are lower than a and c as observed in the average images of the C-zone micrographs (Fig. 4). Note also that interchanging the values of spacings a and c did not significantly affect the computed transform. A further satisfactory feature of the modelling is that the widths of the density peaks demanded by the optical diffraction data are consistent with the appearances of the C-zone micrographs and their microdensitometer traces. The modelling required peaks with 90% of their density in a width of about 130 Å for lines C3, C6, C9 etc. and about 80 Å for lines C4, C5, C7, C8 etc. In the original micrographs the strong lines (C3, C6) often appear broader than the weaker crossbridge lines as the modelling would suggest.

Note finally that the grouping of C-zones in Table 1 is such that $I_4 < I_5$ (group I) as in Figure 7(a) and (b) or $I_4 > I_5$ (groups II and III) as in Figure 7(c) and (d). However, in the latter category some observed patterns (group III) have $I_6 < I_5$. There is uncertainty here whether it is the crossbridge distribution which gives $I_5 < I_4$ or whether limited resolution in the micrograph is such that the crossbridge unit transform falls rapidly from I_4 to I_6. In such a case the crossbridge distribution itself could give an interference function with $I_5 > I_4$ but the transform being sampled could drop sufficiently from peak 4 to peak 5 to peak 6 to give the observed ratios $I_4 > I_5 > I_6$.

In Figures 6 and 7 the extra low density Gaussian peak (the intervening step; Fig. 6(d)) was introduced in an *ad hoc* fashion to give a marginal improvement between the observed and calculated intensities of reflections 1 and 2. However, this feature may have additional significance. One of the puzzling observations revealed by Table 1 is the marked range of spacings for reflection 1. Sometimes the spacing is actually less than 429 Å even though, in the same pattern, reflection 2 has a spacing significantly larger than 429 Å/2. It has already been shown that the mask function can affect the position of this peak, but it seems unlikely that the observed variations could be totally explained in this way. However, the presence of the intervening step could help to explain this anomaly. If the intervening step peaks are given a spacing of 429 Å, then since these peaks are placed midway

between the 434 Å density peaks, their contribution to reflection 1 will be out of phase with and displaced from the 434 Å peak from the lines C3, C6 etc. By adjusting the relative density of the two arrays, in particular by increasing the density of the intervening step, it has been found that the position of reflection 1 can be shifted to a spacing as low as 420 Å to 400 Å. This is due to the fact that two peaks of similar profile but with a slight displacement are being subtracted. The second order is not affected in the same way because now the two structures are diffracting in phase. It was found that an analogous effect on reflection 1 could not be produced by changing the crossbridge array. In no case was a sufficiently strong first order peak produced while conserving the required general form of the crossbridge array. Thus the intervening step, whatever its origin, may be a significant feature of the cryo-sectioned C-zone. Note also that the intervening step with a 429 Å repeat was found not to provide an alternative explanation for the existence of peaks 4 and 5; these peaks are clearly due to the crossbridge array.

4. Discussion

(a) *Summary*

We believe that the analysis presented here has shown beyond reasonable doubt that in the cryo-sectioned human C-zone there are two slightly different axial periods apart from the occasional traces of the 370 to 380 Å actin repeat. In addition the observations and the computer modelling strongly suggest that in this preparation the myosin crossbridges are themselves arranged with an inherent repeat of 429 Å and that there may be a low density "intervening step". The most likely explanation of the prominence of the series C3, C6, C9 etc. is that it is due to the presence of C-protein and we will assume this in the discussion which follows.

(b) *The crossbridge array*

The observed axial displacements of the crossbridge levels from a simple 143 Å repeat may be a result of the preparation procedure used here. For example, it might be an artifact due to drying down of the helically arranged crossbridges onto the grid. But the reproducibility of the observations argues against this. Alternatively it may be due to some form of fixation-induced crossbridge interaction with actin attachment sites which are clearly not spaced at 143 Å intervals. For example, the two "best" models (Fig. 6(b) and (c)) have spacings of $a = 153$ Å (or 163 Å), $b = 113$ Å, $c = 163$ Å (or 153 Å), and $a = 163$ Å, $b = 128$ Å, $c = 138$ Å, and some of these values are very close to multiples of the actin subunit axial translation of 27·5 Å. Considering the actin filament as two long-period helical strands of subunits of pitch about 770 Å, then separations of 110 Å (2×55 Å) and 165 Å (3×55 Å) occur between subunits along the same strand and a separation of 137·5 Å ($2{\cdot}5 \times 55$ Å) occurs from one strand to the other. Two out of three of the observed crossbridge spacings in each model, therefore, correlate well with the known actin repeats. The fact that two slightly different distributions are seen implies that slightly different actin interactions may be involved, due possibly to slightly different filament overlaps. Axial displacements of the actin filaments of

only 100 Å or 200 Å might easily lead to such an effect. However, this need not imply that actin influences a crossbridge array of initial period 143 Å to give the observed spacings. In fact, several features argue against this. Firstly the existence of the true 429 Å period in the crossbridge array would not be explained by actin interaction since the actin repeat is about 370 Å. Secondly there are a number of features of the observed X-ray diffraction patterns from relaxed vertebrate skeletal muscles (i.e. the "forbidden" meridional reflections, see below) which would be explained by the observed forms of crossbridge array. Finally it has been shown by Bennett (1976) that some forms of light meromyosin paracrystal show a sub-repeat of about 3/8 of 429 Å (about 160 Å), and this may be associated with an axial stagger between molecules. We, therefore, conclude that the crossbridge array in relaxed muscle probably does have an intrinsic 429 Å period. The two forms we have seen are probably slight perturbations due to actin interaction of an underlying crossbridge array which has an a spacing of about 160 to 165 Å and b and c spacings of about 110 to 130 Å and 140 to 150 Å. Since isolated A-segments (Hanson *et al.*, 1971) and light meromyosin paracrystals (Bennett, 1976) both tend to show optical diffraction patterns where $I_5 > I_4$, it is possible (indeed likely) that our model in Figure 6(b) is closer to the crossbridge array in relaxed muscle than is Figure 6(c). Note also that the 80 Å axial extent of the crossbridge peaks in the best model suggests that the rather long myosin heads (up to 190 Å; Elliott & Offer, 1978) must be oriented almost perpendicular to the long axis of the myosin filaments in this fixed relaxed preparation.

(c) *Diffraction from the non-helical array of crossbridges*

Although the idea that the crossbridge array might not be exactly helical is not a new one (Huxley & Brown, 1967), previous computer modelling of the X-ray diffraction data has usually assumed perfect helicity (Huxley & Brown, 1967; Squire, 1972,1975; Haselgrove, 1980). It is of interest to consider the effects of non-helicity on this analysis, and initially optical diffraction (Fig. 8) can be used to provide a simple demonstration of the effects. Figure 8(a), (c) and (e) shows projections of the subunits in three different types of three-stranded model for the crossbridge array. Figure 8(a) is the conventional model (Squire, 1972) with crossbridge levels displaced axially by one-third of the repeat of 429 Å. Here the three strands of the array are true helices and the diffraction pattern (Fig. 8(b)) shows the expected result; layer-lines which index as orders of the 429 Å repeat and strong meridional reflections on layer-lines of number $l = 3N$ (N integer). Figure 8(c) and (e) are slight modifications of (a) in that they have subunits which lie along the same three helical tracks as in (a), but their axial separations have now been given the values as in our models in Figure 6(b) and (c). Here, in addition to the layer-line peaks seen in (b), the small axial displacements which give rise to the true 429 Å crossbridge repeat have produced "extra" meridional reflections. The second and fifth orders are strong in (d) and the fourth is marginally stronger than the fifth in (f). It was noted by Huxley & Brown (1967) and Haselgrove (1975) that the forbidden meridional reflection on the second layer-line would not be predicted

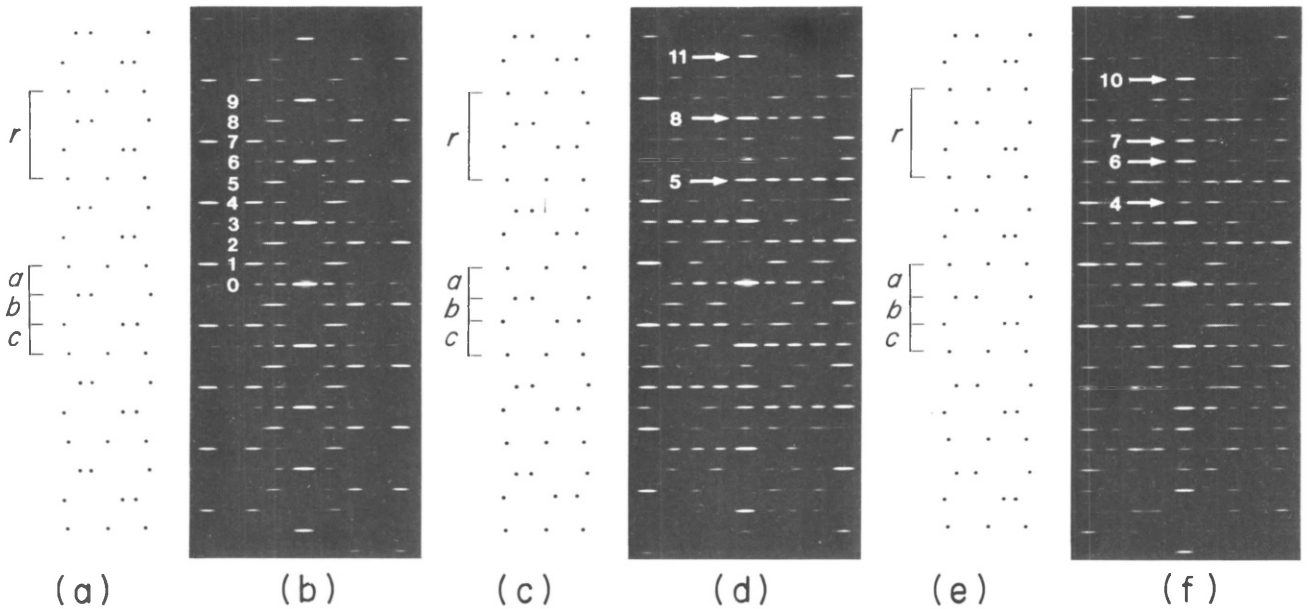


FIG. 8. (a), (c) and (e) Projected views of 3-stranded models for the vertebrate myosin filament but with slightly different crossbridge spacings. In (a) the spacings *a*, *b* and *c* are equal; the structure represents a true helix. In (c) and (e) the crossbridge spacings *a*, *b* and *c* are as in Fig. 6. models (b) and (c), respectively. The differences in the optical diffraction patterns (b), (d) and (f) from (a), (c) and (e), respectively, are described in the text. Note that the models in (a), (c) and (e) only represent a single projected view of the helices (or quasi-helices) involved. Thus the optical diffraction patterns need not be symmetrical across the meridian. Only if the diffraction patterns from all possible projected views were averaged would the symmetry of the helix cross become apparent.

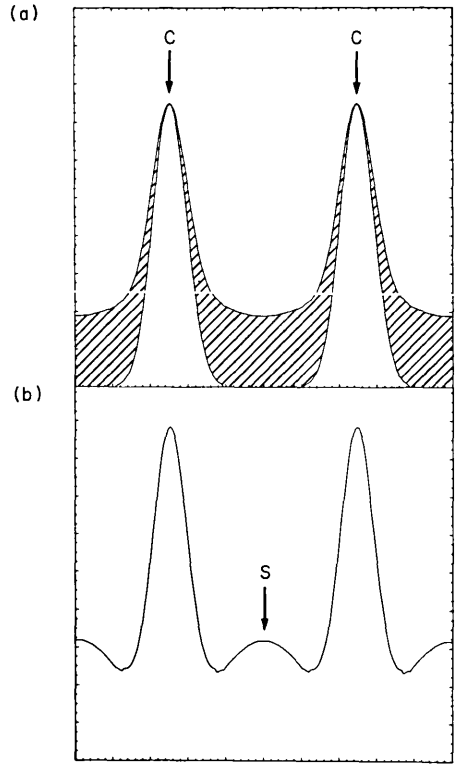


FIG. 9. Possible origin of the intervening step-density. It is assumed in (a) that successive C-protein peaks (C) have stain (shaded) in the gap between them. A plot of transmission as a function of position in (a) is shown in (b). An intervening peak (S) between the prominent peaks has been produced even though no associated protein structure is present at this position in (a).

by a perfect helix (e.g. Fig. 8(a)). However, its existence is readily explained by the distorted structure seen in the cryo-sectioned C-zone and modelled in Figure 8(c). The structure in Figure 8(e) would not explain this observation so well since in (f) the second order peak is relatively weak. Thus, both the A-segments (Hanson *et al.*, 1971) and the observed X-ray data support the idea that the model in Figure 8(c) resembles the true crossbridge arrangement in relaxed muscle. It is of interest to note that any movement of crossbridges from this arrangement towards the model in Figure 8(e), as may occur as a result of actin interaction during contraction, would tend to reduce the intensity of the second order meridional peak and to increase the intensity of the 143 Å reflection (third order; Huxley *et al.*, 1980).

(d) *The origin of the "intervening step" density*

An interesting feature of our analysis of the human C-zone was the improvement in the modelling which was produced by the presence of an "intervening step" density between the strong lines C3, C6, C9, C12, C15, C18 and C21. This

intervening step was, in most cases, a rather broad density peak which was very much shallower than the crossbridge or C-protein peaks. It was sometimes included in the model with a repeat of 429 Å like the crossbridges and thus it could represent some feature of the backbone of the myosin filaments. However, the results are usually not affected if, as is shown in Figure 7, it had a 434 Å repeat. In such a case it could easily be a staining artifact in the cryo-sections. Figure 9 shows that the strong protein features at C3, C6, C9 etc. in the C-zone will tend to have stain piled up against them during negative staining and subsequent drying (Fig. 9(a)). If the transmission through the stain is plotted as a function of position (Fig. 9(b)) then there are strong features of high transmission at positions corresponding to the protein peaks, with low broad peaks (like the intervening step) between these strong features. Thus the intervening step need not correspond to the presence of an additional stain-excluding protein feature, but in some cases it could be entirely due to the staining of the strong peaks. However, if such a feature is needed to explain the variation in spacing of reflection 1 then the step must have a repeat of 429 Å, not 434 Å. In this case it seems clear that the intervening step would have to be due to some feature of the myosin filament backbone, and if so such a feature could explain the need for the intervening step in all of the other models as well. Further work is needed to clarify this point.

(e) *The origin of the 442 Å and 418 Å meridional reflections*

As discussed briefly in the Introduction, the 442 Å and 418 Å meridional reflections in X-ray diffraction patterns from frog sartorius muscle (Huxley & Brown, 1967; Haselgrove, 1975) have previously been accounted for by Rome *et al.* (1973) as being due to an interference effect between the two C-zones in the same A-band. By labelling glycerinated rabbit psoas muscle with antibody to C-protein they found that this part of the meridian of the X-ray pattern was enhanced. However, in their modelling of the meridian they assumed that the C-protein peak from one C-zone was at $1/429\ \text{Å}^{-1}$ and that this was sampled by an interference function of repeat $1/6650\ \text{Å}^{-1}$. At that time, it was thought that there were nine lines of C-protein in each half of the A-band, but the true number has now been shown to be seven (Craig & Offer, 1976). In this case the interference function needs to be increased by about one C-protein period (434 Å) and it becomes about 7080 Å. We have carried out a similar analysis to that of Rome *et al.* (1973) using our best C-zone model in Figure 7(a). The model is shown in Figure 10(c). Here lines C12 in each C-zone are separated by a distance L. The computed intensity distribution of the first order peak due to just one C-zone is shown in Figure 10(a) and that due to interference between both C-zones is shown in Figure 10(b) for $L = 7076$ Å.

Since the interference peaks in Figure 10(b) are sampling an underlying C-protein transform (Fig. 10(a)) with sloping sides, some alteration of position of the peaks from true orders of L might be expected, but we found the shifts to be less than 0·5%. Figure 11(a) compares the calculated positions of orders 16 and 17 of the interference function for a small range of L values and the observed spacings of the meridional X-ray reflections at 441·8 Å and 418·4 Å, together with the uncertainty

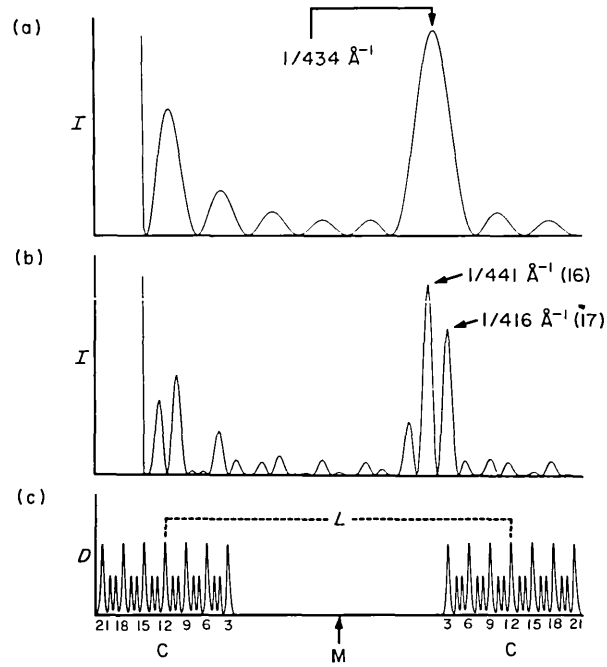


FIG. 10. (a) The intensity profile of reflection 1 in the model shown as Fig. 7(a) and its appearance (b) due to sampling from an interference function of spacing $L = 7076$ Å which would correspond to the separation of the two C-zones in a single A-band as indicated in (c). (Numbers in brackets refer to the order of 7076 Å.)

of $\pm 0{\cdot}5\%$, quoted by Haselgrove (1975). An L value of about 7080 to 7090 Å gives the best agreement between the observed and computed spacings. Figure 11(b) shows the variation of intensity (measured peak height) of the 15th, 16th and 17th order reflections sampling the peak at 1/434 Å in Figure 10(a), as a function of L. Clearly the value of L in Figure 11(a) which gives the best spacings is such that I_{15} is relatively weak and I_{17} is markedly weaker than I_{16}. In the observed X-ray diffraction patterns (Haselgrove, 1975) the 441·8 Å reflection (16) is much stronger than the 418·4 Å reflection (17). But the analysis by Rome *et al.* (1973) with a C-protein peak at 1/429 Å gave these two reflections almost equal intensity. Giving C-protein a slightly longer repeat, as observed here in the cryo-sections of human muscle, tends to increase the ratio I_{16}/I_{17}. Reflection 15 ($\sim$474 Å) is not observed in X-ray patterns and is weak in our modelling with L close to 7080 to 7090 Å. This can be seen in Figure 10(b) which is actually the intensity profile for $L = 7076$ Å. Note that extra protein peaks occur on each side of the C-zone as well. These will also affect the 430 to 440 Å meridional region, but these peaks have been ignored in the present analysis. However, since there are about three or four such lines in the P-zone and another three or four in the D-zone it is likely that the value of L of about 7080 to 7090 Å would still be correct if these lines were included. Furthermore, the presence of these extra peaks, if they were on approximately the same repeat as the myosin or C-protein in the C-zone, would tend to narrow the

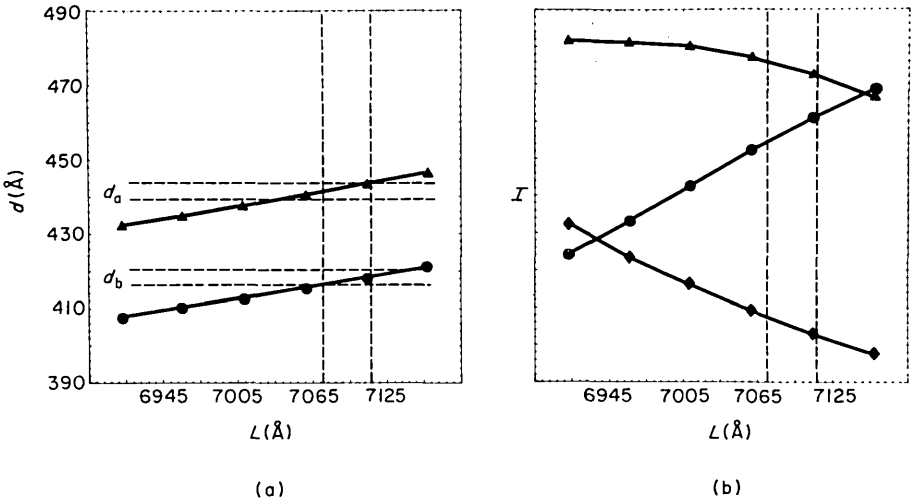


FIG. 11. (a) Values of the positions of orders 16 (▲) and 17 (●) of the interference function L sampling reflection 1 (as in Fig. 10) plotted as a function of L. d_a and d_b are the observed spacings of 441·8 Å (±0·5%) and 418·4 Å (±0·5%) (see Haselgrove, 1975). (b) Intensities of orders 15 (◆), 16 (▲) and 17 (●) of the interference function of period L observed in models like that in Fig. 10 but with different values of L.

peak from that due to a seven-line array to one due to an array with up to 15 lines. The effect on the total transform of doing this could easily be that I_{17} is weakened even further relative to I_{16} than in the case of the simple seven-line array (Fig. 10(b)). We hope to consider this possibility further when analyses of the P and D-zones are carried out. Finally we conclude from this analysis that the model with a C-protein repeat of 434 Å explains the 430 to 440 Å region of the meridional X-ray diffraction pattern rather better than does a model (Rome *et al.*, 1973) with the C-protein and myosin repeats identical.

(f) *The C-protein repeat and filament length determination*

If the two periodicities we have seen are those of C-protein and myosin then their slight difference is puzzling. In many ways it would be very much simpler to model the myosin filament if their repeats were the same but then there would be no known role for C-protein. It is conceivable that the apparent difference is a preparative artifact. For example, it could be argued that the crossbridges which are seen in the cryo-sections are attached to actin and that there is a slight shrinkage in the length of the actin filaments relative to myosin during the preparative procedure. Thus the C-protein repeat would be 429 Å and the apparent crossbridge repeat would be slightly reduced from this. Our own results cannot discount this possibility, although we are not aware of any supporting evidence for it. But the argument from the relative intensities of the 442 and 418 Å meridional X-ray reflections is consistent with (although not proof of) the idea that the C-

protein repeat is different from that of myosin, and for this reason it is of interest to consider the implications of the presence of two A-band periodicities.

The location of C-protein within a restricted part of the A-band has been explained previously in terms of the packing of myosin molecules within the thick filament (Squire, 1973). Both in the P-zone and in the taper regions of the myosin filaments (D-zones) the myosin packing must be changing. Only in the C-zone is it likely to be relatively constant. It was suggested that C-protein may only attach to this regular part of the myosin filament. But why does the thick filament not continue to grow regularly beyond the C-zone with more and more stripes of C-protein binding to it? We have suggested previously (Squire *et al.*, 1976) in a preliminary discussion of this problem, that this continuous growth does not occur because of the effect of the different C-protein period.

Thus, C-protein could be part of the length-determining mechanism of the thick filament. There is not yet enough evidence available to define such a mechanism in detail but the scheme described by Squire *et al.* (1976) shows one class of mechanism which would have the desired effect.

(g) *Myosin filament modelling*

The observed perturbation in the crossbridge array, assuming it is present in native relaxed muscle, could either be due to the effect of the presence of C-protein on myosin molecules packed with a regular 143 Å repeat or it could be due to a true 429 Å packing repeat in the filament backbone. Squire (1979) has described myosin packing models which would account for the latter possibility. Such a perturbation of the crossbridge repeat would also have a marked effect on the layer-line intensities in X-ray diffraction patterns from relaxed muscle. Previous attempts to find the tilt and slew of the relaxed myosin crossbridges by computer modelling of the observed X-ray data (Squire, 1975; Haselgrove, 1980) have all assumed perfect helicity for the crossbridge array. These results must therefore be taken as being preliminary. It should be remembered also that the results presented here describe only the axial component of the crossbridge perturbation. The models in Figure 8 have the crossbridges displaced along the three helical tracks of the three-stranded helix, but this is only one of many possibilities about which there are as yet no data.

5. Conclusion

Although many uncertainties remain about the axial structure of the vertebrate C-zone, it is clear from the results reported here that the study of longitudinal cryo-sections can yield a great deal of new information on A-band structure. In particular we have shown that there are two axial periodicities in the A-band in addition to that due to actin, and we have shown that the myosin crossbridges do not have even axial separations but lie on a true repeat of 429 Å. We are at present extending this work to include studies of human muscles at different sarcomere lengths and also of frog muscles, some of which are at non-overlap sarcomere

lengths to remove the influence of actin. In addition, we are studying human cryosections labelled on the grid (Sjöström & Squire, 1977*b*) with antibody to C-protein. This work and also a detailed discussion of the X-ray diffraction patterns from vertebrate skeletal muscles will be presented elsewhere. Suffice it to say here that the present work, together with a published study of the transverse structure of the A-band (Luther & Squire, 1980) has shown clearly that the vertebrate A-band is much more complicated than has been thought hitherto. Because of the irregularities in the crossbridge array and the randomness in the transverse structure of the A-bands of higher vertebrates (Luther & Squire, 1980), interpretation in terms of crossbridge behaviour of the impressively elegant X-ray diffraction experiments on active frog muscles recently reported by Yu *et al.* (1979) and Huxley *et al.* (1980,1981) is likely to be a formidable undertaking.

We acknowledge the support of grants from the British Medical Research Council, the Science Research Council, the Muscular Dystrophy Association of America and the Swedish Medical Research Council.

We are also indebted to Drs P. K. Luther and A. Freundlich for helpful discussions.

REFERENCES

Bennett, P. M. (1976). *Proc. 6th Eur. Congr. Elec. Microsc., Jerusalem* (Ben Shaul, Y., ed.), vol. 2, pp. 517–519, Tal International, Israel.
Craig, R. W. (1977). *J. Mol. Biol.* **109**, 69–81.
Craig, R. W. & Offer, G. (1976). *Proc. Roy. Soc. ser. B*, **192**, 451–461.
Elliott, A. & Offer, G. (1978). *J. Mol. Biol.* **123**, 505–519.
Fraser, R. D. B. & Millward, G. R. (1970). *J. Ultrastruct. Res.* **31**, 203–211.
Hanson, J., O'Brien, E. J. & Bennett, P. M. (1971). *J. Mol. Biol.* **58**, 865–871.
Haselgrove, J. C. (1975). *J. Mol. Biol.* **92**, 113–143.
Haselgrove, J. C. (1980). *J. Muscle Res. Cell Motil.* **1**, 177–191.
Huxley, H. E. (1963). *J. Mol. Biol.* **7**, 281–308.
Huxley, H. E. (1967). *J. Gen. Physiol.* **50**, 71–83.
Huxley, H. E. & Brown, W. (1967). *J. Mol. Biol.* **30**, 383–434.
Huxley, H. E., Faruqi, A. R., Bordas, J., Koch, M. H. J. & Milch, J. R. (1980). *Nature (London)*, **284**, 140–143.
Huxley, H. E., Simmons, R. M., Faruqi, A. R., Kress, M., Bordas, J. & Koch, M. H. J. (1981). *Proc. Nat. Acad. Sci., U.S.A.* **78**, 2297–2301.
Knappeis, G. G. & Carlsen, F. (1968). *J. Cell. Biol.* **38**, 202–211.
Luther, P. K. & Squire, J. M. (1978). *J. Mol. Biol.* **125**, 313–324.
Luther, P. K. & Squire, J. M. (1980). *J. Mol. Biol.* **141**, 409–439.
Maw, M. C. & Rowe, A. J. (1980). *Nature (London)*, **286**, 412–414.
Moos, C. (1972). *Cold Spring Harbor Symp. Quant. Biol.* **37**, 93–95.
Moos, C., Offer, G., Starr, R. & Bennett, P. M. (1975). *J. Mol. Biol.* **97**, 1–9.
Offer, G. (1972). *Cold Spring Harbor Symp. Quant. Biol.* **37**, 87–96.
Offer, G., Moos, C. S. & Starr, R. (1973). *J. Mol. Biol.* **74**, 653–676.
Pepe, F. A. & Drucker, B. (1975). *J. Mol. Biol.* **99**, 609–617.
Rome, E., Offer, G. & Pepe, F. A. (1973). *Nature New Biol.* **244**, 152–154.
Sjöström, M. & Squire, J. M. (1977*a*). *J. Mol. Biol.* **109**, 49–68.
Sjöström, M. & Squire, J. M. (1977*b*). *J. Microscop.* **111**, 239–278.
Squire, J. M. (1972). *J. Mol. Biol.* **72**, 125–138.
Squire, J. M. (1973). *J. Mol. Biol.* **77**, 291–323.

Squire, J. M. (1975). *Annu. Rev. Biophys. Bioeng.* **4**, 137–163.
Squire, J. M. (1979). In *Fibrous Proteins; Scientific Industrial and Medical Aspects* (Parry, D. A. D. & Creamer, L. K., eds), vol. 1, pp. 27–70, Academic Press, London.
Squire, J. M., Sjöström, M. & Luther, P. K. (1976). *Proc. 6th Eur. Congr. Elec. Microsc., Jerusalem* (Ben Shaul, Y., ed.), pp. 91–95, Tal International, Israel.
Starr, R. & Offer, G. (1978). *Biochem. J.* **171**, 813–816.
Yu, L. C., Hartt, J. E. & Podolsky, R. J. (1979). *J. Mol. Biol.* **132**, 53–68.

Edited by H. E. Huxley